An investigation of the chemistry of silver in biological systems, and the development of silver-containing materials for use as antibacterial agents

Harley D. Betts

School of Physical Sciences
The University of Adelaide

Supervised by Professors Hugh H. Harris and Christopher J. Sumby, and Associate Professor Christopher A. McDevitt

A thesis submitted to the University of Adelaide
for the degree of Doctor of Philosophy

January 2020

THE UNIVERSITY of ADELAIDE

Declaration

I certify that this work contains no material which has been accepted for the award of any other degree or diploma in my name in any university or other tertiary institution and, to the best of my knowledge and belief, contains no material previously published or written by another person, except where due reference has been made in the text. In addition, I certify that no part of this work will, in the future, be used in a submission in my name for any other degree or diploma in any university or other tertiary institution without the prior approval of the University of Adelaide and where applicable, any partner institution responsible for the joint award of this degree.

I give permission for the digital version of my thesis to be made available on the web, via the University's digital research repository, the Library Search and also through web search engines, unless permission has been granted by the University to restrict access for a period of time.

I acknowledge the support I have received for my research through the provision of an Australian Government Research Training Program
Scholarship.

Harley D. Betts
22nd January 2020

Acknowledgements

This doctoral degree has – far and away – been the most difficult endeavour I have undertaken, so far. Mental health, and emotional and physical upheaval have made the last 3-4 years trying, but they have also been full of growth and good company. Without the positive, supporting people around me, this achievement would not have been possible.

Firstly, Professor Hugh Harris. I could not have asked for a more accepting and supporting supervisor, mentor, and friend. He has provided experitise and assistance when asked, but also space for me to develop personally and professionally over the five years that we have worked together.

Secondly, my cosupervisors, the Chrises. Without Chris Sumby, it's hard to see how I would have completed much of my PhD work he has helped to guide many aspects of my research. Without Chris McDevitt, I never would have been introduced to the field of microbiology (a real highlight of my PhD). Admittedly, my undergraduate experience was light in biological electives, but Chris, Steph and the other McDevitt Group members welcomed me and trusted I wouldn't infect them all with golden staph or *E. coli*.

I would be remiss to not give special mention to Dr Steph Neville (née Begg) of the McDevitt group. Steph facilitated much of my biological research; she helped me to crawl, walk and eventually run. She not only taught me valuable lab skills and techniques but was a great mentor and a top-notch friend.

I have been privileged to share these experiences with close friends. Oli, Tash, and Kate have provided more help, support, and joy than they can know. Their comeradery has been a tremendous comfort over these years. Dr Steph Jayne has been an ever-present friend, lab neighbour, and sympathetic ear. To the other Harris group members (James and Jake) – having spent the majority of my candidature as the sole member of the group (sort of), the company has been appreciated and it's been a joy seeing you both start your careers in research.

Finally, my family, especially my parents. Towards the end of my PhD candidature I moved back with my mum and stepdad which has (surprisingly) brought us all closer. It has been a real pleasure to have them be part of this time in my life and they really helped me surmount this final hurdle. The rest of my family have also been a tremendous support, particularly my sister, nanna and dad.

Everyone listed here (and many, many more) has contributed to this achievement and I cannot thank you all enough.

Table of Contents

Declaration iii

Acknowledgements iv

Table of Contents v

Abstract vii

Chapter One: Introduction

1.1 Abbreviations 1

1.2 Introduction 1

1.3 The chemistry of silver and its interactions with the building blocks of life 2

1.4 Silver in bacteria 8

1.5 Silver in humans 14

1.6 Research aims 19

1.7 Techniques 19

1.8 References 22

Chapter Two: Speciation of silver in *S. aureus*, *E. coli* and media

2.1 Abbreviations 33

2.2 Introduction 34

2.3 Methods and procedures 38

2.4 Results 42

2.5 Discussion 67

2.6 Conclusions 77

2.7 Future directions 78

2.8 References 80

2.9 Appendices 85

Chapter Three: The biochemical fate of silver ions in human blood

3.1 Abbreviations 95

3.2 Introduction 95

3.3 Methods and procedures 100

3.4 Results 104

3.5 Discussion 125

3.6 Conclusions 130

3.7 Future directions 131

3.8 References 134

3.9 Appendices 139

Chapter Four: Development of silver-containing materials for use as antibacterial agents

4.1 Abbreviations 151

4.2 Introduction 152

4.3 Experimental and methods 158

4.4 Results and Discussion 166

4.5 Conclusions 202

4.6 Future directions 203

4.7 References 205

4.8 Appendices 211

Chapter Five: Conclusions and future work

5.1 Conclusions and future work 226

Abstract

The antibacterial properties of silver have been known for centuries; however, the threat of antibiotic resistant bacteria has led to renewed focus on the noble metal. Silver is now commonly included in a range of household and medical items to imbue them with bactericidal properties. Despite this, the chemical fate of the metal in mammalian or bacterial biological systems, is poorly understood. Through a metallomics approach, using techniques like X-ray absorption spectroscopy (XAS), and size-exclusion chromatography hyphenated inductively coupled plasma mass spectrometry (SEC-ICP-MS), results are presented that advance our understanding of the chemistry of these interactions.

In bacterial systems, endogenous and exogenous silver ions were found to be predominantly coordinated by thiolate species, likely cysteine residues. Silver in broth was found to be associated exclusively with moderately size species (~30 kDa). Conversely, in *S. aureus* and *E. coli*, silver was bound by a range of species, ranging from 20-30 kDa, to >1220 kDa. Silver was also nonuniformly associated with copper-bound species, suggesting possible cellular processing of the noble metal as nutrient copper. Colocation of Ag with Cu could also provide insight into the cellular distribution of silver, as copper is predominantly found in the extracytoplasmic space of bacteria as it is a strictly regulated nutrient due to potential toxicity.

Exposure of human whole blood to 2 mM $AgNO_3$ resulted in lysis of red blood cells (RBCs), regardless of the isotonicity of the added solution. Despite this, within five minutes ~90% of silver ions were localised in the RBCs. Inside the RBCs Ag^+ interacted predominantly with haemoglobin and no low molecular weight complexes (e.g. glutathione). Linear combination fitting of Ag K-edge XANES of the RBC fraction from a sample of human whole blood treated with $AgNO_3$ indicated ~53% of the experimental spectrum could be described by a silver-haemoglobin model with the remaining percent explained by a silver-cysteine model. In isolated plasma the speciation of silver was found to strongly resemble that of solid silver chloride. Conversely, the speciation of silver in the plasma fraction from whole blood was found to have no contribution from the same AgCl model spectrum. The dominant binder of silver in human plasma was human serum albumin as well as higher molecular weight species.

Finally, the pore environment of UiO-66 was tailored for use as an antibacterial agent. In. general, inclusion of sulfur-containing functionality in the framework resulted in

increased silver ion uptake (relative to the parent material). While sulfhydryl-decorated pores were found to take up significantly more silver, the material did not release significant concentrations of Ag^+. Allyl and alkyl thioethers were found to both increase silver uptake and control release. The silver-loaded materials were successfully embedded into polymer matrices; extending applicability as antibacterial hybrid coatings and providing further control over silver release. Ag XAS revealed that, when loaded with silver ions, the unfunctionalised UiO-66 partially reduced Ag(I) to Ag(0) in the absence of an added reductant. All silver-loaded UiO-66 derivatives embedded in polymer matrices were found to have antibacterial activity against *S. aureus* and *E. coli*.

Chapter One: Introduction

1.1 Abbreviations

AgNP	silver nanoparticle
CSD	Cambridge Structural Database
EXAFS	extended X-ray absorption fine structure
ICP-MS	inductively coupled plasma mass spectrometry
K_{sp}	solubility product
MT	metallothionein
PDB	Protein Data Bank
SEC	size exclusion chromatography
ROS	reactive oxygen species
TEM	transmission electron microscopy
XAS	X-ray absorption spectroscopy
XANES	X-ray absorption near-edge structure

1.2 Introduction

Silver is not an essential macro- or micronutrient for any organism, nor is it involved in any biological process known to date. The antimicrobial properties of silver, however, have been known for centuries.[1] Three common forms of silver include bulk metal, cationic (Ag^+), and nanoparticles (AgNP). Of the three forms, bulk silver is known to have the lowest antibacterial activity due to its resistance to oxidation ($E^0 = +0.80$ V).[2] Ionic and nanoparticulate silver are known to be active antibacterial agents, however, their mechanism(s) of action are still unknown. Whether nanoparticles act as Trojan horses/carriers for Ag^+ to infiltrate the cell, the nanoparticle itself causes the antibacterial response, or a combination of the two is unclear.[3] The mechanism by which Ag^+ acts against bacteria is also yet to be fully understood, however, it is posited to be a dynamic, multimodal process where – if one avenue of attack is blocked – another mode of action is open to the metal ion. While the physiological effects of silver ions on bacteria are well documented, little is understood about the speciation, and molecular targets of silver in biological systems. Through metallomics techniques such as size exclusion chromatography hyphenated inductively coupled plasma mass spectrometry (SEC-ICP-MS), and X-ray absorption spectroscopy (XAS) greater insight into the biochemical fate of silver ions *in vivo* can be achieved.

1.3 The chemistry of silver and its interactions with the building blocks of life

An understanding of silver chemistry and how it interacts with the fundamental building blocks of life can provide stepping-stones to understanding its interactions with higher-order complex molecules in biological systems.

1.3.1 Physical chemistry

Ag^+ is classified by Pearson as a 'soft' metal ion with preference for 'soft' donor atoms such as sulfur and, to a lesser extent, nitrogen.[4] In spite of this, a review of the Cambridge Structural Database (CSD) reveals that a majority of silver-containing structures have silver-oxygen interactions, highlighting the promiscuity of the metal's chemistry (**Appendix 3.9.2**). In structures where silver-sulfur interactions dominate, AgS_2 and AgS_3 coordination spheres are common and result in linear (digonal), and trigonal planar geometries, respectively.[5]

Both silver and copper are group 11/1B elements and Ag(I) and Cu(I) cations exhibit similar chemistries due to their closed shell electronic structures (d^{10}). Cuprous ions exhibit a similar proclivity for soft donor atoms and linear binding geometries.[6] By contrast, Cu(II) ions are considered 'borderline' hard/soft acids, preferring distorted octahedral and square planar geometries with oxygen or nitrogen donors.[4]

While silver(I) is not a biologically essential metal ion, the cuprous and cupric cations are required micronutrients for both prokaryotic and eukaryotic organisms.[7] Therefore, due to the similarities in Cu(I) and Ag(I) chemistry, a knowledge of the biochemistry of copper can be beneficial in understanding silver in biological systems.

The poor aqueous solubility of salts that silver can form with common biological anions (like Cl^-, S^{2-}, O^{2-}, and PO_4^{3-}) is commonly thought to reduce the antibacterial effects of silver ions in biological systems.[3] The solubility products (K_{sp}) of these silver salts span many orders of magnitude from 1.8×10^{-10} (1.93 mg per L of pure water) for AgCl to 8×10^{-51} (0.14 mg per L of pure water) for Ag_2S and have the potential to limit the bioavailability of silver ions by sequestering them as solids.[2] Conversely, the K_{sp} of $AgNO_3$ – a silver salt commonly administered in antibacterial studies – is often not reported due to its high solubility in water (~4.24 kg $AgNO_3$ per litre of water at 25°C).[8]

1.3.2 Amino acids and peptides

One of the most fundamental building blocks in biology are amino acids, of which there are 21 that occur naturally. Polymerisation of these diverse monomers into peptide chains, and proteins facilitates the complex machinations of the cell. The interaction of

metal ions with the side-chain groups of amino acids, resulting in (un)favourable conformations or providing redox activity, is part of how they carry out their biological function *in vivo*. Hence, an understanding of how Ag^+ interacts with amino acids in isolation can, in part, give insight into its behaviour in more complex structures such as proteins and enzymes.

Theoretical binding energies of silver with 20 of the naturally occurring amino acids (stoichiometric ratios of 1:1) suggest that the basic amino acids histidine, lysine, and arginine (**Figure 1**) interact most strongly with Ag^+.[9-10] While the sulfur-containing amino acids – methionine and cysteine (**Figure 1**) – were ranked 5th and 14th, respectively, which is at odds with the experimentally observed chemistry of silver. It is likely that the stoichiometry used (1:1, M to L) and assumptions that binding would not be exclusively through the amino acid side-chains (i.e. all species would be chelated by multiple groups in a single amino acid molecule) resulted in these aberrant conclusions for the sulfur-containing amino acids. Experimentally, Yan and Nan have shown that the affinity, and specificity, of silver for cysteine can be utilised as a probe for the detection of the amino acid in complex biological mixtures at low concentrations (micromolar).[11]

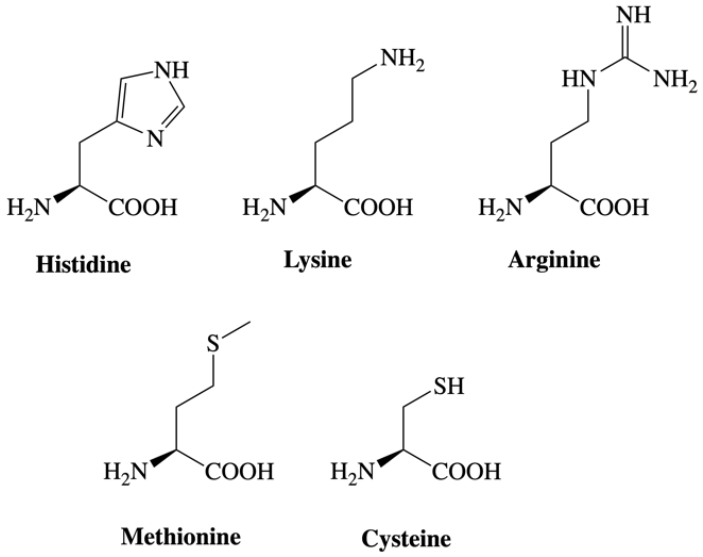

Figure 1: The structures of selected L-amino acid.

Eight different amino acids, including derivatives thereof, have been crystallised as Ag^+ complexes.[5, 12-18] While visualisation of the behaviour of silver with these amino acids is undoubtedly useful, they must be viewed critically. Amino acids are highly pH-sensitive molecules and, unfortunately, the pHs used to crystallise such complexes are often not physiologically relevant (pH 7.4). Mirolo, et al. illustrated this by crystallising complexes

of L-histidine with Ag^+ at acidic and neutral pHs.[18] At neutral pH, two imidazole nitrogens coordinated Ag^+ with a N-Ag-N bond angle of 176° (a nitrate anion balanced the charge), while under acidic conditions each silver cation was solely coordinated through two histidine carboxylate oxygens in a pseudo-linear mode (O-Ag-O bond angle range from 110 to 136°) (**Figure 2**). This difference in coordination was attributed to the fact that at low pH the imidazole nitrogens are protonated (pKa = 6.0) and unavailable for binding.

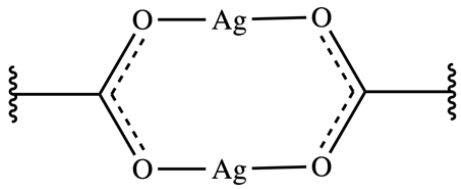

Figure 2: Pseudo-linear coordination of histidine carboxylate oxygens under acidic crystallisation conditions (CSD code: TIGGUN)[18]

In 2013 Leung, *et al.* published the first crystal structure of a cysteinate-silver complex.[5] The structure reported was a coordination polymer where the cysteine sulfur atoms adopted a μ_2 binding mode between two silver atoms, propagating a 1D chain along the *a*-axis. Two silver coordination spheres were observed in the crystal structure (AgS_3 and AgS_2N) with a large range of Ag-S bond lengths (2.450 to 2.802 Å). In the same paper the crystal structure of a complex formed between silver and penicillamine, a derivative of cysteine, was reported. Each silver atom was coordinated by two penicillamine sulfurs in digonal binding geometry. The sulfurs bridged between two silver atoms *via* μ_2 binding and long-range Ag-Ag interactions ranging from 2.954 to 3.089 Å were also observed. In addition to the solid phase data, solution phase characterisation of the complexes formed between silver and cysteine, penicillamine, and glutathione, respectively, was achieved by extended X-ray absorption fine structure (EXAFS), and ^{109}Ag nuclear magnetic resonance (NMR) analysis. The EXAFS data for each of the three systems studied was adequately fit by Ag-S and Ag-Ag interactions. A high value for the Debye-Waller factor (representative of the disorder of the system) for the cysteine and penicillamine systems was attributed to large variation in Ag-S interactions; supported by the aforementioned crystal structures. The overall coordination spheres and bond lengths are summarised in **Table 1**.

Table 1: Summary of EXAFS parameters for solution phase complexes formed between Ag^+ and cysteine, penicillamine, and glutathione

Ligand	N[a]	Ag-S (Å)	σ^2 (Å^2)[b]	N	Ag-Ag (Å)	σ^2 (Å^2)
Cysteine	2.4	2.47	0.085	0.5	2.93	0.014
	2.3	2.47	0.081			
Penicillamine	1.8	2.40	0.072	-	-	-
Glutathione	1.5	2.36	0.0034	-	-	-

[a]Coordination number, [b]Debye-Waller factor

While informative about the behaviour of these sulfur-containing biomolecules, all of the experiments were conducted at high pH (ranging from 9 to 11) and therefore cannot be considered representative of the behaviour of the molecules under physiological conditions. The XAS and NMR work was conducted at elevated pH for consistency between the solid- and solution-phase experiments as the cysteine/penicillamine complexes were crystallised under highly basic conditions.

The interaction between silver and sulfur-containing peptides (glutathione) or small proteins are of particular interest as they are suspected to play important roles as metal ion chaperones and buffering agents in prokaryotic and eukaryotic cells.[19-20]

1.3.3 Proteins

Metallothioneins (MTs) are low molecular weight (~6 kDa), cysteine-rich proteins/polypeptides that are ubiquitous in all forms of life.[21] They traditionally exist intracellularly but have been found in blood plasma and cerebral fluid in higher organisms.[22] Their high sulfur content – with cysteine in its chemically reduced form – imbue these species with some of the highest metal binding affinities of any biomolecule.[23] Expression of MTs have been identified to be induced by exposure of an organism to essential micronutrients (Cu^+/Cu^{2+}, and Zn^{2+} ions) as well as non-essential metals (Cd^{2+}).[24-25] The biological role of these low MW proteins is thought to be about protection as well as supply. Metallothioneins are posited to bind metal ions and prevent adventitious, deleterious interactions with cellular components, but also to act as a buffered pool of the inorganic species to metallate proteins/enzymes.

Scheuhammer and Cherian determined that mammalian hepatic zinc and cadmium MTs were capable of binding up to 18 moles of Ag^+ ions per mole of the protein (displacing the bound Zn(II) and Cd(II) clusters) and that the propensity of other metals to displace silver from the protein was ranked thus: Ag(I) > Cu(II) > Cd(II) > Hg(II) > Zn(II).[26] No crystal structure of a silver-bound MT has been published to date, however,

Peterson, *et al.* reported the first solution phase 3D structure of a silver-substituted (native Cu(I) binding) yeast metallothionein *via* NMR spectroscopy.[27] The MT was found to be devoid of defined structure in the metal-free (apo) form, but formed parallel loops upon exposure to Ag^+; seven silver ions bound by ten cysteine residues.

Veronesi, *et al.* investigated the binding interactions of Ag(I) with a known mammalian copper chaperone (Atox1), as well as rabbit, and yeast MTs by XAS.[6] The EXAFS and X-ray absorption near edge structure (XANES) revealed that Ag(I) was bound by two cysteine residues of the known Cu(I)-binding domain of Atox1 with silver-sulfur bond distances of 2.40 Å. The bonding interactions between Ag(I) and the two metallothioneins were similar with both species thought to have AgS_3 coordination sphere with Ag-S distances ranging from 2.47 to 2.48 Å.

In 2017 a survey of the then 10 (now 13) silver-containing protein structures deposited in the Protein Data Bank (PDB) was conducted.[28] Observations pertaining to structures which contained silver were as follows:

- In all silver-containing structures, the metal was in the +1 oxidation state
- The Ag(I) ions had an average coordination number of 2.3 ± 0.03
- The most frequent coordination number was two with digonal binding geometry (L-Ag-L bond angle >160°) in ~80% of structures
- Three coordinate Ag(I) species always had a trigonal planar binding geometry
- Four coordinate species were tetrahedral
- No correlation was observed between the silver-ligand bond lengths and coordination number
- Silver was bound by the amino acid side chain groups in 96% of structures
- The Ag(I) ion was never coordinated by water
- Ag-S interactions accounted for 44% of all interactions with Ag(I)
    - Cysteine 15% with an average Ag-S bond length of 2.41(3) Å
    - Methionine 29% with an average Ag-S bond length of 2.46(3) Å
- Ag-histidine interactions accounted for 50% of all interactions
    - Average Ag-N bond length: 2.26(3) Å
- Ag-O interactions from aspartate (and, rarely, threonine) were the remaining 6%
    - Average Ag-O bond length: 2.32(4) Å

Caruso also noted that protein crystal structures are susceptible to aberrant results if not crystallised at an appropriate pH. A silver-arginine side-chain interaction was observed in

one structure, but, at physiological pH, the arginine guanidino group would be protonated and unavailable for binding (pKa = 13.8).[29] Since Caruso's review, three additional silver-containing protein structures have been deposited in the PDB. Silver coordination in these structures included linear cysteine/histidine, and cysteine/cysteine binding as well as trigonal pyramidal binding of the metal by two cysteine residues and an isoleucine hydroxyl oxygen.[30-32] Additionally, a solitary structure has been deposited in the Protein Data Bank which shows insertion of silver into an iron/sulfide redox cluster of a bacterial ferredoxin ($AgFe_3S_4$) (**Figure 3**).[33] The activity of the mis-metallated ferredoxin was inhibited until the silver-containing clusters were replaced with the native [Fe_4S_4].

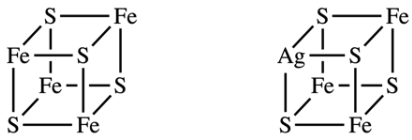

[Fe_4S_4] **[$AgFe_3S_4$]**

Figure 3: Substitution of an [Fe_4S_4] cluster iron with silver (PDB code: 4DHV)[33]

1.3.4 Nitrogenous bases

Silver ions have been shown to have an affinity for the nitrogenous bases of DNA with particular preference for the purine bases adenine and guanine.[34] The majority of crystal structures reported in the CSD for complexes between silver and the nitrogenous bases (including relevant derivatives) are between adenine and Ag(I) (28 out of 40 structures, **Appendix 2.9.3**). In these structures Ag^+ can form linear complexes with the hydrogen bonding moieties of the nitrogenous bases (**Figure 4**). It has been identified that, when treated with sublethal silver sulfadiazine, approximately 15% of silver ions were associated with DNA or RNA in *Pseudomonas aeruginosa*.[35]

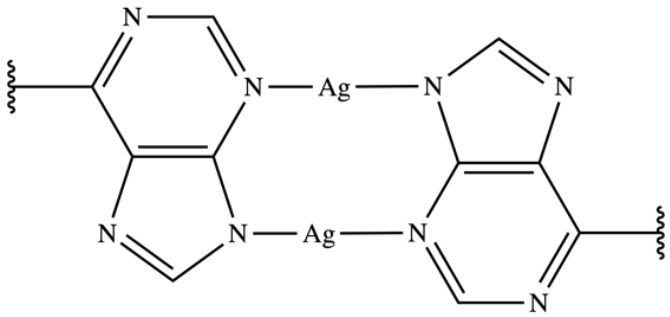

Figure 4: Schematic representation of digonal binding of silver by an adenine derivative (CSD code: MISBEX)[36]

1.4 Silver in bacteria

When bacteria are treated with lethal concentrations of silver, four broad effects have been observed, including:

- Disruption of the cell wall and/or membranes
- Interaction with DNA
- Inhibition of proteins and enzymes
- Generation of Reactive Oxygen Species (ROS)

As such, it has been hypothesised that Ag(I) has the ability to act in a multimodal manner and that if one avenue of action is blocked in the cell, by development of resistance, the metal ion can elicit its antibacterial effect in other ways.[37]

1.4.1 The cell wall and membrane

Species of bacteria can broadly be categorised as: Gram-negative, and Gram-positive. They differ from one another by the thickness of a peptidoglycan cell wall and are named as such due to the discovery by Christian Gram in 1884 that certain bacteria were capable of retaining more crystal violet dye than others.[38]

Gram-positive bacteria, such as *Staphylococcus aureus* (*S. aureus*), possess a thick cell wall (~15-80 nm) and are better able to retain more Gram stain. The cell wall envelopes the phospholipid plasma membrane of the cell (which houses important proteins for respiration and other processes in both groups of bacteria) and is considered the first line of defence for the organism.

Gram-negative bacteria, such as *Escherichia coli* (*E. coli*), have a peptidoglycan layer ~2 nm thick which wraps around the cell. In addition to this, they also possess an external phospholipid membrane which coats the 'cell wall' and can be decorated with porins, liposaccharides and proteins. The sandwich of outer cell membrane, peptidoglycan layer, and inner cell membrane is referred to as the 'periplasmic space'.[38]

Park, *et al.* observed by transmission electron microscopy (TEM) that, when treated with 0.2 ppm solutions of silver nitrate, the cytoplasm of both *S. aureus* and *E. coli* shrank and separated from the 'cell wall'.[39] The degradation and liberation of cellular contents into the extracellular space resulting in cell death was visualised.

1.4.2 Interaction with DNA

Prokaryotic cells, like bacteria, do not possess a membrane-delimited nucleus for the storage of DNA, such as is found in eukaryotic cells; instead the genetic material is located in the nucleoid.[38] In bacterial cells treated with silver nanoparticles, it has been

shown that, while the NPs were not in proximity to the nucleoid (monitored by TEM), the DNA of the organism had condensed and hence was unable to participate in cell replication.[40] The authors reconciled this observation with the presumed interaction of Ag(I), released from the AgNPS, with DNA, causing it to condense.

1.4.3 Inhibition of proteins and enzymes

The various ways in which silver has been observed to interact with amino acids, peptides, and proteins has been discussed above. In isolation these interactions are informative about the chemistry of Ag(I) with biomolecules, however, in biological systems, proteins and enzymes carry out a myriad of different functions. Binding of silver to functionally important moieties in these biomolecules can disrupt their structure and functions, leading to cell death.

Some enzymes utilise iron-sulfur clusters as cofactors in the active site of catalysis. It has been reported – both *in vitro* and *in vivo* – that soft metals, like Ag^+, are able to mis-metallate iron-sulfur clusters by substitution of iron atoms with silver atoms (**Figure 3**). For example, fumarase A is a dehydrogenase enzyme known to be poisoned by silver in a similar way to the ferredoxin structure presented above.[33, 41] Conversely, it was also found that the activity of the Fe_4S_4 cluster-containing NADH dehydrogenase I was not inhibited and the cluster remained unchanged in the presence of Ag(I) ions.[41] This observation was rationalised by the fact that the clusters in dehydrogenase I are buried deep within the protein structure, possibly protecting the clusters against mis-metallation.

Recently, silver-binding protein targets were identified in *E. coli* treated with toxic levels of silver nitrate.[42] No [Fe-S] containing proteins were identified to bind silver, which was reconciled by the fact that such interactions may have degraded the inorganic cluster yielding the apo-enzyme which would not have been detectable by the hyphenated ICP-MS methods used. However, in addition to chromatographic experiments, metabolomics was used to validate whether the identified silver-binding proteins were inhibited by the metal ion. Key enzymes in the tricarboxylic acid (TCA) cycle were found to be inhibited, both *in vitro* and *in vivo*, however, their respective binding substrates were not observed to be accumulated in the cells. The authors hypothesised that upstream [Fe-S] containing proteins in the TCA cycle were also inhibited, which stalled the substrate processing earlier than initially anticipated.

Treatment of *E. coli* with lethal concentrations of silver salts increases the permeability of the cell membrane to protons (H^+) and abolishes the proton gradient of the

cell.[43] The movement of protons in a controlled manner across the cell membrane is an important step in the respiration chain. Collapse of the proton gradient causes the organism to increase the speed of respiration to a point where it becomes independent of the amount of ATP or ADP available, which 'decouples' the respiration chain.[43] The cause of this breakdown of cellular machinery is suggested to be due to the metal ion binding to the NADH dehydrogenase (NDH) enzymes (of which *E. coli* is known to have at least two: NDH-I and -II).

Gordon, *et al.* demonstrated that silver ions released from a silver coordination polymer used in prosthetic coatings were capable of inhibiting the growth of *Staphylococcus epidermidis* (*S. epidermidis*) cultures.[44] They found that the silver ions were bound by cysteine residues of respiratory chain dehydrogenases and, after exposure to silver, generation of ROS was detected.

1.4.4 Generation of reactive oxygen species (ROS)

The generation of reactive oxygen species (singlet oxygen, H_2O_2, and $O_2^{\bullet-}$) by bacteria is a normal part of endogenous metabolic processes in aerobic environments.[45] However, ROS are known to cause damage to cellular contents like DNA, proteins, and membranes.[46] Bacteria have developed various mechanisms to counter the deleterious actions of these reactive species through the expression of scavengers such as catalases, peroxidoredoxins, and superoxide dismutases (SOD).[47] Such species are regulated by sensor proteins such as SoxR and OxyR, which sense $O_2^{\bullet-}$ and H_2O_2 in the cytoplasm, respectively. If the natural defences of the cell are overwhelmed by the generation of ROS, then the organism is considered to be in a state of oxidative stress.

Cysteine and methionine are particularly susceptible to damage by oxidative stress due to their electron-rich sulfur atoms and, in the case of cysteine, the nucleophilic nature of thiolates.[46] Oxidation of cysteine can produce sulfenic acids which are capable of forming disulfide bonds (CysSSCys) with proximal cysteines, and are either irreversibly oxidised further to sulfinic/sulfonic acid or reacted with glutathione (GSH) to eventually regenerate the reduced protein in a process called glutathionylation.[48] Oxidised cysteine residues can be reduced to the free thiol by oxidoreductases like thioredoxins (Trxs) or glutaredoxins (Grxs). These species are, in turn, oxidised and need to be reduced by thioredoxin reductase (TrxR) and glutathione reductase (Gor), respectively. Recently, glutaredoxin 2 (GrxB) was identified as a silver-binding target in *E. coli* treated with toxic levels of silver nitrate.[42] Silver has also previously been identified to bind to this

oxidoreductase through two cysteine residues in the interfacial space between a GrxB homodimer; the metal ion adopted a pseudo-linear geometry (L-Ag-L: 136.5°, PDB code 2MZC).[49]

The oxidation of methionine by ROS can form diastereomers of methionine sulfoxide which can be irreversibly (but rarely) oxidised to sulfones. Oxidised methionine residues can be reduced by methionine sulfoxide reductase (Msrs) which are stereospecific and with MsrA and MsrB catalysing the reduction of the S- and R- substrates, respectively.[50]

Bacterial cells that have been exposed to lethal concentrations of silver ions have been shown to have heightened SoxR activity, suggesting that the superoxide radical anion may be prominent in silver-induced oxidatively stressed organisms.[51]

1.4.5 Detoxification mechanisms in bacteria

Bacteria have developed mechanisms to ameliorate the toxicity of metal ions intracellularly. A silver-resistant strain of *Pseudomonas stutzeri* (*P. stutzeri*) found in the soil of silver mines has been shown to form intra- and extracellular deposits of solid silver when exposed to Ag(I).[52] The composition of these deposits was confirmed to be mixtures of Ag(0), and Ag_2S as well as unidentified components. It is presumed that this is a source of the silver-resistance of the organism. The oxidative effects of such deposits would be more easily managed by the cell than Ag(I) ions, and the oxidative dissolution of the large metal deposits (100-200 nm) would be expected to be slow.

In addition to sequestration of toxic Ag(I) ions, some bacteria have been shown to express a variety of efflux pumps, regulatory systems, and metallothioneins when exposed to silver. A silver-resistant strain of *Salmonella* isolated from a hospital burn ward expresses Ag(I)-specific proteins known as the *sil* ensemble.[53] The operon *silCBAEF* is regulated by the membrane-bound ATP kinase SilS which detects the presence of exogenous silver ions, and also the transcription regulatory protein, SilR, which initiates expression of the *sil* ensemble.[54] SilP is a membrane-bound P-type ATPase and transports cytosolic Ag(I) cations into the periplasmic space. Once in the periplasmic space the soluble proteins, SilE and SilF, bind Ag(I) with high affinity. SilE binds Ag(I) through a histidine motif similar to that of the copper resistance protein PcoE.[53] SilF is homologous to the metallochaperone CusF which forms part of the copper efflux system and binds Ag(I) and Cu(I) *via* methionine and histidine residues.[55] Transport *via* SilE and SilF to the

chemiosmotic cation/proton antiporter SilCBA enables efflux of the metal ion from the cell.[54]

Bacterial metallothioneins were first discovered in the 1980s with the identification of the BmtA family of proteins in cyanobacteria.[25, 56] This family is typified by the ~6 kDa Zn(II) and Cd(II)-responsive protein SmtA (regulated by SmtB) which binds up to four zinc and/or cadmium ions through nine cysteine residues.[57] In 2008 a second family of bacterial MTs was identified in *Mycobacterium tuberculosis* (MymT) that bind copper ions but has been shown to be expressed in the presence of silver, cadmium, zinc, and cobalt ions.[58] Beyond this, surprisingly little is known about MTs in bacteria other than the identification of conserved homologues of the BmtA family of proteins in some bacterial strains.[25]

1.4.6 The role and regulation of copper in bacteria

Unlike silver, copper is a bacterial essential micronutrient that can be used as a cofactor in some enzymes. Its biological functionality *in vivo* likely stems from the two, readily accessible, oxidation states of copper – Cu(I) and Cu(II). The total concentration of copper in *E. coli* is estimated to be ~10 μM and is strictly regulated and almost exclusively localised in the periplasmic space.[59-60]

The presence of exogenous copper is detected by the regulatory protein CueR which induces expression of the P-type ATPase efflux pump, CopA, as well as the multicopper oxidase CueO.[61-62] The sensitivity of CueR to Cu(I) is as low as zeptomolar,[63] providing insight into how stringently copper is regulated in bacteria. CopA transports cytosolic copper into the periplasmic space where Cu(I) is oxidised to Cu(II) by CueO; the cupric ion is thought to be less toxic to the cell.[64] CueR is also sensitive to Ag(I) and the presence of the metal ion induces the expression of CopA and CueO.[63] The copper is cleared from the cytosol by these proteins and retained in the extracytoplasmic space. If the concentration of copper in the periplasm continues to rise (ranging from 70 to 200 μM), the two-component sensor CusR/CusS initiates the expression of the *cusABCF* operon.[61] CusA, a proton antiporter, can export various metal ions from the cell; membrane-bound CusB spans the periplasmic space and CusC is an outer membrane-bound protein.[62] Methionine residues located in the periplasmic domains of CusA and CusB are essential for their ability to transport metal ions to the extracellular space.[65] CusF, an approximately 10 kDa, soluble periplasmic protein, chaperones Cu(I) – and Ag(I) – ions between CusB

and CusC.[66] The crystal structure of CusF shows similar binding motifs for both Ag(I) and Cu(I), consisting of two methionine and one histidine residue.[67] Interestingly, a tryptophan residue appears to 'cap' the binding site of the metal and is thought to prevent adventitious redox reactions occurring between its native Cu(I) metal ion, and other periplasmic species during transport.

Some strains of *E. coli* possess a secondary copper regulatory system which are encoded by the *pcoABCDER* genes, however, the mechanism of copper transport and efflux by this family of proteins is largely unknown.[66] PcoR/PcoS are a two-component regulator system that induces the expression of the other five proteins upon exposure of the organism to copper ions. [68] PcoA – a multicopper oxidase – and PcoC are both exported to the periplasmic space upon expression. PcoD is thought to chaperone cytosolic copper into the periplasm where it is bound by PcoE. Finally, PcoB is predicted to be an outer membrane protein facilitating efflux of the metal ion from the cell.[68-69] However, the putative functionality of this system in responding to Ag^{+} exposure is yet to be determined.[70]

Much is known about systems of bacterial copper efflux, but the mechanisms of uptake and homeostasis are still poorly understood.[71] Transport of the metal ion into the cell is likely a combination of active and passive processes utilising Cu-binding metallophores as well as membrane-bound porins.[72-74] Of the copper-dependent proteins known, most reside in the extracytoplasmic space. The movement of nutrient copper within the cytoplasm is assumed to be facilitated by small, thiolate-containing molecules like glutathione.[75] However, glutathione's affinity for Cu^{+} ions is orders of magnitude lower than that of copper-sensing/regulatory proteins.[76-77] Despite high cytoplasmic glutathione concentrations, and evidence that GSH may be exported to the periplasm,[78] it has been posited that copper is only bound by the peptide in cases of high Cu stress.[75] Additionally, periplasmic extracts indicate that unidentified chaperones or low molecular weight species bind copper.[79-80]

1.5 Silver in humans

1.5.1 Exposure and toxicity

Chronic exposure of humans to silver (ions or nanoparticles) can result in argyria, the primary symptom of which is the subdermal deposition of silver as a mixture of insoluble sulfides and reduced Ag(0) which gives the person a blue appearance.[81-82] Few incidences of argyria are known, however, it is estimated that acute exposure of between 1.4 and 40 x 10^4 μg/kg of soluble salts is required for the condition to be symptomatic.[3] Medical researchers suggest that the staining of the skin is not dangerous and that it is a purely cosmetic concern. However, consumption of the quantities of silver sufficient to develop argyria can also decrease beneficial flora diversity as well as perturbation of liver biochemistry.[83-85]

Exposure of humans to silver was traditionally a rare occurrence, however, heightened use of ionic and nanoparticulate silver in medical and commercial items has increased the rate of incidence.[86] An individual can be exposure to silver by three broadly grouped pathways: inhalation, ingestion, and dermal exposure. Inhalation of silver-containing aerosols or other particulates results in deposition of silver in the lungs and/or absorption into the blood stream. The deposition of particulate silver in the lungs has been identified to be dependent on both particle size and breathing force.[87] Small particles (<1 μm) can be deposited in the alveoli, thus AgNPs penetrate deeply into the lungs and can be in close proximity to the vascular system into which dissociated Ag^+ ions can be incorporated and distributed around the body.[88]

Approximately 10 to 20% of silver ingested is absorbed in the gastrointestinal tract and distributed around the body by the vascular system; the remaining silver is excreted in urine and faeces.[89] In mice fed with silver-doped water (500 ppm $AgNO_3$) the highest concentration of silver was localised in the kidneys (1.2 x 10^4 μg/kg wet weight), followed by the spleen (8.7 x 10^3 μg/kg wet weight), and liver (3.9 x 10^3 μg/kg wet weight).[90] However, other studies suggest that silver is accumulated in the liver and could interfere with copper homeostasis as this is one of the dominant sites of cuproenzyme expression in the body.[85]

Silver can also enter the body by contact of the skin with metal salt solutions or medical/consumer items. Silver sulfadiazine (SSD, **Figure 5**) is commonly used as a topical ointment for the prevention of bacterial infections in burn victims.[86] People treated with SSD or silver salts have been shown to have increased plasma and urine silver concentrations, suggesting that the ion is not restricted to the immediate vicinity of the wound site.[91-92] SSD is an effective antibacterial agent with some studies even suggesting

that use of ionic silver can decrease wound inflammation, however, conflicting evidence in the literature also suggests that the ion can be toxic to host cells and delay wound healing; contradiction between reported *in vitro* and the few *in vivo* experiments are common.[3]

The cellular redundancy of mammalian organisms is one hypothesis for the discrepancy between silver toxicity against eukaryotic and prokaryotic organisms. However, the presence of biological fluids *in vivo* has also been demonstrated to attenuate the potential toxicity of silver.[93] Sequestration *via* sedimentation as insoluble silver salts (chloride, sulfide, etc.) or adsorption to biomolecules in blood serum/extracellularly have been shown to limit the toxicity of silver.[94-95] From these observations it has been highlighted that the speciation of silver *in vivo* is important to understand to try and explain the apparent disparities in toxicity between organisms.[3, 86, 96]

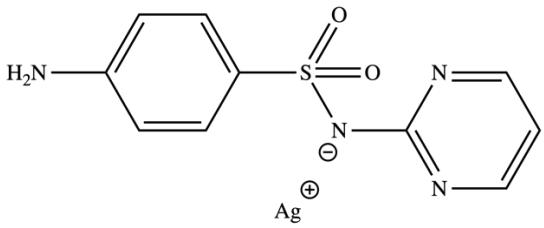

Figure 5: Structure of silver sulfadiazine (SSD); used clinically for treatment of burns

Systemic effects of exposure to silver can include argyrosis of the eyes,[97] leukopenia[98] and liver/kidney damage.[99] Additionally, silver has been claimed to cause brain damage,[100] seizures,[101] and animal deaths.[102] Mice injected with doses of various silver salts sufficient to kill 50% of the population (LD_{50}) displayed signs of ataxia, depression of the central nervous system, and loss of 'right reflex'.[103]

1.5.2 Detoxification and homeostatic mechanisms

The antibacterial efficacy of silver has been shown to be adversely affected *in vitro* by the addition of organic matter, foetal calf serum (FCS) or serum, relative to pure water.[94, 104-105] The cytotoxic effects of silver nitrate against fibroblasts were observed to decrease with increasing FCS content in the media.[104] Such observations have been attributed to the 'cytoprotective' properties of biological fluids with little explanation for the speciation of silver in the experiments conducted. Indeed, sedimentation of silver *in vivo* as a method to mitigate the cytotoxic effects of the metal is likely the origin of the subdermal staining of people afflicted with argyria.

Similar to bacterial systems, the uptake, transport and efflux of silver is thought to be orchestrated by copper homeostatic proteins.[106] CTR1 is a protein responsible for the uptake of nutrient copper (and silver) into human cells; its inactivation leads to copper and iron deficiencies.[107] Iron deficiencies are linked to nutrient copper as FET3 – a copper-dependent ferroxidase – is involved in iron uptake.[106] A second copper-binding protein, CTR2, is homologous with CTR1, however, the role of CTR2 is unclear as it has been shown to have a lower affinity for nutrient copper than CTR1.[108] Introduction of CTR2 into CTR1-inactive yeast cells did not appreciably restore copper uptake.[109]

P-type ATPases in eukaryotic cells are often located in the plasma or endoplasmic reticular membranes. Cu-ATPases such as ATP7A and ATP7B are known to export Cu(I) from the cytosol across the plasma membrane *via* hydrolysis of ATP and the charge balanced importation of biological monovalent ions.[106] Both proteins are purported to transport nutrient copper into intracellular vesicles which release the metal by exocytosis. ATP7A is suggested to funnel copper into the blood stream for redistribution into other tissues or proteins, while that transported by ATP7B is exported for removal from the body with both efflux systems are fed by soluble copper chaperones like Atox1.[62]

All of the copper-binding proteins mentioned have been demonstrated to either interact with Ag^+ upon exposure or be inhibited by the presence of the metal. Both CTR1 and CTR2 can be partially or wholly inactivated by silver ions[107-108] while the ATPases are known to efflux silver from the cells.[110] ATP7A has been shown to export silver from Chinese hamster ovary cells and human fibroblasts.[111-112] While upregulation of ATP7B and active efflux of Ag^+ has been observed upon exposure to silver in other systems.[113]

The crystal structure of copper chaperone Atox1 with Ag^+ has been deposited in the Protein Data Bank (PDB code: 5F0W).[114] Four silver atoms were bound between two monomers of the chaperone. Three of the silver atoms were bound exclusively by cysteine residues and had pseudo-linear geometry (S-Ag-S bond angle range: 133-174°) while the fourth had distorted trigonal planar geometry bound by two cysteine residues and an isoleucine hydroxyl. The silver-cysteine bond lengths ranged from 2.29 Å to 2.66 Å while the silver-oxygen interaction from the isoleucine was very long at 2.87 Å. All silver atoms displayed Ag-Ag interactions ranging from 2.89 Å to 3.01 Å, but these interactions did not appear to influence the atoms geometry.

Solution-phase interactions between the Atox1 and silver ions have also been investigated by X-ray absorption spectroscopy (XAS).[6] Analysis of the extended X-ray absorption fine structure corroborated, in part, the interactions observed in the crystal structure described above. Silver was found to be bound by two cysteine sulfurs with bond

lengths of 2.40 Å and no other interactions were present (in solution) according to the study.

The fate of silver in rats fed on Ag-supplemented diets for 30 days was identified to be the liver where it was incorporated into ceruloplasmin.[85] Ag(I) disrupted the tertiary structure of the metalloprotein and the ceruloplasmin oxidase activity in serum fell to zero. In addition to this, the female rats were found to be infertile. In subsequent studies it was found that a prolonged period of silver supplementation in rats (6 months) resulted in partial restoration in Cp oxidase activity (50% relative to control group), healthy offspring were produced, however, copper and iron homeostatic and transport genes were downregulated.[85]

1.5.3 Medical uses

In addition to topical ointments like silver sulfadiazine or dilute solutions of silver nitrate, a range of silver-containing medical devices exist; including wound dressings, catheters, and prostheses.[92] One of the greatest differences between silver-containing devices is the mode of incorporation of the antibacterial metal. These processes can include coating with metallic silver; incorporation of AgNPs; coating with silver-composite materials like nanocomposites, zeolites, and polymers; or surface modifications.[37]

Coatings of silver metal on implants and megaprostheses have demonstrated good *in vitro* antibacterial activity but poor *in vivo* activity.[115-117] It was postulated that the oxidative dissolution of silver ions from the metallic surface was inefficient. Additionally, silver ions that are released can be quickly sequestered by biomolecules and the recipients of the implants had high levels of blood plasma silver.[115] Conflicting evidence from different case studies revealed that the concentration of silver ions at the wound site of a silver-coated titanium megaprosthesis could reach up to 1.5 ppm, however, despite such high levels of silver ions, integration of the implant by the host did not appear to be impeded.[118] The variable, uncontrolled release of silver ions has led to such implants to be deemed unsafe for use.[3]

Relative to bulk metallic silver, silver nanoparticles have high surface area and undergo oxidative dissolution to release Ag^+ at a faster rate.[119] Particle size effects have been observed for AgNPs with smaller particles (<100 nm) appearing to be more effective antibacterial agents. For example, 500 nm AgNPs embedded in a silicon catheter had

negligible activity, only stunting bacterial growth and failing to stave off infection[120] whereas smaller nanoparticles have been demonstrated to be potent bactericides.[121]

Nanocomposite materials such as TiO_2-AgNPs coated on a titanium implant have been shown to have homogenous distribution on the surface, controlled release of silver ions, but did not discernibly inhibit cell ingrowth onto the implant.[122-123] Coatings, including silver NP/tantalum nitride (TaN-Ag) composites, and silver-doped silica monoliths,[124-125] have shown both favourable biocompatibility as well as prolonged release (up to 28 days, in some cases).[124]

Embedding materials in a polymer matrix or other porous material have been shown to display superior control of silver release while not requiring physical modification of the implant, and providing additional protection for the silver payload.[3] Silver ions can be diffused into porous polymer matrices by immersion in a silver solution; *in situ* reduction of Ag^+ can be achieved by addition of a reductant.[126-127] Hydrogels and a range of polymers, including polyethylene terephthalate and polyacrylamide, have been utilised for such purposes.[128] Chitosan embedded AgNPs have been demonstrated to release silver for up to 90 days.[129] Embedding AgNPs in polymer provides multiple benefits, such as preventing pacification either by biomolecules/insoluble salts or phagocytosis.[130] The rate of diffusion of such loaded materials has been demonstrated to be dependent on the rate of diffusion of water into the material. Because of this it is important that such composites are tested in biologically relevant media. Additionally, the rate of diffusion of the silver has also been shown to be influenced by the crystallinity of the polymer matrix, and nanoparticle morphology.[131]

Silver-doped phosphate glasses are another class of material and are dependent on the degradation of the material to release silver into solution.[132-133] In a similar vein, silver-containing coordination polymers have been demonstrated to have antibacterial activity upon degradation of the framework which liberated Ag^+.[134] Loading of bioactive substances into porous frameworks (like zeolites and metal-organic frameworks) has also been investigated as a means of releasing the species slowly over time.[135-137]

It has been demonstrated that the release of silver from zeolites can be sustained for up to 20 days, and that, in general, the surface charge and pore sizes of the inorganic structure have appreciable impact on the antimicrobial activity of the material. However, zeolites are limited by a lack of scope to alter and modify the overall structure to tailor the material to a specific purpose.[135] Conversely, porous species like metal-organic frameworks allow choice of metal node and organic linker which can be modified pre or post material synthesis. It has been shown that changing the ratio of different organic

linkers included in the MOF synthesis stage can allow 'programming' of payload release, changing release kinetics from the structure.[138-139]

1.6 Research aims

Herein we describe research towards a more indepth understanding of silver chemistry in biological systems and antibacterial materials. In Chapter 2 the chemical fate of sublethal concentrations of silver ions in broth (exogenous) and in *E. coli* and *S. aureus* (endogenous) was investigated. Both endo/exogenously, the chemistry of silver ions, determined by XAS, was dominated by interaction with cysteine residues, and the binding of ions by protein species confirmed by SEC-ICP-MS. Correlation between the silver and copper SEC-ICP-MS traces possibly highlighted that sublethal Ag^+ is treated similarly to nutrient copper in the bacterial cells.

Significant focus is given to the interaction between silver and bacteria, and the metal dismissed as non-toxic to mammals or humans. However, case studies and examples of silver cytotoxicity can be found in literature.[81, 86, 92, 101-102, 140] Upon exposure, transport of silver ions around the body by the vascular system is likely, thus Chapter 3 focuses on the way in which silver ions interact with human whole blood. Silver was found to localise in/on red blood cells where they were predominantly coordinated by cysteine residues on haemoglobin and other protein species.

Finally, increasing concern over antibiotic resistance has led to silver being incorporated in a range of medical and commercial items. For the metal to be successful in prevention or eradication of bacterial infections, the concentration of silver ions released from the item needs to be at a level toxic to the bacteria over a prolonged period of time to prevent non-culturable stasis or reinfection. Chapter 4 investigates the inclusion of ionic and nanoparticulate silver into metal-organic frameworks. Tailoring the pore environments of the frameworks allowed control over the relative uptake of silver in each material which also impacted on the subsequent release of silver. All materials were found to have antibacterial activity.

1.7 Techniques

1.7.1 X-ray absorption spectroscopy

X-ray absorption spectroscopy (XAS) is an element specific technique that enables analysis of the interactions between metals/metalloids and coordinating atoms. An XAS spectrum is obtained through irradiation of a sample with X-rays of increasing energies. Once an appropriate energy is reached core electrons of the element of interest are excited

to a higher bound state which result in the region of an XAS spectrum known as the X-ray absorption near-edge structure (**Figure 6**). This region is sensitive to oxidation state, and coordination geometry of the target atom.[141] Comparison of the experimental XANES through principal component analysis (PCA), target analysis, and linear combination fitting (LCF) to model XANES spectra allows empirical determination of chemical species present in the sample.

At higher energies, the excited electrons can be ejected from the atom as photoelectrons which give rise to the latter part of an XAS spectrum known as the extended X-ray absorption fine structure (**Figure 6**). The ejected electrons can interact with neighbouring atoms to produce oscillations characteristic of the coordination environment, binding atoms, and bond lengths of the target element in the sample.[141]

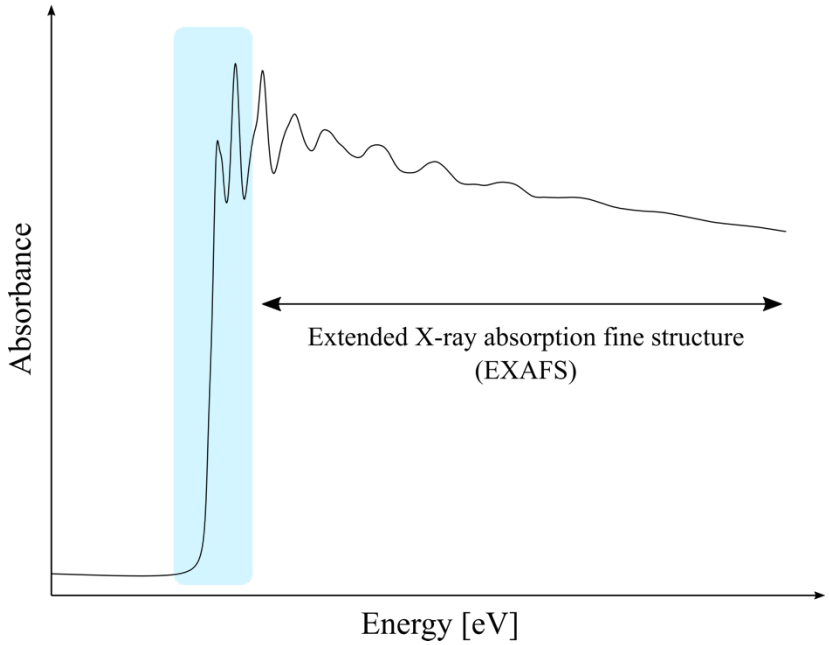

Figure 6: Ag K-edge XAS spectrum of metallic silver displaying the X-ray absorption near-edge structure (XANES, blue), and extended X-ray absorption fine structure (EXAFS) portions of the spectrum.

Identification of the speciation of silver in biological environments through use of XANES and EXAFS have been mentioned already (see above). Some of these include Ag L_3-edge XANES analysis of silver speciation in three strains of bacteria *S. aureus*, *E. coli*, and *L. monocytogenes* which found that silver-nitrogen interactions from amino acids like histidine predominantly bound Ag^+.[142] Interactions between silver ions and homeostatic/transport proteins like Atox1 and rabbit/yeast metallothioneins by XAS have provided validation for the speciation of the metal ion with these biomolecules in solution.[6] The chemical fate of silver has also been investigated in the livers of marine mammals like

dolphins and whales which found that the metal was likely sequestered as both Ag_2Se and Ag_2S chemical species.[143]

1.7.2 SEC-ICP-MS

Size exclusion chromatography (SEC) involves the separation of mixtures based on the 'size,' or more accurately, the hydrodynamic radius of constituents.[144] The technique is commonly used for the separation of proteins in complex biological mixtures, either coupled with anionic or cationic exchange chromatography or manipulation of the pH for an additional dimension of separation.[145] SEC columns can be manually packed or pre-packed for purchase, but the premise of the technique is the same. The resin has well-defined pores which are too small for large (bio)molecules to diffuse in, causing them to elute first while smaller species can diffuse into the resin and elute later. From large to small hydrodynamic radii, the molecules interact progressively more strongly with the column, allowing the separation of complex mixtures. Calibration of the column with protein standards of known molecular weights can enable calculation of the size of the entities eluting at each timepoint in the chromatogram.[146]

Inductively coupled plasma mass spectrometry is a technique traditionally used to simultaneously measure the total concentrations of metal(loid)s but provides almost no information on the speciation of the metals measured. Single cell ICP-MS has been shown to be able to identify the relative uptake of metals of interest by individual cells as opposed to bulk concentrations,[147] and laser-ablation ICP-MS or NanoSIMS techniques can be used to obtain spatially resolved maps of metal localisation in cells,[148-149] however, the techniques are only suitable for larger eukaryotic cells, at present time. ICP-MS in general is considered a highly sensitive technique, with low-interference analytes (like silver) capable of being detected at levels as low as parts per trillion. The amount of analyte present in a sample can be quantitatively determined by comparison against a calibration curve of known analyte concentrations.

However, when SEC is hyphenated with ICP-MS, time-resolved metal traces can be obtained which provide insight into the speciation of the analyte of interest based on size of the eluting species as well as detection of other metals or protein that eluted at a specific time point.

Size exclusion chromatography coupled with inductively coupled plasma mass spectrometry (SEC-ICP-MS) is not a new technique but has been underutilised, likely due to associated infrastructure requirements, namely an ICP-MS-adjacent high-performance liquid chromatography (HPLC) or peristatic pump. To the best of the authors knowledge,

the first paper detailing the use of SEC-ICP-MS was by Crews, *et al.* in 1988 in the Journal of Research of the National Bureau of Standard where it was used in an attempt to identify the speciation of trace elements in artificially digested food.[150] Since the publication by Crews, *et al.* only ~40 papers have been published using the technique. Analyses include speciation of Br, Cu, Fe, Zn, Ru, Os, Nd, and Pt in blood plasma;[151-159] Cu, Cd, I, Mn, Co, Se, S, and Zn in food stuffs like rice, sunflower/chia seeds, goji/açai berries, human breast milk, infant formula, and garlic.[160-168]

1.8 References

1. Alexander, J. W., History of the medical use of silver. *Surg Infect (Larchmt)* **2009,** *10* (3), 289-292.
2. Aylward, G.; Findlay, T., *SI Chemical Data*. 6 ed.; Wiley: 2008.
3. Eckhardt, S., Brunetto, P. S., Gagnon, J., Priebe, M., Giese, B., Fromm, K. M., Nanobio silver: its interactions with peptides and bacteria, and its uses in medicine. *Chem Rev* **2013,** *113* (7), 4708-4754.
4. Pearson, R. G., Hard and soft acids and bases. *J Am Chem Soc* **1963,** *85* (22), 3533-3539.
5. Leung, B. O., Jalilehvand, F., Mah, V., Parvez, M., Wu, Q., Silver(I) complex formation with cysteine, penicillamine, and glutathione. *Inorg Chem* **2013,** *52* (8), 4593-4602.
6. Veronesi, G., Gallon, T., Deniaud, A., Boff, B., Gateau, C., Lebrun, C., Vidaud, C., Rollin-Genetet, F., Carriere, M., Kieffer, I., Mintz, E., Delangle, P., Michaud-Soret, I., XAS investigation of silver(I) coordination in copper(I) biological binding sites. *Inorg Chem* **2015,** *54* (24), 11688-11696.
7. Festa, R. A.; Thiele, D. J., Copper: an essential metal in biology. *Curr Biol* **2011,** *21* (21), R877-883.
8. Seidell, A., Solubilities of inorganic and organic compounds. 2nd edition ed.; D. Van Nostrand Company: New York, 1919; pp 617-619.
9. Jover, J., Bosque, R., Sales, J., A comparison of the binding affinity of the common amino acids with different metal cations. *Dalton Trans* **2008,** 6441-6453.
10. Jover, J.; Bosque, R.; Sales, J., Quantitative structure-property relationship estimation of cation binding affinity of the common amino acids. *J Phys Chem A* **2009,** *113* (15), 3703-3708.
11. Nan, J.; Yan, X. P., A circular dichroism probe for L-cysteine based on the self-assembly of chiral complex nanoparticles. *Chemistry* **2010,** *16* (2), 423-427.
12. Acland, C. B.; Freeman, H. C., Model compounds for metal-protein interaction: Crystal structures of four silver(I) complexes with glycine, glycylglycine, and imidazole. *Chem Comm* **1971,** (17), 1016-1017.
13. Kamwaya, M. E., Papavinasam, E., Teoh, S. G., Rajaram, R. K. Structure of bis(alanine)-disilver(I) dinitrate. *Acta Cryst* **1984,** *40*, 1318-1320.
14. Kasuga, N. C., Yoshikawa, R., Sakai, Y., Nomiya, K., Syntheses, structures, and antimicrobial activities of remarkably light-stable and water-soluble silver complexes with amino acid derivatives, silver(I) N-acetylmethioninates. *Inorg Chem* **2012,** *51* (3), 1640-1647.
15. Nomiya, K.; Yokoyama, H., Syntheses, crystal structures and antimicrobial activities of polymeric silver(I) complexes with three amino-acids [aspartic acid (H_2asp), glycine (Hgly) and asparagine (Hasn)]. *Dalton Trans* **2002,** (12), 2483-2490.

16. Kasuga, N. C.*, et al.*, Molecular design, crystal structure, antimicrobial activity and reactivity of light-stable and water-soluble Ag–O bonding silver(I) complexes, dinuclear silver(I) N-acetylglycinate. *Inorg Chim Acta* **2006**, *359* (13), 4412-4416.
17. Kasuga, N. C., Yamamoto, R., Hara, A., Amano, A., Nomiya, K., Light-stable and antimicrobial active silver(I) complexes composed of triphenylphosphine and amino acid ligands: Synthesis, crystal structure, and antimicrobial activity of silver(I) complexes constructed with hard and soft donor atoms (n∞{[Ag(L)(PPh3)]2} with L=α-ala− or asn− and n=1 or 2). *Inorg Chim Acta* **2008,** *361* (5), 1267-1273.
18. Mirolo, L., Schmidt, T., Eckhardt, S., Meuwly, M., Fromm, K. M. pH-dependent coordination of Ag(I) ions by histidine: experiment, theory, and a model for SilE. *Chemistry* **2013,** *19* (5), 1754-1761.
19. Maryon, E. B., Molloy, S. A., Kaplan, J. H., Cellular glutathione plays a key role in copper uptake mediated by human copper transporter 1. *Am J Physiol Cell Physiol* **2013,** *304* (8), C768-779.
20. Xiong, Y., Uys, J. D., Tew, K. D., Townsend, D. M., S-glutathionylation: from molecular mechanisms to health outcomes. *Antioxid Redox Signal* **2011,** *15* (1), 233-270.
21. Ziller, A.; Fraissinet-Tachet, L., Metallothionein diversity and distribution in the tree of life: A multifunctional protein. *Metallomics* **2018,** *10* (11), 1549-1559.
22. Blindauer, C. A.; Leszczyszyn, O. I., Metallothioneins: unparalleled diversity in structures and functions for metal ion homeostasis and more. *Nat Prod Rep* **2010,** *27* (5), 720-741.
23. Vašák, M., Metal removal and substitution in vertebrate and invertebrate metallothioneins. *Methods Enzymol* **1991,** *205*, 452-458.
24. Robinson, N. J., Whitehall, S. K., Cavet, J. S., Microbial metallthioneins. *Adv Microbial Physiol* **2001,** *44*, 183-213.
25. Liu, T.; Nakashima, S.; Hirose, K; Shibasaka, M.; Katsuhara, M.; Ezaki, B.; Giedroc, D. P.; Kasamo, K, A novel cyanobacterial SmtB/ArsR family repressor regulates the expression of a CPx-ATPase and a metallothionein in response to both Cu(I)/Ag(I) and Zn(II)/Cd(II). *J Biol Chem* **2004,** *279* (17), 17810-17818.
26. Scheuhammer, A. M.; Cherian, M. G., Quantification of metallothioneins by a silver-saturation method. *Toxicol Appl Pharmacol* **1986,** *82*, 417-425.
27. Peterson, C. W., Narula, S. S., Armitage, I. M., 3D solution structure of copper and silver-substituted yeast metallothioneins. *FEBS Lett* **1996,** *379*, 85-93.
28. Carugo, O., Silver and gold in the Protein Data Bank. *J Inorg Biochem* **2017,** *175*, 244-247.
29. Fitch, C. A., Platzer, G., Okon, M., Garcia-Moreno, B. E., McIntosh, L. P., Arginine: Its pKa value revisited. *Protein Sci* **2015,** *24* (5), 752-761.
30. Mazzei, L., Cianci, M., Vara, A. G., Ciurli, S., The structure of urease inactivated by Ag(I): a new paradigm for enzyme inhibition by heavy metals. *Dalton Trans* **2018,** *47* (25), 8240-8247.
31. Wang, H., Wang, M., Sun, H., Structure of silver-bound malate dehydrogenase. 2019.
32. Meury, M., Knop, M., Seebeck, F. P., Structural basis for copper-oxygen mediated C−H bond activation by the formylglycine-generating enzyme. *Angew Chem* **2017,** *56* (28), 8115-8119.
33. Martic, M., Jakab-Simon, I. N., Haahr, L. T., Hagen, W. R., Christensen, H. E., Heterometallic [AgFe3S4] ferredoxin variants: synthesis, characterization, and the first crystal structure of an engineered heterometallic iron-sulfur protein. *J Biol Inorg Chem* **2013,** *18* (2), 261-276.

34. Arakawa, H., Neault, J. F., Tajmir-Riahi, H. A., Silver(I) complexes with DNA and RNA studies by Fourier Transform Infrared Spectroscopy and Capillary Electrophoresis. *Biophys J* **2001,** *81* (3), 1580-1587.
35. Clement, J. L.; Jarrett, P. S., Antibacterial silver. *Metal-Based Drugs* **1994**, *1* (5-6), 467-482.
36. Mishra, A. K., Prajapati, R. K., Verma, S., Coordination site discrimination in substituted bioessential purine ligands. *Indian J Chem A* **2013,** *52*, 1041-1046.
37. Chernousova, S.; Epple, M., Silver as antibacterial agent: ion, nanoparticle, and metal. *Angew Chem* **2013,** *52* (6), 1636-1653.
38. Willey, J. M., Sherwood, L. M., Woolverton, C. J., *Prescott, Harley, and Klein's Microbiology*. 7 ed.; McGraw Hill Higher Education: 2008.
39. Jung, W. K., Koo, H. C., Kim, K. W., Shin, S., Kim, S. H., Park, Y. H., Antibacterial activity and mechanism of action of the silver ion in *Staphylococcus aureus* and *Escherichia coli*. *Appl Environ Microbiol* **2008,** *74* (7), 2171-2178.
40. Feng, Q. L., Wu, J., Chen, G. Q., Cui, F. Z., Kim, T. N., Kim, J. O., A mechanistic study of the antibacterial effect of silver ions on *Escherichia coli* and *Staphylococcus aureus*. *J Biomed Mater Res* **2000,** *52* (4), 662-668.
41. Xu, F. F.; Imlay, J. A., Silver(I), mercury(II), cadmium(II), and zinc(II) target exposed enzymic iron-sulfur clusters when they toxify *Escherichia coli*. *Appl Environ Microbiol* **2012,** *78* (10), 3614-3621.
42. Wang, H., Yan, A., Liu, Z., Yang, X., Xu, Z., Wang, Y., Wang, R., Koohi-Moghadam, M., Hu, L., Xia, W., Tang, H., Wang, Y., Li, H., Sun, H., Deciphering molecular mechanism of silver by integrated omic approaches enables enhancing its antimicrobial efficacy in *E. coli*. *PLoS Biol* **2019,** *17* (6), 1-31.
43. Chappell, J. B.; Greville, G. D., Effect of silver ions on mitochondrial adenosine triphosphatase. *Nature* **1954,** *174*, 930-931.
44. Gordon, O., Vig Slenters, T., Brunetto, P. S., Villaruz, A. E., Sturdevant, D. E., Otto, M., Landmann, R., Fromm, K. M., Silver coordination polymers for prevention of implant infection: thiol interaction, impact on respiratory chain enzymes, and hydroxyl radical induction. *Antimicrob Agents Chemother* **2010,** *54* (10), 4208-4218.
45. Storey, K. B., Oxidative stress: Animal adaptations in nature. *Braz J Med Biol Res* **1997,** *29*, 1715-1733.
46. Ezraty, B., Gennaris, A., Barras, F., Collet, J. F., Oxidative stress, protein damage and repair in bacteria. *Nat Rev Microbiol* **2017,** *15* (7), 385-396.
47. Imlay, J. A., The molecular mechanisms and physiological consequences of oxidative stress: lessons from a model bacterium. *Nat Rev Microbiol* **2013,** *11* (7), 443-454.
48. Imlay, J. A., Cellular defenses against superoxide and hydrogen peroxide. *Annu Rev Biochem* **2008,** *77*, 755-776.
49. Bilinovich, S. M., Caporoso, J. A., Taraboletti, A., Duangjumpa, N., Panzer, M. J., Prokop, J. W., Shriver, L. P., Leeper, T. C., Metal binding of glutaredoxins. 2016.
50. Grimaud, R., Ezraty, B., Mitchell, J. K., Lafitte, D., Briand, C., Derrick, P. J., Barras, F., Repair of oxidized proteins. Identification of a new methionine sulfoxide reductase. *J Biol Chem* **2001,** *276* (52), 48915-48920.
51. Park, H. J., Kim, J. Y., Kim, J., Lee, J. H., Hahn, J. S., Gu, M. B., Yoon, J., Silver-ion-mediated reactive oxygen species generation affecting bactericidal activity. *Water Res* **2009,** *43* (4), 1027-1032.
52. Klaus, T., Joerger, R., Olsson, E., Granqvist, C. G., Silver-based crystalline nanoparticles, microbially fabricated. *PNAS* **1999,** *96* (24), 13611-13614.
53. Gupta, A., Matsui, K., Lo, J. F., Silver, S., Molecular basis for resistance to silver cations in *Salmonella*. *Nat Med* **1999,** *5* (2), 183-188.

54. Silver, S., Bacterial silver resistance: molecular biology and uses and misuses of silver compounds. *FEMS Microbiol Rev* **2003,** *27* (2-3), 341-353.
55. Silver, S., Phung le, T., Silver, G., Silver as biocides in burn and wound dressings and bacterial resistance to silver compounds. *J Ind Microbiol Biotechnol* **2006,** *33* (7), 627-634.
56. Olafson, R. W., McCubbin, W. D., Kay, C. M., Primary- and secondary-structure analysis of a unique prokaryotic metallothionein from a *Synechococcus* sp. *cyanobacterium*. *Biochem J* **1988,** *251*, 691-699.
57. Blindauer, C. A., Harrison, M. D., Parkinson, J. A., Robinson, A. K., Cavet, J. S., Robinson, N. J., Sadler, P. J., A metallothionein containing a zinc finger within a four-metal cluster protects a bacterium from zinc toxicity. *PNAS* **2001,** *98* (17), 9593-9598.
58. Gold, B., Deng, H., Bryk, R., Vargas, D., Eliezer, D., Roberts, J., Jiang, X., Nathan, C., Identification of a copper-binding metallothionein in pathogenic mycobacteria. *Nat Chem Biol* **2008,** *4* (10), 609-616.
59. Finney, L. A.; O'Halloran, T. V., Transition metal speciation in the cell: Insights from the chemistry of metal ion receptors. *Science* **2003,** *300* (5621), 931-936.
60. Outten, C. E.; O'Halloran, T. V., Femtomolar sensitivity of metalloregulatory proteins controlling zinc homeostasis. *Science* **2001,** *292* (5526), 2488-2492.
61. Outten, F. W., Huffman, D. L., Hale, J. A., O'Halloran, T. V., The independent *cue* and *cus* systems confer copper tolerance during aerobic and anaerobic growth in *Escherichia coli*. *J Biol Chem* **2001,** *276* (33), 30670-30677.
62. Robinson, N. J.; Winge, D. R., Copper metallochaperones. *Annu Rev Biochem* **2010,** *79*, 537-562.
63. Changela, A., Chen, K., Xue, Y., Holschen, J., Outten, C. E., O'Halloran, T. V., Mondragón, A., Molecular basis of metal-ion selectivity and zeptomolar sensitivity by CueR. *Science* **2003,** *301* (5638), 1383-1387.
64. Grass, G.; Rensing, C., Genes involved in copper homeostasis in *Escherichia coli*. *J Bacteriol* **2001,** *183* (6), 2145-2147.
65. Franke, S., Grass, G., Rensing, C., Nies, D. H., Molecular analysis of the copper-transporting efflux system CusCFBA of *Escherichia coli*. *J Bacteriol* **2003,** *185* (13), 3804-3812.
66. Osman, D.; Cavet, J. S., Copper homeostasis in bacteria. In *Advances in Applied Microbiology*, Elsevier: 2008; Vol. 65, pp 217-247.
67. Xue, Y., Davis, A. V., Balakrishnan, G., Stasser, J. P., Staehlin, B. M., Focia, P., Spiro, T. G., Penner-Hahn, J. E., O'Halloran, T. V., Cu(I) recognition *via* cation-pi and methionine interactions in CusF. *Nat Chem Biol* **2008,** *4* (2), 107-109.
68. Rensing, C.; Grass, G., *Escherichia coli* mechanisms of copper homeostasis in a changing environment. *FEMS Microbiol Rev* **2003,** *27* (2-3), 197-213.
69. Lee, S. M.; Grass, G.; Rensing, C.; Barrett, S. R.; Yates, C. J. D.; Stoyanov, J. V.; Brown, N. L., The Pco proteins are involved in periplasmic copper hangling in *Escherichia coli*. *Biochem Biophys Res Comm* **2002,** *295*, 616-620.
70. Randall, C. P.; Gupta, A.; Jackson, N.; Busse, D.; O'Neill, A. J., Silver resistance in Gram-negative bacteria: A dissection of endogenous and exogenous mechanisms. *J Antimicrob Chemother* **2015,** *70* (4), 1037-1046.
71. Stewart, L. J.; Thaqi, D.; Kobe, B.; McEwan, A. G.; Waldron, K. J.; Djoko, K. Y., Handling of nutrient copper in the bacterial envelope. *Metallomics* **2019,** *11* (1), 50-63.
72. Li, X.-Z.; Nikaido, H.; Williams, K. E., Silver-resistant mutants of *Escherichia coli* display active efflux of Ag(+) and are deficient in porins. *J Bacteriol* **1997,** *179* (19), 6127-6132.

73. Lee, H. S.; Abdelal, A. H. T.; Clark, M. A.; Ingraham, J. L. Molecular characterization of *nosA*, a *Pseudomonas stutzeri* gene encoding an outer membrane protein required to make copper-containing N_2O reductase. *J Bacteriol* **1991,** *173* (17), 5406-5413.
74. Koh, E. I.; Robinson, A. E.; Bandara, N.; Rogers, B. E.; Henderson, J. P. Copper import in *Escherichia coli* by the yersiniabactin metallophore system. *Nat Chem Biol* **2017,** *13* (9), 1016-1021.
75. Freedman, J. H.; Ciriolo, M. R.; Peisach, J. The role of glutathione in copper metabolism and toxicity. *J Biol Chem* **1989,** *264* (10), 5598-5605.
76. Xiao, Z.; Brose, J.; Schimo, S.; Ackland, S. M.; La Fontaine, S.; Wedd, A. G. Unification of the copper(I) binding affinities of the metallo-chaperones Atx1, Atox1, and related proteins. *J Biol Chem* **2011,** *286* (13), 11047-11055.
77. Morgan, M. T.; Nguyen, L. A. H.; Hancock, H. L.; Fahrni, C. J. Glutathione limits aquacopper(I) to sub-femtomolar concentrations through cooperative assembly of a tetranuclear cluster. *J Biol Chem* **2017,** *292* (52), 21558-21567.
78. Pittman, M. S.; Robinson, H. C.; Poole, R. K. A bacterial glutathione transporter (*Escherichia coli* CydDC) exports reductant to the periplasm. *J Biol Chem* **2005,** *280* (37), 32254-32261.
79. Osman, D.; Waldron, K. J.; Denton, H.; Taylor, C. M.; Grant, A. J.; Mastroeni, P.; Robinson, N. J.; Cavet, J. S. Copper homeostasis in *Salmonella* is atypical and copper-CueP is a major periplasmic metal complex. *J Biol Chem* **2010,** *285* (33), 25259-25268.
80. Waldron, K. J.; Firbank, S. J.; Dainty, S. J.; Perez-Rama, M.; Tottey, S.; Robinson, N. J. Structure and metal loading of a soluble periplasm cuproprotein. *J Biol Chem* **2010,** *285* (42), 32504-32511.
81. Baker, J. W.; Leidy, K. L.; Smith, K. M.; Okeke, U. S. Argyria associated with use of systemic colloidal silver. *Fed Pract* **2011,** *28* (1), 39-42.
82. Hill, W. R.; Pillsburg, D. M., Argyria - the pharmacology of silver. The Williams & Wilkins company: Baltimore, 1939; pp 128-132.
83. Das, P.; Petrof, E. O.; Walker, V. K. Perturbation of a human gut ecosystem by silver chloride colloids. *J Environ Anal Toxicol* **2015,** *5* (294), 1-7.
84. Trop, M.; Novak, M.; Rodl, S.; Hellbom, B.; Kroell, W.; Goessler, W. Silver-coated dressing Acticoat caused raised liver enzymes and argyria-like symptoms in burn patient. *J Trauma* **2006,** *60* (3), 648-652.
85. Ilyechova, E. Y.; Puchkova, L. V.; Shavlovskii, M. M.; Korzhevskii, D. E.; Petrova, E. S.; Tsymbalenko, N. V. Effect of silver ions on copper metabolism during mammalian ontogenesis. *Russ J Develop Biol* **2018,** *49* (3), 166-178.
86. Drake, P. L.; Hazelwood, K. J., Exposure-related health effects of silver and silver compounds: a review. *Ann Occup Hyg* **2005,** *49* (7), 575-585.
87. Casals, E.; Vázquez-Campos, S.; Bastús, N. G.; Puntes, V. Distribution and potential toxicity of engineered inorganic nanoparticles and carbon nanostructures in biological systems. *Trends Anal Chem* **2008,** *27* (8), 672-683.
88. Kim, Y. S.; Song, M. Y.; Park, J. D.; Song, K. S.; Ryu, H. R.; Chung, Y. H.; Chang, H. Y.; Lee, J. H.; Oh, K. H.; Kelman, B. J.; Hwang, I. K.; Yu, I. J. Subchronic oral toxicity of silver nanoparticles. *Particle Fibre Toxicol* **2010,** *7* (20), 1-11.
89. *Toxicological profile for silver*; U. S. Department of Health and Human Services: Atlanta, GA, 1990.
90. Hultman, P.; Enestrom, S.; Turley, S. J.; Pollard, K. M. Selective induction of anti-fibrillarin autoantibodies by silver nitrate in mice. *Clin Exp Immunol* **1994,** *96*, 285-291.

91. Plowman, R.; Graves, N.; Esquivel, J.; Roberts, J. A. An economic model to assess the cost and benefits of the routine use of silver alloy coated urinary catheters to reduce the risk of urinary tract infections in catheterized patients. *J Hosp Infect* **2001,** *48* (1), 33-42.
92. Lansdown, A. B., A pharmacological and toxicological profile of silver as an antimicrobial agent in medical devices. *Adv Pharmacol Sci* **2010,** *2010*, 1-16.
93. Spacciapoli, P.; Buxton, D.; Rothstein, D.; Friden, P., Antimicrobial activity of silver nitrate against periodontal pathogens. *J Periodont Res* **2001,** *36*, 108-113.
94. Zhang, S.; Du, C.; Wang, Z.; Han, X.; Zhang, K.; Liu, L., Reduced cytotoxicity of silver ions to mammalian cells at high concentration due to the formation of silver chloride. *Toxicol In Vitro* **2013,** *27* (2), 739-744.
95. Mariam, J.; Dongre, P. M.; Kothari, D. C., Study of interaction of silver nanoparticles with bovine serum albumin using fluorescence spectroscopy. *J Fluoresc* **2011,** *21* (6), 2193-2199.
96. Marchioni, M.; Jouneau, P.-H.; Chevallet, M.; Michaud-Soret, I.; Deniaud, A., Silver nanoparticle fate in mammals: Bridging *in vitro* and *in vivo* studies. *Coord Chem Rev* **2018,** *364*, 118-136.
97. Scroggs, M. W.; Lewis, J. S.; Proia, A. D., Corneal argyrosis associated with silver soldering. *Cornea* **1992,** *11* (3), 264-269.
98. Fuller, F. W.; Engler, P. E., Leukopenia in non-septic burn patients receiving topical 1% silver sulfadiazine cream therapy: A survey. *JBCR* **1988,** *9* (6), 606-609.
99. Ebabe E., R.; Gaillet, S.; Vide, J.; Romain, C.; Lauret, C.; Rugani, N.; Cristol, J. P.; Rouanet, J. M., Dietary exposure to silver nanoparticles in Sprague-Dawley rats: effects on oxidative stress and inflammation. *Food Chem Toxicol* **2013,** *60*, 297-301.
100. Stepien, K. M.; Morris, R.; Brown, S.; Taylor, A.; Morgan, L., Unintentional silver intoxication following self-medication: an unusual case of corticobasal degeneration. *Ann Clin Biochem* **2009,** *46* (6), 520-522.
101. Ohbo, Y.; Fukuzako, H.; Takeuchi, K.; Takigawa, M., Argyria and convulsive seizures caused by ingestion of silver in a patient with schizophrenia. *Psychiatry Clin Neurosci* **1996,** *50*, 89-90.
102. Hadrup, N.; Lam, H. R., Oral toxicity of silver ions, silver nanoparticles and colloidal silver: a review. *Regul Toxicol Pharmacol* **2014,** *68* (1), 1-7.
103. Horner, H. C.; Roebuck, B. D.; Smith, R. P.; English, J. P., Acute toxicity of some silver salts of sulfonamides in mice and the efficacy of penicillamine in silver poisoning. *Drug Chem Toxicol* **2008,** *6* (3), 267-277.
104. Hildago, E.; Bartolome, R.; Barroso, C.; Moreno, A.; Dominguez, C., Silver nitrate: Antimicrobial activity related to cytotoxicity in cultured human fibroblasts. *Skin Pharmacol Appl Skin Physiol* **1998,** *11*, 140-151.
105. Choi, O.; Deng, K. K.; Kim, N. J.; Ross, L., Jr.; Surampalli, R. Y.; Hu, Z., The inhibitory effects of silver nanoparticles, silver ions, and silver chloride colloids on microbial growth. *Water Res* **2008,** *42* (12), 3066-3074.
106. Gupta, A.; Lutsenko, S., Human copper transporters: mechanism, role in human diseases and therapeutic potential. *Future Med Chem* **2009,** *1* (6), 1125-1142.
107. Bertinato, J.; Cheung, L.; Hoque, R.; Plouffe, L. J., Ctr1 transports silver into mammalian cells. *J Trace Elem Med Biol* **2010,** *24* (3), 178-184.
108. Bertinato, J.; Swist, E.; Plouffe, L. J.; Brooks, S. P. J.; L'Abbé, M. R., Ctr2 is partially localized to the plasma membrane and stimulates copper uptake in COS-7 cells. *Biochem J* **2008,** *409* (3), 731-740.
109. Ohrvik, H.; Thiele, D. J., The role of Ctr1 and Ctr2 in mammalian copper homeostasis and platinum-based chemotherapy. *J Trace Elem Med Biol* **2015,** *31*, 178-182.

110. Monty, J.-F.; Llanos, R. M.; Mercer, J. F. B.; Kramer, D. R., Copper exposure induces trafficking of the Menkes Protein in intestinal epithelium of ATP7A transgenic mice. *Biochem Mol Actions Nut* **2005**, 2762-2766.
111. Verheijen, F. W.; Beerens, C. E. M. T.; Havelaar, A. C.; Kleijer, W. J.; Mancini, G. M. S., Fibroblast silver loading for the diagnosis of Menkes disease. *J Med Genet* **1998,** *35*, 849-851.
112. Petris, M. J.; Mercer, J. F. B.; Culvenor, J. G.; Lockhart, P. L.; Gleeson, P. A.; Camakaris, J., Ligand-regulated transport of the Menkes copper P-type ATPase efflux pump from the Golgi apparatus to the plasma membrane: a novel mechanism of regulated trafficking. *EMBO J* **1996,** *15* (22), 6084-6095.
113. Ibricevic, A.; Brody, S. L.; Youngs, W. J.; Cannon, C. L., ATP7B detoxifies silver in ciliated airway epithelial cells. *Toxicol Appl Pharmacol* **2010,** *243* (3), 315-322.
114. Wei, W.; Wang, F.; Zhao, J., Crystal structure of human copper homeostatic protein Atox1. Worldwide Protein Data Bank, 2017.
115. Massè, A.; Bruno, A.; Bosetti, M.; Biasibetti, A.; Cannas, M.; Gallinaro, P., Prevention of pin track infection in external fixation with silver coated piins: Clinical and microbiological results. *J Biomed Mater Res* **2000**, 600-604.
116. Sheehan, E.; McKenna, J.; Mulhall, K. J.; Marks, P.; McCormack, D., Adhesion of *Staphylococcus* to orthopaedic metals, an *in vivo* study. *J Orthop Res* **2004,** *22*, 39-43.
117. Shivaram, A.; Bose, S.; Bandyopadhyay, A., Understanding long-term silver release from surface modified porous titanium implants. *Acta Biomater* **2017,** *58*, 550-560.
118. Schmidt-Braekling, T.; Streitbuerger, A.; Gosheger, G.; Boettner, F.; Nottrott, M.; Ahrens, H.; Dieckmann, R.; Guder, W.; Andreou, D.; Hauschild, G.; Moellenbeck, B.; Waldstein, W.; Hardes, J., Silver-coated megaprostheses: review of the literature. *Eur J Orthop Surg Traumatol* **2017,** *27* (4), 483-489.
119. Utembe, W.; Potgieter, K.; Stefaniak, A. B.; Gulumian, M., Dissolution and biodurability: Important parameters needed for risk assessment of nanomaterials. *Particle Fibre Toxicol* **2015,** *12*, 1-12.
120. Bayston, R.; Vera, L.; Mills, A.; Ashraf, W.; Stevenson, O.; Howdle, S. M., *In vitro* antimicrobial activity of silver-processed catheters for neurosurgery. *J Antimicrob Chemother* **2010,** *65* (2), 258-265.
121. Duran, N.; Duran, M.; de Jesus, M. B.; Seabra, A. B.; Favaro, W. J.; Nakazato, G., Silver nanoparticles: A new view on mechanistic aspects on antimicrobial activity. *Nanomed* **2016,** *12* (3), 789-799.
122. Hardes, J.; Ahrens, H.; Gebert, C.; Streitbuerger, A.; Buerger, H.; Erren, M.; Gunsel, A.; Wedemeyer, C.; Saxler, G.; Winkelmann, W., Lack of toxicological side-effects in silver-coated megaprostheses in humans. *Biomaterials* **2007,** *28* (18), 2869-2875.
123. Scoccianti, G.; Frenos, F.; Beltrami, G.; Campanacci, D. A.; Capanna, R., Levels of silver ions in body fluids and clinical results in silver-coated megaprostheses after tumour, trauma or failed arthroplasty. *Injury* **2016,** *47*, S11-S16.
124. Huang, H.-L.; Chang, Y.-Y.; Lai, M.-C.; Lin, C.-R.; Lai, C.-H.; Shieh, T.-M., Antibacterial TaN-Ag coatings on titanium dental implants. *Surf Coat Technol* **2010,** *205* (5), 1636-1641.
125. Liu, H.; Chen, Q.; Song, L.; Ye, R.; Lu, J.; Li, H., Ag-doped antibacterial porous materials with slow release of silver ions. *J Non-Cryst Solids* **2008,** *354* (12-13), 1314-1317.
126. Plessers, E.; De Vos, D. E.; Roeffaers, M. B. J., Chemoselective reduction of α,β-unsaturated carbonyl compounds with UiO-66 materials. *J Cat* **2016,** *340*, 136-143.

127. El-Sherif, H.; El-Masry, M.; Kansoh, A., Hydrogels as template nanoreactors for silver nanoparticles formation and their antimicrobial activities. *Macromol Res* **2011,** *19* (11), 1157-1165.
128. Mozumder, M. S.; Mairpady, A.; Mourad, A. I., Polymeric nanobiocomposites for biomedical applications. *J Biomed Mater Res B* **2017,** *105* (5), 1241-1259.
129. Travan, A.; Pelillo, C.; Donati, I.; Marsich, E.; Benincasa, M.; Scarpa, T.; Semeraro, I.; Turco, G.; Gennaro, R.; Paoletti, S., Non-cytotoxic silver nanopartiicle-polysaccharide nanocomposites with antimicrobial activity. *Biomacromol* **2009,** *10*, 1429-1435.
130. Kim, S.; Choi, I.-H., Phagocytosis and endocytosis of silver nanoparticles induce interleukin-8 production in human macrophages. *Yonsei Med J* **2012,** *53* (3), 654-657.
131. Kumar, R.; Munstedt, H., Silver ion release from antimicrobial polyamide/silver composites. *Biomaterials* **2005,** *26* (14), 2081-8.
132. Capela, M. N.; Tobaldi, D. M.; Oliveira, C.; Pereira, A.; Duarte, A. S.; Seabra, M. P.; Fernandes, M. H. V., Bioactivity and antibacterial activity against *E- coli* of calcium-phosphate-based glasses: Effect of silver content and crystallinity. *Ceramics Intl* **2017,** *43* (16), 13800-13809.
133. Lee, S.; Nakano, T.; Kasuga, T., Structure, dissolution behavior, cytocompatibility, and antibacterial activity of silver-containing calcium phosphate invert glasses. *J Biomed Mater Res* **2017,** *105A*, 3127-3135.
134. Young, R. J.; Young, R. J.; Begg, S. L.; Coghlan, C. J.; McDevitt, C. A.; Sumby, C. J., Exploring the use of structure and polumer incorporation to tune silver ion release and antibacterial activity of silver coordination polymers. *Eur J Inorg Chem* **2018,** (30).
135. Dutta, P.; Wang, B., Zeolite-supported silver as antimicrobial agents. *Coord Chem Rev* **2019,** *383*, 1-29.
136. Matsumura, Y.; Yoshikata, K.; Kunisaki, S.; Tsuchido, T., Mode of bactericidal action of silver zeolite and its comparison with that of silver nitrate. *Appl Environ Microbiol* **2003,** *69* (7), 4278-4281.
137. Horcajada, P.; Gref, R.; Baati, T.; Allan, P. K.; Maurin, G.; Couvreur, P.; Ferey, G.; Morris, R. E.; Serre, C., Metal-organic frameworks in biomedicine. *Chem Rev* **2012,** *112* (2), 1232-1268.
138. Dong, Z.; Sun, Y.; Chu, J.; Zhang, X.; Deng, H., Multivariate metal-organic frameworks for dialing-in the binding and programming the release of drug molecules. *J Am Chem Soc* **2017,** *139* (40), 14209-14216.
139. Cai, W.; Wang, J.; Chu, C.; Chen, W.; Wu, C.; Liu, G., Metal-Organic Framework-based stimuli-responsive systems for drug delivery. *Adv Sci (Weinh)* **2019,** *6* (1), 1-20.
140. Kwon, H. B.; Lee. J. H.; Lee, S. H.; Lee, A. Y.; Choi, J. S.; Ahn, Y. S., A case of argyria following colloidal silver ingestion. *Ann Dermatol* **2009,** *21* (3), 308-310.
141. Newville, M., *Fundamentals of XAFS*. Consortium for Advanced Radiation Sources: Chicago, IL, 2004.
142. Bovenkamp, G. L.; Zanzen, U.; Krishna, K. S.; Hormes, J.; Prange, A., X-ray absorption near-edge structure (XANES) spectroscopy study of the interaction of silver ions with *Staphylococcus aureus*, *Listeria monocytogenes*, and *Escherichia coli*. *Appl Environ Microbiol* **2013,** *79* (20), 6385-6390.
143. Nakazawa, E.; Ikemoto, T.; Hokura, A.; Terada, Y.; Kunito, T.; Yamamoto, T.; Yamada, T. K.; Rosas, F. C. W.; Fillmann, G.; Tanabe, S.; Nakai, I., Silver speciation in liver of marine mammals by synchrotron X-ray absorption fine structure and X-ray fluorescence spectroscopies. *J Env Mon* **2011,** *13* (6), 1678-1686.

144. Fekete, S.; Beck, A.; Veuthey, J. L.; Guillarme, D., Theory and practice of size exclusion chromatography for the analysis of protein aggregates. *J Pharm Biomed Anal* **2014,** *101*, 161-173.
145. Hong, P.; Koza, S.; Bouvier, E. S., A review: Size-exclusion chromatography for the analysis of protein biotherapeutics and their aggregates. *J Liq Chromatogr Relat Technol* **2012,** *35* (20), 2923-2950.
146. Manley, S. A.; Byrns, S.; Lyon, A. W.; Brown, P.; Gailer, J., Simultaneous Cu-, Fe-, and Zn-specific detection of metalloproteins contained in rabbit plasma by size-exclusion chromatography-inductively coupled plasma atomic emission spectroscopy. *J Biol Inorg Chem* **2009,** *14* (1), 61-74.
147. Meyer, S.; Lopez-Serrano, A.; Mitze, H.; Jakubowski, N.; Schwerdtle, T., Single-cell analysis by ICP-MS/MS as a fast tool for cellular bioavailability studies of arsenite. *Metallomics* **2018,** *10* (1), 73-76.
148. Urgast, D. S.; Ou, O.; Gordon, M. J.; Raab, A.; Nixon, G. F.; Kwun, I. S.; Beattie, J. H.; Feldmann, J., Microanalytical isotope ratio measurements and elemental mapping using laser ablation ICP-MS for tissue thin sections: Zinc tracer studies in rats. *Anal Bioanal Chem* **2012,** *402* (1), 287-297.
149. Kilburn, M. R.; Clode, P. L., Elemental and isotopic imaging of biological samples using NanoSIMS. In *Electron microscopy: Methods and protocols*, 3 ed.; Kuo, J., Ed. Humana Press: New York, 2014; pp 733-755.
150. Crews, H. M.; Massey, R.; McWeeny, D. J., Trace element speciation in food: a combined enzymolysis SEC-ICP-MS approach. *J Res Nat Bureau Standard* **1988,** *93* (3), 349-350.
151. Liu, D.; Chen, G.; Huo, Z.; Liu, H.; Ji, W.; Liu, H., A study of bromine speciation in human serum and ambroxol determination in rat plasma by liquid chromatography–inductively coupled plasma mass spectrometry. *Chromatographia* **2019,** *82* (6), 927-934.
152. El Balkhi, S.; Poupon, J.; Trocello, J. M.; Massicot, F.; Woimant, F.; Laprevote, O., Human plasma copper proteins speciation by size exclusion chromatography coupled to inductively coupled plasma mass spectrometry. Solutions for columns calibration by sulfur detection. *Anal Chem* **2010,** *82* (16), 6904-6910.
153. Jahromi, E. Z.; White, W.; Wu, Q.; Yamdagni, R.; Gailer, J., Remarkable effect of mobile phase buffer on the SEC-ICP-AES derived Cu, Fe and Zn-metalloproteome pattern of rabbit blood plasma. *Metallomics* **2010,** *2* (7), 460-468.
154. Dziuba, N.; Hardy, J.; Lindahl, P. A., Low-molecular-mass iron in healthy blood plasma is not predominately ferric citrate. *Metallomics* **2018,** *10* (6), 802-817.
155. Sooriyaarachchi, M.; Wedding, J. L., Harris, H. H., Gailer, J., Simultaneous observation of the metabolism of cisplatin and NAMI-A in human plasma *in vitro* by SEC-ICP-AES. *J Biol Inorg Chem* **2014,** *19* (6), 1049-1053.
156. Sarpong-Kumankomah, S.; Gailer, J., Identification of a haptoglobin-hemoglobin complex in human blood plasma. *J Inorg Biochem* **2019,** *201* (110802), 1-8.
157. Harper, B. W. J.; Morris, T. T.; Gailer, J.; Aldrich-Wright, J. R., Probing the interaction of bisintercalating (2,2′:6′,2″-terpyridine)platinum(II) complexes with glutathione and rabbit plasma. *J Inorg Biochem* **2016,** *163*, 95-102.
158. Klose, M. H. M.; Schoberl, A.; Heffeter, P.; Berger, W.; Hartinger, C. G.; Koellensperger, G.; Meier-Menches, S. M.; Keppler, B. K., Serum-binding properties of isosteric ruthenium and osmium anticancer agents elucidated by SEC-ICP-MS. *Monatsh Chem* **2018,** *149* (10), 1719-1726.
159. Sharar, M.; Rodríguez-Solla, H.; Linscheid, M. W.; Montes-Bayón, M., Detection of sulfenic acid in intact proteins by mass spectrometric techniques: application to serum samples. *RSC Adv.* **2017,** *7* (70), 44162-44168.

160. Wei, S.; Guo, B.; Feng, L.; Jiang, T.; Li, M. Y.; Wei, Y., Cadmium distribution and characteristics of cadmium-binding proteins in rice (*Oryza sativa L.*) kernel. *Food Sci Technol Research* **2017,** *23* (5), 661-668.
161. Júnior, C. A. L.; Oliveira, S. R.; Mazzafera, P.; Arruda, M. A. Z., Expanding the information about the influence of cadmium on the metabolism of sunflowers: Evaluation of total, bioavailable, and bioaccessible content and metallobiomolecules in sunflower seeds. *Environ Exp Bot* **2016,** *125*, 87-97.
162. Ruzik, L.; Wojcieszek, J., *In vitro* digestion method for estimation of copper bioaccessibility in Açaí berry. *Monatsh Chem* **2016,** *147*, 1429-1438.
163. Wojcieszek, J.; Kwiatkowski, P.; Ruzik, L., Speciation analysis and bioaccessibility evaluation of trace elements in goji berries (*Lycium Barbarum, L.*). *J Chromatogr A* **2017,** *1492*, 70-78.
164. Wojcieszek, J.; Popowski, D.; Ruzik, L., Ionic liquids as a key medium for efficient extraction of copper complexes from chia seeds (*Salvia hispanica L.*). *Talanta* **2016,** *152*, 482-488.
165. Sanchez, L. F.; Szpunar, J., Speciation analysis for iodine in milk by size-exclusion chromatography with inductively couples plasma mass spectrometric detection. *J Anal Atom Spectrom* **1999,** *14*, 1697-1702.
166. Acosta, M.; Torres, S.; Marino-Repizo, L.; Martinez, L. D.; Gil, R. A., Novel method for metalloproteins determination in human breast milk by size exclusion chromatography coupled to inductively coupled plasma mass spectrometry. *J Pharm Biomed Anal* **2018,** *158*, 209-213.
167. Raab, A.; Ronzan, M.; Feldmann, J., Sulphur fertilization influences the sulphur species composition in *Allium sativum*: sulphomics using HPLC-ICPMS/MS-ESI-MS/MS. *Metallomics* **2017,** *9* (10), 1429-1438.
168. Gomez, B. G.; Perez-Corona, M. T.; Madrid, Y., Availability of zinc from infant formula by in vitro methods (solubility and dialyzability) and size-exclusion chromatography coupled to inductively coupled plasma-mass spectrometry. *J Dairy Sci* **2016,** *99* (12), 9405-9414.

Chapter Two: Speciation of silver in *S. aureus*, *E. coli* and media

2.1 Abbreviations

AEX	anion exchange chromatography
AS	Australian Synchrotron
CSD	Cambridge Structural Database
Cys	cysteine
Da	Daltons
EXAFS	extended X-ray absorption fine structure
FT	Fourier Transform
GSH	glutathione
HEPES	4-(2-hydroxyethyl)-1-piperazineethanesulfonic acid
HMW	high molecular weight
HPLC	high-performance liquid chromatography
ICP-MS	inductively coupled plasma mass spectrometry
IU	international units
LB	Luria Bertani
LCF	linear combination fitting
LMW	low molecular weight
MIC	minimum inhibitory concentration
NP	nanoparticles
OD_{600}	optical density at 600 nm
PCA	principal component analysis
PDB	Protein Data Bank
ROS	reactive oxygen species
SDS-PAGE	sodium dodecylsulfate polyacrylamide gel electrophoresis
SEC	size exclusion chromatography
SEM	scanning electron microscopy
SOD	superoxide dismutase
TEM	transmission electron microscopy
t_r	retention time
v_0	void volume
XANES	X-ray absorption near-edge structure
XAS	X-ray absorption spectroscopy

2.2 Introduction

The antibacterial properties of silver have been known for centuries but the discovery of molecular antibiotics in the early 20th century saw a decline in its use.[1] Today silver is still used as a treatment for wounds, ulcers, and other maladies.[2] However, while antibiotics are effective bactericidal agents, their singular modes of action enable cellular resistances to develop.[3] Conversely, the antibacterial activity of silver has been shown to be multifaceted and its modes of action can be broadly grouped as such: interaction between Ag and the cell wall/membrane; DNA; proteins/enzymes; and generation of reactive oxygen species (ROS).[4] Having multiple modes of action is beneficial as, if resistance against a single pathway was to develop, the metal can still elicit its antibacterial activity in other ways; however, some silver-resistant strains of bacteria have been identified.[5-6] The down-stream impacts of silver exposure on bacteria are well documented (e.g. detection of ROS,[7-9] cell lysis,[10-11] up/down regulation of genes[12-14]) but little is known about specific intracellular molecular targets and mechanisms of the metal.[15-17]

A sizeable disparity exists between the toxic level of silver for microorganisms (μM levels for $AgNO_3$), and for humans (acute toxicity estimated to require 1.4 to 40 x 10^4 μg Ag/kg).[4] Such a broad 'therapeutic window' coupled with an increase in antibiotic resistant bacteria has led to renewed interest in silver as an antibacterial agent. Today silver is included in a range of medical and commercial products to imbue them with antibacterial qualities.[18]

Chronic exposure of silver to humans and mammals causes a condition called argyria. The most apparent symptom of argyria is the deposition of silver under the skin giving the person a blueish appearance that can be permanent.[19] Medical professionals suggest that the change in skin colour is purely aesthetic and poses no threat to human health.[20] However, people afflicted with argyria can have reduced beneficial gut flora and a weakened immune response potentially leading to contraction of secondary infections, like pneumonia.[21] Few cases of argyria have been reported and highlight the need to better understand the mode(s) of action of silver as an antibacterial agent to develop more targeted silver-treatments. To do so, understanding of the molecular mechanisms by which the metal acts as an antibacterial agent is crucial.

Bacteria can be broadly categorised as Gram-negative or Gram-positive.[22] Gram-negative bacteria, like *Escherichia coli* (*E. coli*), have inner and outer cell membranes, with the 'periplasmic space' sandwiched between. Gram-positive bacteria, like *Staphylococcus aureus* (*S. aureus*), have a single cell membrane which is enveloped by a

thick peptidoglycan cell wall and the space between the membrane and the cell wall is referred to as the 'extracytoplasmic space'.[22]

Silver biochemistry has been closely linked to that of copper in biological systems. To date, no known biological process in any organism requires silver, however, both the Cu^{+} and Cu^{2+} ions are essential micronutrients for most organisms.[23] The cuprous and cupric ions are likely utilised due to the readily accessible oxidation states and redox potential. Both Ag^{+} and Cu^{+} are 'spectroscopically silent' due to their d^{10} electronic structures and lack of distinctive interactions with light.[24] The difficulty of studying these silent metals is likely, in part, why there are still significant gaps in knowledge about endogenous copper metabolic and homeostatic pathways in bacteria.[25] Despite being an essential micronutrient, copper can also be toxic to bacterial cells through generation of ROS, peroxidation of cell membranes, mismetallation of proteins, and induction of protein misfolding and as such the metal is strictly regulated intracellularly.[25] Unless bound as a cofactor, nutrient copper is thought to be relegated to the periplasmic/extracytoplasmic space of bacteria.[25] In cases of copper stress both *E. coli* and *S. aureus* can express CopZ which chaperones cytoplasmic Cu to the inner membrane-bound efflux protein, CopA, which ejects the ions into the periplasm/extracytoplasmic space;[26] this is largely the extent of understanding of copper homeostasis in *S. aureus*. However, for *E. coli*, once in the periplasm, multicopper oxidases (MCOs) like CueO, oxidise Cu^{+} to Cu^{2+}, which is considered less toxic to the organism.[27] If the concentration of copper ions in the periplasm increases too much, soluble chaperones, like CusF, bind and transport cuprous ions to membrane-bound cation/proton antiporters, like CusCBA, which efflux Cu^{+} into the extracellular space.[28] Beyond these efflux and homeostatic proteins, little is known about the cellular metabolism of copper in bacteria, for example, how copper-dependent enzymes are metallated or the identity of low molecular weight copper-buffering molecules.[25] Cuproenzymes expressed by some strains of bacteria include nitrous oxide reductases, nitric reductases, [Cu, Zn]-superoxide dismutases (SOD), and haem-respiratory oxidases.[29] The latter contain cytochrome c, and quinol oxidases which are terminal enzymes in the respiratory chain of the organism.[30]

Copper stress in *S. aureus* has been shown to inhibit the cytoplasmic protein glyceraldehyde-3-phosphate dehydrogenase (GapA), a key enzyme in the glycolytic cycle.[31] GapA is not a metalloprotein, but binding of Cu^{+} *via* a cysteine residue in the active site of the enzyme during Cu stress is thought to be a source of inhibition.[31] Also inhibited by copper is dihydrolipoyl dehydrogenase (LpdA), a disulfide reductase, which catalyses electron transfer from a substrate (NADH) through intramolecular redox active

cysteine residues to a flavin cofactor for continuation along an electron transport chain.[32-33] Both GapA and LpdA were recently identified by Wang *et al.* to be silver-binding molecular targets in *E. coli* cells treated with the minimum inhibitory concentration of silver nitrate.[34] Inhibition studies revealed that GapA retained ~50% activity when treated with silver *in vitro*.

2.2.1 Research aims

The aim of the study presented herein is to understand the biochemical fate of silver ions in two clinically relevant model microorganisms (*E. coli* and *S. aureus*) exposed to sublethal concentrations of the metal. Identification of individual, intracellular silver-binding targets at sublethal concentrations could improve our understanding of the toxic molecular mechanisms of action of the metal at higher concentrations. In addition to intracellular speciation, the speciation of silver ions in bacterial media was also investigated. To ensure only biologically relevant silver interactions were recorded, metallomics techniques were used, namely, X-ray absorption spectroscopy (XAS), and size exclusion chromatography coupled with ICP-MS (SEC-ICP-MS).

2.2.2 X-ray absorption spectroscopy

X-ray absorption spectroscopy (XAS) is an element-specific technique used for speciation studies of elements larger than silicon. The technique requires little sample preparation meaning that the risk of analyte chemistry perturbation is reduced. A spectrum is obtained by irradiation of a sample over a range of energies with high intensity X-rays. An XAS spectrum consists of the X-ray absorption near edge structure (XANES) and the extended X-ray absorption fine structure (EXAFS). The XANES are sensitive to oxidation state and local coordination environment of the element of interest, while the EXAFS provide information about bond lengths, coordinating atoms and coordination number.

XANES analysis involves comparison of unknown experimental data against reference ‘model’ spectra. These comparisons allow the indentification of possible components of the unknown system, however, to do so requires foresight into possible chemistry present in the experimental sample, collection of relevant model spectra or access to a library of relevant data.

For example, analysis of the Cu K-edge XANES recently found that the oxidation state of copper associated with various strains of bacteria was Cu(I), regardless of the species of copper to which the organism was exposed.[35] This is despite the fact that, under aerobic, atmospheric conditions, Cu(II) ion would be expected to predominate.[36 37]

Recently, a group identified differences in the speciation of zinc at various stages of bacterial growth in *B. subtilis* and *P. putida* through use of high resolution XANES.[38] Traditionally, XAS techniques struggle to differentiate between coordinating atoms of similar atomic number (e.g. nitrogen vs. oxygen). However, the high resolution XANES were capable of differentiating between carboxyl and phosphoryl binding as well as identification of imidazole and cysteine interactions.

2.2.3 Size exclusion chromatography hyphenated with ICP-MS

Solution ICP-MS by itself is a technique commonly used to simultaneously detect the concentrations of metals (as well as metalloids and sometimes non-metals) in a digested aqueous sample. However, when coupled with size exclusion chromatography, time-resolved ICP-MS allows simultaneous online detection of metal-binding species separated by SEC. A 'metal trace' is produced which can be overlaid with the size exclusion chromatogram to provide information about the metal-binding species in the sample.

The proteomes of most organisms are often vast lists of 1000's of proteins, which can be difficult to deconvolute or analyse. Comparatively, a subset of the proteome (namely the metalloproteome) can be relatively smaller yet provide an appreciable amount of information about the fates of inorganic species in biological systems. Comparison of the trace of an analyte of interest against other 'native' metal traces can provide insight into the biochemical fate of the metal species of interest.[39-40] SEC-ICP-MS has previously been used for analysis of a wide range of biological samples including analysis of a wide range of elements in blood plasma as well as food stuffs like rice, sunflower seeds, chia seeds, goji and açai berries, human breast milk, infant formula, and garlic.[41-47]

Analysis of bacterial metalloproteomes by SEC-ICP-MS is a relatively recent application; only a solitary published piece of work could be found.[48] Within the study the authors exposed *E. coli* to a range of different sized silver nanoparticles (as well as silver ions) at 10, 50, and 90% of the inhibitory concentration for the organism. Treatment of the cells to isolate extracytoplasmic/cell wall, and cytoplasmic extracts enabled the group to identify that the localisation of the silver in the cell was predominantly in the extracellular medium (24 – 60% of total silver) or the cell wall/membrane (25 – 64% of total silver) with only a small percentage associated with the cytoplasmic extracts (6 – 15% of total silver).

2.3 Methods and procedures

Materials

Protease inhibitory cocktail (Roche, cOmplete, EDTA-free); Lysostaphin (CAS 9011-93-2; lyophilised powder from *Staphylococcus staphylolyticus*; protein 50-70% by biuret; >500 units/mg protein); silver nitrate (CAS 7761-88-8; >99%); 4-(2-hydroxyethyl)-1-piperazinethanesulfonic acid (HEPES; CAS 7365-45-9; >99.5%); human haemoglobin (CAS 9008-02-0, lyophilized powder); bovine serum albumin (CAS 9048-46-8; ≥98.0%); L-cysteine (CAS 52-90-4; 97%); L-methionine (CAS 63-68-3; ≥98%); thiamine mononitrate (CAS 532-43-4; ≥98%); L-histidine (CAS 71-00-1; ≥99%); glycine (CAS 56-40-6; ≥99%); biotin (CAS 58-89-5; ≥99%) were purchased from Sigma Aldrich. Thyroglobulin; ferritin; aldolase; conalbumin; carbonic anhydrase; ribonuclease; aprotinin; and ovalbumin were purchased from GE Healthcare, Life Sciences. Ultra-pure MilliQ water (Merck Millipore purification system) with resistivity of 18 MΩ.cm^{-1} was used. All chemicals were used as received.

Methods

General experimental

Buffers

HEPES (100 mM) was prepared by dissolving the relevant solid in the appropriate volume of ultra-pure water. The pH was adjusted to 7.4 by the addition of NaOH (6M) (Orion Star pH Meter, Thermo Scientific). For size exclusion experiments, the mobile phase was passed through a 0.45 μm nylon-membrane filter before use.

SEC-ICP-MS

The SEC-ICP-MS consisted of a high-performance liquid chromatography (HPLC) pump (Agilent 1200 Infinity Series, Santa Clara, CA, USA) and an inductively coupled plasma mass spectrometer (Agilent QQQ 8900, Santa Clara, CA, USA). A prepacked Agilent AdvanceBio SEC 130Å size exclusion column (7.8 x 300 mm I.D., particle size: 2.7 μm, fractionation range: 120 – 0.1 kDa, Agilent) was used with a 100 mM HEPES mobile phase at a flow rate of 0.3 mL/min (column temperature: ~20°C). The void volume (v_o) was determined experimentally by injection of bacterial cell lysate (t_r = 5.79 min) detected by a variable wavelength detector (1200 series, VWD, Agilent) measuring absorbance of the effluent liquid at 280 nm. The inclusion volume (v_i) was determined by the injection of uracil (t_r = 13.74 min) detected as above. Standards used to construct a calibration curve included ovalbumin (4 mg/mL), carbonic anhydrase (3 mg/mL),

ribonuclease A (3 mg/mL), aprotinin (3 mg/mL) (GE Healthcare), and uracil (3 mg/mL) (Sigma).

A prepacked Agilent AdvanceBio SEC 300Å size exclusion column (300 x 7.8 mm I.D., particle size: 2.7 μm, fractionation range 1200 – 5 kDa) was used with a 100 mM HEPES mobile phase at a flow rate of 0.3 mL/min (column temperature: ~20°C). The void volume (v_o) and inclusion volume (v_i) were determined by detection of the thyroglobulin dimer (t_r = 6.75 min), and aprotinin (t_r = 15.13 min), respectively; detected by a variable wavelength detector (1200 series, VWD, Agilent) measuring absorbance of the column effluent at 280 nm. Protein standards used to construct a calibration curve were thyroglobulin (5 mg/mL), ferritin (0.3 mg/mL), conalbumin (3 mg/mL), ribonuclease A (3 mg/mL), and aprotinin (3 mg/mL) (GE Healthcare). See **Appendix 2.9.1** for operational parameters.

X-ray absorption spectroscopy

Data collection. Silver K-edge X-ray absorption spectra were recorded on the X-ray absorption spectroscopy (XAS) beamline at the Australian Synchrotron (AS), Victoria, Australia. The energy of the electron beam was 3.0 GeV with a current of ~200 mA, and an X-ray beam was sourced from a wiggler, monochromated by the Si(111) monochromator, and harmonic rejection achieved using a rhodium-coated mirror. Samples were positioned at ~45° to a 100-element germanium fluorescence detector which was placed at 90° to the incident beam. The energy ranges used for EXAFS spectra collection were: pre-edge region 25.3140 – 25.4941 keV (0.003 eV steps); XANES region 25.4941 – 25.5641 keV (0.0003 eV steps); and EXAFS region 25.5641 – 25.700 keV. During data collection the samples were maintained at a temperature of ~ 10 K using a Cryo Industries (Manchester, NH, USA) cryostat. The spectrum of a silver foil, recorded in transmission mode downstream from the sample, was used as an internal standard to calibrate the energy scale for the first peak of the first derivative of the elemental silver edge (25.5156 keV). 1 to 4 scans per sample were collected for EXAFS spectra.

Data analysis. Calibration, averaging, background subtraction of all spectra and principle component, target, and multiple linear regression analyses of XANES spectra were performed using the EXAFSPAK software package (G. N. George, SSRL). Single and multiple-scattering fits of EXAFS data were carried out using EXAFSPAK and the FEFF8 code.[49] The model compounds for target analysis and XANES linear combination fitting were prepared, and spectra recorded at the AS, Victoria, Australia.

Model spectra. Glassed solutions of silver nitrate with relevant amino acids, B vitamins, and proteins in 100 mM HEPES buffer were used to obtain model spectra for XANES fitting of biological samples and EXAFS analysis. The amino acid and vitamin samples had a molar ratio of 5:1 with a 2 mM final concentration of silver. Protein models had a molar ratio of 2:1 ligand to metal with a final silver concentration of 2 mM.

2. Bacteria

2.1 Cell culture

A single colony of *Escherichia coli* (*E. coli*) MG1655 or *Staphylococcus aureus* (*S. aureus*) Newman were inoculated into Luria-Bertani (LB) broth (20 mL) and incubated overnight (37°C, 200 rpm).

2.2 Minimum inhibitory concentration (MIC) studies

Inoculum prepared as per *2.1* was added to fresh samples of LB broth to a starting optical density (OD_{600}) of 0.04 and used as the inoculum. LB broth with silver nitrate acted as the positive control and broth alone acted as the negative control. Columns 1 and 12 A-H, and row H 1-12 of the plate were unused. Into column 2 was added LB broth (100 μL), and silver nitrate (*E. coli*: 50 μL, 512 μg/mL; *S. aureus*: 50 μL, 128 μg/mL) in MilliQ water. Two-fold microdilutions were carried out to reach a minimum concentration of 0.5 μg/mL (*E. coli*), and 0.125 μg/mL (*S. aureus*) in column 11. Column 12 was left as untreated with $AgNO_3$. Columns 2-12, rows C-G were inoculated to a final OD_{600} of 0.01 through addition of the above bacterial culture (50 μL). Optical densities were recorded every 15 min during incubation with constant shaking (BMG FLUOStar spectrophotometer, 37°C, 600 rpm); the MIC was read after 22 h (**Appendix 2.9.2**)

2.3 X-ray absorption spectroscopy

Cell pellets and depleted broth. Fresh samples of LB broth (19 mL) were spiked with a stock solution of $AgNO_3$ (1 mL, 10 mg/mL) in MilliQ water. Inoculum prepared as per *2.1* was added to the spiked broth to a starting optical density of 0.05 and incubated overnight (37°C, 200 rpm). The cultures were centrifuged (3750 g, 15 min, 8°C), supernatant broth removed, and the cell pellet resuspended in HEPES buffer (100 mM, 10 mL, pH 7.4). The suspension was centrifuged (as above) and the supernatant buffer removed. Both the supernatant broth and the cell pellet were freeze dried (1.0 mbar, -80°C)

and the resultant solids loaded into Lucite holders secured with Kapton tape and stored at -180°C until analysis.

Doped broth. Silver nitrate (10 or 100 mg/mL) in MilliQ water was added to LB broth (20 mL, final; 0.5 or 1 μg/mL, respectively). The doped broth was incubated overnight (37°C, 200 rpm) and freeze dried (1.0 mbar, -80°C). The resultant solid was loaded into a Lucite sample holder secured with Kapton tape and stored at -180°C until analysis.

2.4 SEC-ICP-MS

E. coli was cultured as per XAS samples (*2.3*), however, the cell pellet was suspended in HEPES (100 mM, pH 7.4, 10 mL) and the cells lysed (Cell Disruptor, Constant Systems Ltd., 0.4 bar, 6°C, 10 times). The resultant mixture was centrifuged (14,000 rpm, 15 min, 8°C) and a protease cocktail inhibitor (26 mg/mL, 600 μL) added, the lysate aliquoted (200 μL) and stored at -80°C.

S. aureus was cultured as per XAS samples (*2.3*), however, the cell pellet was suspended in HEPES (100 mM, pH 7.4, 1 mL), lysostaphin (10 units/μL, 25 μL) added, and the mixture incubated (37°C, 200 rpm, 1 h). The sample was centrifuged (14,000 rpm, 15 min, 4°C), the supernatant liquid removed, a protease cocktail inhibitor (10 μg/mL) added, the lysate aliquoted (200 μL) and stored at -80°C.

2.4 Results

X-ray absorption spectroscopy

Model XANES spectra – Interactions between Ag^+ and discrete biomolecules

Silver K-edge XANES spectra of biologically relevant molecules and silver nitrate buffered at pH 7.4 displayed a range of different peak shapes dependent on the local Ag environment (**Figure 1**). The structures of some of the (bio)molecules are displayed in **Figure 2**. These data, in addition to others collected elsewhere by our research group,[50] allowed the expansion of a library of model silver K-edge XAS spectra. Comparison of model spectra against biological samples aided the identification of silver speciation *in vitro*.

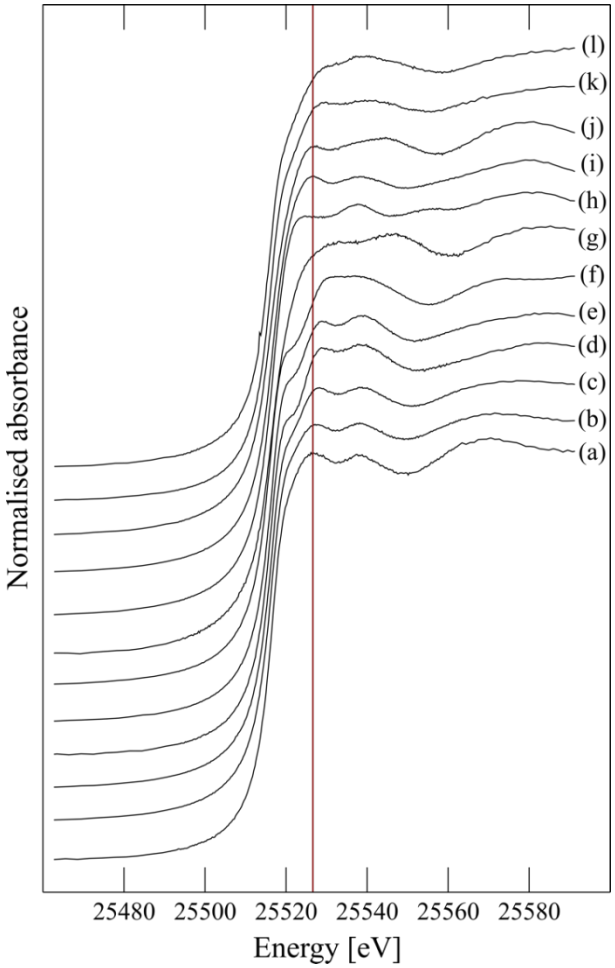

Figure 1: Ag K-edge XANES spectra of model compounds containing silver nitrate with (**a**) buffer alone; (**b**) glycine, pH 7; (**c**) glycine, pH 8; (**d**) glycine, pH 10; (**e**) glycine, Tris, pH 7; (**f**) histidine; (**g**) thiamine; (**h**) biotin; (**i**) methionine; (**j**) cysteine; (**k**) bovine serum albumin (2:1 ligand to metal); (**l**) haemoglobin (2:1 ligand to metal). Unless otherwise stated, all samples contained 2 mM $AgNO_3$ and 10 mM ligand and were prepared using 100 mM HEPES buffer at pH 7.4.

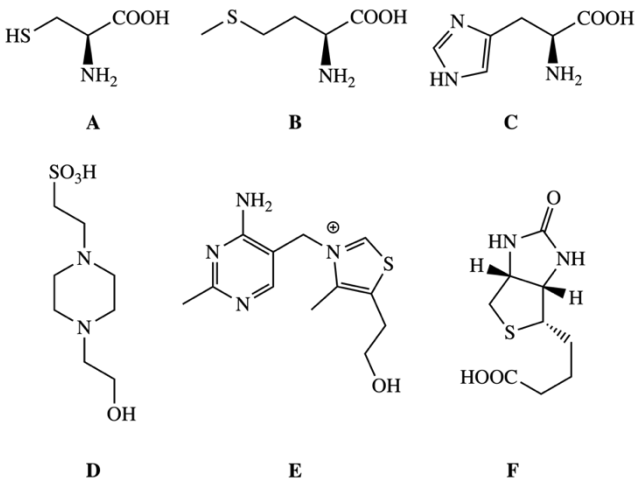

Figure 2: Structures of biologically relevant molecules used in XANES and EXAFS model spectra presented in **Figures 1** and **6**. (**A**) L-cysteine; (**B**) L-methionine; (**C**) L-histidine; (**D**) HEPES; (**E**) thiamine; (**F**) biotin.

Figure 3 shows a comparison of spectra collected from silver nitrate dissolved in excess buffered glycine across a range of pH values. Significant variation included that, with increasing pH, a shoulder near the top of the rising edge appeared (likely due to increasing deprotonation of glycine-NH_3^+ allowing nitrogen to coordinate silver). Additionally, an increase in the energy of a broad peak from 25,570 eV at pH 8 to more than 25,580 at pH 10.

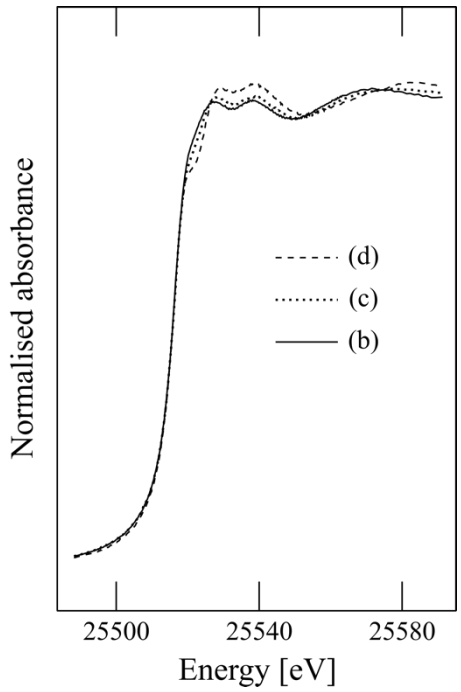

Figure 3: Superimposed Ag K-edge XANES spectra of buffered glycine/silver nitrate solutions with molar ratios of 5:1 glycine to silver at (**b**) pH 7, (**c**) pH 8, (**d**) pH 10.

A shoulder feature on the rising edge similar to that observed for the glycine models was present in spectra of silver in solution with glycine in Tris buffer at pH 7 (**Figure 1e**), and histidine in HEPES buffer at pH 7.4 (**Figure 1f**). Similar variation between the spectra of the two glycine samples at pH 7 (one buffered by HEPES, and the other Tris) may have been due to the presence of the primary amine of Tris coordinating silver, as has been seen for other heavy metals.[39] Based on pKa and physiological pH, the percentage of deprotonated nitrogen functional groups available for coordination in both histidine and Tris would be: histidine imidazole (100%), histidine amine (~2%), and Tris (~10%).

Spectra of samples with sulfur-containing molecules (**Figure 1g** to **j**) did not display a shoulder feature. Thiamine (**Figure 1g**), biotin (**h**), and methionine (**i**) all possess thioether-like functionality that would be expected to have a strong affinity for silver. However, no common post-edge feature was identified for them and they each resulted in unique XANES spectra. The silver-cysteine spectrum (**Figure 1i**) displayed similar features to that of methionine (j), such as an initial peak atop the rising edge and a broad, low frequency oscillation at 25,580 eV.

For studies concerning silver speciation in human blood (**Chapter 3**) spectra of human haemoglobin (Hb) (**Figure 1k**), and bovine serum albumin (BSA) (**l**) in two-fold excess with buffered silver nitrate were recorded. The post-edge oscillations of the silver-protein spectra were much broader and lacked strong features relative to most of the silver-small molecule model spectra.

XANES of bacterial cell pellets and broth

The minimum inhibitory concentration (MIC) of $AgNO_3$ against *E. coli* and *S. aureus* was experimentally determined to be 1 and 2 μg/mL, respectively (**Appendix 2.9.2**). Thus, samples of Luria Bertani (LB) broth were spiked to final concentrations of 0.5 and 1 μg/mL $AgNO_3$, inoculated with *E. coli* and *S. aureus*, respectively, and incubated. This allowed the organisms to grow in the presence of sublethal $AgNO_3$ and when pelleted, the sample was designated as 'growth' cell pellets (**Figure 4a** and **c**). Bacterial cultures that had been allowed to grow to maturity before exposure to sublethal concentrations of $AgNO_3$, incubated for a further ~16 h, and then pelletised were designated 'shock' cell pellets (**Figure 4b** and **d**).

The bacterial cell pellet spectra (**Figure 4a** to **d**) appeared visually similar bar small shifts in energy of the second post-edge peak annotated with a red line. However, *E. coli*

'growth' (**Figure 4c**), in addition to a higher signal-to-noise ratio, lacked a clear peak atop the rising edge as well as a subsequent trough.

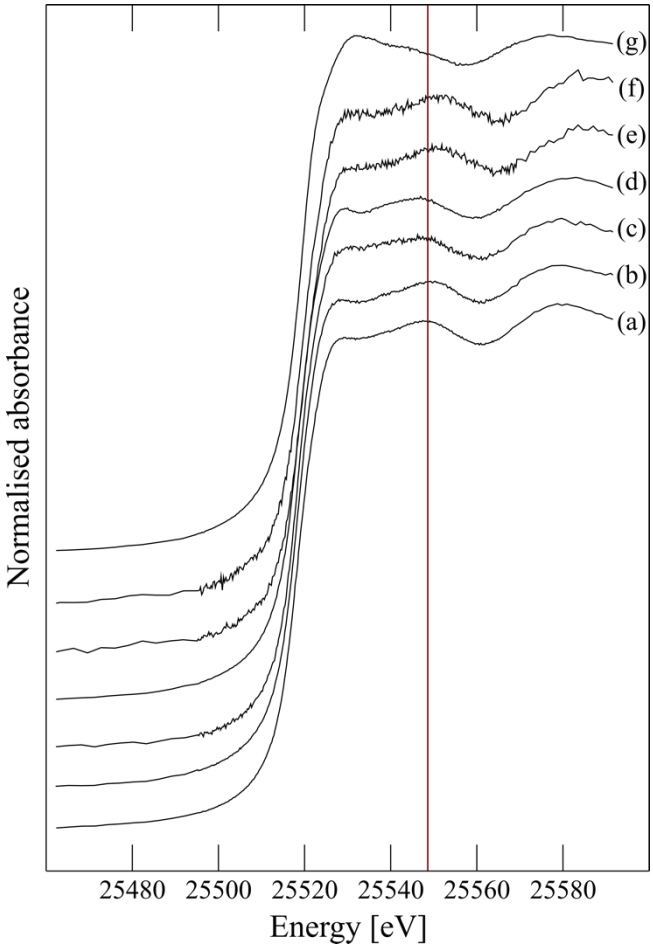

Figure 4: Ag K-edge XANES spectra of (**a**) *S. aureus* growth; (**b**) *S. aureus* shock; (**c**) *E. coli* growth; (**d***) E. coli* shock; (**e**) broth 10 μg/mL; (**f**) broth 0.5 μg/mL; and (**g**) 1:1 broth/HEPES buffer.

In **Figure 4,** spectra (**e**) and (**f**) represent freeze-dried LB broth spiked with 10 μg/mL, and 0.5 μg/mL $AgNO_3$, respectively. Despite a 20-fold difference in [$AgNO_3$] between the broth samples, the XANES spectra appeared similar. A freeze-dried sample of 50:50 LB broth (10 μg/mL $AgNO_3$) and 100 mM HEPES buffer solution – **Figure 4g** – displayed significantly different post-edge features to those of neat broth spiked with silver (**e** and **f**). The peak atop the rising edge increased in intensity and energy in broth:buffer sample, and the trough at ~25,555 eV was ~10 eV lower in energy than that of 10 μg/mL $AgNO_3$ broth (**Figure 4e**). This would suggest a perturbation in silver speciation due to the presence of the buffer.

Principal component analysis (PCA) of the bacteria/broth XANES dataset, shown in **Figure 4**, determined that three components were required for the data to be adequately

described. Target transformation of the bacterial and broth XANES spectra against the model spectra, shown in **Figure 1**, allowed visual identification of similar spectra as well as calculation of residuals. Visually the model spectra of silver with cysteine, and silver with thiamine shared similarities with those of the bacterial/broth dataset as well as the lowest calculated target transform residuals (not shown). No XANES spectrum in the model library could account for the peak atop the rising edge of the 50:50 broth:HEPES (**Figure 4g**), however, it was still included in the dataset. Linear combination fitting (LCF) allowed the ratio of each model component identified above to be calculated for the experimental cell pellet and broth spectra (**Table 1** & **Figure 5**).

Table 1 shows the ratio of silver-cysteine and silver-thiamine model spectra fit to the experimental bacterial cell pellet and broth data. Proportions of the Ag-Cys model spectrum fit ranged from 75 to 90% while the remaining proportion was that of the silver-thiamine model. The largest variation observed in the LCF values was between *S. aureus* growth (75% cysteine, 25% thiamine) and *S. aureus* 'shock' (87% cysteine, 12% thiamine) cell pellet spectra. The ratio of cysteine fit to the *E. coli* growth and *E. coli* 'shock' spectra, and also the 0.5 μg/mL and 10 μg/mL $AgNO_3$ broth spectra did not significantly change between the respective treatments of relevant samples (i.e. growth vs. shock, and 0.5 vs. 10).

Table 1: Ratio of Ag species in E. coli and S. aureus cell pellets, and broth, as estimated by linear combination of model XANES spectra.[a]

Sample	Ratio of component fitted		N_{tot}[b]	Residual
	Cysteine	Thiamine		
S. aureus growth	0.75(3)	0.25(3)	1.00	0.056
S. aureus shock	0.87(3)	0.12(3)	0.99	0.117
E. coli growth	0.85(3)	0.14(3)	0.99	0.061
E. coli shock	0.82(3)	0.18(2)	1.00	0.047
10 μg/mL $AgNO_3$ broth	0.87(2)	0.11(2)	0.98	0.112
0.5 μg/mL $AgNO_3$ broth	0.90(4)	0.08(4)	0.98	0.135

[a]Values in parentheses are the estimated standard deviation derived from the diagonal elements of the covariance matrix and are a measure of precision. [b]N_{tot} is the sum of the fractions

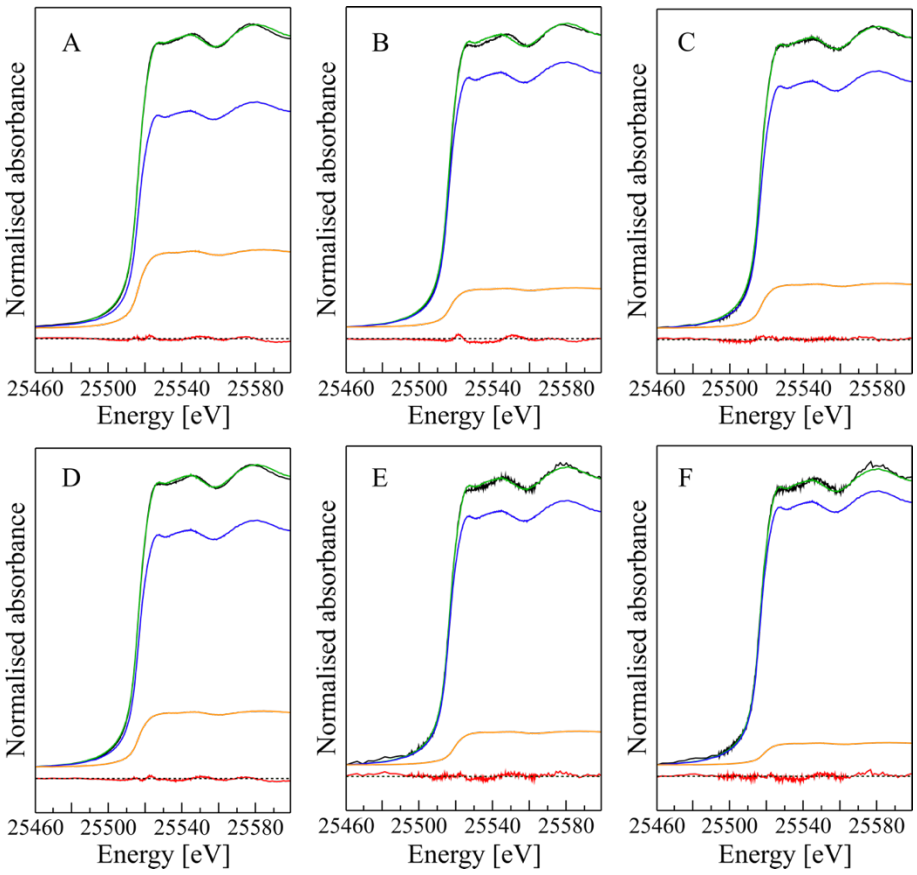

Figure 5: Linear combination fit of Ag K-edge XANES of (**A**) *S. aureus* growth cell pellet; (**B**) *S. aureus* 'shock' cell pellet; (**C**) *E. coli* growth cell pellet; (**D**) *E. coli* 'shock' cell pellet; (**E**) 10 μg/mL $AgNO_3$ broth; (**F**) 0.5 μg/mL $AgNO_3$ broth. The experimental spectra (black) was fit with a linear combination fit (green) comprised of silver-cysteine (blue) and silver-thiamine (orange) model XANES spectra as components with the residual (red) shown offset. Results of linear combination analysis are shown in **Table 1**.

EXAFS of model spectra

Ag K-edge EXAFS spectra were also collected for a range of biologically relevant molecules in buffered solutions with silver nitrate (**Figure 6**). Silver, sulfur, nitrogen, oxygen or carbon back scatterers were fit to the spectra, depending on the functional groups present in the molecules in the sample. Sulfur back scatterers were the dominant interactions in the cysteine and methionine spectra (**Figure 6A** and **B**) with Ag-S interactions of 2.48 and 2.56 Å, respectively. The increased bond length for methionine was consistent with typical silver-thioether interactions, according to a survey of the CSD (**Chapter 3**, and **Appendix 3.9.2**). The cysteine spectrum displayed a secondary peak at larger R, which was fit by an Ag-Ag interaction with a distance of 2.96 Å; conversely, no such interaction was visible for the methionine spectrum. Instead an asymmetry of the main peak was thought to be due to an unresolved peak at lower R and was adequately fit by a silver-nitrogen interaction at 2.36 Å. With both nitrogen and sulfur interactions in the coordination sphere of the silver-methionine sample, it was possible that the amino acid

was chelating Ag^+ (**Figure 7**). However, were chelation to occur, the methionine molecule would likely be held in a sufficiently rigid orientation to allow multiple backscattering to occur, but no such features were observed in the EXAFS FT. However, the absence of backscattering in the spectrum does not preclude the presence of such a chemical species.

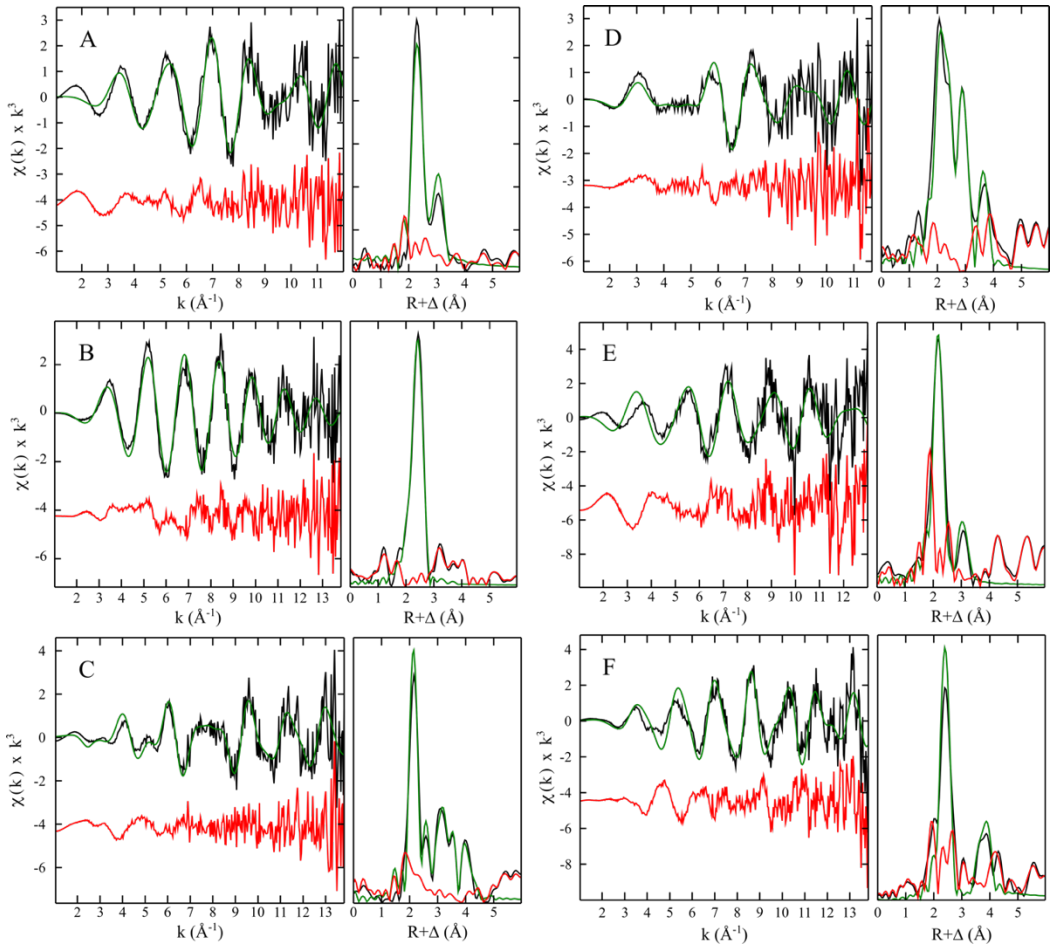

Figure 6: Ag K-edge EXAFS spectra (left panel) and corresponding Fourier Transform (right panel) of buffered solutions of Ag^+ in excess (**A**) cysteine, (**B**) methionine, (**C**) histidine, (**D**) HEPES, (**E**) thiamine, (**F**) biotin showing experimental (**black**) and calculated (green) data with the residual (red) shown offset. Fit parameters are shown in **Table 2**.

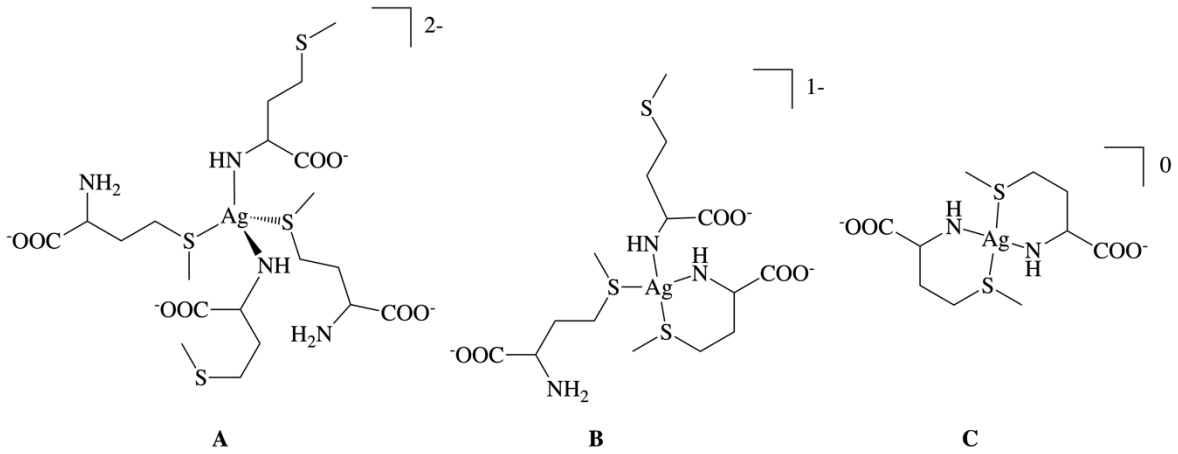

Figure 7: Possible modes of binding between methionine and silver(I) based on the calculated EXAFS fit parameters in **Table 2**. The expected mode of coordination of a four-coordinate silver complex would be tetrahedral, however, this was omitted from some structures for clarity.

Table 2: Parameters fit to EXAFS spectra of biologically relevant molecules with silver shown in **Figure 6**.[a]

Ligand	Scatterer	CN	Distance (Å)	DWF (Å^2)	-E_0	Fit error
Cysteine	S	2	2.477(5)	0.0059(3)	20(1)	0.54
	Ag	1	2.955(7)	0.0074(4)		
Methionine	N/O	2	2.36(1)	0.007(1)	14(1)	0.48
	S	2	2.560(6)	0.0053(3)		
Histidine	N	2	2.158(2)	0.0012(2)	5(1)	0.67
	N	1	2.729	0.0033		
	C	4	3.151	0.0044		
	C	4	3.567	0.0058		
	C	4	4.163	0.0045		
	Ag-C-N-Ag	6	3.298	0.0055		
	C	4	4.074	0.0089		
HEPES	N/O	2	2.221(9)	0.0066(9)	20(2)	0.71
	N/O	1	2.56(1)	0.004(2)		
	N/O	2	3.07(1)	0.0034(8)		
	N/O	2	4.01(2)	0.005(2)		
Thiamine	N	4	2.266(6)	0.0045(4)	13(1)	0.78
	C	2	3.20(1)	0.0012(9)		
Biotin	S	2	2.486(4)	0.0043(2)	14(1)	0.63
	Ag	1	3.922(6)	0.0047(4)		

[a]k-ranges used for fitting each spectrum were cysteine = 1-12 Å; methionine, histidine and biotin = 1-14 Å; HEPES = 1-11.5 Å; thiamine = 1-13 Å with a scale factor (S_0^2) of 0.9. $\Delta E_0 = E_0 - 25515$ eV where E_0 is the threshold energy. Values in parentheses are the estimated standard deviation derived from the diagonal elements of the covariance matric and are a measure of precision. The fit error is defined as $[\Sigma k^6(\chi_{exp}-\chi_{calc})^2/\Sigma k^6\chi_{exp}^2]^{½}$.

A multiple scattering fit was calculated from a crystal structure of a digonal silver-imidazole complex[51] and refined against the silver-histidine EXAFS oscillations (**Figure 6C**). The fit parameters for the histidine sample in **Table 2** show two imidazole nitrogen-silver interactions with distances of 2.16 Å. All other interactions listed were not representative of direct bonding interactions but due to the planar, rigid nature of the histidine imidazole ring; they were the result of the photoelectrons emitted from the silver absorbing atom interacting with the other atoms in the ring, known as multiple scattering.

The EXAFS spectrum of silver nitrate in HEPES buffer (**Figure 6D**) was expected to be a representation of the coordination sphere of aqueous silver cations at pH 7. Instead it was observed that, ~10 min after mixing the metal salt with the buffer solution, a crystalline, white solid was deposited from solution. Unit cell determination of a single crystal extracted from the sample provided cell axes and angles identical to a Ag-HEPES complex reported by Bilinovich, *et al.*; namely, a two-dimensional framework with silver ions bound by all functional groups in the buffer molecule.[52] Relevant structural parameters from the crystal structure are reported in **Table 3**. In light of this, immediately after mixing the solution of silver nitrate with buffer, it was flash frozen and presented to the beamline before solid was visible. However, the EXAFS fit of the $AgNO_3$ in HEPES sample still displayed Ag- nitrogen/oxygen interactions at distances similar to those observed for the silver-HEPES crystal structure collected (**Table 3**). The additional, longer Ag-N/O components at ~3 and 4 Å may have been caused by the beginnings of crystal growth in the solution, prior to freezing.

Table 3: Selected interatomic distances and angles for the silver-HEPES crystal structure.

Distance (Å)		Angle (°)	
Ag(1)-N(1)	2.253	N(1)-Ag(1)-N(2)	168.49
Ag(1)-N(2)	2.273	O(1)-Ag(1)-O(2)	87.44
Ag(1)-O(1) (OH)	2.587		
Ag(1)-O(2) (SO_3)	2.686		

Thiamine and biotin are the only sulfur-containing B vitamins (**Figure 2E** and **F**) and the XAS spectra of their interaction with silver at biological pH were recorded due to high levels of B vitamins in LB broth and the likely affinity of sulfur for silver. The EXAFS of the silver-biotin model was fit with a sulfur component at ~2.49 Å (**Figure 6F**), however, fitting the silver-thiamine EXAFS with sulfur backscatterers resulted in physically unrealistic fit parameters (not shown). A survey of the CSD (**Appendix 2.9.3**)

revealed that metal ions (such as Cu(I), Hg(II), and Cd(II)) were almost exclusively coordinated by the pyrimidine nitrogens of thiamine. In all other metal ion/thiamine-derivative structures, the metal either did not bond (forming an overall negatively charged halide complex through and acting as the counterion to the positive charge of the thiazole nitrogen) or interacted with the hydroxyl 'tail'. Four nitrogen backscatterers at distances of 2.27 Å provided an adequate fit for the EXAFS spectrum of thiamine (**Figure 6E**, **Table 2**). Additional carbon and nitrogen interactions could be fit to longer R peaks in the spectrum – at distances in agreement with those measured from a silver-pyrimidine crystal structure[53] (**Figure 8**) – however, the fit error was only marginally reduced in doing so (~1% per additional component). The silver-carbon interaction at 3.20 Å was included as validation that the mode of binding was likely through the pyrimidine ring and not the thiazole sulfur.

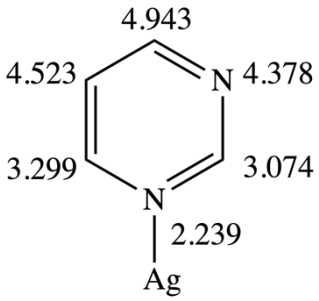

Figure 8: Distances (through space, in angstroms) of a coordinated silver atom to each atom of a pyrimidine ring, measured from crystal structure. CSD code: MESCAT.[53]

EXAFS of bacterial cell pellets and broth

Figure 9 shows the EXAFS spectra of *E. coli* growth and 'shock' cell pellets with fit parameters summarised in **Table 4**. Both spectra were adequately fit with sulfur and silver back scatterers. The sulfur distances varied by only 0.02 Å between the growth and 'shock' samples and the silver distances were refined to be 2.94 Å for both samples. The large fit error of the *E. coli* growth EXAFS (**A**) was likely due to the low signal-to-noise ratio observed for these samples.

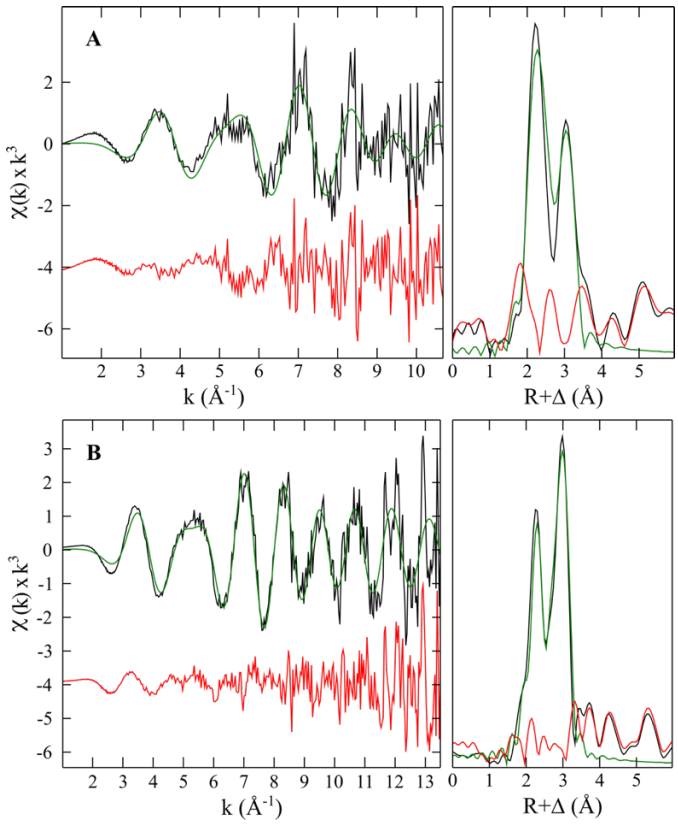

Figure 9: Ag K-edge EXAFS spectra (left panel) and corresponding Fourier transform (right panel) of (**A**) *E. coli* growth cell pellet, (**B**) *E. coli* 'shock' cell pellet showing experimental (**black**) and calculated (green) data with the residual (red) shown offset. Fit parameters reported in **Table 4**.

Table 4: Parameters fit to Ag K-edge EXAFS spectra of pelletized, freeze-dried (**A**) *E. coli* growth and (**B**) *E. coli* 'shock'.[a]

Sample	Scatterer	CN	Distance (Å)	DWF (Å^2)	-E_0 (eV)	Fit error
Growth (A)	S	2	2.46(1)	0.0101(7)	20(2)	0.70
	Ag	2	2.94(1)	0.0110(6)		
'Shock' (B)	S	2	2.48	0.0101	20(1)	0.54
	Ag	2	2.94	0.0079		

[a]The *k*-range was 1-11 and 1-13.5 Å^{-1} for A and B, respectively, with a scale factor (S_0^2) of 0.9. $\Delta E_0 = E_0 - 25515$ eV where E_0 is the threshold energy. Values in parentheses are the estimated standard deviation derived from the diagonal elements of the covariance matric and are a measure of precision. The fit error is defined as $[\Sigma k^6(\chi_{exp}-\chi_{calc})^2/\Sigma k^6\chi_{exp}^2]^{½}$.

The *S. aureus* growth Fourier Transform in **Figure 10A** displayed three prominent, resolved peaks between 2 and 3 Å. The calculated fit parameters (**Table 5**) revealed interaction of sulfur, silver, and nitrogen/oxygen backscattering atoms; a feature unique to the *S. aureus* growth cell pellet. The 'shock' sample FT also displayed three peaks, however, they were broader and more widely spaced than those observed in the growth sample spectrum. The peaks in the spectrum of the 'shock' sample were fit by a single sulfur interaction, as well as short and long silver interactions. The reduced intensities of the Ag-Ag interactions, relative to the prominent sulfur peak, were due to the dampening of the EXAFS oscillations at higher *k*-space; the oscillations became dampened at ~9 $Å^{-1}$ in spectrum **B** but the oscillated of spectrum **A** continued until ~11 $Å^{-1}$.

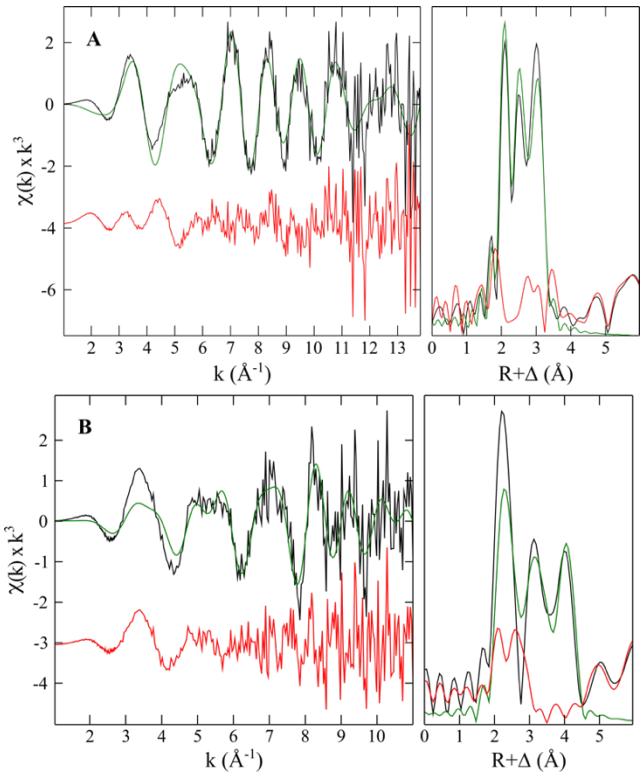

Figure 10: Ag K-edge EXAFS spectra (left panel) and corresponding Fourier Transform (right panel) of (**A**) *S. aureus* growth, (**B**) *S. aureus* 'shock' showing experimental (**black**) and calculated (green) data with the residual (red) shown offset. Fit parameters reported in **Table 5**.

Table 5: Parameters fit to Ag K-edge EXAFS of pelletized, freeze-dried (**A**) *S. aureus* growth cell pellet, and (**B**) *S. aureus* 'shock' cell pellet.[a]

Sample	Scatterer	CN	Distance	DWF	$-E_0$	Fit error
Growth (A)	N/O	2	2.243(6)	0.0030(4)	17(1)	0.60
	S	1	2.544(6)	0.0035(4)		
	Ag	2	2.945(5)	0.0089(3)		
'Shock' (B)	S	1	2.465(8)	0.0047(6)	18(1)	0.84
	Ag	1	2.949(8)	0.0073(5)		
	Ag	2	4.05(1)	0.0086(5)		

[a]The *k*-range was 1-11 and 1-14 $Å^{-1}$ for A and B, respectively, with a scale factor (S_0^2) of 0.9. $\Delta E_0 = E_0 - 25515$ eV where E_0 is the threshold energy. Values in parentheses are the estimated standard deviation derived from the diagonal elements of the covariance matric and are a measure of precision. The fit error is defined as $[\Sigma k^6(\chi_{exp}-\chi_{calc})^2/\Sigma k^6\chi_{exp}^2]^{½}$.

The EXAFS oscillations of the broth sample treated with 0.5 μg/mL $AgNO_3$ (**Figure 11A**) were reduced in intensity until ~7 $Å^{-1}$, which suggested strong interaction of the absorbing silver atom with other heavy atoms (such as another silver atom). Conversely, the EXAFS spectrum of 10 μg/mL $AgNO_3$ in broth (**Figure 11B**) displayed more intense, low *k* undulations. This observation which was reflected in the emergence of a secondary low R peak at ~2 Å in the EXAFS FT of **B**. As such, lighter backscatters (like N/O) were included in the EXAFS fit parameters, in addition to sulfur (**Table 6**).

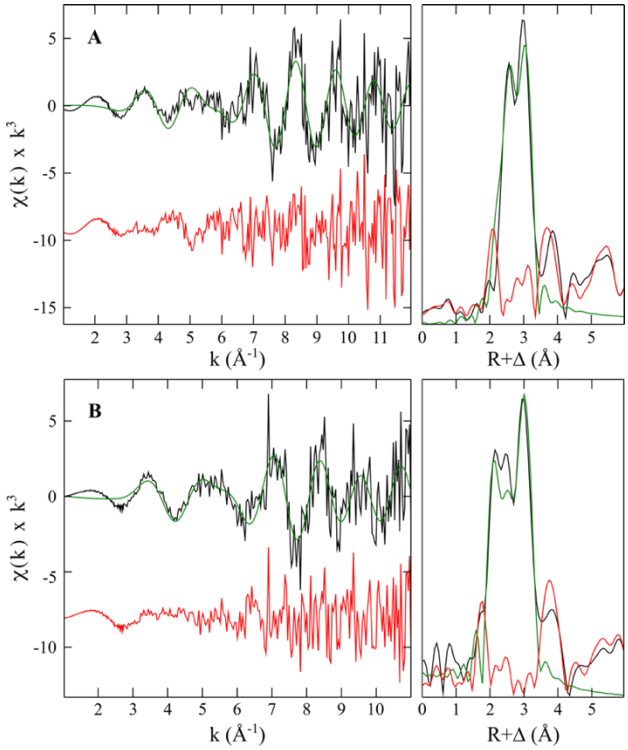

Figure 11: Ag K-edge EXAFS spectra (**left panel**) and corresponding Fourier Transform (**right panel**) of (**A**) 0.5 µg/mL $AgNO_3$ Luria Bertani broth, (**B**) 10 µg/mL $AgNO_3$ in Luria Bertani broth showing experimental (**black**) and calculated (green) data with the residual (red) shown offset. Fit parameters reported in **Table 6**.

Table 6: Parameters fit to Ag K-edge EXAFS of Luria Bertani broth spiked with $AgNO_3$[a]

Sample	Interaction	CN	Distance	DWF	$-E_0$	Fit error
(**A**) 0.5 µg/mL	S	2	2.54(2)	0.008(1)	15(2)	0.77
$AgNO_3$	Ag	2	2.93(1)	0.0060(4)		
(**B**) 10 µg/mL	N/O	2	2.30(2)	0.005(3)	19(2)	0.74
$AgNO_3$	S	1	2.47(4)	0.010(5)		
	Ag	2	2.92(1)	0.0065(5)		

[a]The *k*-range was 1-12 and 1-11 $Å^{-1}$ for A and B, respectively, with a scale factor (S_0^2) of 0.9. $\Delta E_0 = E_0 - 25515$ eV where E_0 is the threshold energy. Values in parentheses are the estimated standard deviation derived from the diagonal elements of the covariance matric and are a measure of precision. The fit error is defined as $[\Sigma k^6(\chi_{exp}-\chi_{calc})^2/\Sigma k^6\chi_{exp}^2]^{½}$.

Size exclusion chromatography coupled with ICP-MS

SEC and ICP-MS of bacterial broth

To follow the biochemical fate of silver in bacteria, one starting point is the speciation of exogenous Ag, prior to uptake by the organism. Luria Bertani broth is a liquid medium used for bacterial culture. It is an 'undefined' medium comprised of amino acids, low molecular weight (LMW) peptides, B vitamins, and minerals from reconstituted yeast extract and digested casein (tryptone). Due to its inconsistent composition, a single batch of LB was used for all experiments. SEC chromatograms of untreated and silver-spiked LB broth are shown in **Figure 12**. No species with absorbance at 280 nm eluted at, or near, the void volume of the column (fractionation range: 120 to 0.1 kDa).

Absorbance of the column effluent was monitored at 280 nm for untreated broth (purple), broth spiked with 0.5 μg/mL $AgNO_3$ (blue), and 10 μg/mL $AgNO_3$ (green) (**Figure 12**). A constant injection volume (100 μL) was used allowing direct comparison between the absorbance traces of each sample. Residuals (dotted lines) were calculated by subtraction of the untreated 280 nm trace from those of the Ag-spiked broth. In the treated broth samples, the elution of silver-bound species (highlighted in yellow) was determined by fractionation (one-minute time slices) of the column effluent followed by analysis of each fraction by ICP-MS to identify if silver was present. The 0.5 μg/mL SEC residual (**Figure 12**) did not show significant perturbation of the broth elution profile due to addition of silver. Fluctuation in the 0.5 μg/mL residual at ~18.5 min (and elsewhere) was likely due to conformational changes of species present which would alter their elution times. As silver was not found to elute at high retention time it was unlikely the metal contributed to these changes. The 0.5 μg/mL residual showed no variation in the 280 nm trace occurred where silver-bound species were known to elute (between 7 and 9 minutes). Conversely, a shoulder feature could be seen in the 10 μg/mL residual at 7.40 minutes.

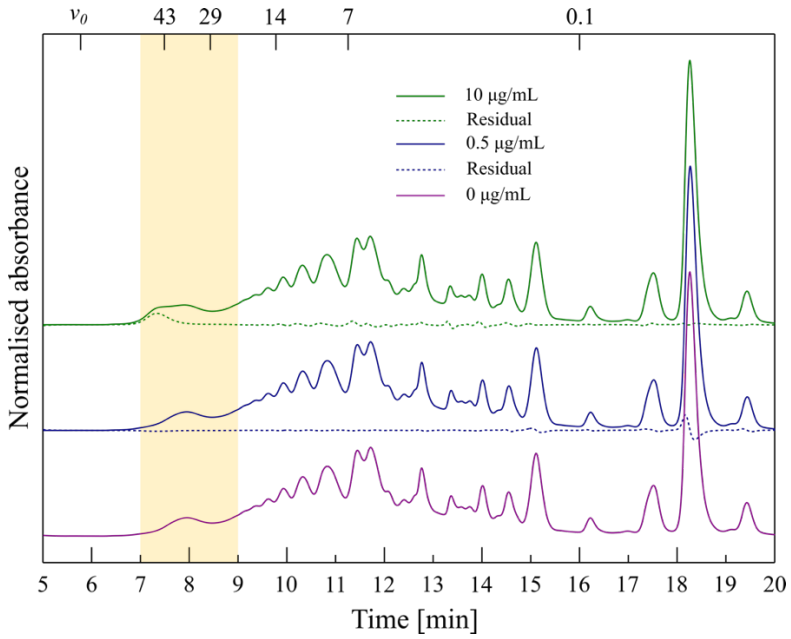

Figure 12: Size exclusion chromatograms of Luria Bertani (LB) broth spiked to a final concentration of 10 (green), 1 (blue), and 0 µg/mL (purple) of $AgNO_3$ monitored at 280 nm for the detection of short chain peptides and amino acids. Dashed residuals were calculated by subtraction of the 0 µg/mL 280 nm trace from the silver-spiked 280 nm traces. The samples were fractionated into a 96-well plate with one-minute intervals and each fraction tested for the presence of ^{107}Ag via ICP-MS (yellow). Column: Agilent AdvanceBio SEC 130Å (7.8 x 300 mm I.D.; 2.7 µm particle size); temperature: ~20°C; mobile phase: 100 mM HEPES, pH 7.4; flow rate: 0.3 mL/min; injection volume: 100 µL; detector: Agilent Infinity 1200 variable wavelength detector set at 280 nm. The void volume of the column (v_0) and elution times of molecular weight markers are shown at the top of the plot in kDa.

A calibration curve constructed from the elution times and molecular weights of known protein standards (**Appendix 2.9.4**) enabled calculation of the molecular weights of unknown species based on elution time. However, it must be noted that calculated molecular weights are only accurate if solely non-specific interactions are present between the eluting species and the column resin.[54] The MWs of the silver-bound species that eluted at 7.40 and 7.90 min in **Figure 12** were calculated to be ~65 and 46 kDa, respectively, and likely represented partially digested protein as the peak in the SEC chromatogram was present in the absence of Ag^+. Given the composition of LB broth (high amounts of short chain peptides and small molecules) the additional peak was likely due to aggregation of various smaller species; fluctuations in the higher concentration residual trace could indicate the source of the aggregated species.

After incubation of *E. coli* and *S. aureus* cultures in the presence of sublethal $AgNO_3$, the cells were pelletized, and the supernatant broth analysed by SEC and ICP-MS. The elution profiles of silver-spiked broth pre and post bacterial growth were compared

(**Figure 13**). Residuals (dashed purple) were calculated by subtraction of the 'pre growth' 280 nm trace (green) from the 'post growth' trace (blue). The residual traces highlighted the species taken up from the broth by the two bacterial strains during incubation.

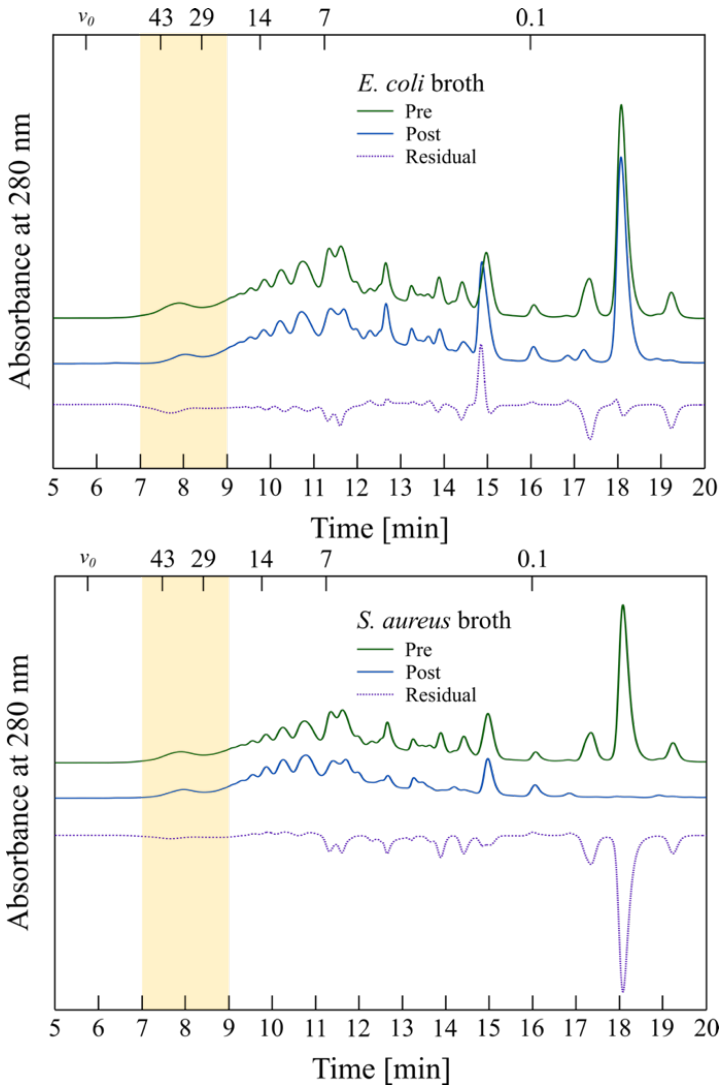

Figure 13: Size exclusion chromatograms of silver-spiked Luria Bertani (LB) broth pre growth (green) and post growth (blue) of *E. coli* (**top**) and *S. aureus* (**bottom**). Column effluent was monitored at 280 nm to detect short chain peptides, amino acids and UV-absorbing LMW molecules. Residuals (dashed purple) were calculated by subtraction of the pre-growth trace from the post-growth trace. The samples were fractionated into a 96-well plate with one-minute intervals and each fraction tested for the presence of ^{107}Ag via ICP-MS (yellow) (Note: S. aureus 'post' sample had no detectable ^{107}Ag). Column: Agilent AdvanceBio SEC 130Å (7.8 x 300 mm I.D.; 2.7 µm particle size); temperature: ~20°C; mobile phase: 100 mM HEPES, pH 7.4; flow rate: 0.3 mL/min; injection volume: 100 µL; detector: Agilent Infinity 1200 variable wavelength detector set at 280 nm. The void volume of the column (v_0) and elution times of molecular weight markers are shown at the top of the plot in kDa.

All peaks in the residuals were inverted relative to the UV traces, except for the peak at ~15 min in the *E. coli* residual. Based on how the residuals were calculated (pre-minus post growth UV trace), inverted peaks indicated that components of the broth were taken up by the bacteria, and minimal efflux of cellular detritus occurred. Significant uptake of the most intense peak (~18 min) by *S. aureus*, but not *E. coli*, was the largest difference between the post-growth broth traces. If efflux had occurred, the post-growth broth elution profile would be expected to appear significantly different either in elution profile or the relative intensities of species present. For both strains the uptake of silver-bound species (eluted between 7 and 9 minutes) was visible as a small decrease in the residual between those time points. ICP-MS analysis of the *S. aureus* post-growth broth (not shown) did not detect any exogenous silver remaining in solution which would suggest that the bacteria were not sufficiently metal-stressed to express Cu(I)/Ag(I) efflux systems. Conversely, the *E. coli* post-growth broth still contained detectable levels of silver; despite *E. coli* being exposed to half the amount of silver that *S. aureus* due to their respective MICs. While it was possible *E. coli* effluxed silver from its cells, it would be unlikely that the majority of silver would still exist intracellularly after incubation for ~16 h.

Size exclusion chromatograms of LB broth in which *E. coli* and *S. aureus* were grown in the presence and absence of $AgNO_3$ were also recorded (**Figure 14**). The presence of sublethal silver nitrate did not appear to greatly change the elution profile of the post-growth broth. This would suggest that the presence of silver ions did not greatly affect uptake of nutrients or other exogenous species from broth. Fluctuation in the *E. coli* residual at larger elution times was likely due to shifts in elution times of the peaks at ~15 and 18 minutes.

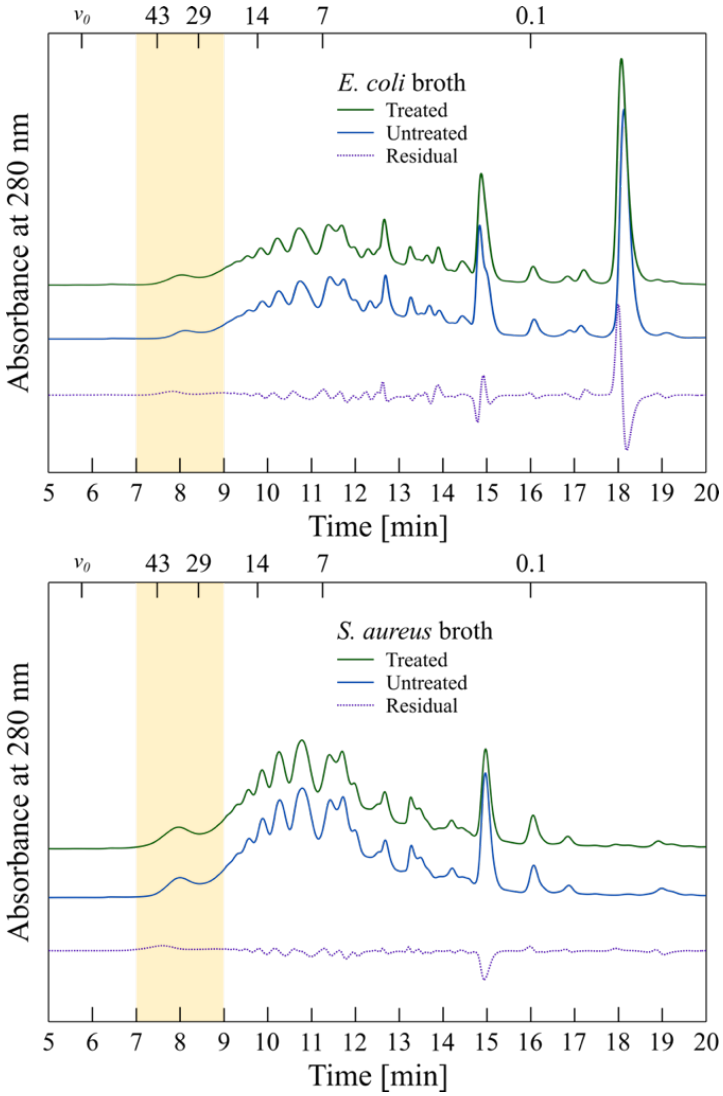

Figure 14: Size exclusion chromatograms of Luria Bertani (LB) broth in which *E. coli* (**top**) and *S. aureus* (**bottom**) were treated (green) or untreated (blue) by $AgNO_3$. Column effluent was monitored at 280 nm to detect short chain peptides, amino acids and UV-absorbing LMW molecules. Residuals (dashed purple) were calculated by subtraction of the 'treated' trace from the 'untreated' trace. Samples spiked with $AgNO_3$ were fractionated into a 96-well plate with one-minute intervals and each fraction tested for the presence of ^{107}Ag via ICP-MS (yellow). The fractions that contained silver (determined by ICP-MS) are highlighted (yellow). The void volume of the column (v_0) and elution times of molecular weight markers are shown at the top of the plot in kDa.

Hyphenated SEC and ICP-MS of E. coli and S. aureus cell lysates

Analysis of bacterial lysates with a low molecular weight (LMW) range column (fractionation range: 120 to 0.1 kDa) revealed that all silver-bound species eluted close to the void volume (between 6 and 8 minutes) for both strains, suggesting that the metal was associated with high molecular weight (HMW) species (**Figure 15**). The lower signal-to-noise ratio of the *S. aureus* ^{107}Ag ICP-MS data (yellow bar graph, **Figure 15**), relative to *E. coli*, was due to reduced cell lysis of the Gram-positive cells into buffer post silver treatment. For subsequent analyses *S. aureus* was chemically lysed with the commercially available lysing agent, Lysostaphin (10 IU).

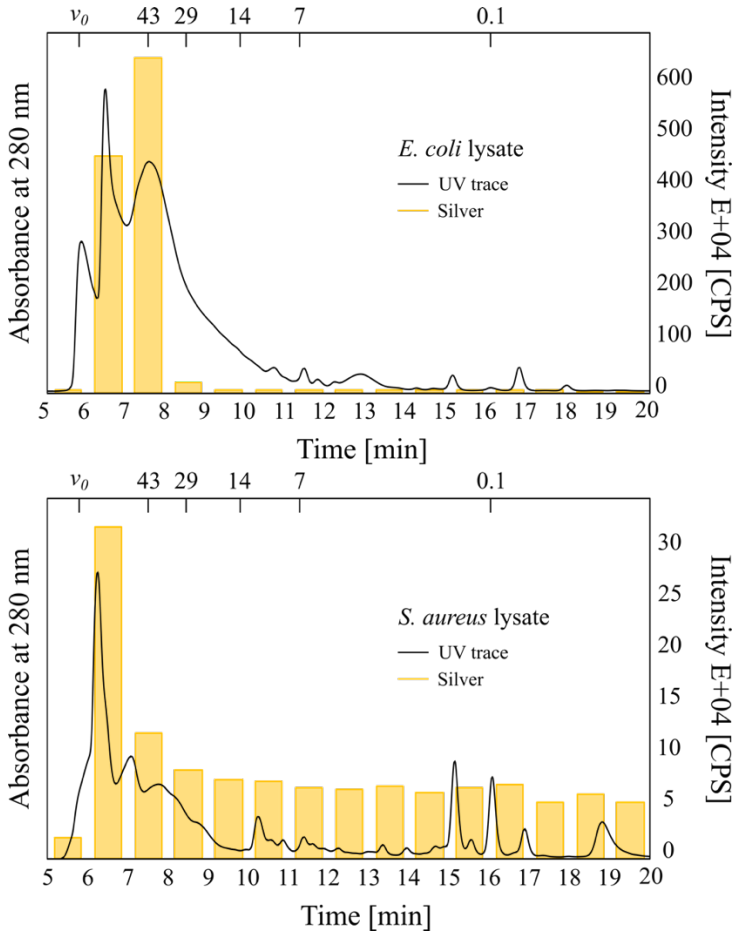

Figure 15: SEC chromatograms of *E. coli* (**top**) and *S. aureus* (**bottom**) lysate of cells grown in the presence of 0.5 and 1.0 µg/mL $AgNO_3$, respectively. The presence of protein was monitored by absorbance at 280 nm (**black**). The samples were fractionated into a 96-well plate with one-minute intervals and each fraction tested for the presence of ^{107}Ag via ICP-MS (yellow). Column: Agilent AdvanceBio SEC 130Å (7.8 x 300 mm I.D.; 2.7 µm particle size); temperature: ~20°C; mobile phase: 100 mM HEPES, pH 7.4; flow rate: 0.3 mL/min; injection volume: 100 µL; detector: Agilent Infinity 1200 variable wavelength detector set at 280 nm. The void volume of the column (v_0) and elution times of molecular weight markers are shown at the top of the plot in kDa.

E. coli lysate passed over a high molecular weight fractionating column (fractionation range: 1200 to 5 kDa) resulted in better resolved ^{107}Ag ICP-MS and 280 nm traces (**Figure 16**, **top**). Integration of the area under the silver trace revealed that 87% of detected silver in the sample eluted between 8 and 11 minutes with the major silver peak at 9.27 min; 6% was eluted at the void volume (**Table 7**). The molecular weights of the silver-bound species were calculated (**Table 8**) using a calibration curve constructed from the elution times and molecular weights of known protein standards (**Appendix 2.9.4**). In addition to silver, multiple biologically relevant metals (Mn, Fe, Co, Ni, Zn, Cu) were simultaneously monitored during the experiment and all silver-bound species in the *E. coli* lysate were found to coelute with copper-bound species. However, the non-uniformity of the coelution of ^{107}Ag and ^{65}Cu peaks could represent incorporation of Ag^{+} into Cu(I)-specific cellular Cu(I) metabolic pathways.

The ^{107}Ag traces of *S. aureus* lysate (**Figure 16**, **bottom**) displayed a more diverse elution profile than that of *E. coli*; multiple non-baseline resolved silver peaks were observed between 5 and 13 minutes. The percentage of silver eluted between various time ranges of the chromatogram (determined by integration of eluted peaks) is shown in **Table 7**, and the calculated molecular weights of discrete ^{107}Ag peaks are shown in **Table 8**.

Similarities between the ^{107}Ag and ^{65}Cu traces of the *S. aureus* lysate were more prominent than for *E. coli*; clear mirroring of the traces was observed between 9.5 and 12.5 minutes. The only point where silver did not coelute with copper was the shoulder peak at ~8 minutes; while the count rate of the copper trace was elevated relative to background levels, the silver trace displayed a clear shoulder peak which was not present for copper.

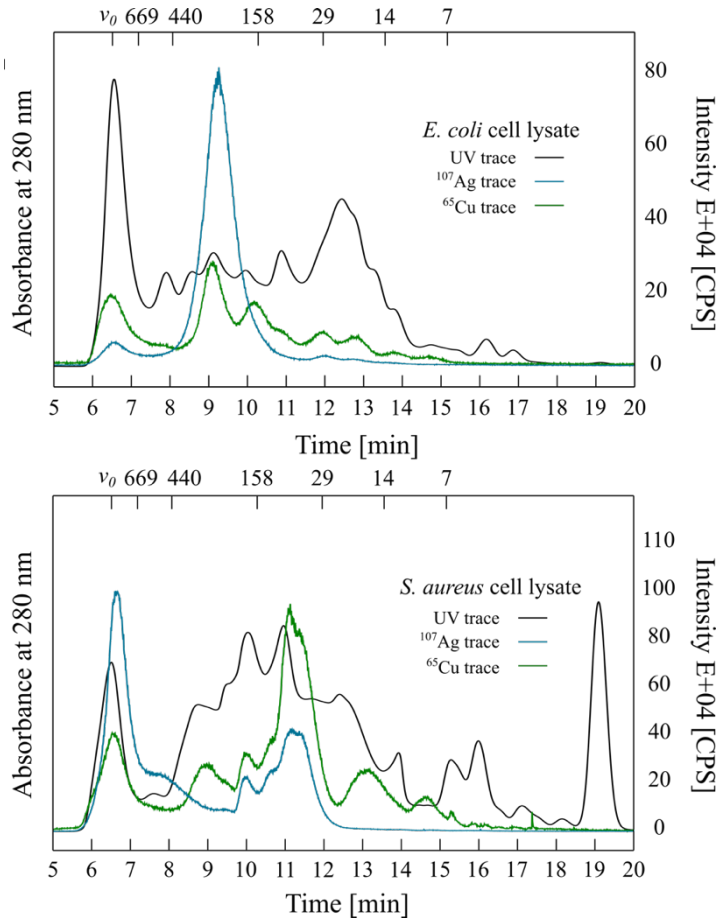

Figure 16: SEC-ICP-MS chromatograms of lysed *E. coli* (**top**) and *S. aureus* (**bottom**) cells grown in the presence of 0.5 and 1.0 µg/mL $AgNO_3$, respectively. The presence of protein was monitored by absorbance of the column effluent at 280 nm (**black**). Multiple ICP-MS metal traces were measured simultaneously; ^{107}Ag (blue) and ^{65}Cu (green) traces are shown. Column: Agilent AdvanceBio SEC 300Å (7.8 x 300 mm I.D.; 2.7 µm particle size); temperature: ~20°C; mobile phase: 100 mM HEPES, pH 7.4; flow rate: 0.3 mL/min; injection volume: 100 µL; detector: Agilent Infinity 1200 variable wavelength detector set at 280 nm, and Agilent QQQ 8900 ICP-MS. The void volume of the column (v_0) and retention times of molecular weight markers are shown at the top of the plot in kDa.

Table 7: Time ranges and percentage of total silver calculated by integration under the ^{107} Ag ICP-MS trace for *E. coli* and *S. aureus* lysate chromatograms in **Figure 16**

Organism	Time range [min]	% silver
E. coli	6 – 7	6
	8 – 10.5	87
S. aureus	5.5 – 7	38
	7 – 9.5	24
	9.5 – 12.5	35

Table 8: Molecular weights of discrete peaks observed in the ^{107}Ag ICP-MS traces for *E. coli* and *S. aureus* lysates, calculated from a calibration curve created from the elution times and MWs of known protein standards

Organism	Elution time [min]	Calculated MW [kDa]
E. coli	Void volume	≥1220
	9.27	198
	12.01	38
	12.90	22
S. aureus	Void volume	≥1220
	7.66 (shoulder)	529
	9.91	134
	10.53	92
	11.13	64

Gel electrophoresis of SEC fractions

The bacterial lysates were again passed over the high molecular weight SEC column and fractionated into a 96-well plate for subsequent analysis. The SEC-ICP-MS traces reported above (**Figure 16**) facilitated identification of silver-containing fractions which were subjected to SDS-PAGE conditions, stained with Coomassie blue, and imaged (**Figure 17**).

E. coli SEC fractions known to contain silver were loaded into lanes 2-4 and *S. aureus* silver-containing fractions loaded into lanes 6-10. The difference in protein concentration between the two organisms was visibly apparent as the intensity of stained bands are related to the concentration of protein present. For example, more protein was present in the *S. aureus* SEC fractions (lanes 6-10) and were stained darker relative to those of *E. coli* (lanes 2-5). The difference in protein concentration was a result of chemical vs. mechanical lysis. *S. aureus* cells were lysed with a chemical specific for lysis of the organism (Lysostaphin) which resulted in a high concentration of protein in the lysate buffer solution passed over the column (~3 mg/mL, as estimated by absorbance at 280 nm relative to a blank). However, *E. coli* cells were mechanically lysed, which required suspension of the unlysed cells in ~10 mL of buffer, diluting the protein concentration of the lysate (~0.3 mg/mL relative to blank).

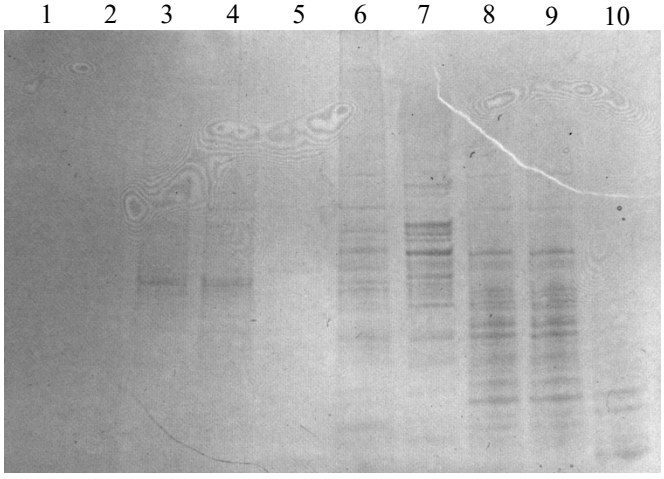

Figure 17: Image of a stained (Coomassie Brilliant Blue) SDS PAGE gel used to further separate *E. coli* (lanes 2-4) and *S. aureus* (lanes 6-10) lysate SEC fractions that were identified as containing silver from SEC-ICP-MS chromatograms.

The number of bands visible in the *S. aureus* lanes showed that, at each time point of the SEC-ICP-MS chromatograms shown in **Figure 16**, many protein species eluted frustrating attempts to identify specific silver-bound proteins. This was unsurprising as the elution profile of the chromatograms between ~5 and 20 minutes represented the entire

bacterial proteome of both organisms (containing thousands of proteins). Further identification of silver-bound species was attempted by blotting of gels (like that displayed in **Figure 17**) onto polymer membranes and analysis by X-ray fluorescence microscopy (XFM).[55] However, the level of silver (and all other biologically relevant metals) was found to be below the detection limit of the technique (data not shown).

Summary of key results

Linear combination fitting of the Ag K-edge XANES spectra of *E. coli* and *S. aureus* cell pellets, whether growth or shock treatments, calculated consistently high contributions from the silver-cysteine (Ag-Cys) model spectrum (75 – 90%) with the remaining percentage coming from a silver-thiamine model spectrum. The EXAFS spectrum of the silver-cysteine model was fit with sulfur and silver backscattering interactions at 2.48 and 2.96 Å, respectively. Coordination spheres similar to Ag-Cys were successfully fit to all *E. coli* and *S. aureus* experimental spectra. The Ag-S distances ranged from 2.46 – 2.54 Å and Ag-Ag distances were 2.94 Å, corroborating the LCF results which indicated silver/cysteine-like interactions were present. However, the small percentage of silver-thiamine model spectrum fit to all bacterial spectra did not appear to be substantiated by the EXAFS analysis, as only the *S. aureus* growth sample was fit with N/O interactions. The proportion of the thiamine spectrum fitted to all experimental spectra was so low that the already dampened features of the silver-thiamine XANES were almost completely obscured, bar minor oscillations. While pyrimidine-containing molecules are prominent in cellular biochemistry,[56] it was likely that the fitting of the thiamine model spectrum was not a true component but merely added amplitude to the fit of the cysteine model spectrum.

Size exclusion chromatography hyphenated ICP-MS of Ag-treated *E. coli* and *S. aureus* lysates revealed that all silver in the system was associated with high to medium molecular weight species (>1220 to 22 kDa). In both organism lysates, it was found that silver coeluted with select peaks in the ^{65}Cu trace. While the ^{107}Ag elution profile of the *E. coli* lysate appeared relatively simple, with only an intense major peak and four smaller peaks, subsequent analysis of the SEC fractions by SDS PAGE revealed that many species eluted at each time point in the chromatogram. Relative to the ^{107}Ag trace of *E. coli*, the *S. aureus* trace was more complex with clear mirroring of the ^{65}Cu trace in parts.

2.5 Discussion

X-ray absorption spectroscopy

Few X-ray absorption spectroscopy studies have been carried out on silver-treated bacteria, however, one group of researchers reported the Ag L_3-edge XANES of *S. aureus*, *E. coli*, and *L. monocytogenes* exposed to Ag^+.[57] The researchers treated the three strains of bacteria with either silver nitrate or acetate (5 mM), and found that the XANES spectra of intracellular Ag species differed significantly from the XANES spectra of the administered silver salts. The group did not provide explanation for why EXAFS analysis was not carried out, but it was likely that low levels of silver in the cell pellets prevented adequate data collection. However, through use of linear combination fitting, the relative proportions of model XANES were fit to the experimental spectra; model spectra used included samples of silver with cysteine, histidine, alanine, and DL-aspartic acid. The dominant contributions were found to be from histidine in *S. aureus* and *L. monocytogenes* (47%) and alanine in *E. coli* (37%) while only minor contributions from the cysteine model were calculated across all strains of bacteria tested (10 – 24%). From their LCF analysis, silver-nitrogen interactions were determined to be the dominant features of silver speciation in bacteria, with 'non-dominant' Ag-S interactions also present. This was in stark contrast to the results reported herein which, through both XANES and EXAFS analysis, identified sulfur as the dominant donor atom in the Ag^+ coordination sphere. In the previous work, the methods by which the silver model spectra were prepared for XANES collection were not carefully outlined; no mention was made of the buffer system used, solution pH, or stoichiometric metal-to-ligand ratios in the models. In addition, the silver-cysteine sample was prepared according to the protocol of a paper which investigated the gelation of silver/cysteine solutions.[58] Finally, it was stated that compositions of the samples were validated by 'X-ray diffraction,' a technique often used for characterisation of solid-state substances; despite the standard being compared against an aqueous biological system. Such inconsistencies raise questions about the validity of the results obtained by the group, and whether biologically relevant interactions were recorded.

Even with appropriate model sample preparation, the silver XAS spectra of metal/amino acid solutions at pH 7.4 may not be representative of biologically relevant interactions between the Ag^+ and amino acid residue sidechains in proteins. The silver-methionine EXAFS spectrum presented here was fit with two nitrogen and two sulfur backscattering interactions. The nitrogen backscattering component was likely due to

interaction with the primary amine of methionine, in addition to the thioether sulfur. In protein structures the primary amine of the amino acid backbone form amide bonds with the carboxylic acid of a neighbouring amino acid in the sequence. While some metals have been shown to be bound by amide linkages (Cu^{2+}), the functional group has been demonstrated to be a poor ligand for soft metals like Cu^{+}.[59] Thus, the silver-methionine model XAS spectrum could be considered unrepresentative of the interactions likely to occur between proteinaceous methionine and silver ions (unless the coordination sphere of the Ag^{+} ion happened to be S_2N_2, with appropriate bonding distances). A review of the Protein Data Bank (PDB) in 2017 revealed the most common silver-binding residues; histidine (50%), methionine (29%), and cysteine (15%).[60] Many bacterial copper transport, efflux or homeostatic proteins are rich in methionine residues while being comparatively poor in cysteine residues. As such, it may have been the case that the high proportion of silver-cysteine model calculated for the bacterial cell pellet XANES in this work (74 – 90%) could have represented a mixture of Cys and Met residue binding. A review of the CSD indicated an appreciable overlap between silver-cysteine and silver-methionine bond distances (**Appendix 3.9.2**). To determine whether this was the case, it would be informative to collect Ag K-edge XANES data of solely Ag-$S_{thioether}$ interactions for comparison against the experimental cell pellet spectra. However, it was also possible that the coordination sphere of silver in bacterial cells was dominated by interactions with cysteine residues, given the known affinity of the amino acid for Ag^{+}.[61] Regardless, there is a stark contrast between the results reported herein which show binding of Ag^{+} to cysteine (and possibly methionine), and some previously reported results which suggested limited involvement of these amino acids.

In 2013 the interactions between Ag^{+} and the Cu^{+} chaperone protein, Atox1, as well as silver-substituted rabbit, and yeast metallothioneins were investigated by XAS.[62] Analysis of XANES (and EXAFS) identified that silver was coordinated exclusively by cysteine residues (an attribute for which MTs are renowned). The silver K-edge XANES data collected in their study (in which silver was bound by cysteine residues) bore striking similarities to the experimental cell pellets, and silver-cysteine model spectra reported herein (**Figure 1**). Such similarities may indicate that the chemistry of silver in bacteria was indeed dominated by interactions with cysteine.

The linear combination fits of all silver K-edge XANES of cell pellets and broth indicated a minor contribution (8–25%) from the Ag-thiamine model spectrum but the flat, dampened features of the thiamine spectrum raised doubts about its validity as a

component of the experimental XANES spectra. The thiamine model was included as Luria Bertani broth is known to be rich in B vitamins and, as one of the few sulfur-containing vitamins, it was thought to have some affinity for silver ions. However, analysis of the thiamine EXAFS, coupled with a survey of the CSD, revealed that the most likely binding interaction with silver was *via* the aromatic pyrimidine nitrogens.

Intracellularly, thiamine can be utilised as a cofactor for a number of enzymes, two of which participate in the tricarboxylic acid cycle (TCA); pyruvate dehydrogenase complex (PDC), and α-ketoglutarate dehydrogenase complex (KGDHC).[63] Thiamine deficiency has been shown to result in decreased activity of these vitamin-dependent enzymes of the TCA, which also contributed to significant inhibition of other non-thiamine-dependent members of the cycle.[63] In some cases, the non-thiamine-dependent enzymes (namely succinate dehydrogenase (SucD), and malate dehydrogenase (Mdh)) can be more significantly reduced in activity than the dependent enzymes. A recent investigation revealed SucD and Mdh as silver-binding targets in *E. coli* grown in the presence of toxic levels of silver nitrate (4 μg/mL) – see below.[34]

Pyrimidine functionality is widespread in molecular biology. Thus, if the silver ions interacted with the thiamine-pyrimidine in the model spectrum, the proportion fit to the experimental cell pellet/broth XANES could be representative of interactions with other pyrimidine-containing biomolecules. Possibly the most well-known pyrimidine-containing biomolecules are the nitrogenous bases that form part of DNA and RNA. In *E. coli* approximately 15% of accumulated silver has previously been found to be associated with nucleic acids (DNA/RNA).[64] In the lysates of *E. coli* and *S. aureus* examined herein, the ^{107}Ag traces indicated some silver eluted with the void volume of the column, suggesting interaction with very high molecular weight species; the maximum fractionation range of the column used here was ~1220 kDa. A relatively small bacterial plasmid of ~35 kilo base pairs would exceed this fraction range (~1300 kDa) and elute with the void volume of the column.[65] As such, interaction between silver ions and the pyrimidine/purine nitrogenous bases of DNA or RNA could explain the proportion of silver that eluted at the void volume in the SEC-ICP-MS chromatogram of *E. coli* and *S. aureus* lysates as well as the component of the bacterial cell pellet Ag XANES fit by the thiamine model spectrum. The CSD revealed that silver ions have an affinity for the purine base adenine with 28 of 40 crystal structures of silver-nitrogenous base complexes containing solely these two molecules or derivatives thereof (**Appendix 2.9.3**).

Unexpectedly, there was no indication of any silver chloride in the XANES or EXAFS of any bacterial samples (cell pellet or broth). Given the high concentration of NaCl in LB broth, it was anticipated that some AgCl would be formed. The formation of insoluble salts is often hypothesised to limit the antibacterial activity of silver in biological systems. However, in the systems studied here, it appeared that the formation of insoluble solids did not occur.

Size exclusion chromatography ICP-MS

Escherichia coli

Recently the Sun group investigated molecular mechanisms by which Ag^+ acts as an antibacterial agent against *E. coli*.[34] Through development of ICP-MS coupled with liquid chromatography (LC) and gel electrophoresis (GE) (LC-GE-ICP-MS) they identified 34 individual proteins to which Ag^+ was bound. The proteins that were identified were associated with a range of cellular processes including the tricarboxylic acid cycle (found to be impeded by the presence of silver), the glyoxylate cycle, glycolysis, translation, responses to oxidative stress, and regulation of internal pH.

It was found that the molecular weights of the proteins identified were of moderate size (<50 kDa), which was partially consistent with the calculated MWs of the silver peaks observed in the ^{107}Ag SEC-ICP-MS trace of *E. coli* lysate reported herein (198, 38, and 22 kDa). The proteins identified by Wang *et al.*[34] were low MW, however, there was limited discussion about the size of the biologically relevant species; expected to be maintained with the metallomics techniques used in the study presented in this thesis. For example, one of the proteins identified to bind Ag^+ (Dps) is involved in DNA protection during starvation. Dps itself is a low molecular weight protein (18.7 kDa) but within the cell it functions as a homododecameric species with a molecular weight of ~224 kDa.[66] Similarly, two of the proteins identified to be strongly inhibited by Ag^+ (by Wang *et al.*), isocitrate dehydrogenase (Idh) and malate dehydrogenase (Mdh), have nominal molecular weights of ~46 and 32 kDa, respectively, but both form homodimeric species intracellularly and have MWs of 92 and 64 kDa, respectively. However, the first dimension of separation of the bacterial lysates used by the Sun group involved manipulation of pH which would have disrupted protein-protein interactions; changing the pH would alter the surface environment of the protein subunits, disrupting intermolecular interactions, causing protein complexes to degrade.[67]

Of the 34 proteins identified by Wang *et al.*,[34] only two are known to bind copper, the zinc transporter ZraP,[68] and Dps, which has been implicated in the homeostasis of

copper as well as transport and oxidation of ferrous ions.[66] However, the authors also acknowledged that their experiments did not provide an exhaustive list of silver-binding proteins in the organism. Iron-sulfur cluster-containing proteins, such as NADH dehydrogenases, have been demonstrated to be poisoned by silver ions, leading to degradation of the cluster and generation of the apo-enzyme.[69] Thus, the absence of the copper-binding proteins identified by Wang *et al* does not preclude the results observed here. It is worth noting that the experimental design of the work published by the Sun group, and that of the experiments reported herein were subtly different. The work presented here was conducted at a concentration below the minimal inhibitory concentration (MIC) of silver nitrate against *E. coli*. The MIC was experimentally determined to be ~2.0 μg/mL $AgNO_3$, and all *E. coli* cells were cultured in the presence of 0.5 μg/mL silver nitrate. This ensured that cell death was not a significant factor and that all silver-associated species were true representations of the biochemical fate of the metal instead of adventitious metallation of cellular detritus. Comparitively, the work by the Sun group was carried out at the experimentally determined MIC_{50} value for *E. coli* (4 μg/mL) which would have resulted in a significant amount of silver-stress exerted on the organism and may have been a snapshot of a different biochemical fate for Ag^+. However, in the study presented here, no measurements to quantify the level of metal-associated stress were carried out.

In their study, Wang *et al.* fidentified proteins involved in important cellular processes, such as the TCA cycle, pH regulation, and maintenance of cysteine-derived redox activity, were targeted; an observation consistent with previously reported antibacterial and inhibitory properties of silver.[70] Additionally, the group identified that the enzymatic activities of succinate dehydrogenase (SucD), isocitrate lyase (AceA), and malate synthase (AceB) increased upon exposure to silver before decreasing. This phenomenon has been reported elsewhere for the decoupling of enzyme activity from available ATP or ADP.[71-72] Analysis from Wang *et al.* identified the TCA to be significantly targeted by the Ag^+ with isocitrate dehydrogenase (Idh) and malate dehydrogenase (Mdh) having up to 80% of their enzymatic activity inhibited by silver from 5 min post exposure, and for the duration of the experiment (60 min). Intracellularly the organism attempted to mitigate the effect of the inhibition of these enzymes in the oxidative branch of the tricarboxylic acid cycle by switching to the glyoxylate cycle, however, silver eventually inhibited that cellular process as well.

Nutrient copper is a double-edged sword for bacteria with it being an essential micronutrient but also having antibacterial activity against the organisms.[73] As the

chemistry of silver has been likened to that of copper in the +1 oxidation state, it is likely that, when exposed to sublethal concentrations of $AgNO_3$, the biochemical fate of Ag^+ would be similar to that of endogenous Cu^+. Thus, the colocalisation of the metals observed for the work reported here appears to be consistent with work reported elsewhere, namely that protein species known to bind Cu^+ often also bind Ag^+.[62, 74-75]

In 2019 a group reported on the localisation and 'speciation' of silver ions and nanoparticles in *E. coli* when the organism was treated with concentrations 10, 50, and 90% of the minimal inhibitory concentration (of the NPs and silver nitrate).[48] Treatment of the cells to isolate extracytoplasmic/cell wall, and cytoplasmic extracts enabled the group to identify that the localisation of the silver in the cell was predominantly in the extracellular medium (24 – 60% of total silver) or the cell wall/membrane (25 – 64% of total silver) with only a small percentage associated with the cytoplasmic extracts (6 – 15% of total silver). Significant gaps in bacterial copper biochemistry are known, but *in vivo* Cu(I/II) is throught to be strictly regulated and relegated to extracytoplasmic regions of the cell to manage the toxicity of the metal.[25] As such, localisation of the majority of cell-associated silver with the cell wall/membrane extracts of the organism is consistent with the observed colocalisation of silver and copper in the study presented in this thesis.

Despite claims of speciation analysis by Dong *et al.*, the presented results did not shed significant light on the topic.[48] The pore size of the column was excessive (1000 Å) which, at a flow rate of 0.5 mL/min, caused analysed samples to elute within 4 minutes with poor resolution. Additionally, there was no reference to column calibration with known standards for comparison with experimentally eluted species. Further to this, the experimental setup contained many opportunities for perturbation of analyte chemistry, such as the unbuffered elution solvent consisting exclusively of 2% v/v FL-70 (contains ~1.5% Na_2EDTA, $NaHCO_3$, triethanolamine, etc.) and 2 mM $Na_2S_2O_3$. As such the claims of the authors to be able to visualise "free" Ag^+ (which is unlikely to be present in any case) and other microbiologically relevant silver species was dubious.

The proteome of *E. coli* MG1655 strain (UniProt code: UP000000625), the same strain used by this study and that by Wang *et al.*[34] contains ~25 known copper-binding proteins; the majority of which are associated with the periplasmic space or the inner/outer membranes of the cell.[25] While some of the copper-binding proteins are known to exist in the cytoplasm of the cell, they are thought to function as copper chaperones tasked with removal of copper from the cytoplasm to the periplasmic space, like CutC, or

transcriptional regulator proteins like CueR.[28] Thus the observation by Wang *et al.* that the bulk of silver identified in their study was associated with cytoplasmic proteins appeared to be inconsistent with ours and others observations[48, 64] but may have been a result of the concentrations of silver used (as mentioned above). It has been reported that copper stress in *S. aureus* leads to copper-binding by GapA,[31] which was also identified by Wang *et al.* as a silver-binding protein. Thus, the colocalisation of silver and copper is not inconsistent with previous results.

It has, however, been observed that protein-bound copper can display significant lability when conducting size exclusion experiments with low molecular weight species in rabbit blood plasma shown to be demetallated and degraded within 30 min of blood collection.[76] Thus, it is possible that the sample processing for the SEC experiments, albeit minimal, resulted in mismetallation in the lysate chromatograms. However, the presence of low molecular weight copper-bound species in the *S. aureus* and *E. coli* chromatograms (MW ranging from ~29 to 7 kDa) could be an indication that the observed phenomena in rabbit plasma may not be universally true. Time dependent studies in which the cell lysate was run immediately, and at set time points, post lysis would need to be conducted to identify whether cellular contents were degraded over time.

Little is known about the uptake of copper by bacteria, however, appreciably more is known about its efflux and homeostasis in the cell. In the proteome of the strain of *E. coli* used for this study (MG1655) there are ~25 known copper binding proteins; including the *cus*, *cut*, *cue*, and *cop* ensembles. CusF is a soluble, low MW Cu-chaperone that transports Cu^{+} ions in the periplasm to the CusCBA cation/proton antiporter for ejection from the cell, the expression of the *cus* operon is regulated by CusR/S. CueR regulates the expression of the multicopper oxidase, CueO, and the P-type ATPase exporter, CopA. Cytoplasmic copper is delivered to CopA by the chaperone, CopZ, where the Cu^{+} is exported to the periplasm and oxidised by CueO to the 'less toxic' Cu^{2+}.

Several proteins that utilised nutrient copper as a cofactor are also encoded in the proteome of *E. coli*, including zinc uptake/transport proteins (ZupT), and metabolic proteins (RhaB, YfiH, YpdE, TynA). In Gram-negative bacteria (like *E. coli*) the periplasm between the inner and outer membranes is known to have a more oxidative redox potential than the cytoplasm. A result of the more oxidising environment is that surface exposed cysteine residues tend to be oxidised to CysSSCys and contribute to the structural integrity of the protein. The Dsb family of periplasmic proteins (DsbABCDG) corrects the formation of adventitious disulfide bonds, as well as reduces isolated cysteine residues;

DsbD is a known copper-binding protein.[77] As mentioned above, Dps, a homododecameric protein involved in DNA protection during starvation, is known to bind copper and iron (up to 500 Fe^{3+} ions) and has been implicated in Cu homeostasis, however, its role is unclear.[66]

Staphylococcus aureus

Compared to the ^{107}Ag trace of *E. coli*, the silver trace of *S. aureus* appeared appreciably more complex. Not only were more silver peaks and shoulders present in the chromatogram, there was also clear mirroring of the ^{65}Cu trace in parts, strengthening the idea that the two metals were colocalised. Mining of the proteome of *S. aureus* Newman strain revealed only four known copper-binding proteins; the copper chaperone, CopZ (7.2 kDa), copper efflux ATPase, CopA (87.9 kDa) (known to be present in all sequenced *S. aureus* strains),[78] as well as the haem-copper oxidases quinol oxidase 1, and quinol oxidase 2 (QoxA and B). According to the *S. aureus* SEC chromatogram the calculated MWs of Ag-bound species ranged from >1220 – 64 kDa, thus, CopZ was unlikely to be involved in silver binding in this system. CopA could likely be excluded from the pool of possible Ag-binding species as it is a copper efflux protein suggesting that interaction with Ag^+ would result in the metal's ejection from the cell. It was found in this study that no detectable silver remained in the supernatant broth in which *S. aureus* was cultured suggesting all exogenous Ag^+ was taken up and retained by the organism. It was unclear whether the concentration of silver to which *S. aureus* was exposed was sufficient to trigger induction of the *copAZ* operon, as it is been shown that the expression of the corresponding proteins is dependent on copper (and possibly silver) concentrations.[78] Thus the identities of the silver (and copper) binding proteins are still unclear. However, within the proteome of *S. aureus* Newman (UniProt code: UP000006386) there are hundreds of entries whose functions and properties are yet to be elucidated and are listed as 'uncharacterised protein'. It is likely that many copper-binding proteins in *S. aureus* are yet to be identified and characterised. Conversely, a similar argument regarding the lability of copper in size exclusion experiments (see above) could be applied to this system.

Some proteins that are known to require copper as a cofactor include nitrous oxide reductases, and nitrite reductases, but they have not been identified in the *S. aureus* or *E. coli* proteomes. However, two additional groups of cuproenzymes – superoxide reductases, and haem-copper oxidases – have been identified in *E. coli* and *S. aureus*.

Superoxide dismutases (SOD) are an important group of proteins responsible for the degradation of the superoxide radical and mitigation of oxidative stress.[29] Many different types of SODs exist in nature, including one that utilises copper and zinc as cofactors and is found widely in bacteria (SodC).[79] SodC is a homodimer where each monomer binds one solvent-accessible copper atom as an active site. This protein exists in the extracytoplasmic space of the organism as a soluble protein in most Gram-negative bacteria or an anchored protein in Gram-positive bacteria.[80] SodC is hypothesised to be metallated by the soluble periplasmic chaperone protein CueP. CueP binds one Cu(I) atom with high affinity *in vitro* through a combination of cysteine and histidine residues.[81] Additionally, CueP is suspected to act as a copper sink in the periplasm to aid copper tolerance.[82-83] The proteome of the strain of *E. coli* used in the study presented here contains SodC and could represent one of the colocalised Cu/Ag peaks in the SEC-ICP-MS chromatogram of *E. coli* lysate. However, CueP has not been identified in the *E. coli* proteome and neither protein species have been identified in *S. aureus* Newman. At toxic concentrations of silver, were the Ag^+ to inhibit the antioxidant activity of SodC in addition to generation of ROS, the organisms could experience significant oxidative damage.

Haem-copper oxidases (HCO) are a group of proteins that catalyse the terminal step of the respiratory electron transport chain *via* the reduction of O_2 to H_2O.[25] All HCOs contain a buried mononuclear copper centre where the reduction of molecular oxygen occurs while some have an additional binuclear copper centre located in a soluble periplasmic subunit.[25] The insertion of Cu into HCOs is possibly due to metallochaperones like the lipoprotein, Sco, which binds Cu(I) through a histidine and two cysteine residues *in vitro*.[84] The proteome of the strain of *S. aureus* used herein (Newman, UniProt code: UP000006386) is known to contain two HCOs; quinol oxidase 1 (QoxA), and quinol oxidase 2 (QoxB). In this current study, the concentration of silver was sublethal to the bacteria, however, inhibition of these terminal HCOs at higher $AgNO_3$ concentrations would trap electrons in the transport chain and generate reactive oxygen species. In fact, the HCO cytochrome BD oxidase subunit II (CydB) in *E. coli* was found to be a silver-binding molecular target by Wang *et al.*[34]

A key difference between Ag^+ and Cu^+ cations is silver's lack of accessible oxidation states. Under physiological conditions, copper can readily switch between the +1 and +2 oxidation states and is thought to be included in some proteins/enzymes to facilitate redox activity or reactions.[23] According to the Irving-Williams series, of the first-row transition metals, copper forms some of the most stable complexes with biomolecules.[85]

Thus it could also be expected that silver would form an even stronger complex than copper in biological binding sites.[85] Potentially providing insight into the first cellular processes targeted and 'poisoned' by bactericidal concentrations of Ag^{+}.

All silver detected in the study presented here was found to be associated with moderate to high molecular weight, likely proteinaceous, species. No low molecular weight metal-buffering species, such as glutathione-bound Ag^{+}, were identified. While unexpected, some metals have demonstrated a preference for interaction with proteins while others have shown a stronger affinity for interaction with small molecules like glutathione. An example of this is the fate of cadmium ions, and mercury ions in red blood cells; Cd^{2+} primarily associates with cellular glutathione, while Hg^{2+} primarily associate with haemoglobin (the dominant proteins in red blood cells).[39]

From the results presented here, it would indicate that Ag^{+} forms more stable complexes with proteins, relative to glutathione or other small molecules. However, under atmospheric conditions, reduced GSH will readily be oxidised to GSSG and be less likely to interact with silver ions. To determine whether this occurred, it would be informative to 'fortify' the SEC-ICP-MS elution solvent with physiologically relevant concentrations of glutathione to observe if the ^{107}Ag elution profile was altered, as has been achieved elsewhere for other analytes.[39]

2.6 Conclusions

Through use of metallomics techniques, namely size exclusion chromatography hyphenated with ICP-MS, and X-ray absorption spectroscopy, greater insight into the speciation and chemistry of silver ions in *E. coli*, and *S. aureus* cultured in the presence of sublethal concentrations of $AgNO_3$ was achieved.

Upon addition of micromolar concentrations of silver nitrate into Luria Bertani broth, XANES and EXAFS analysis revealed that the Ag^+ ions were likely complexed by thiolate-containing species of moderate size (MW ~30-50 kDa). Despite high concentrations of sodium chloride in solution (5 g/L), no formation of silver chloride occurred; validated by linear combination fitting of Ag-broth XANES spectra.

Neither the XANES nor the EXAFS spectra of silver nitrate in broth changed appreciably when the concentration of $AgNO_3$ was increased 20-fold. However, the SEC and ICP-MS chromatograms of the same Ag-broth samples displayed an additional shoulder feature in the region silver was known to elute. When considering both the XAS and SEC ICP-MS data for the silver in broth samples, it would appear that the increase in silver concentration caused aggregation of low molecular weight species.

The Ag K-edge XANES of silver ions in *E. coli* and *S. aureus* cell pellets did not significantly differ from exogenous silver in broth suggesting similar coordination environments in all samples. However, the size exclusion chromatography ^{107}Ag ICP-MS trace showed that silver in both bacterial lysates was bound by high molecular weight, likely proteinaceous, biomolecules significantly larger in size than the species in broth. For this to have occurred, the silver would have to be taken up by the bacteria, possibly by some unidentified copper uptake mechanism or cross the cell membranes *via* porins/other uptake mechanisms. The ^{107}Ag and ^{65}Cu ICP-MS traces of *E. coli* and *S. aureus* lysates showed non-uniform colocation of silver and copper, possibly indicating incorporation of silver ions into other cellular processes (likely Cu(I) metabolic pathways). The partial colocation of silver with copper in the metalloprotein elution profile is consistent with previous observations of Ag exposure resulting in upregulation of, or an affinity for, Cu-transport/homeostatic proteins. Analysis of the post-bacterial growth supernatant (SN) broth by SEC and ICP-MS found that the elution profile (monitored by absorbance at 280 nm) was not significantly altered relative to samples of fresh silver-spiked broth from the same stock. Paired with this, the observation that the SN broth of *S. aureus* contained undetectable levels of silver ions it could be further stated that the organism did not identify silver ions as a toxic species to efflux from the cell; were this the case, silver would likely have been detectable in the SN post-growth broth. The proteome of the strain

of *S. aureus* used herein (Newman) contains only two known copper-binding proteins, namely the Cu-chaperone CopZ which transports Cu^{+} to the Cu-efflux protein CopA. However, the proteome of *S. aureus* Newman also contains hundreds of uncharacterised proteins. The SEC-ICP-MS chromatogram (in particular the ^{65}Cu trace) of the organism lysate indicates that there are numerous unidentified Cu-metalloproteins and that this technique could be beneficial in isolating and further characterising these biomolecules.

While the silver signal in *E. coli* post-growth broth was reduced relative to the pre-growth broth, the metal was still detectable after culturing the organism. As such, some of the silver associated with copper in the *E. coli* lysate SEC-ICP-MS chromatogram was possibly bound by components of copper efflux and homeostatic systems. The strain of *E. coli* used (MG1655) contains ~25 known Cu-binding proteins including the Cus, Cut and Cop copper homeostatic and efflux ensembles. Several species that use copper as a cofactor are also known, including proteins involved in zinc uptake (ZupT), thiol/disulfide interchange (DsbD), metabolism (TynA, RhaB, YpdE), and DNA protection (Dps). This may provide insight into how silver ions transition from a benign to toxic entity in the organisms as cellular processes (such as DNA replication and metabolism) have been shown to be inhibited or adversely effected by the noble metal. These findings represent a new understanding of the chemistry of silver when it is not acting as an antibacterial agent in Gram-positive and Gram-negative organisms.

2.7 Future directions

If silver is incorporated into the copper metabolic pathways of bacterial Gram-positive and Gram-negative bacteria it could provide clues regarding the initial cellular response of the microorganism to toxic concentrations of silver ions. While the general trend of colocation of silver ions with copper was observed through size exclusion chromatography hyphenated with ICP-MS of cell lysates, the separation provided by SEC alone did not allow identification of individual silver-bound molecular targets. A useful technique to provide a second dimension to the size-based SEC chromatogram is anion exchange chromatography (AEX) which can separate proteins based on their isoelectric points.[86]

Throughout this study all solutions were maintained at pH 7.4 by HEPES buffer. HEPES was chosen due to its buffering capacity at physiological pH and its demonstrated lack of affinity for various heavy metals, meaning it would be unlikely to perturb the 'natural' chemistry of silver.[87] Unfortunately, an unforeseen consequence of this buffer choice was that the sulfonate group of HEPES is completely deprotonated at pH 7.4. The

result of this was that attempts to carry out anion exchange chromatography were unsuccessful as HEPES molecules saturated the cationic binding sites of the column resin, causing all protein to elute with the void volume of the column as, presumably the biomolecules could not compete with the buffer for the positive binding sites. One of the main focuses of this project was the speciation and chemistry of silver in bacterial systems, and, as XAS synchrotron experiments had already been carried out in HEPES buffer, it was deemed unnecessary to alter a variable, such as buffer choice, mid project.

As such, lysis of bacterial cells into a non-anionic buffer, like Tris, would enable a second dimension of separation of the cellular components in addition to size exclusion. The added purification of the cell lysate may allow greater resolution of the localisation of silver, as monitored by ICP-MS which could aid the identification of individual silver-binding molecular targets. If a sufficiently pure sample of individual or small groups of proteins could be attained, trypsin digestion, analysis of the resultant fragments by electrospray ionisation mass spectrometry, and comparison of the fragments to a proteomic database like MASCOT could enable identification of proteins that bind sublethal silver in *S. aureus* and *E. coli*; as has been achieved for gold in another bacterial system.[88] Analysis of the binding profile of silver in bacteria cultured in the presence of silver nitrate concentrations ranging from sublethal to toxic could provide significant insight into the transition of Ag(I) from benign copper mimic to toxic antibacterial agent. This would help pinpoint the pathways and molecular mechanisms by which silver elicits its toxic effect which could aid in more targeted use of the metal.

As was mentioned above, there are significant gaps in the knowledge of copper uptake, metabolism, and homeostasis in bacterial cells. Within this study, many new copper binding proteins were identified in the *S. aureus* Newman strain as the multiple peaks of the ^{65}Cu trace appeared inconsistent with the four copper-binding proteins known in the organisms' proteome. Further purification of the copper-containing fractions of the bacterial lysates could provide a greater understanding of unknown aspects of copper biochemistry. For example, low molecular weight molecules like glutathione and other unidentified peptide/proteins have been hypothesised to act as a copper buffering pool.[25] In the chromatograms presented herein two small, broad peaks were observed in the copper trace of *S. aureus* which could be representative of LMW buffered copper as the broadness of the peaks would suggest poorly defined conformation, as would be expected for metal-peptide complexes.

2.8 References

1. Alexander, J. W., History of the medical use of silver. *Surg Infect (Larchmt)* **2009,** *10* (3), 289-292.
2. Politano, A. D.; Campbell, K. T.; Rosenberger, L. H.; Sawyer, R. G., Use of silver in the prevention and treatment of infections: silver review. *Surg Infect (Larchmt)* **2013,** *14* (1), 8-20.
3. Ventola, C. L., The antibiotic resistance crisis. *P&T* **2015,** *40* (4), 277-283.
4. Eckhardt, S.; Brunetto, P. S.; Gagnon, J.; Priebe, M.; Giese, B.; Fromm, K. M., Nanobio silver: its interactions with peptides and bacteria, and its uses in medicine. *Chem Rev* **2013,** *113* (7), 4708-4754.
5. Gupta, A.; Matsui, K.; Lo, J. F.; Silver, S., Molecular basis for resistance to silver cations in *Salmonella*. *Nat Med* **1999,** *5* (2), 183-188.
6. Slawson, R. M.; Lohmeier-Vogel, E. M.; Lee, H.; Trevors, J. T., Silver resistance in *Pseudomonas stutzeri*. *BioMetals* **1994,** *7*, 30-40.
7. Park, H. J.; Kim, J. Y.; Kim, J.; Lee, J. H.; Hahn, J. S.; Gu, M. B.; Yoon, J., Silver-ion-mediated reactive oxygen species generation affecting bactericidal activity. *Water Res* **2009,** *43* (4), 1027-1032.
8. Aurore, V.; Caldana, F.; Blanchard, M.; Kharoubi Hess, S.; Lannes, N.; Mantel, P. Y.; Filgueira, L.; Walch, M., Silver-nanoparticles increase bactericidal activity and radical oxygen responses against bacterial pathogens in human osteoclasts. *Nanomedicine* **2018,** *14* (2), 601-607.
9. Xu, H.; Qu, F.; Xu, H.; Lai, W.; Wang, Y. A.; Aguilar, Z. P.; Wei, H., Role of reactive oxygen species in the antibacterial mechanism of silver nanoparticles on *Escherichia coli* O157:H7. *Biometals* **2012,** *25* (1), 45-53.
10. Aruguete, D. M.; Hochella, M. F., Bacteria - nanoparticle interactions and their environmental implications. *Environ Chem* **2010,** *7* (1), 3-9.
11. Kim, S.-H.; Lee, H.-S.; Ryu, D.-S.; Choi, S.-J.; Lee, D.-S., Antibacterial activity of silver-nanoparticles against *Staphylococcus aureus* and *Escherichia coli*. *Korean J Microbiol Biotechnol* **2011,** *39* (1), 77-85.
12. Hobman, J. L.; Yamamoto, K.; Oshima, T., Transcriptomic responses of bacterial cells to sublethal metal ion stress. In *Molecular microbiology of heavy metals*, Nies, D. H.; Silver, S., Eds. Springer: Berlin, Heidelburg, 2007; Vol. 6, pp 73-115.
13. McQuillan, J. S.; Shaw, A. M., Differential gene regulation in the Ag nanoparticle and Ag(I)-induced silver stress response in *Escherichia coli*: a full transcriptomic profile. *Nanotoxicology* **2014,** *8 S1*, 177-184.
14. Li, Y.; Yan, N.; Wong, T. Y.; Wang, W.-X.; Liu, H., Interaction of antibacterial silver nanoparticles and microbiota-dependent holobionts revealed by metatranscriptomic analysis. *Environ Sci: Nano* **2019,** *6* (11), 3242-3255.
15. Marchioni, M.; Jouneau, P.-H.; Chevallet, M.; Michaud-Soret, I.; Deniaud, A., Silver nanoparticle fate in mammals: Bridging *in vitro* and *in vivo* studies. *Coord Chem Rev* **2018,** *364*, 118-136.
16. Jiravova, J.; Tomankova, K. B.; Harvanova, M.; Malina, L.; Malohlava, J.; Luhova, L.; Panacek, A.; Manisova, B.; Kolarova, H., The effect of silver nanoparticles and silver ions on mammalian and plant cells *in vitro*. *Food Chem Toxicol* **2016,** *96*, 50-61.
17. Huang, H.; Lai, W.; Cui, M.; Liang, L.; Lin, Y.; Fang, Q.; Liu, Y.; Xie, L., An evaluation of blood compatibility of silver nanoparticles. *Sci Rep* **2016,** *6* (25518), 1-15.
18. Sim, W.; Barnard, R. T.; Blaskovich, M. A. T.; Ziora, Z. M., Antimicrobial silver in medicinal and consumer applications: A patent review of the past decade (2007-2017). *Antibiotics (Basel)* **2018,** *7* (93), 1-15.

19. Baker, J. W.; Leidy, K. L.; Smith, K. M.; Okeke, U. S., Argyria associated with use of systemic colloidal silver. *Fed Pract* **2011,** *28* (1), 39-42.
20. *Toxicological profile for silver*; U. S. Department of Health and Human Services: Atlanta, GA, 1990.
21. Stepien, K. M.; Morris, R.; Brown, S.; Taylor, A.; Morgan, L., Unintentional silver intoxication following self-medication: an unusual case of corticobasal degeneration. *Ann Clin Biochem* **2009,** *46* (6), 520-522.
22. Willey, J. M.*, et al.*, *Prescott, Harley, and Klein's Microbiology*. 7 ed.; McGraw Hill Higher Education: 2008.
23. Festa, R. A.; Thiele, D. J., Copper: an essential metal in biology. *Curr Biol* **2011,** *21* (21), R877-883.
24. Penner-Hahn, J. E., Characterization of "spectroscopically quiet" metals in biology. *Coord Chem Rev* **2005,** *249*, 161-177.
25. Stewart, L. J.; Thaqi, D.; Kobe, B.; McEwan, A. G.; Waldron, K. J.; Djoko, K. Y., Handling of nutrient copper in the bacterial envelope. *Metallomics* **2019,** *11* (1), 50-63.
26. Rensing, C.; Fan, B.; Sharma, R.; Mitra, B.; Rosen, B. P., CopA: An *Escherichia coli* Cu(I)-translocating P-type ATPase. *PNAS* **2000,** *97* (2), 652-656.
27. Sakurai, T.; Kataoka, K., Basic and applied features of multicopper oxidases, CueO, bilirubin oxidase, and laccase. *Chem Rec* **2007,** *7* (4), 220-229.
28. Rensing, C.; Grass, G., *Escherichia coli* mechanisms of copper homeostasis in a changing environment. *FEMS Microbiol Rev* **2003,** *27* (2-3), 197-213.
29. Mondola, P.; Damiano, S.; Sasso, A.; Santillo, M., The Cu, Zn superoxide dismutase: not only a dismutase enzyme. *Front Physiol* **2016,** *7* (594), 1-8.
30. Osman, D.; Cavet, J. S., Copper homeostasis in bacteria. In *Advances in Applied Microbiology*, Elsevier: 2008; Vol. 65, pp 217-247.
31. Tarrant, E.; Riboldi, G. P.; McIlvin, M. R.; Stevenson, J.; Barwinska-Sendra, A. Stewart, L. J.; Saito, M. A.; Waldron, K. J., Copper stress in *Staphylococcus aureus* leads to adaptive changes in central carbon metabolism. *Metallomics* **2019,** *11* (1), 183-200.
32. Argyrou, A.; Blanchard, J. S., Flavoprotein disulfide reductases: advances in chemistry and function. *Prog Nucleic Acid Res Mol Biol* **2004,** *78*, 89-142.
33. Gutierrez-Correa, J.; Stoppani, A. O., Inactivation of heart dihydrolipoamide dehydrogenase by copper Fenton systems. Effect of thiol compounds and metal chelators. *Free Radic Res* **1995,** *22* (3), 239-250.
34. Wang, H.; Yan, A.; Liu, Z.; Yang, X.; Xu, Z.; Wang, Y.; Wang, R.; Koohi-Moghadam, M.; Hu, L.; Xia, W.; Tang, H.; Wang, Y.; Li, H.; Sun, H., Deciphering molecular mechanism of silver by integrated omic approaches enables enhancing its antimicrobial efficacy in *E. coli*. *PLoS Biol* **2019,** *17* (6), 1-31.
35. Zanzen, U.; Bovenkamp-Langlois, L.; Klysubun, W.; Hormes, J.; Prange, A., The interaction of copper ions with *Staphylococcus aureus*, *Pseudomonas aeruginosa*, and *Escherichia coli*: an X-ray absorption near-edge structure (XANES) spectroscopy study. *Arch Microbiol* **2018,** *200* (3), 401-412.
36. Conry, R. R., Copper: inorganic and coordination chemistry. In *Encyclopedia of Inorganic Chemistry*, Wiley: 2006.
37. Grass, G.; Rensing, C., Genes involved in copper homeostasis in *Escherichia coli*. *J Bacteriol* **2001,** *183* (6), 2145-2147.
38. Thomas, S. A.; Mishra, B.; Myneni, S. C. B., High energy resolution-X-ray absorption near edge structure spectroscopy reveals Zn ligation in whole cell bacteria. *J Phys Chem Lett* **2019,** *10* (10), 2585-2592.

39. Gibson, M. A.; Sarpong-Kumankomah, S.; Nehzati, S.; George, G. N.; Gailer, J., Remarkable differences in the biochemical fate of Cd(II), Hg(II), CH_3Hg^+ and thiomerosal in red blood cell lysate. *Metallomics* **2017,** *9* (8), 1060-1072.
40. Manley, S. A.; Byrns, S.; Lyon, A. W.; Brown, P.; Gailer, J., Simultaneous Cu-, Fe-, and Zn-specific detection of metalloproteins contained in rabbit plasma by size-exclusion chromatography-inductively coupled plasma atomic emission spectroscopy. *J Biol Inorg Chem* **2009,** *14* (1), 61-74.
41. Acosta, M.; Torres, S.; Marino-Repizo, L.; Martinez, L. D.; Gil, R. A., Novel method for metalloproteins determination in human breast milk by size exclusion chromatography coupled to inductively coupled plasma mass spectrometry. *J Pharm Biomed Anal* **2018,** *158*, 209-213.
42. Hare, D. J.; Grubman, A.; Ryan, T. M.; Lothian, A.; Liddell, J. R.; Grimm, R.; Matsuda, T.; Doble, P. A.; Cherny, R. A.; Bush, A. I.; White, A. R.; Masters, C. L.; Roberts, B. R., Profiling the iron, copper and zinc content in primary neuron and astrocyte cultures by rapid online quantitative size exclusion chromatography-inductively coupled plasma-mass spectrometry. *Metallomics* **2013,** *5* (12), 1656-1662.
43. Ruzik, L.; Wojcieszek, J., *In vitro* digestion method for estimation of copper bioaccessibility in Açaí berry. *Monatsh Chem* **2016,** *147*, 1429-1438.
44. Sanchez, L. F.; Szpunar, J., Speciation analysis for iodine in milk by size-exclusion chromatography with inductively couples plasma mass spectrometric detection. *J Anal Atom Spectrom* **1999,** *14*, 1697-1702.
45. Thomas, O. R.; Ganio, K.; Roberts, B. R.; Swearer, S. E., Trace element-protein interactions in endolymph from the inner ear of fish: implications for environmental reconstructions using fish otolith chemistry. *Metallomics* **2017,** *9* (3), 239-249.
46. Venkatesan, A. K.; Gan, W.; Ashani, H.; Herckes, P.; Westerhoff, P., Size exclusion chromatography with online ICP-MS enables molecular weight fractionation of dissolved phosphorus species in water samples. *Water Res* **2018,** *133*, 264-271.
47. Wojcieszek, J.; Kwiatkowski, P.; Ruzik, L., Speciation analysis and bioaccessibility evaluation of trace elements in goji berries (*Lycium Barbarum, L.*). *J Chromatogr A* **2017,** *1492*, 70-78.
48. Dong, L.-J.; Lai, Y.-J.; Yu, S.-J.; Liu, J.-F., Speciation analysis of the uptake and biodistribution of nanoparticulate and ionic silver in *Escherichia coli*. *Anal Chem* **2019,** *91* (19), 12525-12530.
49. Ankudinov, A. L.; Ravel, B.; Rehr, J. J.; Conradson, S. D., Real-space multiple-scattering calculation and interpretation of X-ray absorption near-edge structure. *Phys Rev B* **1998,** *58* (12), 7565-7576.
50. Doolette, C. L.; McLaughlin, M. J.; Kirby, J. K.; Batstone, D. J.; Harris, H. H.; Ge, H.; Cornelis, G., Transformation of PVP coated silver nanoparticles in a simulated wastewater treatment process and the effect on microbial communities. *Chem Cent J* **2013,** *7* (46), 1-18.
51. Acland, C. B.; Freeman, H. C., Model compounds for metal-protein interaction: Crystal structures of four silver(I) complexes with glycine, glycylglycine, and imidazole. *Chem Comm* **1971,** (17), 1016-1017.
52. Bilinovich, S. M.; Panzner, M. J.; Youngs, W. J.; Leeper, T. C., Poly[[{mu(3)-2-[4-(2-hy-droxy-eth-yl)piperazin-1-yl]ethane-sulfonato}-silver(I)] trihydrate]. *Acta Crystallogr Sect E Struct Rep Online* **2011,** *67* (9), m1178-1179.
53. Sharma, C. V. K.; Rogers, R. D., Discrete macrocycles to infinite polymeric frames: Crystal engineering studies of Ag(I):pyrimidine complexes. *Crystal Engineering* **1998,** *1* (1), 19-38.

54. Fekete, S.; Beck, A.; Veuthey, J. L.; Guillarme, D., Theory and practice of size exclusion chromatography for the analysis of protein aggregates. *J Pharm Biomed Anal* **2014,** *101*, 161-173.
55. Finney, L. A.; Chishti, Y.; Khare, T.; Giometti, C.; Levina, A.; Lay, P. A.; Vogt, S., Imaging metals in protein by combining electrophoresis with rapid X-ray fluorescence mapping. *ACS Chem Biol* **2010,** *5* (6), 577-587.
56. Lagoja, I. M., Pyrimidine as constituent of natural biologically active compounds. *Chem Biodivers* **2005,** *2*, 1-50.
57. Bovenkamp, G. L.; Zanzen, U.; Krishna, K. S.; Hormes, J.; Prange, A., X-ray absorption near-edge structure (XANES) spectroscopy study of the interaction of silver ions with *Staphylococcus aureus*, *Listeria monocytogenes*, and *Escherichia coli*. *Appl Environ Microbiol* **2013,** *79* (20), 6385-6390.
58. Pakhomov, P. M.; Ovchinnikov, M. M.; Khizhnyak, S. D.; Lavrienko, M. V.; Nierling, W.; Lechnoer, M. D., Study of gelation in aqueous solutions of cysteine and silver nitrate. *Coll J* **2004,** *66* (1), 65-70.
59. Sendzik, M.; Pushie, M. J.; Stefaniak, E.; Haas, K. L., Structure and affinity of Cu(I) bound to human serum albumin. *Inorg Chem* **2017,** *56* (24), 15057-15065.
60. Carugo, O., Silver and gold in the Protein Data Bank. *J Inorg Biochem* **2017,** *175*, 244-247.
61. Nan, J.; Yan, X. P., A circular dichroism probe for L-cysteine based on the self-assembly of chiral complex nanoparticles. *Chemistry* **2010,** *16* (2), 423-427.
62. Veronesi, G.; Gallon, T.; Deniaud, A.; Boff, B.; Gateau, C.; Lebrun, C.; Vidaud, C.; Rollin-Genetet, F.; Carriere, M.; Kieffer, I.; Mintz, E.; Delangle, P.; Michaud-Soret, I., XAS investigation of silver(I) coordination in copper(I) biological binding sites. *Inorg Chem* **2015,** *54* (24), 11688-11696.
63. Bubber, P.; Ke, Z. J.; Gibson, G. E., Tricarboxylic acid cycle enzymes following thiamine deficiency. *Neurochem Int* **2004,** *45* (7), 1021-1028.
64. Clement, J. L.; Jarrett, P. S., Antibacterial silver. *Metal-Based Drugs* **1994,** *1* (5-6), 467-482.
65. Lodish, H.; Berk, A.; Zipursky, S. L.; Matsudaira, P.; Baltimore, D.; Darnell, J., DNA cloning with plasmid vectors. In *Molecular Cell Biology*, 4th ed.; W. H. Freeman: New York, 2000.
66. Thieme, D.; Grass, G., The Dps protein of *Escherichia coli* is involved in copper homeostasis. *Microbiol Res* **2010,** *165* (2), 108-115.
67. Nooren, I. M. A.; Thornton, J. M., Diversity of protein-protein interactions. *EMBO J* **2003,** *22* (14), 3486-3492.
68. Blindauer, C. A., Advances in the molecular understanding of biological zinc transport. *Chem Commun (Camb)* **2015,** *51* (22), 4544-4563.
69. Xu, F. F.; Imlay, J. A., Silver(I), mercury(II), cadmium(II), and zinc(II) target exposed enzymic iron-sulfur clusters when they toxify *Escherichia coli*. *Appl Environ Microbiol* **2012,** *78* (10), 3614-3621.
70. Gugala, N.; Lemire, J.; Chatfield-Reed, K.; Yan, Y.; Chua, G.; Turner, R. J., Using a chemical genetic screen to enhance our understanding of the antibacterial properties of silver. *Genes (Basel)* **2018,** *9* (7), 1-21.
71. Holt, K. B.; Bard, A. J., Interaction of silver(I) ions with the respiratory chain of *Escherichia coli*: an electrochemical and scanning electrochemical microscopy study of the antimicrobial mechanism of micromolar Ag(I). *Biochemistry* **2005,** *44* (39), 13214-13223.
72. Bragg, P. D.; Rainnie, D. J., The effect of silver ions on the respiratory chain of *Escherchia coli*. *Can J Microbiol* **1974,** *20*, 883-889.
73. Chandrangsu, P.; Chandrangsu, P.; Rensing, C.; Helmann, J. D., Metal homeostasis and resistance in bacteria. *Nat Rev Microbiol* **2017,** *15* (6), 338-350.

74. Loftin, I. R.; Franke, S.; Blackburn, N. J.; McEvoy, M. M., Unusual Cu(I)/Ag(I) coordination of *Escherichia coli* CusF as revealed by atomic resolution crystallography and X-ray absorption spectroscopy. *Protein Sci* **2007,** *16* (10), 2287-2293.
75. Gudipaty, S. A.; Larsen, A. S.; Rensing, C.; McEvoy, M. M., Regulation of Cu(I)/Ag(I) efflux genes in *Escherichia coli* by the sensor kinase CusS. *FEMS Microbiol Lett* **2012,** *330* (1), 30-37.
76. Jahromi, E. Z.; White, W.; Wu, Q.; Yamdagni, R.; Gailer, J., Remarkable effect of mobile phase buffer on the SEC-ICP-AES derived Cu, Fe and Zn-metalloproteome pattern of rabbit blood plasma. *Metallomics* **2010,** *2* (7), 460-468.
77. Ezraty, B.; Gennaris, A.; Barras, F.; Collet, J. F., Oxidative stress, protein damage and repair in bacteria. *Nat Rev Microbiol* **2017,** *15* (7), 385-396.
78. Sitthisak, S.; Knutsson, L.; Webb, J. W.; Jayaswal, R. K., Molecular characterization of the copper transport system in *Staphylococcus aureus*. *Microbiology* **2007,** *153* (12), 4274-4283.
79. Dunn, K. L.; Farrant, J. L.; Langford, P. R.; Kroll, J. S., Bacterial [Cu,Zn]-cofactored superoxide dismutase protects opsonized, encapsulated *Neisseria meningitidis* from phagocytosis by human monocytes/macrophages. *Infect Immun* **2003,** *71* (3), 1604-1607.
80. Fenlon, L. A.; Slauch, J. M., Cytoplasmic copper detoxification in *Salmonella* can contribute to SodC metalation bit is dispensable during systemic infection. *J Bacteriol* **2017,** *199* (24), 1-13.
81. Yoon, B.-Y.; Kim, Y.-H.; Kim, N.; Yun, B.-Y.; Kim, J.-S.; Lee, J.-H.; Cho, H.-S.; Lee, K.; Ha, N.-C., Structure of the periplasmic copper-binding protein CueP from *Salmonella enterica* serovar Typhimurium. *Acta Cryst D* **2014,** *70* (7), 2053-2053.
82. Osman, D*., et al.*, The copper supply pathway to a *Salmonella* Cu,Zn-superoxide dismutase (SodCII) involves P(1B)-type ATPase copper efflux and periplasmic CueP. *Mol Microbiol* **2013,** *87* (3), 466-477.
83. Osman, D.; Patterson, C. J.; Bailey, K.; Fisher, K.; Robinson, N. J.; Rigby, S. E.; Cavet, J. S., Copper homeostasis in *Salmonella* is atypical and copper-CueP is a major periplasmic metal complex. *J Biol Chem* **2010,** *285* (33), 25259-25268.
84. McEwan, A. G.; Lewin, A.; Davy, S. L.; Boetzel, R.; Leech, A.; Walker, D.; Wood, T.; Moore, G. R., PrrC from *Rhodobacter sphaeroides*, a homologue of eukaryotic Sco proteins, is a copper-binding protein and may have a thiol-disulfide oxidoreductase activity. *FEBS Lett* **2002,** *518*, 10-16.
85. Robinson, N. J.; Winge, D. R., Copper metallochaperones. *Annu Rev Biochem* **2010,** *79*, 537-562.
86. Hong, P.; Koza, S.; Bouvier, E. S., A review: Size-exclusion chromatography for the analysis of protein biotherapeutics and their aggregates. *J Liq Chromatogr Relat Technol* **2012,** *35* (20), 2923-2950.
87. Ferreira, C. M. H.; Pinto, I. S. S.; Soares, E. V.; Soares, H. M. V. M., (Un)suitability of the use of pH buffers in biological, biochemical and environmental studies and their interaction with metal ions – a review. *RSC Adv* **2015,** *5* (39), 30989-31003.
88. Zammit, C. M.; Weiland, F.; Brugger, J.; Wade, B.; Winderbaum, L. J.; Nies, D. H.; Southam, G.; Hoffmann, P.; Reith, F., Proteomic responses to gold(III)-toxicity in the bacterium *Cupriavidus metallidurans* CH34. *Metallomics* **2016,** *8* (11), 1204-1216.

2.9 Appendices

Appendix 2.9.1 Operating parameters

Table 9: Typical operating parameters for SEC-ICP-MS experiments

Agilent 1200 LC	
Mobile phase	100 mM HEPES, pH 7.4
Column	Agilent AdvancedBio SEC 130 or 300 Å
Particle size	2.7 μm
Pore size	130 or 300 Å
Flow rate	0.3 mL/min
Injection volume	10 – 100 μL
Column dimensions	7.8 mm x 300 mm
Agilent ICP-MS QQQ 8900	
RF power	1550 W
Sample depth	10.0 mm
Carrier gas	15.0 L/min
Makeup gas	0.90 L/min
Spray chamber temp	2°C
Extracts 1, 2	-6.0 V, -250.0 V
Omega bias, lens	-150 V, 7.5 V
Deflect, plate bias	2.0 V, -60 V
Cell entrance, exit	-70 V, -80 V
Octopole bias, RF	-18.0 V, 170 V
Collision gas	He, 3.5 mL/min

Appendix 2.9.2 Experimentally determined minimum inhibitory concentrations (MIC)

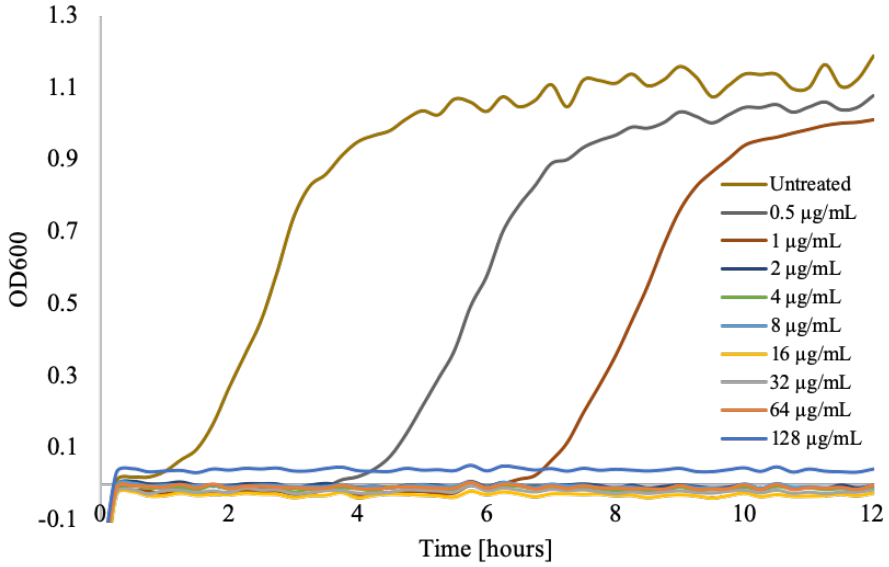

Figure 18: Blank-corrected growth curves of *E. coli* MG1655 strain, as measured by the optical density (OD) at 600 nm, incubated at 37°C with a range of concentrations of $AgNO_3$ (0 µg/mL to 128 µg/mL) for 16 hours. Time point >12 hours were discarded as the natural cell death was expected beyond this time frame. The minimum inhibitory concentration (MIC) was determined to be >2 µg/mL.

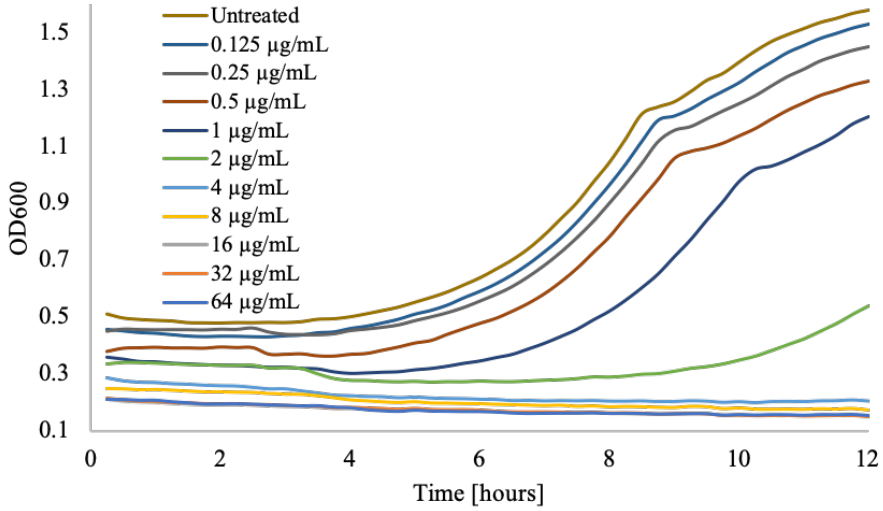

Figure 19: Blank-corrected growth curves of *S. aureus* Newman strain, as measured by the optical density (OD) at 600 nm, incubated at 37°C with a range of concentrations of $AgNO_3$ (0 µg/mL to 128 µg/mL) for 16 hours. Time point >12 hours were discarded as the natural cell death was expected beyond this time frame. The minimum inhibitory concentration (MIC) was determined to be >4 µg/mL.

Appendix 2.9.3 Cambridge Structural Database (CSD) survey results and references

Table 10: Survey of silver-nitrogenous bases (and relevant derivatives thereof) in CSD version 5.40 (Nov 2018)

CSD Code	Reference	Nitrogenous base
ADAGPC	Gagnon, C., *et al.*, *Inorg Chem*, **1977**, 16, 2469	Adenine
EBILIM	Venkatesh, V., *et al.*, *CrystEngComm*, **2011**, 13, 6030	
EBILOS	Venkatesh, V., *et al.*, *CrystEngComm*, **2011**, 13, 6030	
EKAYUL	Mishra, A. K., *et al.*, *Dalton Trans*, **2010**, 39, 10034	
EKAZAS	Mishra, A. K., *et al.*, *Dalton Trans*, **2010**, 39, 10034	
EKAZEW	Mishra, A. K., *et al.*, *Dalton Trans*, **2010**, 39, 10034	
EKAZIA	Mishra, A. K., *et al.*, *Dalton Trans*, **2010**, 39, 10034	
EKAZOG	Mishra, A. K., *et al.*, *Dalton Trans*, **2010**, 39, 10034	
FIHJOX	Prajapati, R. K., *et al.*, *CrystEngComm*, **2013**, 15, 9316	
FIHJUD	Prajapati, R. K., *et al.*, *CrystEngComm*, **2013**, 15, 9316	
FIHKAK	Prajapati, R. K., *et al.*, *CrystEngComm*, **2013**, 15, 9316	
FIHKEO	Prajapati, R. K., *et al.*, *CrystEngComm*, **2013**, 15, 9316	
FIHKIS	Prajapati, R. K., *et al.*, *CrystEngComm*, **2013**, 15, 9316	
GIRHAR	Purohit, C. S., *et al.*, *Inorg Chem*, **2007**, 46, 8493	
GIRHEV	Purohit, C. S., *et al.*, *Inorg Chem*, **2007**, 46, 8493	
GIRHIZ	Purohit, C. S., *et al.*, *Inorg Chem*, **2007**, 46, 8493	
JEFGEH	Purohit, C. J., *et al.*, *J Am Chem Soc*, **2006**, 128, 400	
MADAGN01	Gagnon, C. *et al.*, *Acta Cryst B.*, **1977**, 33, 1448	
MADAGN10	Cagnon, C., *et al.*, *Inorganica Chim Acta*, **1975**, 14, L52	
MASVOT	Kumar, J., *et al.*, *CrystEngComm*, **2012**, 14, 3012	
MISBAT	Mishra, A. K., *et al.*, *Indian J Chem*, **2013**, 52, 1041	
MISBEX	Mishra, A. K., *et al.*, *Indian J Chem*, **2013**, 52, 1041	
OLALOE	Kumar, J., *et al.*, *Inorganica Chim Acta*, **2016**, 452, 214	
OLALUK	Kumar, J., *et al.*, *Inorganica Chim Acta*, **2016**, 452, 214	
QEZLOX	Purohit, C. J., *et al.*, *J Am Chem Soc*, **2007**, 129, 3488	
VUGLAK	Menzer, S., *et al.*, *J Am Chem Soc*, **1992**, 114, 4644	
WERYOH	Rother, I. B., *et al.*, *Inorganica Chim Acta*, **2000**, 300	
XINRER	Rother, I. B., *et al.*, *Supramol Chem*, **2002**, 14, 189	
AWICEP	Khutia, A., *et al*, *Chem Euro J*, **2011**, 17, 4205	Cytosine
DEFFEC	Terrón, A., *et al CrystEngComm*, **2017**, 19, 5830	
ETASAU	Khutia, A., *et al*, *Chem Euro J*, **2011**, 17, 4205	
FATBIL	Schollhorn, H., *et al*, *Inorganica Chim Acta*, **1987**, 135	
MCYTAG10	Kistenmacher, T. J., *et al*, *Inorg Chem*, **1979**, 18, 240	
VUGLAK	Menzer, S., *et al*, *J Am Chem Soc*, **1992**, 114, 4644	
PEWTIU	Menzer, S., *et al*, *Inorganica Chim Acta*, **1993**, 210, 167	Guanine
AGMTHY	Guay, F., *et al*, *J Am Chem Soc*, **1979**, 101, 6260	Thymine/uracil
CEZGAP	Aoki, K., *et al*, *Acta Cryst C*, **1984**, 40, 775	
EPITUT	Barcelo-Oliver, M., *et al*, *Chem Comm*, **2011**, 47, 4646	
EPITUT01	Barceló-Oliver, M., *et al*, *Dalton Trans*, **2013**, 42, 763	
NAZNOT	Nong, P.-S., *et al*, *Synth React Inorg M*, **2012**, 42, 313	

Table 11: Survey of silver-biotin structures in CSD version 5.40 (Nov 2018)

CSD Code	Reference	Interaction	Bond length (Å)
BECQAD	Altaf, M., Stoeckli-Evans, H., *CSD Comm,* **2012**	Ag-S Ag-S Ag-O_{ketone} Ag-$OClO_3$ Ag-S Ag-O_{ketone}	2.438 2.517 2.393 2.549 2.520 2.393
CEGKAA	Aoki, K., *et al.*, *J Inorg Biochem*, **1983**, 19, 269	Ag-S Ag-S Ag-ONO_3 Ag-O_{ketone}	2.392 2.514 2.451 2.68
LERDIX	Altaf, M., Stoeckli-Evans, H., *Acta Crystallographica Section C*, **2013**, 69, 127	Ag-S Ag-S Ag-O_{acid} Ag-O_{acid} Ag-O_{ketone}	2.564 2.515 2.895[a] 2.299[a] 2.515
LERDOD	Altaf, M., Stoeckli-Evans, H., *Acta Crystallographica Section C*, **2013**, 69, 127	Ag-S Ag-S Ag-ONO_2 Ag-ONO_2 Ag-O_{ketone}	2.439 2.464 2.801[a] 2.396[a] 2.529
LERDUJ	Altaf, M., Stoeckli-Evans, H., *Acta Crystallographica Section C*, **2013**, 69, 127	Ag-S Ag-S Ag-O_{acid} Ag-O_{acid}	2.423 2.452 2.753 2.518
LERFAR	Altaf, M., Stoeckli-Evans, H., *Acta Crystallographica Section C*, **2013**, 69, 127	Ag-S Ag-S Ag-O_{acid}	2.419 2.450 2.440

[a] Ligand chelated

Table 12: Survey of silver-methionine (and derivatives thereof) structures in CSD version 5.40 (Nov 2018)

CSD Code	Reference	Interaction	Bond length (Å)
DAPJUB (N-acetyl methionine)	Kasuga, N. C., *et al.*, *Inorg Chem*, **2012**, 51, 1640	Ag-Ag Ag-S Ag-S Ag-O Ag-O	2.899 2.994 2.497 2.209 2.345
DAPKAI	Kasuga, N. C., *et al.*, *Inorg Chem*, **2012**, 51, 1640	Ag-S Ag-O Ag-O Ag-N	2.395 2.585 2.453[a] 2.241[a]
EQIYAG	Chabert, V., *et al*, *CSD Comm*, **2016**	Ag-S Ag-S Ag-O	2.501 2.487 2.346
EQIYAG01	Chabert, V., *et al.*, *Chem Comm*, **2017**, 53, 6105	Ag-S Ag-S Ag-O	2.454 2.487 2.338
LEYLUX (Crystallised with Cu)	Luo, T.-T., *et al*, *Inorg Chem*, **2007**, 46, 1532	Ag-S Ag-S Ag-S Ag-OH_2	2.514 2.586 2.613 2.519

[a] Ligand chelated

Table 13: Survey of silver-histidine (and derivatives thereof) structures in CSD version 5.40 (Nov 2018)

CSD Code	Reference	Interaction	Bond length (Å)
DILGIP (N-acetyl histidine)	Kasuga, N. C., *et al.*, *Acta Crystallographica Section E*, **2007**, 63, m2440	Ag-O Ag-O Ag-O Ag-N_{ring}	2.257 2.528 2.650[a] 2.175[a]
TIGGUN	Mirolo, L., *et al.*, *Chem Euro J*, **2013**, 19, 1754	Ag-O Ag-O Ag-O Ag-ONO_2	2.300 2.250 2.456 2.567
TIGHAU	Mirolo, L., *et al.*, *Chem Eur J*, **2013**, 19, 1754	Ag-O Ag-O Ag-ONO_2 Ag-O Ag-O Ag-O Ag-ONO_2 Ag-ONO_2	2.226 2.216 2.392 2.243 2.716 2.299 2.500[a] 2.603[a]
TIGHEY	Mirolo, L., *et al.*, *Chem Euro J*, **2013**, 19, 1754	Ag-N_{ring} Ag-N_{ring}	2.109 2.099
UMOTAS	Kasuga, N. C., *et al.*, *Inorg Chim Acta*, **2011**, 368, 44	Ag-Ag Ag-Ag Ag-N_{ring} Ag-N Ag-O	3.038 3.083 2.102 2.146[a] 2.659[a]
UMOTEW	Kasuga, N. C., *et al.*, *Inorg Chim Acta*, **2011**, 368, 44	Ag-N_{amine} Ag-N_{ring}	2.131 2.093
WIJDUO	Nomiya, K., *et al.*, *Inorg Chem*, **2000**, 39, 3301	Ag-N_{amine} Ag-N_{ring}	2.125 2.097

[a] Ligand chelated

Table 14: Survey of silver-cysteine (and derivatives thereof) structures in CSD version 5.40 (Nov 2018)

CSD Code	Reference	Interaction	Bond length (Å)
NIQWIV	Leung, B. O., *et al.*, *Inorg Chem*, **2013**, 52, 4593	Ag-S Ag-S Ag-S Ag-N Ag-S Ag-S Ag-S	2.657 2.515 2.802[a] 2.306[a] 2.450 2.573 2.530
DAPKEM (S-methyl cysteine)	Kasuga, N. C., *et al.*, *Inorg Chem,* **2012**, 51, 1640	Ag-S Ag-N Ag-O_{COO-} Ag-O_{COO-}	2.844[a] 2.212[a] 2.188 2.590
NIQWOB (Penicillamine)	Leung, B. O. *et al.*, *Inorg Chem*, **2013**, 52, 4593	Ag-S Ag-S	2.377 2.376

[a] Ligand chelated

Table 15: Survey of metal-thiamine (and derivatives thereof) structures in CSD version 5.40 (Nov 2018)

CSD Code	Reference	Metal	Interaction
CEJHAA	Cramer, R. E., *et al.*, *J Am Chem Soc*, **1984**, 106, 111,	Cu(I)	Cu-N (LHPN)[a] Cu-Cl (x2)
CLTMCD	Cramer, R. E., *et al.*, *J Am Chem Soc*, **1981**, 103, 76	Cd(II)	Cd-N (LHPN) Cd-Cl (x3)
DEWRAY	Aoki, K., *et al.*, *J Am Chem Soc*, **1985**, 107, 6242	Rh(I)	Rh-N (LHPN) Rh-O (x4) Rh-Rh NOTE: dinuclear
FURPAJ	Cramer, R. E., *et al.*, *Inorg Chem*, **1988**, 27, 123	Pt(II)	Pt-N (LHPN) Pt-Cl (x3)
GETZAG	Bencini, A, *et al.*, *Inorg Chim Acta*, **1987**, 135, 85	Zn(II)	Zn-N (LHPN) Zn-Cl (x3)
GETZAG01	Pengjun, L., *et al.*, *Yingyong Huaxue*, **1989**, 6, 40-42	Zn(II)	Zn-N (LHPN) Zn-Cl (x3)
GIFZEA	Bau, R., *et al.*, *Inorg Chim Acta*, **1988**, 150, 107	Co(II)	Co-N (LHPN) Co-Cl (x3) NOTE: Non-aromatic thiazole ring
HOXZID	Hu, N.-H., *et al.*, *Polyhedron*, **1999**, 18, 2987	Cd(II)	Cd-N (LHPN) Cd-Cl (x3)
HOXZOJ	Hu, N.-H., *et al.*, *Polyhedron*, **1999**, 18, 2987	Cd(II)	Cd-N (LHPN) Cd-Br (x3)
HOXZUP	Hu, N.-H., *et al.*, *Polyhedron*, **1999**, 18, 2987	Hg(II)	Hg-N (LHPN) Hg-Cl (x3) NOTE: dinuclear
HOYBAY	Hu, N.-H., *et al.*, *Polyhedron*, **1999**, 18, 2987	Hg(II)	Hg-N (LHPN) Hg-Br (x3) NOTE: dinuclear
HOYBEC	Hu, N.-H., *et al.*, *Polyhedron*, **1999**, 18, 2987	Pt(II)	Pt-N (LHPN) Pt-ONO
JAHGEE	Archibong, E., *et al.*, *Inorg Chim Acta*, **1989**, 156, 77	Cu(I)	Cu-N (LHPN) Cu-Br (x2)
JOGJOE	Zhong-Sheng, J., *et al.*, *Chinese Sci Bull*, **1990**, 35, 383	Hg(II)	Hg-O (OH tail) Hg-Cl (x3) NOTE: counterion and multinuclear
KIBVEW	Louloudi, M. *et al.*, *J Am Chem Soc*, **1990**, 112, 7233	Hg(II)	Hg-N (LHPN) Hg-Cl (x3)
LATLAT	Cramer, R. E., Carrie, M. J. J. *Inorg Chem*, **1993**, 32, 3509	Pt(II)	Pt-N (LHPN) Pt-Cl (x2) Pt-S (DMSO)
NODXUZ	Hu, N.-H., *Inorg Chim Acta*, **2001**, 325, 9	Pt(II)	Pt-N (LHPN) Pt-ONO (x2) Pt-NO_2
SISHIL	Aoki, K., *et al.*, *Inorg Chim Acta*, **1990**, 175, 247	Co(II)	Co-N (LHPN) Co-Cl (x3)
SISHOR	Aoki, K., *et al.*, *Inorg Chim Acta*, **1990**, 175, 247	Zn(II)	Zn-N (LHPN) Zn-Br (x3)
SORXUS	Malik, K.M.A., *et al.*, J *Bangladesh Chem Soc*, **1990**, 3, 205	Co(II)	Co-N (LHPN) Co-Cl (x3)
SORYAZ	Malik, K.M.A., *et al.*, J *Bangladesh Chem Soc*, **1990**, 3, 205	Zn(II)	Zn-N (LHPN) Zn-Cl (x3)
SOSMES	Hu, N.-H., *Inorg Chim Acta*, **1991**, 186, 209	Mn(II)	Mn-N (LHPN) Mn-OH_2 Mn-Cl (x2) Mn-O (OH tail)
TUBJIJ	Dodi, K. *et al.*, *Inorg Chem*, **1996**, 35, 6513	Hg(II)	Hg-N (LHPN) (x2)

			Hg-Cl (x2)
VISCEF	Aoki, K., *et al.*, *Inorg Chim Acta*, **1991**, 180, 117	Zn(II)	Zn-N (LHPN) Zn-NCS (x3)
VISCIJ	Aoki, K., *et al.*, *Inorg Chim Acta*, **1991**, 180, 117	Cd(II)	Cd-O (OH tail) Cd-NCS (x3) Cd-SCN (x2)
YUBNAK	Casas, J.S., *et al.*, *Inorg Chem*, **1995**, 34, 2430	Cd(II)	Cd-N (LHPN) Cd-Cl (x3) Cd-O (OH tail)
ZADCAI	Casas, J.S., *et al.*, *Polyhedron*, **1995**, 14, 1825	Cd(II)	Cd-N (LHPN) (x2) Cd-Cl (x4)
ZADCAI01	Marsh, R.E., *Acta Crystallographica, Section B*, 1999, 55, 93	Cd(II)	Cd-N (LHPN) (x2) Cd-Cl (x4)

[a] LHPN = least hindered pyrimidine nitrogen

Table 16: Survey of silver-porphyrin interactions in CSD version 5.40 (Nov 2018)

CSD Code	Reference	Av. Ag-N (Å)
ABOSOZ	Ishii, T., *et al.*, *Inorg Chim Acta*, **2001**, 317, 81	2.089
AYOHOM	Liao, J.-X., *et al.*, *Acta Crystallographica Section E*, **2011**, 67, m1316	2.084
BICQUZ	Wong, W.-K., *et al.*, *Dalton Transactions*, **1999**, 615	2.094
BOPVUY	Epple, L. *et al.*, *Fullerenes, Nanotubes, Carbon Nanostructures,* **2009***, 67*	2.088
DOWRAI	Scheidt, Y.-J., *et al.*, *Inorg Chem*, **1986**, 25, 795	2.092
LICRAR	Xu, Y.-J., *et al.*, *Acta Crystallographica Section E*, **2007**, 63, m1437	2.099
QAKTUR	Senge, M.O., *et al.*, *Tetrahedron*, **2000**, 56, 8927	2.087
QOMCUR	Epple, L., *et al.*, *Chem Comm*, **2008**, 5610	2.093
QOMCUR	Epple, L., *et al.*, *Chem Comm*, **2008**, 5610	2.101
RUVHEX	Jiang, W., *et al.*, *Chem Comm*, **2016**, 52, 1373	2.080
TEJBAO	Singh, A. K., *et al.*, *Ange Chemie, Intl Ed*, **2017**, 56, 8849	2.091
TEJBAO	Singh, A. K., *et al.*, *Ange Chemie, Intl Ed*, **2017**, 56, 8849	2.095
TEJBES	Singh, A. K., *et al.*, *Ange Chemie, Intl Ed*, **2017**, 56, 8849	2.025
TEJBES	Singh, A. K., *et al.*, *Ange Chemie, Intl Ed*, **2017**, 56, 8849	2.089
TEJBOC	Singh, A. K., *et al.*, *Ange Chemie, Intl Ed*, **2017**, 56, 8849	2.031
TEJBOC	Singh, A. K., *et al.*, *Ange Chemie, Intl Ed*, **2017**, 56, 8849	2.035
TPSTPP	Schneider, M.L., *Dalton Transactions*, **1972**, 1093	2.063
UPOTEZ	Carlucci, L., *et al.*, *J Porphyrins Phthalocyanines*, **2010**, 14, 804	2.071
UPOTID	Carlucci, L., *et al.*, *J Porphyrins Phthalocyanines*, **2010**, 14, 804	2.080
XIQLAN	Wand, H.-H., *et al.*, *Chinese Chem Lett*, **2018**, 29, 1404	2.099
XOMCIM	So, M.-H., *et al.*, *Chem Asian J*, **2008**, 3, 1968	2.084

Appendix 2.9.4 Size exclusion column calibration and molecular weight markers

Table 17: SEC calibration proteins (Figure 21, blue series), molecular weights and concentrations of solutions injected onto the column. GE standards were diluted in HEPES buffer from 20 mg/mL to desired concentration.

Protein	Molecular weight [kDa]	Concentration [mg/mL]	Source
Thyroglobulin	669	5	Gel filtration HMW calibration kit (product ID: 28403841, GE Healthcare Life Sciences, US
Ferritin	440	0.3	
Conalbumin	75	3	
Carbonic anhydrase	30	3	Gel filtration LMW calibration kit (product ID: 28403842, GE Healthcare Life Sciences, US
Ribonuclease A	13.7	3	
Aprotinin	6.5	3	
Bovine serum albumin (BSA)	66.5	1	Sigma Aldrich, CAS 9008-02-0, lyophilized powder
Human haemoglobin (Hb)	64.5	1	Sigma Aldrich, CAS 9048-46-8; ≥98.0%

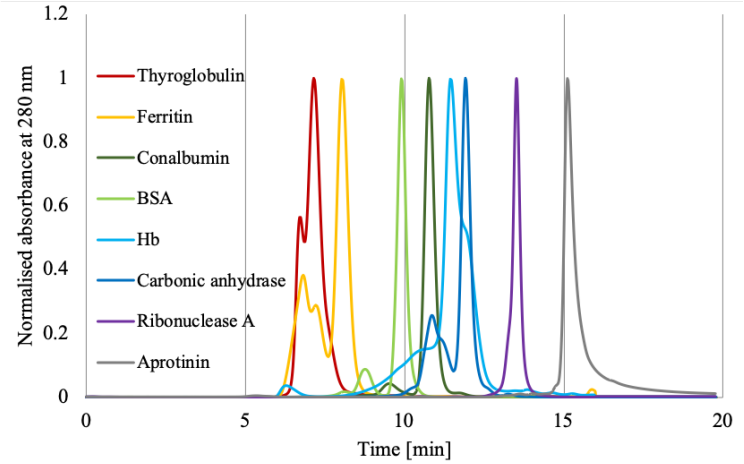

Figure 20: Normalised size exclusion chromatograms of protein standards. Agilent AdvanceBio SEC 300Å column (7.8 x 300 mm I.D.; 2.7 µm particle size); temperature: ~20°C; mobile phase: 100 mM HEPES, pH 7.4; flow rate: 0.3 mL/min; injection volume: 10 µL; detector: Agilent Infinity 1200 variable wavelength detector set at 280 nm. Naturally occurring thyroglobulin dimer (shoulder on low retention time edge of monomer peak, MW ~1338 kDa) was identified as the void volume of the column. Calibration protein standards used are shown in **Table 17**.

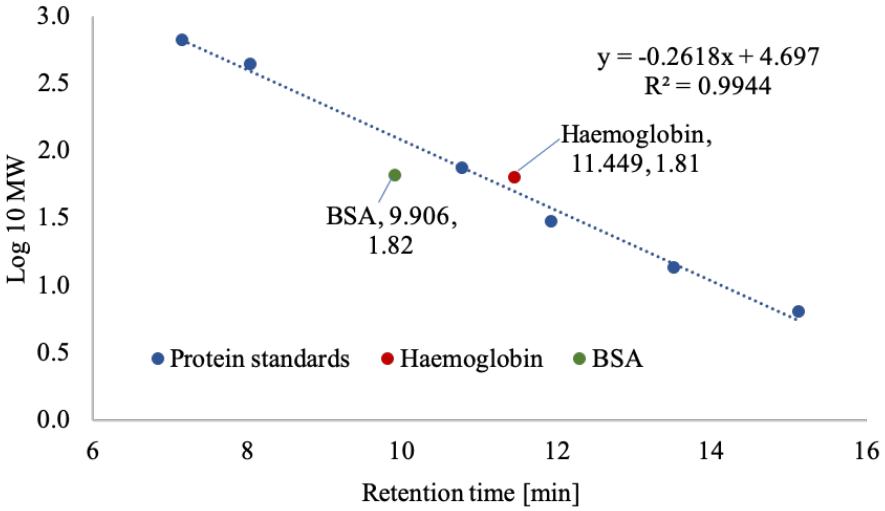

Figure 21: Calibration curve of $\log_{10}$ protein standard molecular weights and retention times, as determined by monitoring column effluent at 280 nm. Agilent AdvanceBio SEC 300Å column (7.8 x 300 mm I.D.; 2.7 µm particle size); temperature: ~20°C; mobile phase: 100 mM HEPES, pH 7.4; flow rate: 0.3 mL/min; injection volume: 10 µL; detector: Agilent Infinity 1200 variable wavelength detector set at 280 nm.

Chapter Three: The biochemical fate of silver ions in human blood

3.1 Abbreviations

AS	Australian Synchrotron
BSA	bovine serum albumin
CSD	Cambridge Structural Database
Cys	cysteine
EXAFS	extended X-ray absorption fine structure
FCS	foetal calf serum
FT	Fourier transform
GSH	glutathione
Hb	haemoglobin
HEPES	4-(2-hydroxyethyl)-1-piperazinethane sulfonic acid
HSA	human serum albumin
LCF	linear combination fitting
PCA	principal component analysis
RBC	red blood cell
v_i	inclusion volume
v_o	void volume
WHO	World Health Organisation
XANES	X-ray absorption near-edge structure
XAS	X-ray absorption spectroscopy

3.2 Introduction

Historically 'lunar caustic' (silver nitrate) was applied to wounds to aid healing.[1] During the First World War, silver salts were used to treat burns or wounds to 'cleanse them'.[2] However, the discovery of molecular antibiotics in the early 20th century led to a decline in use of silver. A lack of novel antibiotic drug discovery or research, coupled with over prescription and misuse, has seen the efficacy of these drugs waning as bacteria develop resistances against them.[3] Rising concern over an antibacterial resistance crisis has seen an increase in materials for medical and commercial use which contain silver to imbue them with bactericidal properties.[4] While silver has traditionally been viewed as non-toxic to humans, adverse side effects have been reported if used inappropriately.[5-11] Chronic exposure to silver leads to a condition called argyria, the primary symptom of which is the permanent subdermal deposition of silver as Ag(0) and sulfides which gives the person a blue appearance.[6] Several case studies involving chronic exposure of

individuals to silver show a mixture of symptoms, ranging from staining of the skin (but otherwise asymptomatic), to weight loss, anaemia, contraction of secondary infections (pneumonia), and neurodegenerative conditions.[9-10, 12] Mice receiving daily silver 'supplementation,' displayed reduction in ceruloplasmin activity, and infertility, from which the mice recovered when silver dosing was stopped.[13] Conversely, inclusion of silver in some prosthetic implants has been shown to have no adverse effects on the recipient while preventing bacterial infection and increasing wound healing or showing no adverse effects.[14] To better understand the reported variability and inconsistency between *in vivo* and *in vitro* results, a greater understanding of the biochemical fate and speciation of silver in biological systems is needed.

Three main routes of exposure to silver exist: dermal, inhalation, and ingestion, all of which bring the metal in close proximity to the vascular system.[15] Patients treated with silver-based wound dressings or implants have been shown to have elevated plasma silver concentrations, indicating that the metal is not localised to a wound site once used.[16] Particulate silver lodged in the lungs can undergo oxidative dissolution and the released silver ions absorbed into the blood stream *via* the alveoli.[17] Finally, if ingested, approximately 10 to 20% of the total silver consumed is absorbed from the small intestines into the blood stream while the remaining amount is excreted from the body.[18] As such, the speciation and biochemical fate of silver ions in human whole blood is important to understand when considering the metal's interaction with humans.

Previous studies concerning the effect of silver ions in blood have found that the metal can lyse red blood cells (possibly by scrambling membranes and lipid peroxidation), disruption of KCl efflux, impede clotting and reduce cellular ATP concentrations.[19-20] In the case of AgNPs, unless intravenously injected, only silver ions released from the particles are expected to be present in the vascular system. Once in the blood, it has been suggested that Ag^+ could interact with reduced thiolates and proteinaceous species as well as formation of chloride salts.[21-22] However, such studies were only conducted *via* dynamic light scattering techniques which provide little to no information on chemical speciation.

3.2.1 Research aims

With increased use of silver in medical and commercial spheres, the rate of human exposure to the metal has increased. While only mildly toxic against mammals or humans the speciation of the metal within these systems is important to understand as adverse effects of the use of silver have been reported.[5, 7-11, 23]

We aim to investigate the biochemical fate of silver ions in human whole blood and related biological fluids. Analysis of a sub-population of the whole blood proteome (the metalloproteome) could aid in identification of specific silver-binding targets. Localisation of silver in whole blood was also investigated. To ensure only biologically relevant silver interactions were recorded, metallomics techniques were used, namely, X-ray absorption spectroscopy (XAS), and size exclusion chromatography coupled with ICP-MS (SEC-ICP-MS). Limited speciation studies regarding the interaction between silver ions and whole blood or mammalian biological fluids have been reported. However, other inorganic species in blood or relevant fluids have been investigated through use of metallomics techniques like X-ray absorption spectroscopy (XAS), and size exclusion chromatography coupled with ICP-MS or ICP-AES (SEC-ICP-MS/AES).

3.2.2 X-ray absorption spectroscopy

While not directly related to speciation of silver in blood, an XAS study to investigate the speciation and distribution of silver in marine mammals indicated that Ag_2S or Ag_2Se species predominated in the animals' livers.[24] The minimal sample preparation required means that there is little risk of perturbation of naturally occurring species or introduction of processing artefacts. Another study involved the collection of hair and blood from citizens of a town in China which is in close proximity to a mercury mine.[25] Analysis of the Hg L_3-edge of the samples revealed that while inorganic Hg^{2+} was the dominant species in hair (~92%), there was a 50:50 split between methyl mercury and Hg^{2+} in the blood.

The use of XAS is not limited to toxicants or heavy metals, a species of worm *Ascidia certodes* (*A. ceratodes*) is known to have naturally high concentrations of vanadium in its blood.[26] Analysis of the V K-edge of two different species known to be closely related but geographically isolated indicated that the two organisms had significantly different vanadium blood chemistry. In another study by the same group on the same organism, sulfur K-edge XAS enabled a greater understanding of the range of different sulfur-containing species in the worm's blood.[27]

Speciation of a drug or supplement is an important consideration for human health and the efficacy of the administered medicine. An XAS study regarding the biochemistry of non-toxic chromium(III) supplements, purported to have antidiabetic properties, showed that the Cr(III) species induced oxidative stress in the blood and was oxidised to toxic Cr(VI) or Cr(V) oxidation states, presenting potentially health risks.[28]

It has also been shown by XAS that the breakdown of various vanadium(V) and (IV) anticancer and antidiabetic drugs in human blood result in the formation of the same V-containing metabolic products.[29] By principal component analysis and linear combination fitting the vanadium metabolite was found to be in the (IV) oxidation state, coordinated by carbohydrate/citrate-like ligands (65-85%), as well as in the (V) oxidation state bound by protein (15-35%).

XAS can also be used to characterise the binding sites of a metal ion in a purified sample of protein or biomolecule, for example, Sendzik *et al*., identified a Cu^{+} binding site on human serum albumin (HSA).[30] Analysis of the Cu K-edge EXAFS showed the Cu^{2+} was bound by the ATCUN motif and, upon reduction with ascorbate, Cu^{+} was bound by a different site consisting of two histidine residues. Long range backscattering interactions can sometimes be observed in the EXAFS Fourier Transform (FT) if the analyte is coordinated by a rigid, planar species (like a histidine imidazole).

The binding interactions of silver ions in proteins known to be involved in copper homeostasis were probed by XANES and EXAFS analysis of the Ag K-edge.[31] Silver was found to be bound by the Cu^{+} binding loop of the copper chaperone Atox1, namely digonal binding with two cysteine residues. Also investigated was the silver coordination in rabbit and yeast metallothioneins, which were dominated by Ag-S interactions typical of AgS_3 geometry.

3.2.3 Size exclusion chromatography hyphenated with ICP-MS

Size exclusion chromatography enables the separation of complex samples based on the components' hydrodynamic radius, which can be correlated to molecular weight.[32] Hyphenation of SEC with a secondary analytical technique like ICP-MS or ICP-AES allows visualisation of metal-bound species and estimation of molecular weight. Simultaneous detection of multiple analytes by ICP-MS provides some deconvolution of eluting species in the biological sample. Regarding silver, a solitary study investigating the fate of Ag^{+} and AgNPs in *E. coli* by use of SEC-ICP-MS has been reported.[33] However, speciation experiments of other inorganic analytes in whole blood or related biological fluids have been carried out.

Copper, zinc, and iron are essential micronutrients for all organisms and are involved in a range of biological processes. In 2009, Manley, *et al.*, analysed healthy human plasma by SEC-ICP-AES and identified multiple Cu/Zn/Fe metalloproteins; including, ceruloplasmin, human serum albumin, and possible superoxide dismutases.[34] In the study a peak in the iron trace was thought to correspond to the Fe storage protein

ferritin, but was recently confirmed to be the first identification of the haptoglobin-haemoglobin complex[35] which serves to free haemoglobin from reaching the kidneys.[36] Such findings, and identification of important plasma proteins in healthy individuals, could allow for non-invasive blood screening and diagnosis of diseases associated with metal-binding plasma proteins.[37] For example, a patient with Wilson's disease will characteristically have low ceruloplasmin plasma levels, conversely, a person with hemochromatosis (an overload of iron) will typically have elevated holo transferrin levels.[38-39]

In addition to monitoring biologically relevant metal ions, the technique can shed light on important biochemical processing of toxic heavy metals in blood. Gibson *et al.*, investigated the fate of Cd^{2+}, Hg^{2+}, CH_3Hg^+, and thimerosal in red blood cell lysate by SEC-ICP-AES.[40] They identified that the majority of cadmium was associated with haemoglobin (Hb) (85%) with a much smaller proportion associated with reduced glutathione (~13%). The inverse was found to be true for Hg^{2+} with only 6% Hg eluting with Hb and 94% bound as GSH complexes, confirming previously trends reported for the speciation of the metals in RBCs.[41-42] The biochemical fate of methyl mercury and thimerosal was found to be similar to mercuric ions with 5-12% associated with haemoglobin after 6 hours and the authors posited that the interaction between the heavy metal and Hb could be a source of its toxicity against mammals. Additionally, the study was supported by Hg L_3-edge X-ray absorption spectroscopy which indicated the metal was predominantly bound by sulfur.

Combination therapy of two metal-based anticancer drugs, cisplatin (Pt) and NAMI-A (Ru), has been demonstrated to be more effective in treatment of lung metastasis than when administered alone.[43] SEC-ICP-AES was used to determine, in human plasma, whether exposure to both drugs resulted in unfavourable or toxic metabolites.[44] The technique also indicated that the two drugs have distinct metabolic and hydrolytic chemistries in plasma; cisplatin largely remained as the molecular species with a minor component consisting of protein bound species, conversely, NAMI-A was immediately hydrolysed and bound by plasma proteins (<10 min post exposure).

The technique can also be used to guide drug design under a similar premise to the above study. Harper *et al.*, investigated the degradation products of a range of platinum-containing complexes in the presence of glutathione spiked rabbit plasma over time which allowed selection of the species least susceptible to inhibition in plasma.[45]

3.3 Methods and procedures

Materials

Silver nitrate (CAS 7761-88-8; >99%); 4-(2-hydroxyethyl)-1-piperazinethanesulfonic acid (HEPES; CAS 7365-45-9; >99.5%); human haemoglobin (CAS 9008-02-0, lyophilized powder); bovine serum albumin (CAS 9048-46-8; ≥98.0%); L-cysteine (CAS 52-90-4; 97%); L-methionine (CAS 63-68-3; ≥98%); thiamine mononitrate (CAS 532-43-4; ≥98%); L-histidine (CAS 71-00-1; ≥99%); glycine (CAS 56-40-6; ≥99%); biotin (CAS 58-89-5; ≥99%) were purchased from Sigma Aldrich. Thyroglobulin; ferritin; aldolase; conalbumin; carbonic anhydrase; ribonuclease; aprotinin; ovalbumin were purchased from GE Healthcare, Life Sciences. Ultra-pure MilliQ water (Merck Millipore purification system) with resistivity of 18 MΩ.cm^{-1} was used. All chemicals were used as received.

Methods

General experimental

Buffers

HEPES (100 mM) was prepared by dissolving the relevant solid in the appropriate volume of ultra-pure water. The pH was adjusted to 7.4 by the addition of NaOH (6M) (Orion Star pH Meter, Thermo Scientific). For size exclusion experiments, the mobile phase was passed through a 0.45 μm nylon-membrane filter before use.

SEC-ICP-MS

The SEC-ICP-MS was comprised of a high-performance liquid chromatography (HPLC) pump (Agilent 1200 Infinity Series, Santa Clara, CA, USA) and an inductively coupled plasma mass spectrometer (Agilent QQQ 8900, Santa Clara, CA, USA). A prepacked Agilent AdvanceBio SEC 300Å size exclusion column (7.8 mm x 300 I.D., particle size: 2.7 μm, fractionation range 1200 – 5 kDa) was used with a 100 mM HEPES mobile phase at a flow rate of 0.3 mL/min (column temperature: ~20°C). The void volume (v_o) and inclusion volume (v_i) were determined by the injection of thyroglobulin – which naturally contains the thyroglobulin dimer (t_r = 6.75 min), and aprotinin (t_r = 15.13 min), respectively; each detected by a variable wavelength detector (1200 series, VWD, Agilent) measuring absorbance of the column effluent at 280 nm. Protein standards used to construct a calibration curve were thyroglobulin (5 mg/mL), ferritin (0.3 mg/mL), conalbumin (3 mg/mL), ribonuclease A (3 mg/mL), and aprotinin (3 mg/mL) (GE Healthcare).

X-ray absorption spectroscopy

Data collection. Silver K-edge X-ray absorption spectra were recorded on the X-ray absorption spectroscopy (XAS) beamline at the Australian Synchrotron (AS), Victoria, Australia. The energy of the electron beam was 3.0 GeV with a current of ~200 mA, and an X-ray beam was sourced from a wiggler, monochromated by the Si(111) monochromator, and harmonic rejection achieved using a rhodium-coated mirror. Samples were positioned at ~45° to a 100-element germanium fluorescence detector which was placed at 90° to the incident beam. The energy ranges used for EXAFS spectra collection were: pre-edge region 25.3140 – 25.4941 keV (0.003 eV steps); XANES region 25.4941 – 25.5641 keV (0.0003 eV steps); and EXAFS region 25.5641 – 25.700 keV. During data collection the samples were maintained at a temperature of ~ 10 K using a Cryo Industries (Manchester, NH, USA) cryostat. The spectrum of a silver foil, recorded in transmission downstream from the sample, was used as an internal standard to calibrate the energy scale for the first peak of the first derivative of the elemental silver edge (25.5156 keV). 1 to 4 scans per sample were collected for EXAFS spectra.

Data analysis. Calibration, averaging, background subtraction of all spectra and principle component, target, and multiple linear regression analyses of XANES spectra were performed using the EXAFSPAK software package (G. N. George, SSRL). Single and multiple-scattering fits of EXAFS data were carried out using EXAFSPAK and the FEFF8 code.[46] The model compounds for target analysis and XANES linear combination fitting were prepared, and spectra recorded at the AS, Victoria, Australia.

Model spectra. Glassed solutions of relevant amino acids, B vitamins, and proteins in 100 mM HEPES buffer were used to obtain model spectra for XANES fitting of biological samples and EXAFS analysis. The amino acid and vitamin samples had a molar ratio of 5:1 with a 2 mM final concentration of silver. Protein models had a molar ratio of 2:1 ligand to metal with a final silver concentration of 2 mM.

Human blood

3.1 Blood collection

Whole blood donated by the author, was collected into heparin-coated Vacutainer tubes (Becton Dickinson), stored on ice prior to experimentation, and used within 1 h of collection.

3.2 Silver localisation study

A silver nitrate stock solution (50 mM, 40 μL) was added to whole blood (960 μL) and incubated (37°C, 200 rpm, 60 min). The sample was centrifuged (4000 rpm, 5 min, 4°C), the plasma and RBCs separated, and stored on ice. The procedure was carried out simultaneously on six samples of whole blood which differed in the time of incubation with silver nitrate (5, 10, 20, 30, 40, 50 min). A zero min sample was prepared by the addition of silver nitrate to an ice-cold sample of blood followed by immediate centrifugation (as above). The RBCs were lysed by diluting the sample in HEPES buffer (1:4). The concentration of silver in both the plasma and red blood cell fractions was determined by AAS.

3.3 X-ray absorption spectroscopy of human blood

A portion of the blood collected in *3.1* was centrifuged (2000 rpm, 10 min, 4°C) and the supernatant plasma removed to be used as a sample of isolated plasma. A silver nitrate solution (50 mM) in MilliQ water was prepared in the hour preceding the experiment and added to whole blood (20 μL), isolated plasma, or serum to give a final volume of 0.5 mL, and a final Ag(I) concentration of 2.0 mM.

Two whole blood samples were centrifuged (2000 rpm, 10 min, 4°C) to separate the plasma and RBC fractions for 'whole blood – plasma/RBC fraction' samples. All samples were loaded, neat, into Lucite XAS samples holders, secured with Kapton tape, flash frozen to form a glass and stored at -180°C until analysis.

3.4 SEC-ICP-MS

Whole blood (960 μL) was treated with silver nitrate (50 mM, 40 μL) and incubated (37°C, 200 rpm, 1 h). The sample was briefly cooled on ice, centrifuged (4,000 rpm, 4°C, 5 min), and the plasma and RBC fractions isolated. The RBC fraction was diluted in HEPES buffer (1:10) and the cells lysed (BioRuptor, 8°C, 15 min). Both the

plasma and lysed RBCs were centrifuged (14,000 rpm, 4°C, 15 min) to remove cellular detritus and unlysed cells prior to SEC experiments.

To prepare a blood sample with low silver concentration whole blood (984 μL) was spiked with silver nitrate (6 mM, 16 μL) and treated as above. The plasma fraction was isolated and used for SEC analysis.

To assist the identification of haemoglobin (Hb) and human serum albumin (HSA), a solution of each (bovine serum albumin used in lieu of HSA) (3 mg/mL) was injected (10 μL) onto a SEC column (300 Å, 0.3 mL/min, ~280 bar) and the UV absorbance monitored at 280 nm (t_r = 11.47 min, Hb; t_r = 9.92 min, BSA).

3.4 Results

X-ray absorption spectroscopy

XANES of silver in blood

The Ag K-edge XANES of human blood and related biological fluids spiked with $AgNO_3$ are displayed in **Figure 1**. A range of post-edge shapes and features were observed which could be loosely grouped thusly: spectra (**a**) to (**e**), which displayed low intensity oscillations with few distinct features, and spectra (**f**) and (**g**) with intense, high-frequency oscillations which were consistent between the two samples.

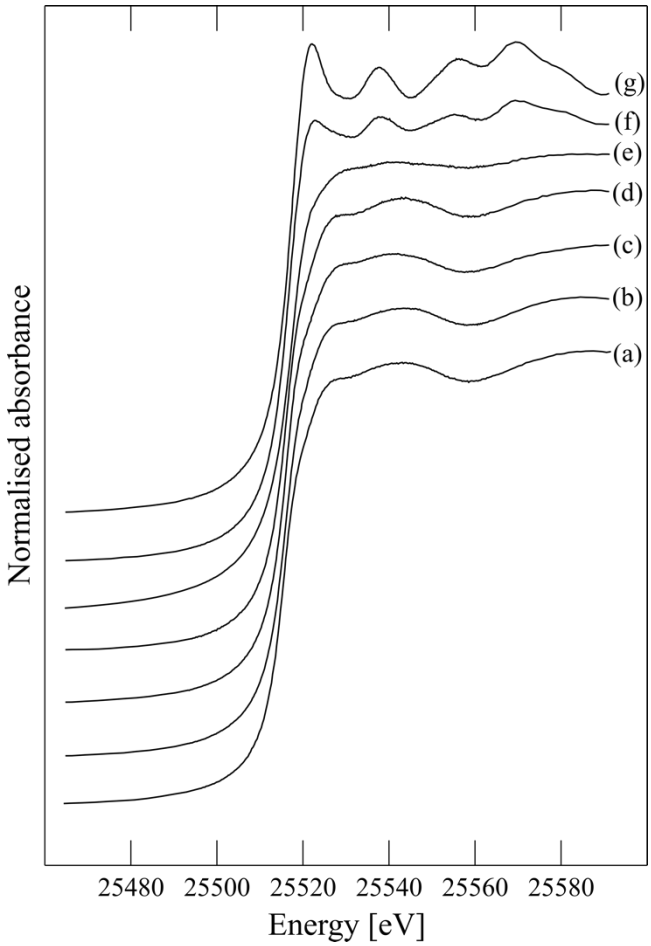

Figure 1: Ag K-edge XANES spectra of biological fluids incubated at 37°C with 2 mM $AgNO_3$ for 1 hr: (**a**) human whole blood; (**b**) RBC fraction from whole blood; (**c**) plasma fraction from whole blood; (**d**) RBC lysate; (**e**) precipitate that formed when $AgNO_3$ was added to (d) and subsequently isolated by centrifugation; (**f**) isolated plasma; (**g**) foetal calf serum.

Fresh human whole blood was spiked with silver nitrate to a final concentration of 2 mM, and incubated at 37°C for 1 hr; the Ag K-edge XANES are displayed in **Figure 1a**. Additional samples of whole blood were treated as above and separated into plasma and red blood cell (RBC) fractions, **Figure 1b** and **c**, respectively. The three whole blood samples (**a**), (**b**), and (**c**) displayed similar XANES features including a change in the slope

of the rising edge at ~25,518 eV (seen previously for nitrogen-coordinated species **Chapter 2**), the energy of the peak atop the rising edge (25,525 eV) and a trough at 25,560 eV. However, the first and second broad post-edge peaks at 25,545 and 25,585 eV shifted by -5 eV and +10 eV, respectively, between the RBC and plasma spectra.

To investigate possible changes in speciation of silver in processed biological fluids, (such as RBC lysate), relative to whole blood, the Ag K-edge XANES of RBC lysate spiked with $AgNO_3$ (post-lysis) was recorded (**Figure 1d**). The spectra of the RBC fraction of whole blood (**b**), and RBC lysate (**d**) were similar, with all significant post-edge features (including the change in the slope of the rising edge at 25,525 eV) consistent between them. However, the first two post-edge peaks of the RBC lysate were moderately more intense than those of the RBC fraction isolated from whole blood that had been spiked with $AgNO_3$.

The similarity of the whole blood RBC spectrum and that of the RBC lysate was unexpected as the addition of the silver nitrate solution to the lysate generated a significant amount of reddish-black precipitate. The precipitate was isolated, freeze-dried and XANES recorded (**Figure 1e**). The XANES spectrum of the precipitate was, overall, flat and featureless, however, a peak atop the rising edge (25,530 eV), a subsequent peak at 25,540 eV, and a trough at 25,560 eV were discernible; all features shared by spectra (**a**) to (**d**).

Other processed biological fluids such as isolated plasma, and foetal calf serum (FCS) were also incubated with $AgNO_3$ at 37°C for 1 hr. The Ag K-edge XANES of both the isolated plasma (**Figure 1f**) and FCS (**g**) had very different post-edge features compared to the RBC lysate/precipitate and whole blood samples. The intensity of the peaks in the spectrum of isolated plasma were lower in intensity than those of the FCS XANES. Strong post-edge oscillations continuing to high energy suggested a well-ordered local environment around the absorbing silver atoms, e.g. a solid/colloid.

Principal component analysis (PCA) of the blood XANES dataset presented in **Figure 1** indicated that three to four spectral components were required for the data to be adequately described. Target transformation of the blood XANES spectra against a library of model Ag K-edge XANES spectra allowed qualitative identification of species that may have been present in each experimental sample. Visually, the XANES of solid silver chloride, aqueous silver-cysteine, silver-haemoglobin, and silver-BSA models shared features with those of the experimental blood dataset. The ratio of each model spectrum required to describe the experimental spectra was calculated by linear combination fitting (LCF) (**Table 1** & **Figure 2**).

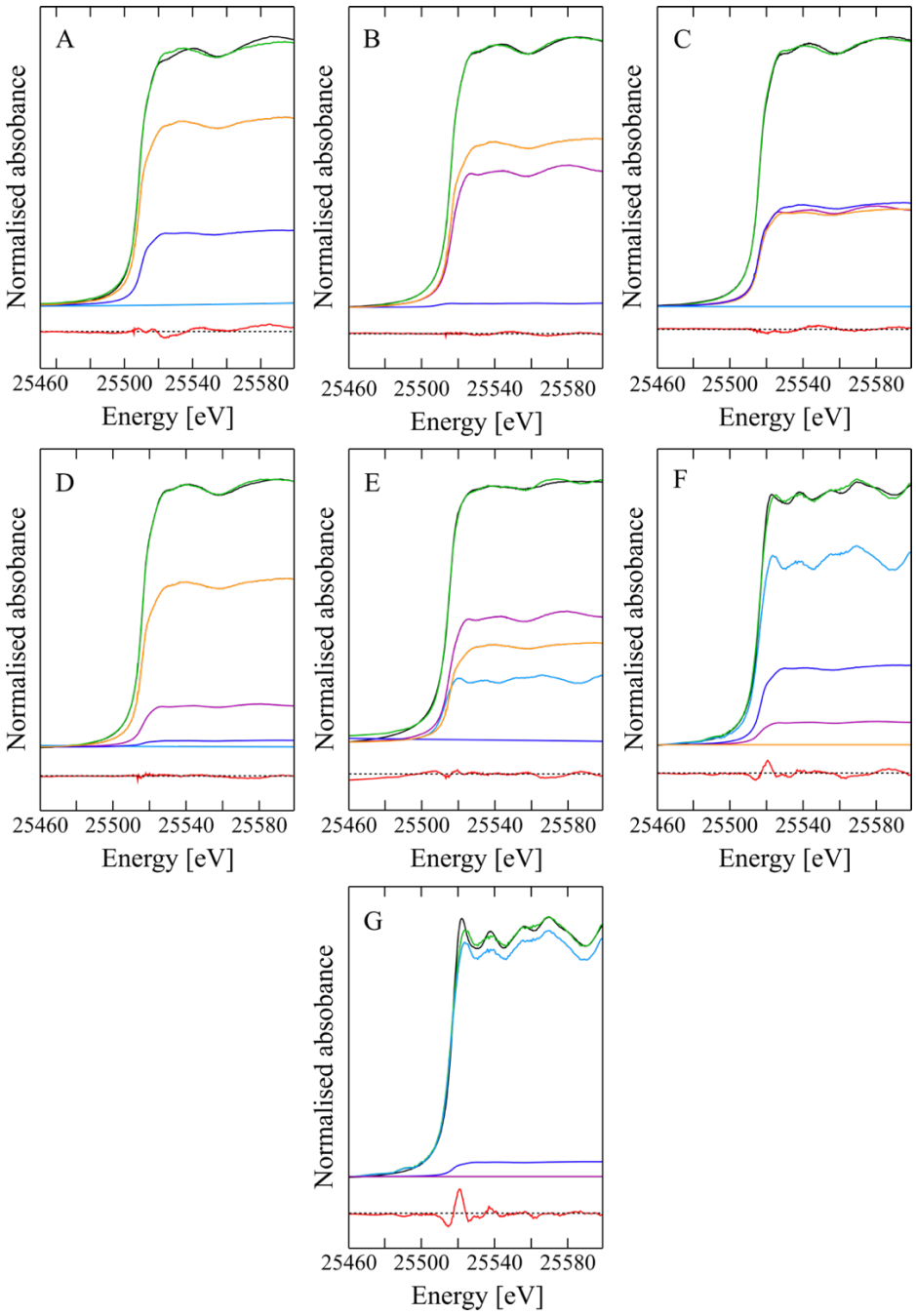

Figure 2: Linear combination fits of Ag K-edge XANES of biological fluids incubated at 37°C with 2 mM $AgNO_3$ for 1 hr: (**A**) human whole blood; (**B**) RBC fraction from whole blood; (**C**) plasma fraction from whole blood; (**D**) lysed RBCs; (**E**) precipitate that formed when $AgNO_3$ was added to (D) and subsequently isolated by centrifugation; (**F**) isolated plasma; (**G**) foetal calf serum. The experimental spectra (**black**) were fit with a linear combination fit (green) comprised of model XANES spectra of silver-BSA (dark blue), silver-haemoglobin (orange), solid bulk silver chloride (light blue), silver-cysteine (purple) with the residual (red) shown offset. Numerical results of linear combination analysis are shown in **Table 1**.

Silver chloride was found to be the dominant contribution in the silver-spiked isolated plasma and FCS XANES (**Figure 2F** and **G**), accounting for 65 and 95% of the experimental spectra, respectively. The second largest contribution was from BSA (27 and 5%, respectively), while cysteine (Cys) contributed ~8% of the isolated plasma (**Table 1** &

Figure 2). While it was evident that silver chloride was a large component of the isolated plasma and FCS samples, the model spectrum of bulk solid silver chloride was not a perfect model for the experimental spectra. Upon addition of silver nitrate to isolated plasma or FCS no white, flocculent precipitate was observed (which would be expected for precipitation of AgCl). This would suggest that the silver chloride in solution may have formed nanoparticles/a colloidal suspension or possibly existed as a charged polychloride species (e.g. $AgCl_2^-$/$AgCl_3^{2-}$, etc.). The latter, however, would not be expected to display similar XANES features to that of solid AgCl as polychlorido silver would likely exist as discrete, water-soluble species. While the post-edge features of the plasma and FCS XANES shared clear similarities with that of bulk silver chloride, the intensities of the oscillations in the bulk AgCl XANES did not match those of the experimental samples; a phenomenon previously observed for nanoparticulate species vs. bulk material.[47-48] Haemoglobin (Hb) was included in the LCF of isolated plasma and FCS spectra but found to have negligible contributions.

Table 1: Calculated ratios of Ag species in biological fluids treated with 2 mM $AgNO_3$ and incubated for 1 hr at 37°C, as estimated by linear combination of model XANES spectra.[a]

Sample	Ratio of component fitted				N_{tot}[b]	Residual
	Haemoglobin	BSA	Cysteine	Chloride		
Whole blood	0.71(7)	0.24(7)	-	-	0.95	0.25
Whole blood – RBC	0.53(1)	-	0.45(1)	-	0.98	0.024
Whole blood – plasma	0.34(5)	0.32(6)	0.33(4)	-	0.99	0.11
RBC lysate	0.68(2)	0.049(3)	0.27(2)	-	0.99	0.021
RBC lysate ppt.	0.32(2)	-	0.43(2)	0.214(9)	0.96	0.082
Isolated plasma	-	0.27(5)	0.078(5)	0.65(2)	1.00	0.34
Foetal calf serum	-	0.051(4)	-	0.95(4)	1.00	1.19

[a]Values in parentheses are the estimated standard deviation derived from the diagonal elements of the covariance matric and are a measure of precision. [b]N_{tot} is the sum of fractions.

A high contribution from haemoglobin in the whole blood LCF (**Figure 2A**) was consistent with the general trend observed for the localisation of silver in whole blood (see localisation study, **Figure 7**), which showed that ~90% of Ag was localised in the RBCs. All fractionated whole blood or RBC lysate/precipitate XANES (**B**) to (**E**) were found to have mixed contributions from haemoglobin, BSA, and cysteine-bound silver. The linear combination fit of the plasma fraction from whole blood was approximately a three-way split between the aforementioned model spectra, including haemoglobin. Haemolysis of erythrocytes in whole blood spiked with 2 mM $AgNO_3$ was observed within 5 minutes of the addition of a solution of silver nitrate (40 μL in 960 μL of blood), regardless of

isotonicity. This meant that the plasma fraction of whole blood was contaminated with RBC cellular contents, including haemoglobin, which was identified by the LCF calculation, showing ~33% contribution from Ag-Hb (**Table 1**).

Comparison of the proportions of components fit to the RBC fraction from spiked whole blood and spiked RBC lysate (**Table 1**) showed some similarities between the two samples. The Ag-haemoglobin model had the largest contribution of both spectra followed by cysteine, and 5% BSA for the lysate. The composition of the reddish-black precipitate that formed upon addition of $AgNO_3$ into RBC lysate was found to be a mixture of species including silver bound to cysteine, haemoglobin, and chloride.

CSD survey of interactions between silver and biologically relevant moieties

A survey of the Cambridge Structural Database (CSD) was conducted for interactions between silver and biologically relevant functional groups (**Table 2**). Silver coordination spheres consisting of only one type of donor atom (i.e. only sulfur, nitrogen or oxygen) were surveyed for total coordination numbers of two, three, and four; the most common coordination numbers for silver in biological systems.[49] Across all systems investigated (bar AgO_3) an increase in total coordination number correlated with an increase in average bond length, however, a surprisingly broad range of bond lengths was observed. Additionally, the average bond lengths of sulfur (thiolate and thioether) were found to be longer than for silver to nitrogen, as would be expected based on atomic radii. However, the average Ag-carboxylate bond lengths did not follow the periodic trend. All interactions investigated resulted in broad bond length ranges (min. vs. max. values, **Table 2**) with the breadth of Ag-O interactions being the largest (2.087 to 2.981 Å for AgO_2 coordination spheres); suggesting that silver coordination bond lengths could vary widely.

The mode values of each dataset were provided to give insight into whether the calculated average bond length for each coordination sphere was representative of the most frequently occurring bond distances; the mode of datasets with low total numbers of structures were excluded (e.g. AgS_4 thiolate). For most of the datasets the mode agreed well with the calculated averages.

Table 2: Survey of interactions between silver and biologically relevant moieties in CSD version 5.40 (Nov 2018). See **Appendix 3.9.2** for 'raw' data and references.

	Coord. sphere	Number of structures	Av. distance (Å)	Std. dev. (Å)	Min. (Å)	Max. (Å)	Mode (Å)
Thiolate	AgS_2	57	2.39	0.03	2.29	2.48	2.37
	AgS_3	21	2.53	0.03	2.46	2.57	2.52
	AgS_4	6	2.58	0.05	2.50	2.63	-
Thioether	AgS_2	12	2.45	0.06	2.41	2.64	-
	AgS_3	10	2.53	0.02	2.51	2.57	-
	AgS_4	42	2.59	0.03	2.51	2.69	2.58
Amine	AgN_2	110	2.18	0.08	2.05	2.51	2.14
	AgN_3	29	2.30	0.04	2.23	2.43	2.29
	AgN_4	44	2.37	0.10	2.15	2.48	2.40
Carboxylate	AgO_2	108	2.35	0.15	2.11	2.75	2.12
	AgO_3	30	2.32	0.07	2.24	2.59	2.31
	AgO_4	10	2.38	0.05	2.33	2.51	-

Speciation of silver with human haemoglobin and bovine serum albumin

Two of the most abundant proteins in human blood are haemoglobin (309 g/L in healthy RBCs)[50] and human serum albumin (HSA) (36-53 g/L).[51] Thus, understanding the association of silver with these proteins in isolation is useful when considering the speciation of silver in whole blood. Bovine serum albumin was used in lieu of HSA as the two proteins share a sequence similarity of 76% and are considered analogous biomolecules.[52] The silver K-edge EXAFS spectra of BSA and Hb in buffered solutions with 2 mM $AgNO_3$ are shown in **Figure 3**. Only a two-fold excess of protein relative to silver was used as this was the highest ratio achievable before protein solubility issues arose. The Fourier Transforms (FTs) of the BSA and Hb EXAFS displayed three resolved peaks centred around ~2 Å, the relative intensities of which varied between each sample. Additionally, the width of the most intense peak in the BSA sample was greater than for haemoglobin. The EXAFS oscillations (**Figure 3**, **left panel**) for BSA were not evident beyond 12 $Å^{-1}$ while the oscillations of the Hb spectrum were present up to 14 $Å^{-1}$.

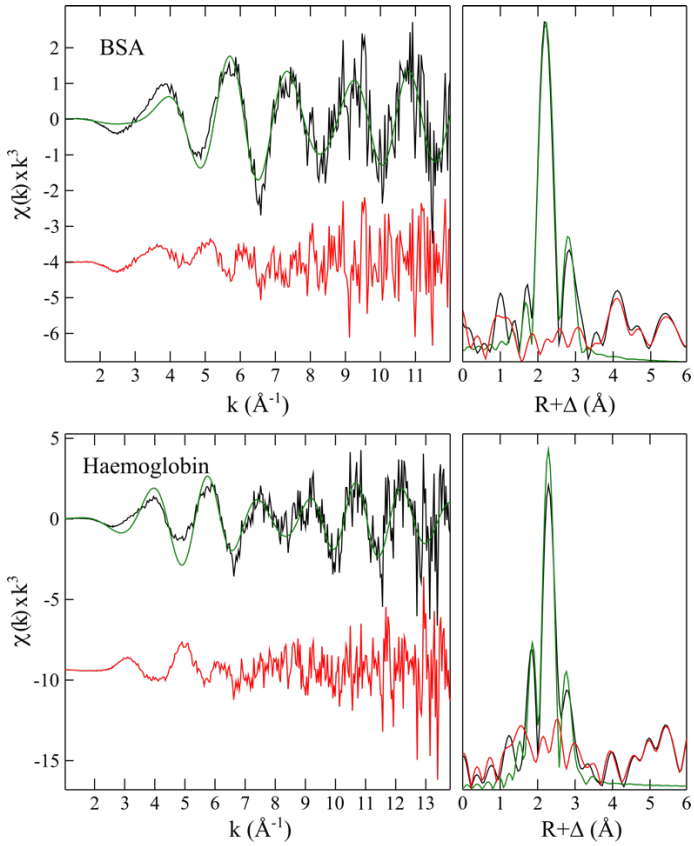

Figure 3: Ag K-edge EXAFS spectra (left panel) and corresponding Fourier Transform (right panel) of bovine serum albumin (BSA) (**top**), and human haemoglobin (**bottom**) in buffered solutions of silver nitrate (final metal to protein ratio of 1:2), showing experimental (black) and calculated (green) data with the residual (red) shown offset. Fit parameters are shown in **Table 3**.

The parameters fit to the EXAFS in **Figure 3** are summarised in **Table 3**. Both the haemoglobin and BSA spectra were successfully fit with S_2N/O silver coordination spheres with short and long silver-sulfur interactions. Variation in fit error was likely due to the relative noise level of each spectrum, as evident in the fit residuals. The short Ag-S distances at 2.35 and 2.38 Å for BSA and Hb, respectively, were consistent with silver-thiolate (cysteine) interactions observed for a number of small molecule crystal structures, according to a survey of the CSD (**Table 2**). The Ag-S distances at ~2.9 Å were longer than would be expected for silver-thiolate or thioether interactions, however, only sulfur (and chlorine) backscattering atoms provided physically realistic fit parameters and visually acceptable fits. While it would not be possible to differentiate between sulfur and chlorine backscattering atoms when fitting the EXAFS, it was unlikely to be an Ag-Cl interaction as care was taken to prevent introduction of chloride anions when preparing the samples (such as use of MilliQ water and pH adjustment of buffers with HNO_3 instead of HCl, etc) to avoid precipitation of AgCl. As silver-thioether bonds tend to be longer than equivalent thiolates it was assumed that the longer Ag-S distance was due to interaction with methionine residues in the respective proteins.

A short Ag-S interaction symmetrically fit the prominent peak in the haemoglobin FT in **Figure 3**, however, the same interaction was asymmetrically fit to the BSA FT, thus an additional nitrogen/oxygen component at 2.24 Å was added. In the EXAFS FT of Hb a N/O backscatterer at 2.08 Å adequately fit the peak at ~2 Å. An Ag-N/O interaction at 2.08 Å was shorter than would be expected for amine species (**Table 2**) but matched exactly the average Ag-N distance observed in silver-porphyrin structures (average Ag-N distance: 2.08 ± 0.02 Å) (**Appendix 2.9.3**, **Table 16**). However, beyond the aforementioned bonding interaction, no evidence for the inclusion of silver in the heme porphyrin moieties of haemoglobin was observed (e.g. Ag-Fe interactions in the EXAFS, or multiple scattering interactions due to the rigid porphyrin ring). Similar short bond lengths have previously been reported for silver-imidazole (histidine), water, and carboxylate interactions (**Table 2** and **Appendix 2.9.3**). It was possible that the interaction fitted could be one, or all, of those mentioned as XAS data represents a weighted average of all silver environments.

Table 3: Parameters fit to EXAFS spectra of bovine serum albumin, and human haemoglobin in buffered solutions with silver nitrate shown in **Figure 3**.

Sample	Scatterer	CN	Distance	DWF	$-E_0$	Fit error
Bovine serum albumin	N/O	1	2.24(2)	0.003(2)	17(1)	0.60
	S	1	2.350(9)	0.006(2)		
	S	1	2.905(8)	0.007(1)		
Human haemoglobin	N/O	1	2.03(1)	0.003(1)	17(1)	0.75
	S	1	2.370(3)	0.0045(3)		
	S	1	2.93(1)	0.005(1)		

[a]k-ranges used for fitting each spectrum were: BSA 1-12 $Å^{-1}$; Hb 1-13.8 $Å^{-1}$ with scale factors (S_0^2) of 0.9. $\Delta E_0 = E_0 - 25515$ eV where E_0 is the threshold energy. Values in parentheses are the estimated standard deviation derived from the diagonal elements of the covariance matric and are a measure of precision. The fit error is defined as $[\Sigma k^6(\chi_{exp}-\chi_{calc})^2/\Sigma k^6\chi_{exp}^2]^{½}$.

Differences observed between the Ag K-edge EXAFS of buffered solutions of BSA, and Hb with silver nitrate were likely attributable to the differences in the amino acid residues present in each protein. Bovine serum albumin (and HSA) has 35 cysteine residues in its amino acid sequence, however, only one the residues exists as reduced cysteine (Cys-SH); the remaining 34 form structural disulfide bonds (Cys-S-S-Cys)[53] and are unavailable to interact with silver. As analysis of the Ag K-edge XAS identified that silver ions predominantly interacted with cysteine, the location of the metal on BSA could be pinpointed to the solitary reduced cysteine residue (Cys34) in the protein crystal structure (PDB code: 3V03).[54] The only sulfur-containing residue in BSA within proximity to Cys34 is Met87; ~8.5 Å away, sulfur-atom-to-sulfur-atom. While a linear geometry was not feasible for silver with a total coordination number of three, summing the refined silver-sulfur bond lengths together with the ionic diameter (twice the Ag^+ ionic radius – 1.7 Å) resulted in a distance of ~8.7 Å; (2.91 Å + 3.4 Å + 2.35 Å = 8.66 Å); adding weight to the possibility that Cys34 and Met87 coordinated the silver ion. Thus, binding *via* the Cys34 and Met87 residues could account for the 2.35 and 2.91 Å Ag-S distances fit to the BSA Ag K-edge EXAFS spectrum (**Table 3**). If Ag^+ ions were bound by Cys34 and Met87, several N/O-containing residues – glutamine (Gln33), tyrosine (Tyr84) or threonine (Thr83) – were present in the immediate area and available to complete the coordination sphere of silver which was identified here as S_2N/O.

Conversely, the localisation of silver in haemoglobin was less clear. While BSA is a monomeric protein, human haemoglobin is tetrameric and comprises four protein subunits with molecular weights of ~15 kDa each. Adult humans possess two to three forms of haemoglobin, the dominant 'A' form which accounts for 97% of Hb, the A_2 form,

and the residual F form retained from infancy; the 'A' form will exclusively discussed due to its prevalence and will simply be referred to as 'haemoglobin'.[55] Haemoglobin ('A' form) consists of two 'α chains' (1 Cys each), and two 'β chains' (2 Cys each) (all present as reduced Cys-SH; PDB code: 1A3N),[56-57] thus, per haemoglobin tetramer, six cysteine residues are present; three unique Cys residues, based on symmetry. The interaction of silver with the different local environments surrounding each of the three non-symmetry-related cysteine residues (Cys104, 93, and 112) would result in the EXAFS spectrum being a weighted average of silver coordination interactions. Thus, while the EXAFS fit parameters (**Table 3**) indicated similarities in silver coordination between the two proteins, each produced unique spectra.

EXAFS of silver in blood

Ag K-edge EXAFS were also collected for the blood dataset. The RBC and plasma fractions of whole blood were fit with sulfur back scatterers at similar distances (2.393 and 2.373 Å, respectively). A survey of the CSD indicated that the average silver-thiolate distance for a silver coordination number of two was 2.39 ± 0.03 Å, thus the refined distances fit to the EXAFS spectra were consistent with interactions between silver and cysteine residues. Conversely, while both spectra were successfully fit with silver back scatterers, the silver-silver distances varied between the plasma and RBC fractions. Plasma whole blood was fit with an Ag-Ag distance of 3.29 Å while the RBC fraction spectrum was fit with a shorter interaction at 2.92 Å. The absence of well-defined oscillations in the corresponding XANES spectra for plasma and RBCs (**Figure 4D** and **E**, left panel) suggested that the silver in solution remained as Ag(I) (not bulk metal or nanoparticles), thus the silver-silver interactions were likely due to bridging by cysteine sulfur atoms between multiple metal centres resulting in S-Ag-S scattering. The EXAFS FT of whole blood (**C**) appeared visually similar to the FT of the RBC fraction (**E**) and both were fit with silver and sulfur backscattering atoms. However, in the whole blood spectrum two nitrogen/oxygen interaction was also fit at appropriate bond lengths (**Table 4**).

The EXAFS of isolated plasma spiked with $AgNO_3$ (**Figure 4B**) was fit with a multiple scattering (MS) model generated from a published crystal structure of silver chloride.[58] However, upon refinement, and rejection of components that contributed less than 4% of the fit, it was revealed that the spectrum was adequately described by three single scattering interactions (**Table 4**). The coordination numbers (CNs) reported for the FCS and isolated plasma spectra were determined by the 'best-integer fits' function of EXAFSPAK with all other parameters floated to identify the CN that provided the lowest fit-error.

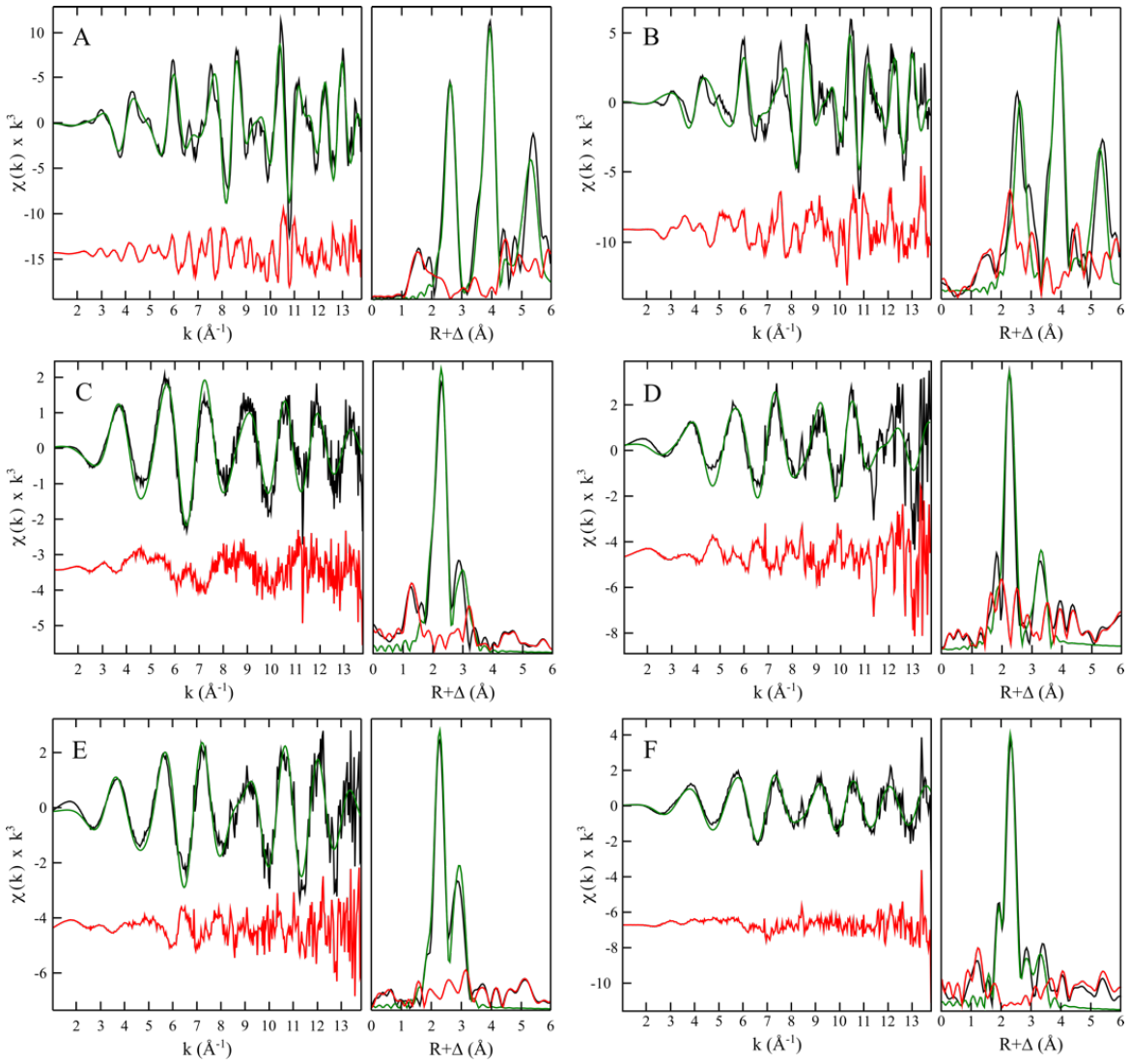

Figure 4: Ag K-edge EXAFS spectra (left panel) and corresponding Fourier Transform (right panel) of biological fluids treated with 2 mM $AgNO_3$ and incubated at 37°C for 1 hr: (**A**) foetal calf serum, (**B**) plasma isolated from whole blood, (**C**) whole blood, (**D**) plasma fraction from whole blood, (**E**) RBC fraction from whole blood, and (**F**) RBC lysate, showing experimental (**black**) and calculated (green) data with the residual (red) shown offset. Fit parameters are shown in **Table 4**. Physically unrealistic peaks at distances <1.5 Å in the non-phase corrected FT of the EXAF spectra of C and D were filtered out and subtracted from the EXAFS oscillations, see **Appendix 3.9.3** for unfiltered FTs.

Table 4: Parameters fit to EXAFS spectra of biological fluids spiked with silver shown in **Figure 4**.[a]

Sample	Scatterer	CN	Distance	DWF	$-E_0$	Fit error
Foetal calf serum	Cl (010)	6	2.752(4)	0.0072(3)	14(1)	0.41
(MS)	Ag (020)	12	3.906(3)	0.0073(1)		
	Ag (020)	4	5.370(2)	0.0012(2)		
Isolated plasma	Cl (010)	5	2.762(7)	0.0111(6)	15(1)	0.53
(MS)	Ag (020)	5	3.901(4)	0.0057(2)		
	Ag (020)	5	5.363(5)	0.0043(3)		
Whole blood	N/O	2	2.212(7)	0.0061(6)	13(1)	0.42
	S	1	2.427(4)	0.0030(2)		
	Ag	1	2.949(5)	0.0092(4)		
Plasma fraction	S	2	2.373(5)	0.0053(2)	20(1)	0.64
from whole blood	Ag	1	3.294(7)	0.0065(4)		
RBC fraction	S	2	2.393(3)	0.0056(2)	19(1)	0.45
from whole blood	Ag	1	2.924(3)	0.0064(2)		
RBC lysate	N	1	2.14(1)	0.0047(9)	15(1)	0.49
	S	1	2.402(4)	0.0018(2)		
	Ag	1	2.94(1)	0.014(1)		
	Ag	1	3.31(2)	0.013(1)		

[a] k-ranges used for fitting each spectrum were 1-13.8 $Å^{-1}$ with a scale factor (S_0^2) of 0.9. $\Delta E_0 = E_0 - 25515$ eV where E_0 is the threshold energy. Values in parentheses are the estimated standard deviation derived from the diagonal elements of the covariance matric and are a measure of precision. The fit error is defined as $[\Sigma k^6(\chi_{exp}-\chi_{calc})^2/\Sigma k^6\chi_{exp}^2]^{½}$.

Size exclusion chromatography hyphenated with ICP-MS (SEC-ICP-MS)

Analysis of human blood by SEC-ICP-MS

To further investigate the speciation of silver in human blood, size exclusion chromatography hyphenated with ICP-MS chromatograms of plasma and RBC lysate were recorded. Silver nitrate was spiked into human whole blood to a final concentration of 2 mM, incubated for 1 hr at 37°C and separated into plasma and RBC fractions. Prior to passing the biological fluids over the size exclusion column the plasma was centrifuged (15,000 rpm, 4°C, 20 min) to remove particulate matter, while the red blood cells were lysed by 1:4 dilution into buffer followed by centrifugation (as above); the resultant chromatograms and ICP-MS traces for both fractions are shown in **Figure 5**. All ICP-MS traces were corrected by -15 seconds to account for the travel time between the UV detector of the HPLC and the ICP-MS; this represented 70 μL at the flow rate used for all samples (0.3 mL/min).

The maximum intensity of the ^{107}Ag ICP-MS traces of the plasma and RBCs fractions were an order of magnitude greater than the maximum intensity of the naturally occurring metal ions in human blood. To allow comparison between the ^{107}Ag, ^{57}Fe, ^{65}Cu, and ^{66}Zn traces, their intensities were normalised as shown on the second y-axes (**Figure 5**). Both stable copper isotopes (^{63}Cu and ^{65}Cu) were monitored simultaneously, however, the ^{65}Cu trace was used for analysis due to likely interference in the ^{63}Cu trace from ^{23}Na-^{40}Ar and ^{23}Na-^{40}K species generated in the ICP-MS plasma.[59] Elution times of BSA and human haemoglobin were denoted at the top of each SEC-ICP-MS plot and were determined by passing 1 mg/mL solutions of each protein over the column and monitoring absorbance at 280 nm in the column effluent.

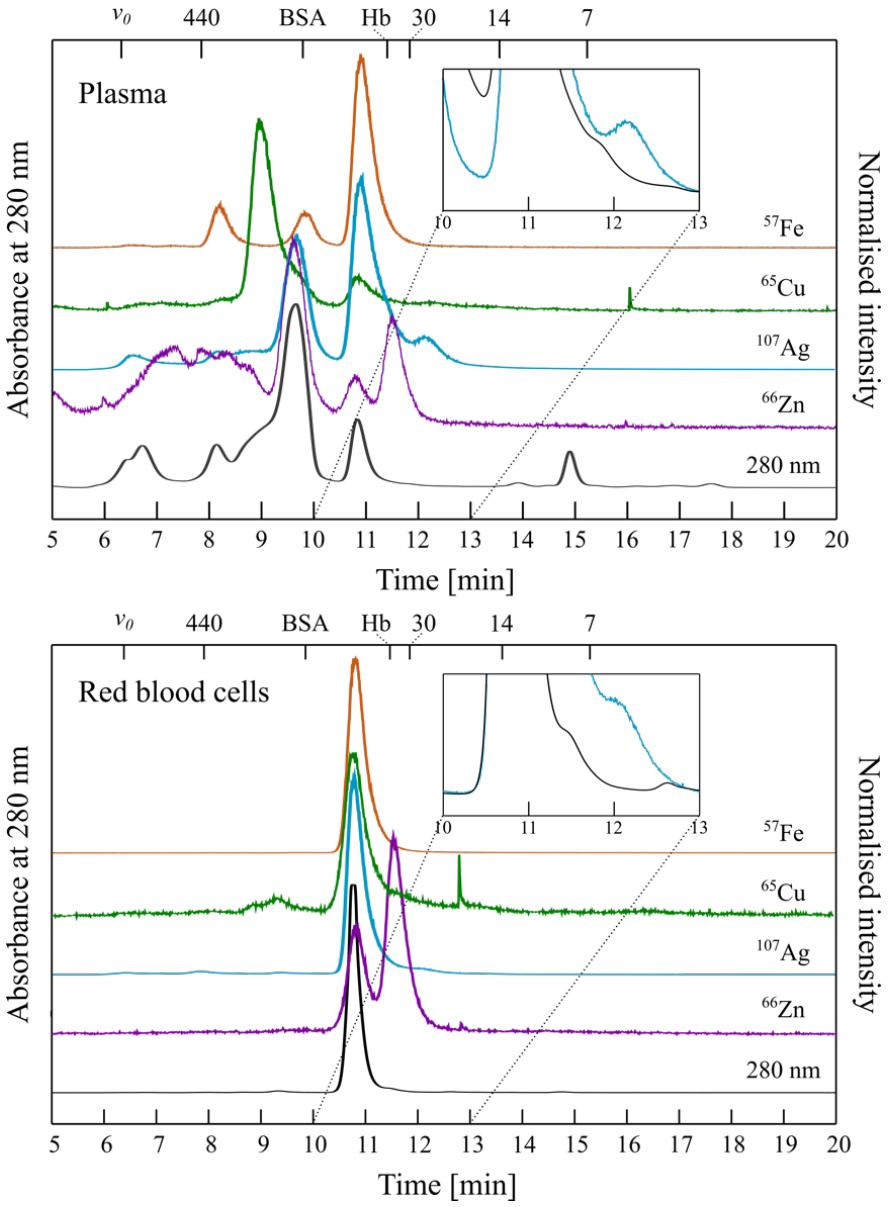

Figure 5: SEC-ICP-MS chromatograms of plasma (**top**) and red blood cells (**bottom**) from a sample of human whole blood spiked with $AgNO_3$ (final conc. 2 mM), incubated at 37°C for 1 hr and fractionated. RBCs were lysed by dilution in HEPES buffer (1:4) at pH 7.4. The presence of protein was monitored by absorbance of the column effluent at 280 nm (**black**). ^{107}Ag (blue), ^{65}Cu (green), ^{57}Fe (orange), and ^{66}Zn (purple) ICP-MS traces of the column effluent were recorded; all metal trace elution times were corrected by -15 seconds (~70 µL) to account for time taken to reach the ICP-MS. Column: Agilent AdvanceBio SEC 300Å (7.8 x 300 mm I.D.; 2.7 µm particle size); temperature: ~20°C; mobile phase: 100 mM HEPES, pH 7.4; flow rate: 0.3 mL/min; injection volume: 10 µL; detector: Agilent Infinity 1200 variable wavelength detector set at 280 nm, and Agilent QQQ 8900 ICP-MS. The void volume of the column (v_0) and retention times of molecular weight markers are shown at the top of the plot in kDa.

A single, intense peak was observed in the 280 nm trace of RBC lysate at 10.78 min, with which was associated elevated ^{57}Fe and ^{107}Ag signals (**Figure 5**, **bottom**). This large peak was qualitatively identified to be haemoglobin based on the colocation of the

intense iron peak; however, the elution time of 'native' Hb in the lysate was reduced relative to that observed for the human haemoglobin standard (t_r = 11.45 min). A shoulder on the high retention time edge of the haemoglobin 280 nm peak (shown inset, **Figure 5**, **bottom**) was concomitant with a peak in the ^{66}Zn trace (11.52 min) and likely indicated the elution of the zinc-bearing metalloprotein, carbonic anhydrase (CA). In RBCs the absolute amount of carbonic anhydrase is unclear however, it has been shown to be low relative to haemoglobin (~2 to 12 mg CA per g Hb)[60] and the corresponding shoulder at ~11.5 min in the 280 nm trace was almost completely obscured by the magnitude of the Hb peak. The apparent offset in the 280 nm and ^{107}Ag traces (inset **Figure 5**, **bottom**) was due to the tailing observed in the silver trace, likely the result of analyte/machine adsorptive effects caused by the high concentration of analyte present (CPS of ^{107}Ag trace were ~17 times greater than ^{57}Fe). Peaks in the ^{65}Cu and ^{66}Zn traces that eluted with Hb (10.78 min) could represent Hb-bound copper and zinc[61-62] or coelution of other metalloproteins such as [Cu, Zn] superoxide dismutases (SOD). Low intensity, broad peaks were present at low elution time in the 280 nm and ^{107}Ag traces which were likely due to the presence of remnant plasma in the RBC fraction. The peaks matched well with the chromatogram of plasma and the contamination likely resulted from not washing the RBCs prior to lysis. The additional peaks accounted for <5% of the total area of the plot. The RBC fraction was not washed as buffers used for this purpose tend to be high in halide and (bi)carbonate anions which, if present, have the potential to perturb silver speciation upon lysis.

Table 5: Elution times and calculated molecular weights of peaks observed in the 280 nm and ICP-MS traces of the SEC-ICP-MS plots of plasma and RBCs treated with 2 mM $AgNO_3$ (**Figure 5**).

Fraction	Elution time [min]	Calculated MW [kDa]
Plasma	6.46	1037
	6.74	878
	8.16	375
	9.00 (shoulder)	227
	9.70	150
	10.86	75
	11.98	38
	12.28 (Ag/Cu trace)	32
	14.07	11
	14.57	8
	14.95	6
Red blood cells	10.78	78
	11.50	51

As mentioned above, haemolysis of RBCs occurred upon addition of 2 mM $AgNO_3$ to whole blood, thus the plasma fraction passed over the SEC column was contaminated with red blood cell contents (mostly haemoglobin) and was red in colour instead of straw yellow. The 2 mM concentration of Ag was chosen to provide good data for XAS experiments and was kept constant to enable comparison between XAS and SEC-ICP-MS data. The retention time of haemoglobin in the plasma fraction was in good agreement with the RBC lysate (10.78 min vs. 10.86 min) and again identified by the high amount of iron associated with the peak. Additionally, when the ICP-MS was disconnected and the column effluent fractionated into a 96 well plate, the fractions corresponding to the elution of the peak at 10.78 min were bright red while all other fractions were colourless (not shown).

Human blood plasma is comprised of over a thousand individual proteins,[63] thus all peaks observed in the 280 nm trace shown in **Figure 5**, **top** were likely representative of coelution of multiple species. Analysis of a subsection of the proteome, namely the metalloproteome, can provide insight into which proteins may have been present. The copper transport protein, ceruloplasmin, was posited to elute at 9.00 min due to the high elution of copper. Iron transport proteins ferritin and transferrin likely eluted at 8.26 and 9.94 min, respectively, based on elution of iron and molecular weight (e.g. larger proteins are expected to elute at lower elution time). Human serum albumin is the most abundant protein in plasma and a known zinc-binding protein, thus the magnitude of the 280 nm peak at 9.70 min as well as coelution with a peak in the ^{66}Zn trace, suggested the presence of HSA. Silver was found to elute with almost all peaks observed in the UV trace with elution times <13 min. Notable exceptions from this observation included the peaks at 6.46 and 6.74 min.

To investigate whether the haemolysis induced by addition of 2 mM $AgNO_3$ altered the elution profile of the silver, a sample of human blood was spiked to a final concentration of 0.1 mM $AgNO_3$ and the plasma fraction analysed by SEC-ICP-MS (**Figure 6**). When treated with the lower concentration of silver, even when added in non-isotonic MilliQ water, no lysis of RBCs was visually observed after incubation for 1 hr at 37°C.

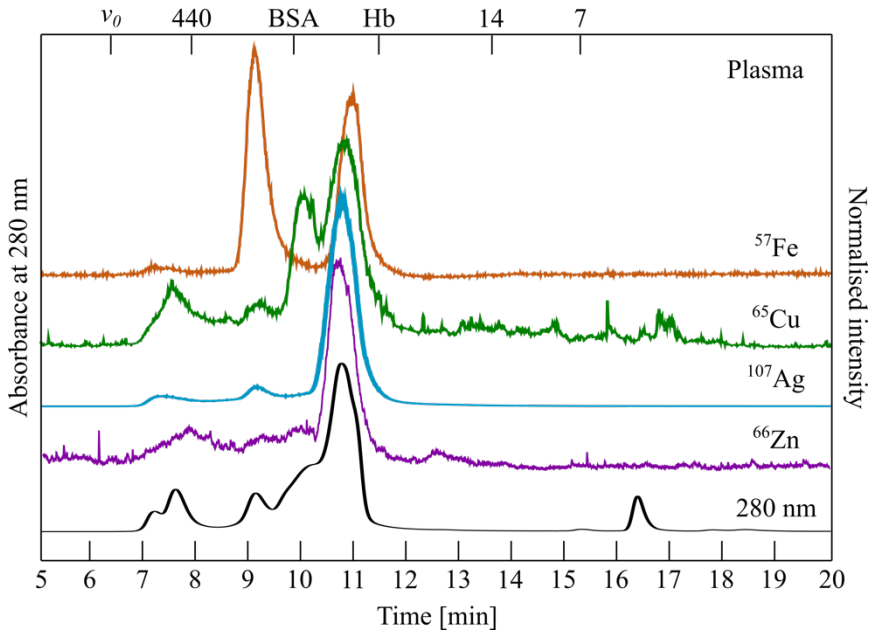

Figure 6: SEC-ICP-MS chromatogram of human plasma from a sample of whole blood spiked to a final concentration of 0.1 mM $AgNO_3$, incubated at 37°C for 1 hr and fractionated. The presence of protein was monitored by absorbance of the column effluent at 280 nm **(black)**. ^{107}Ag (blue), ^{65}Cu (green), ^{57}Fe (orange), and ^{66}Zn (purple) ICP-MS traces of the column effluent were recorded.; all metal trace elution times were corrected by -15 seconds (~70 µL) to account for time taken to reach the ICP-MS. Column: Agilent AdvanceBio SEC 300Å (7.8 x 300 mm I.D.; 2.7 µm particle size); temperature: ~20°C; mobile phase: 100 mM HEPES, pH 7.4; flow rate: 0.3 mL/min; injection volume: 10 µL; detector: Agilent Infinity 1200 variable wavelength detector set at 280 nm, and Agilent QQQ 8900 ICP-MS. The void volume of the column (v_0) and retention times of molecular weight markers are shown at the top of the plot in kDa; BSA and Hb are 66.5 and 64.5 kDa, respectively

When passed over the size exclusion column, the elution profile shape of plasma spiked with 0.1 mM $AgNO_3$ was similar to that of the 2 mM $AgNO_3$ sample (**Figure 5**, **top**) – bar the absence of the Hb peak. Most notably, however, all elution times of the 0.1 mM $AgNO_3$ plasma sample peaks were shifted approximately +60 seconds (**Table 6**). The cause of the observed change in elution time was unclear, however, it may have been due to a reduced protein load injected onto the column Hb was absent in the 0.1 mM sample (the same injection volume was used between the two samples). Haemoglobin was one of the final major proteins observed to elute from the column in the 2 mM $AgNO_3$ plasma fraction, suggesting it had a stronger affinity for the column resin than the other proteins in the sample. If the protein loading was high, and Hb occupied a significant amount of the column pore volume, diffusion of the other plasma proteins into the resin pores would likely be impeded. As a result, they would pass through the column faster and have reduced elution times (relative to a sample where haemoglobin was absent); this was observed for the 2 and 0.1 mM $AgNO_3$-treated plasma samples.

In the absence of haemoglobin, the highest proportion of silver was found to elute with the dominant peak in the 280 nm trace at 10.74 min, likely to contain human serum albumin. The poor alignment of the UV, ^{107}Ag, and ^{65}Cu traces with that of the ^{57}Fe trace at 10.74 min may confirm the coelution of multiple species such as transferrin (80 kDa) and HSA (66 kDa) based on the iron, and copper/zinc traces, respectively.

Table 6: Elution times and calculated molecular weights of peaks observed in the 280 nm and ICP-MS traces of the SEC-ICP-MS plots of plasma from whole blood treated with 0.1 mM $AgNO_3$ (**Figure 6**).

Elution time [min]	Calculated MW [kDa]
7.23	655
7.61	522
9.14	209
10.10 (shoulder)	118
10.74	80

Localisation of silver in human blood

The localisation of silver ions in the plasma and red blood cell fractions of human whole blood over time is shown in **Figure 7**. Each time point represents a discrete sample of whole blood spiked with 2 mM $AgNO_3$ and incubated at 37°C for 5 to 60 minutes before centrifugation. The zero-minute time point was an ice-cooled sample of whole blood to which was added silver nitrate and centrifuged immediately (for 5 min). At zero minutes 69% of the silver was located in the RBC fraction, which increased to 94% by 30 minutes and then decreased to 86% after 60 minutes. The plasma fraction trend mirrored that of the RBC fraction with a decrease in the moles of silver in the plasma from 0 to 30 minutes followed by an increase from 30 to 60 minutes. The sum of the moles of silver in the plasma and RBC fractions was, on average, 1.92 ± 0.01 µmol, indicating only a small loss of silver during the experiment (total Ag per sample of whole blood was 2 µmol).

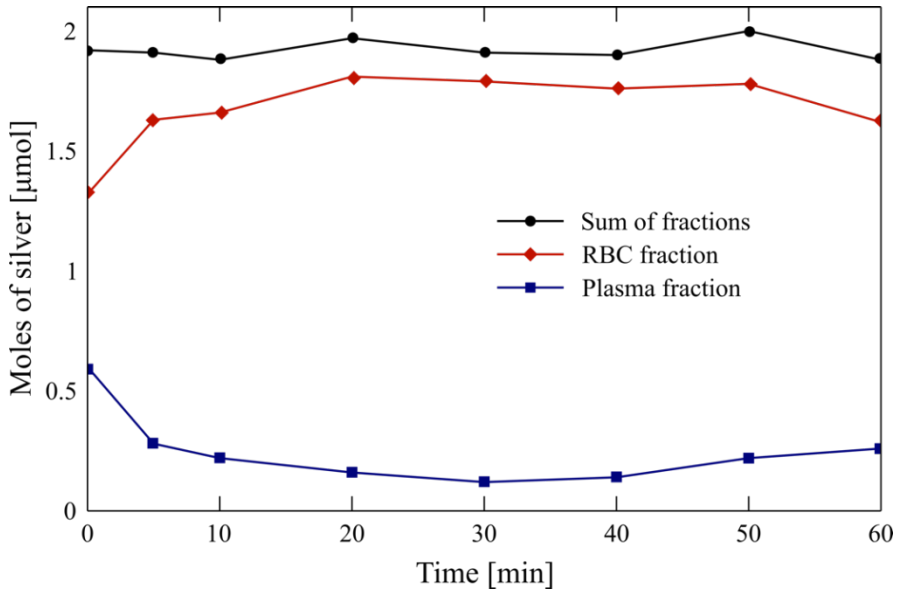

Figure 7: Time-dependent localisation of silver in human whole blood. Silver in red blood cell (red) and plasma (blue) fractions of eight samples of human whole blood spiked with 2 mM $AgNO_3$ (2 µmol per individual sample), incubated for 0 to 60 minutes at 37°C and separated into plasma and RBC fractions. The sum of moles in the RBC and plasma fractions at each time point is shown (**black**). The amount of silver was measured by atomic absorption spectroscopy through use of a calibration curve of known silver standards.

As has been stated above, addition of 2 mM $AgNO_3$ to whole blood resulted in immediate lysis of some RBCs thus it was likely that the percentage of silver localised in the plasma fraction would have been even lower than that measured if lysis had not occurred. The decrease in moles of silver in the RBC fraction at time >30 min was possibly due to subsequent lysis of erythrocytes (additional to that which initially occurred) releasing endogenous silver into the surrounding plasma.

Summary of results

Ag K-edge XANES of human whole blood spiked with 2 mM $AgNO_3$ were described by silver-Hb and silver-BSA model spectra (~70 and 30%, respectively, as determined by linear combination fitting); a trend corroborated by the localisation study which showed ~90% of the silver migrated to the red blood cell (RBC) fraction of whole blood. The SEC-ICP-MS ^{107}Ag trace of lysed RBCs showed interaction between silver, haemoglobin (10.78 min) and carbonic anhydrase (~11.5 min). Fitting of the whole blood EXAFS with a S_2N/OAg coordination sphere provided physically sensible fit parameters and shared similarities to the parameters fit to the Ag-Hb/BSA model EXAFS (S_2N/O).

LCF of the plasma fraction of whole blood treated with silver calculated approximate one third contributions from Hb, BSA, and cysteine model spectra, respectively. Lysis of RBCs was observed upon exposure of whole blood to 2 mM $AgNO_3$ which accounted for the haemoglobin component. SEC-ICP-MS revealed that the greatest proportion of silver in the plasma was associated with Hb, human serum albumin (HSA), and other high molecular weight proteins. Similarly, at a concentration of $AgNO_3$ where haemolysis was not observed (~0.1 mM) HSA was the dominant binder of Ag^+. Isolation of the plasma fraction followed by treatment with Ag^+ displayed significantly different speciation of silver. Both LCF and EXAFS fitting determined that solid silver chloride was formed; a similar result was observed for treatment of foetal calf serum (an analogous biological fluid). To the best of the authors' knowledge, presented herein was the first metallomics study of silver speciation in human blood. However, speciation of other analytes by similar techniques have been reported and help contextualise the data collected.

3.5 Discussion

Silver in human blood plasma

Elsewhere it has been identified that the antibacterial properties of silver ions are impeded upon exposure to blood plasma.[64] The hypothesis behind this observation is that the Ag^+ ions are sequestered as solid silver chloride limiting antibacterial properties due to poor aqueous solubility. Indeed, as reported here, addition of silver nitrate solution to isolated human blood plasma resulted in the formation of solid silver chloride (as determined by XAS analysis), however, this appeared to be an aberrant result. The speciation of silver ions in the plasma fraction of human whole blood treated with 2 mM $AgNO_3$ was found to be primarily thiolate-bound from interaction with haemoglobin, HSA, and other unidentified plasma proteins. No contribution from a solid silver chloride model spectrum was found for the whole blood plasma fraction despite inclusion of the model in the linear combination fit analysis. Conversely, 65 and 95% contribution from the $AgCl_{(s)}$ model spectrum was found for isolated plasma and foetal calf serum, respectively. This disparity in speciation highlights the need to investigate the biochemical fates of analytes as whole systems, not simply the sum of their parts.

It was possible that the speciation of Ag^+ in the plasma fraction of whole blood was perturbed due to lysis of red blood cells contaminating the plasma. However, the plasma fraction of a sample of whole blood treated with ~0.1 mM $AgNO_3$ did not visually display signs of RBC lysis, nor was a haemoglobin peak apparent in the SEC-ICP-MS chromatogram, confirming decreased or complete absence of haemolysis. All detected Ag^+, as monitored by the ^{107}Ag ICP-MS trace, was also associated with high molecular weight protein species. If Ag^+ was present as particulate or colloidal silver chloride, three things could be expected: (1) pelletisation of solid AgCl upon centrifugation of the sample prior to chromatographic analysis – carried out for all samples (10,000 g, 20 min, 4°C); (2) a significant increase in HPLC back pressure due to clogging of the column with silver chloride particulate when analysed; (3) elution and detection of low molecular weight-bound Ag^+ (if silver chloride colloids reached the ICP-MS). None of these observations occurred, indicating that formation of silver chloride in the isolated plasma sample was not representative of the biochemical fate of silver in whole blood. By extension, likely nor were the results reported elsewhere indicating a reduction in the antibacterial properties of silver in isolated plasma.[65-66]

Analysis of blood plasma by similar chromatographic techniques by other allowed qualitative identification of plasma proteins detected by the SEC-ICP-MS traces of biologically relevant metal (^{65}Cu, ^{66}Zn, and ^{57}Fe) reported here.[35]

Regarding the ^{57}Fe ICP-MS trace of plasma, the two low elution time peaks (8.29, and 9.91 min) have previously been identified as the haptoglobin-haemoglobin complex (Hp-Hb, MW: ~470 kDa),[35] and the iron transport protein holo-transferrin (hTf, MW: 79.7 kDa), respectively.[34] The major peak of the ^{65}Cu trace (9.00 min) was the dominant plasma copper transport protein, ceruloplasmin (Cp, MW: 151 kDa) while the shoulder on the high elution time edge of Cp was Cu-bound albumin.[34] In the ^{66}Zn trace, the poorly defined peaks at elution times >9 min likely included zinc-bound entities like α_2-macroglobulin (MW: 725 kDa) and a number of unidentified zinc metalloproteins,[34] and the most intense peak in the ^{66}Zn trace was likely Zn-bound albumin.[67] Peaks that eluted at >10.5 min were presumed to be contaminants from haemolysis of RBCs as they matched well with the elution profile of RBC lysate and were absent in the 0.1 mM $AgNO_3$ treated whole blood plasma fraction. Considering the peaks at >10.5 min likely originated from RBC cellular contents, the second largest peak in the ^{66}Zn trace (11.65 min) may correspond to the zinc-metalloprotein, carbonic anhydrase.[60] The collocation of copper and zinc at 10.95 min may be associated with haemoglobin,[61-62] however, it could also represent elution of [Cu,Zn] superoxide dismutases (SOD) like the extracellular sensory, homotetrameric SOD3 (MW 130 kDa)[68] or the soluble, homodimeric SOD1 (MW: 32 kDa).[69]

Silver in red blood cells

Haemolysis has been reported to occur when RBCs are exposed to various metals, including copper,[70-71] cadmium,[72-73] lead,[74-75] gold,[76-77] and silver.[20, 78] Nanomolar concentrations of silver nitrate can induce dose-dependent membrane scrambling, efflux of intracellular potassium chloride, activation of protein kinase C, and disruption of nitric oxide homeostasis, resulting in RBC lysis.[20] Therefore, the haemolysis observed upon exposure of whole blood to 2 mM $AgNO_3$ in this study was consistent with previously reported results and explains why, even when added as an isotonic solution, RBC lysis was observed.

Considering the low concentrations of silver nitrate required to induce haemolysis (<500 nM)[20] the plasma fraction of whole blood treated with 0.1 mM $AgNO_3$ (analysed by SEC-ICP-MS), was likely not devoid of RBC lysis. The absence of identifiable haemoglobin peaks in the ^{57}Fe traces of the plasma fraction may have been due to the Hb

scavenging ability of haptoglobin, a biochemical mechanism which ensures free haemoglobin is not present in plasma.[36] Indeed, haptoglobin itself does not naturally contain any iron,[79] so the identification of the lowest elution time peak of the ^{57}Fe trace as the Hp-Hb complex suggests that some lysis occurred but was not sufficient to overwhelm the natural mechanisms in whole blood.

Localisation in intact erythrocytes has been shown to occur for several heavy metals, however, it has not previously been reported for silver nitrate. The rapid migration of Hg^{2+} into RBCs was observed *via* ^{1}H NMR studies.[42] The study found that equilibration of mercury concentration within the RBCs was reached within less than 5 minutes post exposure; a result consistent with the migration of silver ions reported herein. In addition to the short equilibration time, RBC lysis occurred, the dominant interactions with Hg^{2+} were from Hb cysteine residues, and the metal was mainly associated with haemoglobin as opposed to GSH, a result that has been replicated elsewhere.[40] Similarly, ^{1}H NMR studies indicated that ~90% of Cd^{2+} ions localise within intact erythrocytes,[41] however it was found that cadmium interacted predominantly with glutathione, a result that has been validated by recent size exclusion studies.[40] The bulk of lead in the human body is eventually sequestered in bone, however, upon initial exposure, up to 99% of the blood lead burden is within the RBCs.[74] Therefore, the rapid migration and high proportion of silver ions localised in the red blood cell fraction of human whole blood was consistent with the reported chemistry of other heavy metals.

SEC-ICP-MS analysis of the plasma and RBC fractions of silver-treated whole blood reported here revealed silver was exclusively bound by medium/high molecular weight protein species (>30 kDa). Interaction between Ag^{+} and high concentration blood proteins (like haemoglobin or human serum albumin) was expected, however, no low molecular weight-bound silver species were identified in the 280 nm or ^{107}Ag traces. Glutathione (GSH) is present at high concentrations in RBC cytosol (~2.5 mM)[80] but no interactions between silver ions and GSH were observed. Previous studies have identified that some heavy metals interact predominantly with haemoglobin or GSH (e.g. mercury, and cadmium, respectively), thus it may be possible that silver ions interact strongly with Hb, but not glutathione in RBCs.

A previous study has linked decreased reduced glutathione levels in plasma (as well as RBC cytosol) with the formation of a GS-Ag species.[81] However, while a dose-dependent decrease in GSH levels over 2 hours upon exposure to $AgNO_3$ was apparent,

whether it was a result of direct interaction with Ag^+ or generation of reactive oxygen species was not clear. Results presented here would suggest that silver ions do not interact directly with GSH and that discrete $(GS)_xAg$ species were not formed.

In a size exclusion metallomics study of RBC lysate, perturbation of zinc and phosphorous speciation (after incubation for two hours) was attributed to oxidation events linked to the rapid oxidation of GSH under atmospheric conditions at pH 7.4.[40] To moderate the loss of GSH redox activity, the SEC mobile phase was fortified with 2.5 mM GSH (physiological RBC concentration), which mitigated the previously observed changes in speciation. Thus, it was possible that absence of glutathione-bound silver species in the SEC-ICP-MS study reported here, was due to auto-oxidation of GSH under atmospheric oxygen and/or generation of ROS. The experiments reported herein involved exposure of whole human blood to 2 mM $AgNO_3$, incubation at 37°C for 1 hour followed by fractionation and lysis of RBCs. Upon lysis (which was carried out by dilution into buffer) the sample vials were capped immediately and kept at ~4°C until analysis (always <1 hour, post lysis), thus, if perturbation of GSH binding of Ag^+ did occur, it was likely an artefact of chromatographic analysis (as reported by Gibson, *et al.*).[40]

In addition to oxidative stress possibly placed on the system by perturbation of GSH/GSSG ratios, there is evidence in the literature for the rapid degradation of metalloprotein/peptide species in blood plasma (<30 min post sample collection).[34] Degradation of Cu-bound proteins in rabbit plasma has been reported where proteins, such as blood coagulation factor V, were only detectable if the plasma was analysed within 30 minutes of collection. Beyond this time, the copper signal corresponding to blood coagulation factor V (as well as other non-baseline separated species) disappeared completely. Similarly, a >50% reduction in the intensity of a low molecular weight bound copper species that eluted at large elution time was observed between 30 min and 1 hour.

Post blood collection, the whole blood sample used here was exposed to 2 mM $AgNO_3$ and incubated at 37°C for one hour, therefore it is possible that low molecular weight proteins/peptides were degraded before analysis by SEC-ICP-MS. Were low molecular weight silver-bound species present in plasma or RBC lysate they would likely elute at high retention time. Although glutathione does not absorb strongly at 280 nm,(due to absence of aromatic amino acid residues) a peak in the ^{107}Ag trace would be expected, however, no peak corresponding to LMW-bound silver (or any biologically relevant metal) was observed.

The retention times of human serum albumin and haemoglobin were similar but did not match the protein standards of lyophilised BSA, and human haemoglobin dissolved in elution buffer. The standard protein samples tended to elute at larger retention times relative to the 'native' protein species, which could be due to the absence of naturally occurring peptides capable of binding to protein species, altering their hydrodynamic radii.[35]

Indeed, transient mixed-ligand metal-bound species such as GS-Hg-Hb have been observed in ^{1}H NMR studies[42] and such species would likely have shorter elution times due to the increase in size (relative to the unmodified protein). In the case of BSA, the discrepancy may be associated with the 24% dissimilarity in amino acid sequence relative to HSA which could lead to differences in their hydrodynamic radii.[52] In the 2 mM $AgNO_3$ whole blood plasma sample HSA eluted ~10 seconds earlier than the BSA standard. However, HSA eluted ~60 seconds after the BSA standard in the plasma whole blood sample treated with 0.1 mM $AgNO_3$. In fact, all peaks in the low concentration silver nitrate plasma SEC-ICP-MS chromatogram were shifted to higher elution times by ~60 seconds. A major difference between the two plasma samples (other than [Ag^{+}]) was the presence of haemoglobin and other RBC cellular contents in the 2 mM sample. Both samples were applied to the column as 10 μL injection volumes under identical HPLC running conditions, thus, the change in retention times was likely as result of the reduced protein concentration of the plasma due to the absence of the RBC contamination, as mentioned above.

3.6 Conclusions

Humans are increasingly exposed to silver through its inclusion in a vast array of medical and consumer items. Despite this, the biochemical fate and speciation of silver ions in mammals is relatively unknown. Through use of metallomics techniques, namely size exclusion chromatography hyphenated with ICP-MS, and X-ray absorption spectroscopy, greater insight into the speciation and chemistry of silver ions in human whole blood and relevant biological fluids was achieved.

Silver nitrate was found to localise within the red blood cell fraction of the human whole blood within five minutes, post exposure. In conjunction with this, significant lysis of the erythrocytes was observed. Both observations are consistent with previously reported effects of heavy metals on blood (like Hg^{2+}) Once inside the RBCs silver was found to be predominantly associated with haemoglobin and possibly carbonic anhydrase, the two most abundant proteins in erythrocytes. This observation was also consistent with the chemistry Hg^{2+} ions in red blood cells, while other heavy metals, such as cadmium, appear to have a higher affinity for reduced glutathione in the cells, the concentration of which is ~2.5 mM. XANES analysis, corroborated by EXAFS fitting, revealed the silver coordination environment in the red blood cell fraction was dominated by sulfurous molecules such as cysteine, or cysteine-like ligands. The silver-methionine XAS model spectrum was found to be physically unrepresentative of the interactions likely to occur between Ag^{+} and proteinaceous methionine residues due to binding through the amine nitrogen, so the proportion of silver associated with the thioether-containing amino acid could not be quantified.

Binding of silver to human haemoglobin and bovine serum albumin was identified to be three-coordinate; consistent with other silver-biomolecule coordination numbers.[49] S_2N/O coordination spheres fit to the EXAFS of both spectra with contributions from cysteine, methionine and an unidentified nitrogen/oxygen-containing residue. For BSA this identified the binding of silver to likely be through the sole reduced cysteine residue in the protein sequence, Cys34. The Ag K-edge XANES of whole blood samples could be described by linear combination fitting by a combination of silver-haemoglobin, BSA, and cysteine model spectra; no solid silver chloride component was identified. Conversely, the speciation of silver in ‘incomplete’ biological systems (e.g. isolated plasma) was determined to likely be that of colloidal silver chloride through XANES and EXAFS analysis.

At the concentration of silver used in this study, haemolysis of red blood cells was unavoidable. As such, the plasma fraction of silver-treated whole blood was contaminated

with RBC cellular contents and the prevalent binder of Ag^+ in the plasma was found to be haemoglobin. At a lower concentration of $AgNO_3$, in the perceived absence of haemolysis, the dominant binder of Ag^+ in plasma was identified to be human serum albumin as well as other unidentified high molecular weight proteins. No low molecular weight-bound silver was present in any analysis of RBC lysate or plasma which suggested that does not interact significantly with glutathione or metallothioneins.

Through SEC-ICP-MS of plasma it was found that silver ions were bound by numerous serum proteins. Analysis of a subset of the plasma proteome, namely the metalloproteome, enabled some of the silver-bound species to be qualitatively identified. After haemoglobin, the dominant protein associated with silver was human serum albumin, as well as carbonic anhydrase and ceruloplasmin. The lack of toxicity of silver ions towards humans and mammals, especially relative to other heavy elements like mercury, would suggest that while silver has a wide binding profile in plasma that the coordination of the metal to these proteins, does not result in adverse effect on the protein function.

A common argument against the use of silver as an antibacterial agent is the sequestration of the metal as insoluble salts like silver chloride. It was found in this study that silver chloride only formed in 'incomplete' systems such as isolated plasma or foetal calf serum. This is consistent with previously observed studies regarding the supplementation of silver solutions used for antibacterial testing with broth, plasma or serum reducing the metal ions efficacy. However, the results presented here in indicates that this may not necessarily represent biologically relevant chemistries, highlighting the need to study biological systems as a 'whole,' not the sum of its parts. This was evident from the XAS and SEC-ICP-MS analysis that revealed no silver chloride formed in human whole blood treated with silver: either 2 mM or ~0.1 mM $AgNO_3$, final concentration.

3.7 Future directions

Throughout this study all solutions were maintained at pH 7.4 by HEPES buffer. HEPES was chosen due to its buffering capacity at physiological pH and demonstrated low affinity for various heavy metals.[82] Unfortunately, an unforeseen consequence of this buffer choice was that the sulfonate group of the molecule would be completely deprotonated at the pH 7.4. A technique commonly used in conjunction with size exclusion chromatography is anion (or cation) exchange chromatography (AEX). This technique adds a second dimension of separation based on the isoelectric points (pIs) of the protein species present in solution. While some of the proteins could be qualitatively identified in the SEC-ICP-MS chromatograms of plasma and red blood cell lysate, multiple species

were likely eluting at any given time point of the plot. As such, the second dimension of separation and purification of the native proteins could allow for more accurate identification of the silver-binding species as well as testing by kit assays for enzymatic activity of some of the components of human plasma or red blood cells.[35] This could be particularly useful for the RBC lysate sample where the sheer magnitude of the haemoglobin UV trace peak possibly obscured some of the less abundant intracellular proteins. Choice of a non-anionic buffer like Tris or bis-Tris would facilitate such analysis. As the purpose of the study presented herein was to determine the speciation of Ag^+ in human blood and the XAS spectra and models were collected while in HEPES buffer, it was deemed inappropriate to change buffer system as the results from SEC-ICP-MS and XAS would not be directly comparable.

As was mentioned above, previous groups have identified that exposure of red blood cell lysate to atmospheric oxygen can lead to the degradation of glutathione *via* oxidation to GSSG.[40] As both plasma and RBCs are known to have high levels of GSH, it was surprising that no identifiable glutathione-metal ion species were detected, either for silver ions or any native metal ions. As such it would be informative to see whether fortification of the elution buffer with physiological GSH concentrations altered the speciation of silver in human blood. Additionally, due to financial and time constraints an untreated sample of human plasma and RBC lysate was not analysed by SEC-ICP-MS. Comparison of the untreated plasma and RBC metal traces with those of the silver-treated samples would be informative to see whether significant mismetallation or degradation of metalloproteins occurred during treatment, incubation or chromatographic development.

All samples of whole blood treated with silver nitrate herein were incubated at 37°C for 1 hours to ensure any biochemical reactions between added silver ions and the native biomolecules were allowed to occur. Other studies have found that copper-bound plasma proteins and low molecular weight species have been observed to be significantly degraded within 30 minutes of blood collection.[34] Even halving of the incubation time with silver would thus lead to degradation of some of the blood components. As such a murine model experiment involving the addition of silver (likely as nitrate) to the animals' food or water could provide better insight into the chemistry of silver *in vivo*. Approximately 10-20% of silver to which mammals are exposed to orally is introduced into the vascular system by absorption through the small intestines. Collection of the mouse blood and immediate analysis by SEC-ICP-MS would ensure that the blood chemistry and chemical integrity is maintained as much as possible. In addition to this, were the animals humanely euthanised and dissected, the organs could be later analysed by either/or XAS and X-ray

fluorescence microscopy for more speciation/localisation information. Conflicting evidence is present in the literature regarding the organ targets for localisation of silver ions. Some studies suggest the kidneys were the site of silver localisation while others point to the liver.[13] XAS and XFM experiments coupled with bulk ICP-MS techniques for total metal content and SEC-ICP-MS for further speciation analysis could provide a much more complete understanding of the biochemical fate of silver in mammals.

Were some of the mice subjected to levels of silver high enough for symptomatic argyria to appear, detailed analysis of the subdermal silver deposits that form as a result of the condition could be examined by XFM and XAS, as well. While the composition of the deposits has been reported to contain reduced silver, and sulfide species, an unidentified component has also been identified.[15] Mapping portions of the animals' skin by XFM could allow greater understanding of the speciation of the metal deposits.

When human whole blood was treated with 2 mM silver nitrate significant lysis was observed. This concentration was chosen to ensure good data collection from XAS experiments and was maintained through the SEC-ICP-MS experiments for consistency. While no AgCl formation was identified from XANES of human whole blood and both the plasma and RBC fractions from silver-treated whole blood, what was unclear was the extent to which the contamination of the plasma fraction altered Ag^+ speciation. When whole blood was treated with 0.1 mM $AgNO_3$ no visible lysis was observed, as validated by the plasma SEC-ICP-MS chromatogram which showed no haemoglobin peak. While a concentration of 0.1 mM $AgNO_3$ would likely be insufficient to collect EXAFS spectra, especially from the plasma fraction which is now known to contain <10% of the total added silver, collection of XANES may be possible. Analysis of the Ag K-edge XANES of the un-haemolysed plasma sample, in particular, would validate that silver chloride is not formed upon exposure of whole blood to silver.

3.8 References

1. Alexander, J. W., History of the medical use of silver. *Surg Infect (Larchmt)* **2009,** *10* (3), 289-292.
2. Shen, L., *Silver: Nature and culture*. Reakton Books: 2017.
3. Ventola, C. L., The antibiotic resistance crisis. *P&T* **2015,** *40* (4), 277-283.
4. Sim, W.; Barnard, R. T.; Blaskovich, M. A. T.; Ziora, Z. M., Antimicrobial silver in medicinal and consumer applications: A patent review of the past decade (2007-2017). *Antibiotics (Basel)* **2018,** *7* (93), 1-15.
5. Baker, J. W.; Leidy, K. L.; Smith, K. M.; Okeke, U. S., Argyria associated with use of systemic colloidal silver. *Fed Pract* **2011,** *28* (1), 39-42.
6. Hill, W. R.; Pillsburg, D. M., Argyria - the pharmacology of silver. The Williams & Wilkins company: Baltimore, 1939; pp 128-132.
7. Kwon, H. B.; Lee. J. H.; Lee, S. H.; Lee, A. Y.; Choi, J. S.; Ahn, Y. S., A case of argyria following colloidal silver ingestion. *Ann Dermatol* **2009,** *21* (3), 308-310.
8. Lansdown, A. B., A pharmacological and toxicological profile of silver as an antimicrobial agent in medical devices. *Adv Pharmacol Sci* **2010,** *2010*, 1-16.
9. Ohbo, Y.; Fukuzako, H.; Takeuchi, K.; Takigawa, M., Argyria and convulsive seizures caused by ingestion of silver in a patient with schizophrenia. *Psychiatry Clin Neurosci* **1996,** *50*, 89-90.
10. Stepien, K. M.; Morris, R.; Brown, S.; Taylor, A.; Morgan, L., Unintentional silver intoxication following self-medication: an unusual case of corticobasal degeneration. *Ann Clin Biochem* **2009,** *46* (6), 520-522.
11. Trop, M.; Novak, M.; Rodl, S.; Hellbom, B.; Kroell, W.; Goessler, W., Silver-coated dressing Acticoat caused raised liver enzymes and argyria-like symptoms in burn patient. *J Trauma* **2006,** *60* (3), 648-652.
12. Mirsattari, S. M.; Hammond, R. R.; Sharpe, M. D.; Leung, F. Y.; Young, G. B., Myoclonic status epilepticus following repeated oral ingestion of colloidal silver. *Neurology* **2004,** *62*, 1408-1410.
13. Ilyechova, E. Y.; Puchkova, L. V.; Shavlovskii, M. M.; Korzhevskii, D. E.; Petrova, E. S.; Tsymbalenko, N. V., Effect of silver ions on copper metabolism during mammalian ontogenesis. *Russ J Develop Biol* **2018,** *49* (3), 166-178.
14. Lampé, I.; Beke, D; Biri, S; Csarnovics, I; Csík, A; Dombrádi, Z.; Hajdu, P.; Hegedűs, V.; Rácz, R.; Varga, I.; Hegedűs, C., Investigation of silver nanoparticles on titanium surface created by ion implantation technology. *Int J Nanomed* **2019,** *14*, 4709-4721.
15. Eckhardt, S.; Brunetto, P. S.; Gagnon, J.; Priebe, M.; Giese, B.; Fromm, K. M., Nanobio silver: its interactions with peptides and bacteria, and its uses in medicine. *Chem Rev* **2013,** *113* (7), 4708-4754.
16. Barillo, D. J.; Croutch, C. R.; Reid, F.; Culley, T.; Sosna, W.; Roseman, J., Blood and tissue silver levels following application of silver-based dressings to sulfur mustard chemical burns. *J Burn Care Res* **2017,** *38* (5), e818-e823.
17. Kim, Y. S.; Song, M. Y.; Park, J. D.; Song, K. S.; Ryu, H. R.; Chung, Y. H.; Chang, H. Y.; Lee, J. H.; Oh, K. H.; Kelman, B. J.; Hwang, I. K.; Yu, I. J., Subchronic oral toxicity of silver nanoparticles. *Particle Fibre Toxicol* **2010,** *7* (20), 1-11.
18. *Toxicological profile for silver*; U. S. Department of Health and Human Services: Atlanta, GA, 1990.
19. Kapadia, N. P.; Kristol, D.; Spillert, C. R., Effect of endotoxin and silver ion on the clotting time of blood. In *IEEE*, 2005.
20. Sopjani, M.; Foller, M.; Haendeler, J.; Gotz, F.; Lang, F., Silver ion-induced suicidal erythrocyte death. *J Appl Toxicol* **2009,** *29* (6), 531-536.

21. Liu, J.; Wang, Z.; Liu, F. D.; Kane, A. B.; Hurt, R. H., Chemical transformation of nanosilver in biological environments. *ACS Nano* **2012,** *6* (11), 9887-9899.
22. Marchioni, M.; Jouneau, P.-H.; Chevallet, M.; Michaud-Soret, I.; Deniaud, A., Silver nanoparticle fate in mammals: Bridging *in vitro* and *in vivo* studies. *Coord Chem Rev* **2018,** *364*, 118-136.
23. Hadrup, N.; Lam, H. R., Oral toxicity of silver ions, silver nanoparticles and colloidal silver: a review. *Regul Toxicol Pharmacol* **2014,** *68* (1), 1-7.
24. Nakazawa, E.; Ikemoto, T.; Hokura, A.; Terada, Y.; Kunito, T.; Yamamoto, T.; Yamada, T. K.; Rosas, F. C. W.; Fillmann, G.; Tanabe, S.; Nakai, I., Silver speciation in liver of marine mammals by synchrotron X-ray absorption fine structure and X-ray fluorescence spectroscopies. *J Env Mon* **2011,** *13* (6), 1678-1686.
25. Li, Y. F.; Chen, C.; Li, B.; Li, W.; Qu, L.; Dong, Z.; Nomura, M.; Gao, Y.; Zhao, J.; Hu, W.; Zhao, Y.; Chai, Z., Mercury in human hair and blood samples from people living in Wanshan mercury mine area, Guizhou, China: an XAS study. *J Inorg Biochem* **2008,** *102* (3), 500-506.
26. Frank, P.; Carlson, R. M. K.; Carlson, E. J.; Hodgson, K. O., The vanadium environment in blood cells of *Ascidia ceratodes* is divergent at all organismal levels: an XAS and EPR spectroscopic study. *J Inorg Biochem* **2003,** *94* (1-2), 59-71.
27. Frank, P.; Hedman, B.; Hodgson, K. O., XAS spectroscopy, sulfur, and the brew within blood cells from *Ascidia ceratodes*. *J Inorg Biochem* **2014,** *131*, 99-108.
28. Wu, L. E.; Levina, A.; Harris, H. H.; Cai, Z.; Lai, B.; Vogt, S.; James, D. E.; Lay, P. A., Carcinogenic chromium (VI) compounds formed by intracellular oxidation of chromium (III) dietary supplement by adipocytes. *Angew Chem* **2016,** *55* (1), 1742-1745.
29. Levina, A.; McLeod, A. I.; Gasparini, S. J.; Nguyen, A.; De Silva, W. G.; Aitken, J. B.; Harris, H. H.; Glover, C.; Johannessen, B.; Lay, P. A., Reactivity and speciation of anti-diabetic vanadium complexes in whole blood and its components: The important role of red blood cells. *Inorg Chem* **2015,** *54* (16), 7753-7766.
30. Sendzik, M.; Pushie, M. J.; Stefaniak, E.; Haas, K. L., Structure and affinity of Cu(I) bound to human serum albumin. *Inorg Chem* **2017,** *56* (24), 15057-15065.
31. Veronesi, G.; Gallon, T.; Deniaud, A.; Boff, B.; Gateau, C.; Lebrun, C.; Vidaud, C.; Rollin-Genetet, F.; Carriere, M.; Kieffer, I.; Mintz, E.; Delangle, P.; Michaud-Soret, I., XAS investigation of silver(I) coordination in copper(I) biological binding sites. *Inorg Chem* **2015,** *54* (24), 11688-11696.
32. Barth, H. G.; Boyes, B. E.; Jackson, C., Size exclusion chromatography. *Anal Chem* **1996,** *68*, 445R-466R.
33. Dong, L.-J.; Lai, Y.-J.; Yu, S.-J.; Liu, J.-F., Speciation analysis of the uptake and biodistribution of nanoparticulate and ionic silver in *Escherichia coli*. *Anal Chem* **2019,** *91* (19), 12525-12530.
34. Manley, S. A.; Byrns, S.; Lyon, A. W.; Brown, P.; Gailer, J., Simultaneous Cu-, Fe-, and Zn-specific detection of metalloproteins contained in rabbit plasma by size-exclusion chromatography-inductively coupled plasma atomic emission spectroscopy. *J Biol Inorg Chem* **2009,** *14* (1), 61-74.
35. Sarpong-Kumankomah, S.; Gailer, J., Identification of a haptoglobin-hemoglobin complex in human blood plasma. *J Inorg Biochem* **2019,** *201* (110802), 1-8.
36. Deuel, J. W.; Schaer, C. A.; Boretti, F. S.; Opitz, L.; Garcia-Rubio, I.; Baek, J. H.; Spahn, D. R.; Buehler, P. W.; Schaer, D. J., Hemoglobinuria-related acute kidney injury is driven by intrarenal oxidative reactions triggering a heme toxicity response. *Cell Death Dis* **2016,** *7* (e2064), 1-12.

37. Kodali, P.; Chitta, K. R.; Landero Figueroa, J. A.; Caruso, J. A.; Adeoye, O., Detection of metals and metalloproteins in the plasma of stroke patients by mass spectrometry methods. *Metallomics* **2012,** *4* (10), 1077-1087.
38. Tavill, A. S.; Adams, P. C., A diagnostic approach to hemochromatosis. *Can J Gastroenterol* **2006,** *20* (8), 535-540.
39. Cauza, E.; Maier-Dobersberger, T.; Polli, C.; Kaserer, K.; Kramer, L.; Ferenci, P. Screening for Wilson's disease in patients with liver diseases by serum ceruloplasmin. *J Hepatol* **1997,** *27*, 358-362.
40. Gibson, M. A.; Sarpong-Kumankomah, S.; Nehzati, S.; George, G. N.; Gailer, J., Remarkable differences in the biochemical fate of Cd(II), Hg(II), CH_3Hg^+ and thiomerosal in red blood cell lysate. *Metallomics* **2017,** *9* (8), 1060-1072.
41. Rabenstein, D. L.; Isab, A. A.; Kadima, W.; Mohanakrishnan, P., A proton nuclear magnetic resonance study of the interaction of cadmium with human erythrocytes. *Biochim Biophys Acta* **1983,** *762*, 531-541.
42. Weed, R.; Eber, J.; Rothstein, A., Interaction of mercury with human erythrocytes. *J Gen Physio* **1962,** *45*, 395-410.
43. Khalaila, I.; Bergamo, A.; Bussy, F.; Sava, G.; Dyson, P. J., The role of cisplatin and NAMI-A plasma-protein interactions in relation to combination therapy. *Int J Oncol* **2006,** *29* (1), 261-268.
44. Sooriyaarachchi, M.; Wedding, J. L.; Harris, H. H.; Gailer, J., Simultaneous observation of the metabolism of cisplatin and NAMI-A in human plasma *in vitro* by SEC-ICP-AES. *J Biol Inorg Chem* **2014,** *19* (6), 1049-1053.
45. Harper, B. W. J.; Morris, T. T.; Gailer, J.; Aldrich-Wright, J. R., Probing the interaction of bisintercalating (2,2′:6′,2″-terpyridine)platinum(II) complexes with glutathione and rabbit plasma. *J Inorg Biochem* **2016,** *163*, 95-102.
46. Ankudinov, A. L.; Ravel, B.; Rehr, J. J.; Conradson, S. D., Real-space multiple-scattering calculation and interpretation of X-ray absorption near-edge structure. *Phys Rev B* **1998,** *58* (12), 7565-7576.
47. Anderson, D. P.; Adnan, R. H.; Alvino, J. F.; Shipper, O.; Donoeva, B.; Ruzicka, J.-Y.; Qahtani, H. A.; Harris, H. H.; Cowie, B.; Aitken, J. B.; Golovko, V. B.; Metha, G. F.; Andersson, G. G., Chemically synthesised atomically precise gold cluster deposited and activated on titania. Part II. *Phys Chem Chem Phys* **2013,** *15*, 14806-14813.
48. Doolette, C. L.; McLaughlin, M. J.; Kirby, J. K.; Batstone, D. J.; Harris, H. H.; Ge, H.; Cornelis, G., Transformation of PVP coated silver nanoparticles in a simulated wastewater treatment process and the effect on microbial communities. *Chem Cent J* **2013,** *7* (46), 1-18.
49. Carugo, O., Silver and gold in the Protein Data Bank. *J Inorg Biochem* **2017,** *175*, 244-247.
50. Park, Y.-K.; Diez-Silva, M.; Popescu, G.; Lykotrafitis, G.; Choi, W.; Feld, M. S.; Suresh, S., Refractive index maps and membrane dynamics of human red blood cells parasitized by *Plasmodium falciparum*. *PNAS* **2008,** *105* (37), 13730-13735.
51. Craig, W. Y.; Ledue, T. B.; Ritchie, R. F., *Plasma proteins: clinical utility and interpretation*. Foundation for Blood Research: 2000.
52. Gelamo, E. L.; Silver, C. H. T. P.; Imasato, H.; Tabak, M., Interaction in bovine (BSA) and human (HSA) serum albumin with ionic surfactants: spectroscopy and modelling. *Biochim Biophys Acta* **2002,** *1594*, 84-99.
53. Siriwardana, K.; Wang, A.; Gadogbe, M.; Collier, W. E.; Fitzkee, N. C.; Zhang, D., Studying the effects of cysteine residues on protein interactions with silver nanoparticles. *J Phys Chem C* **2015,** *119* (5), 2910-2916.
54. Majorek, K. A.; Porebski, P. J.; Dayal, A.; Zimmerman, M. D.; Jablonska, K.; Stewart, A. J.; Chruszcz, M.; Minor, W., Structural and immunologic

characterization of bovine, horse, and rabbit serum albumins. *Mol Immunol* **2012,** *52* (3-4), 174-182.
55. Neildez-Nguyen, T. M. A.; Wajcman, H.; Marden, M. C.; Bensidhoum, M.; Moncollin, V.; Giarratana, M.-C.; Kobari, L.; Thierry, D.; Douay, L., Human erythroid cells produced *ex vivo* at large scale differentiate into red blood cells *in vivo*. *Nat Biotechnol* **2002,** *20*, 467-472.
56. Tame, J. R. H.; Vallone, B., The structures of deoxy human haemoglobin and the mutant Hb Tyralpha42His at 120 K. *Acta Cryst D* **2000,** *D56*, 805-811.
57. Brinkman, R.; Jonxis, J. H. P., The occurrence of several kinds of haemoglobin in human blood. *J Physiol* **1935,** *85* (2), 117-127.
58. Hull, S.; Keen, D. A., Pressure-induced phase transitions in AgCl, AgBr, AgI. *Phys Rev B* **1999,** *59*, 750-761.
59. Chrastný, V.; Komárek, M., Copper determination using ICP-MS with hexapole collision cell. *Chemical Papers* **2009,** *63* (5), 512-519.
60. Funakoshi, S.; Deutsch, H. F., Human carbonic anhydrases. Immunochemical studies. *J Biol Chem* **1970,** *245* (11), 2852-2856.
61. Rifkind, J. M.; Lauer, L. D.; Chiang, S. C.; Li, N. C., Copper and the oxidation of hemoglobin: A comparison of horse and human hemoglobins. *Biochem* **1976,** *15* (24), 5336-5343.
62. Oelshlegel, F. J.; Brewer, G. J.; Knutsen, C.; Prasad, A. S.; Schoomaker, B., Studies on the interaction of zinc with human hemoglobin. *Biochem Biophys* **1974,** *163*, 742-748.
63. Pieper, R.; Gatlin, C. L.; Makusky, A. J.; Russo, P. S.; Schatz, C. R.; Miller, S. S.; Su, Q.; McGrath, A. M.; Estock, M. A.; Parmar, P. P.; Zhao, M.; Huang, S. T.; Zhou, J.; Wang, F.; Esquer-Blasco, R.; Anderson, N. L.; Taylor, J.; Steiner, S. The human serum proteome: Display of nearly 3700 chromatographically separated protein spots on two-dimension electrophoresis gels and identification of 325 distinct proteins. *Proteomics* **2003,** *3*.
64. Hildago, E.; Bartolome, R.; Barroso, C.; Moreno, A.; Dominguez, C., Silver nitrate: Antimicrobial activity related to cytotoxicity in cultured human fibroblasts. *Skin Pharmacol Appl Skin Physiol* **1998,** *11*, 140-151.
65. Zhang, S.; Du, C.; Wang, Z.; Han, X.; Zhang, K.; Liu, L., Reduced cytotoxicity of silver ions to mammalian cells at high concentration due to the formation of silver chloride. *Toxicol In Vitro* **2013,** *27* (2), 739-744.
66. Choi, O.; Deng, K. K.; Kim, N. J.; Ross, L., Jr.; Surampalli, R. Y.; Hu, Z., The inhibitory effects of silver nanoparticles, silver ions, and silver chloride colloids on microbial growth. *Water Res* **2008,** *42* (12), 3066-3074.
67. Marrack, J. R.; Hoch, H., Serum proteins: a review. *J Clin Path* **1949,** *2*, 161-192.
68. Antonyuk, S. V.; Strange, R. W.; Marklund, S. L.; Hasnain, S. S.. The structure of human extracellular copper-zinc superoxide dismutase at 1.7 A resolution: insights into heparin and collagen binding. *J Mol Biol* **2009,** *388* (2), 310-326.
69. Bartlett, S. E.; Singala, R.; Hashikawa, A.; Shaw, L.; Hendry, I. A., Development and characterization of human and house specific antibodies to CuZn-superoxide dismutase (SOD1). *J Neuro Met* **2000,** *98*, 63-67.
70. Caffrey, J. M.; Smith, H. A.; Schmitz, J. C.; Merchant, A.; Frieden, E., Hemolysis of rabbit erythrocytes in the presence of copper ions. *Biol Trace Element Res* **1990,** *25*, 11-19.
71. Lang, P. A.; Schenck, M.; Nicolay, J. P.; Becker, J. U.; Kempe, D. S.; Lupescu, A.; Koka, S.; Eisele, K.; Klarl, B. A.; Rubben, H.; Schmid, K. W.; Mann, K.; Hildenbrand, S.; Hefter, H.; Huber, S. M.; Wieder, T.; Erhardt, A.; Haussinger, D.; Gulbins, E.; Lang, F., Liver cell death and anemia in Wilson disease involve acid sphingomyelinase and ceramide. *Nat Med* **2007,** *13* (2), 164-170.

72. Horiguchi, H.; Oguma, E.; Kayama, F., Cadmium induces anemia through interdependent progress of hemolysis, body iron accumulation, and insufficient erythropoietin production in rats. *Toxicol Sci* **2011,** *122* (1), 198-210.
73. Sopjani, M.; Föller, M.; Dreischer, P.; Lang, F., Stimulation of eryptosis by cadmium ions. *Cell Physio Biochem* **2008,** *22*, 245-252.
74. Ray, R. R., Haemotoxic effect of lead: A review. *Proc Zool Soc* **2015,** *69* (2), 161-172.
75. Gelman, B. B.; Michaelson, I. A.; Bus, J. S., The effect of lead on oxidative hemolysis and erythrocyte defense mechanism in the rat. *Toxicol Appl Pharmacol* **1978,** *45*, 119-129.
76. Sopjani, M.; Foller, M.; Lang, F., Gold stimulates Ca(II) entry into and subsequent suicidal death of erythrocytes. *Toxicology* **2008,** *244* (2-3), 271-279.
77. Aseichev, A. V.; Azizova, O. A.; Beckman, E. M.; Skotnikova, O. I.; Dudnik, L. B.; Schcheglovitova, O. N.; Sergienko, V. I., Effects of gold nanoparticles on erythrocyte hemolysis. *Bull Exp Biol Med* **2014,** *156* (4), 496-498.
78. Laloy, J.; Minet, V.; Alpan, L.; Mullier, F.; Beken, S.; Toussaint, O.; Lucas, S.; Dogne, J. M., Impact of silver nanoparticles on haemolysis, platelet function and coagulation. *Nanobiomed* **2014,** *1* (4), 1-9.
79. Andersen, C. B. F.; Torvund-Jensen, M.; Nielsen, M. J.; Pinto de Oliveira, C. L.; Hersleth, H.-P.; Andersen, N. H.; Pedersen, J. S.; Andersen, G. R.; Moestrup, S. K., Structure of the haptoglobin-haemoglobin complex. *Nature* **2012,** *489*, 456-459.
80. van 't Erve, T. J.; Wagner, B. A.; Ryckman, K. K.; Raife, T. J.; Buettner, G. R., The concentration of glutathione in human erythrocytes is a heritable trait. *Free Radic Biol Med* **2013,** *65*, 742-749.
81. Khan, H.; Khan, M. F.; Rehman, A. U.; Jan, S. U.; Ullah, N., The protective role of glutathione in silver induced toxicity in blood components. *Pak J Pharm Sci* **2011,** *24* (2), 123-128.
82. Ferreira, C. M. H.; Pinto, I. S. S.; Soares, E. V.; Soares, H. M. V. M., (Un)suitability of the use of pH buffers in biological, biochemical and environmental studies and their interaction with metal ions – a review. *RSC Adv* **2015,** *5* (39), 30989-31003.

3.9 Appendices

Appendix 3.9.1 Operating parameters

Table 7: Typical operating parameters for SEC-ICP-MS experiments

Agilent 1200 LC	
Mobile phase	100 mM HEPES, pH 7.4
Column	Agilent AdvancedBio SEC 130 or 300 Å
Particle size	2.7 μm
Pore size	130 or 300 Å
Flow rate	0.3 mL/min
Injection volume	10 – 100 μL
Column dimensions	7.8 mm x 300 mm
Agilent ICP-MS QQQ 8900	
RF power	1550 W
Sample depth	10.0 mm
Carrier gas	15.0 L/min
Makeup gas	0.90 L/min
Spray chamber temp	2°C
Extracts 1, 2	-6.0 V, -250.0 V
Omega bias, lens	-150 V, 7.5 V
Deflect, plate bias	2.0 V, -60 V
Cell entrance, exit	-70 V, -80 V
Octopole bias, RF	-18.0 V, 170 V
Collision gas	He, 3.5 mL/min

Appendix 3.9.2 Cambridge Structural Database (CSD) survey results/references

Table 8: Survey of AgS_2 THIOETHER structures in CSD version 5.40 (Nov 2018)

CSD Code	Reference	Av. Ag-S (Å)
FOFVED	Kim, S., *et al.*, *Inorganica Chim Acta*, **2014**, 417, 171	2.440
FOFVIH	Kim, S., *et al.*, *Inorganica Chim Acta*, **2014**, 417, 171	2.414
IFUWUB	Bu, X.-H., *et al.*, *Cryst Growth Des*, **2002**, 2, 303	2.423
KEMGOB	Seo, S., *et al.*, *CrystEngComm*, **2017**, 19, 7185	2.420
MEFLEP	Hu, T.-L., *et al.*, *Cryst Growth Des*, **2006**, 6, 648	2.411
OLOMIL	Fainerman-Melnikova, M., *et al.*, *Acta Cryst E*, **2003**, 59, m880	2.641
REXDUU	Lee, J. Y., *et al.*, *Org Lett*, **2007**, 9, 493	2.495
WEMMOS	Lee, E., Shim Sung Lee, S. S., *CrystEngComm*, **2013**, 15, 1814	2.419
WUGLUF	Brammer, L., *et al.*, *Dalton Trans*, **2002**, 4134	2.409
WUGMAM	Brammer, L., *et al.*, *Dalton Trans*, **2002**, 4134	2.437
XAKFUL	Okada, T., *et al.*, *Chem Comm*, **2005**, 1484	2.455
XAYWEZ	Meier, H., *et al.*, *CSD Comm*, **2000**	2.438

Table 9: Survey of AgS_3 THIOETHER structures in CSD version 5.40 (Nov 2018)

CSD Code	Reference	Av. Ag-S (Å)
ACEHOG	Li, J.-R., *et al.*, *J Chem Cryst*, **2004**, 34, 501	2.521
AGTRTH	Domenicano, A., *et al.*, *J Chem Soc A*, **1968**, 866	2.548
COJGEN	Noren, B., *et al.*, *Acta Chem A Phys Inorg Chem*, **1984**, 38, 479	2.506
EFAXEP	Iyoshi, S., *et al.*, *Inorg Chem*, **2008**, 47, 3946	2.545
FIKSAU	Li, J.-R., *et al.*, *Dalton Trans*, **2005**, 464	2.515
NIYLAK	Siewe, A. D., *et al.*, *Inorg Chem*, **2014**, 53, 393	2.537
POPKIP	Awaleh, M.O., *et al.*, *J Chem Cryst*, **2009**, 39, 122	2.522
UCOCAQ	Brooks, N.R., *et al.*, *Dalton Trans*, **2001**, 2530	2.534
ULEKUR	Li, J.-R., *et al.*, *Cryst Growth Des*, **2003**, 3, 829	2.527
ULELEC	Li, J.-R., *et al.*, *Cryst Growth Des*, **2003**, 3, 829	2.566

Table 10: Survey of AgS_4 THIOETHER structures in CSD version 5.40 (Nov 2018)

CSD Code	Reference	Av. Ag-S (Å)
AFASEF	Yamaguchi, T., *et al.*, *Acta Cryst C*, **2002**, 58, m213	2.564
AQOJUN	Iwatsuki, S., *et al*., *Dalton Trans*, **2016**, 45, 12548	2.566
AQOKAU	Iwatsuki, S., *et al*., *Dalton Trans*, **2016**, 45, 12548	2.560
BULZOY	Galindo, M.A., *et al.*, *Inorg Chem*, **2009**, 48, 10295	2.563
EREXUU	Park, K.-M., *et al*., *Supramolecular Chem*, **2004**, 16, 51	2.620
FIKQUM	Li, J.-R., *et al.*, *Dalton Trans*, **2005**, 464	2.587
FIKROH	Li, J.-R., *et al.*, *Dalton Trans*, **2005**, 464	2.558
FITDOB	Kuppers, H.-J., *et al.*, *Angew Chem, Int Ed*, **1987**, 26, 575	2.603
GUBYIM	Qureshi, N., *et al.*, *Dalton Trans*, **2009**, 5708	2.583
HIJKUG	Drexler, H.-J., *et al.*, *Chemische Berichte*, **1996**, 129, 807	2.686
HOPDOF	Ishikawa, J., *et al.*, *Dalton Trans*, **1999**, 191	2.582
HOPDUL	Ishikawa, J., *et al.*, *Dalton Trans*, **1999**, 191	2.605
ICACAQ	Chen, W., *et al.*, *Acta Cryst E,* **2001**, 57, m213	2.629
JAFDAY	Grosu, I. G., *et al.*, *Molecules*, **2015**, 20, 8020	2. 552
JEDQEO	Blake, A.J., *et al.*, *Dalton Trans*, **1998**, 2931	
JEMKOB	Blake, A.J., *et al.*, *Chem Comm*, **1990**, 974	2.596
JEMKOB10	Blake, A.J., *et al.*, *Dalton Trans*, **1993**, 521	2.596
KILGOD	Frank, N. C., *et al.*, *Chem Euro J*, **2013**, 19, 14076	2.601
LIWZIB	Huang, D., *et al.*, *Chem Comm*, **2008**, 1305	2.511
LIWZOH	Huang, D., *et al.*, *Chem Comm*, **2008**, 1305	2.583
NIYLEO	Siewe, A. D., *et al.*, *Inorg Chem*, **2014**, 53, 393	2.566
NOJYOA	Jenkins, H.A., *et al.*, *Inorganica Chim Acta*, **1996**, 246, 207	2.548
NOJYUG	Jenkins, H.A., *et al.*, *Inorganica Chim Acta*, **1996**, 246, 207	2.571
NOJZAN	Jenkins, H.A., *et al.*, *Inorganica Chim Acta*, **1996**, 246, 207	2.578
QAHPAR	Pickardt, J., *et al.*, *Zeitschrift fur Naturforschung,B*, **2004**, 59, 1077	2.590

SIMKEE	de Groot, B., *et al.*, *Chem Comm*, **1990**, 1755	2.556
SIMKEE10	de Groot, B., *et al.*, *Inorg Chem*, **1992**, 31, 203	2.556
SOLHIK	de Groot, B., *et al.*, *Inorg Chem*, **1991**, 30, 3103	2.550
SUHDAA	Blake, A.J., *et al.*, *Dalton Trans*, **1993**, 521	2.611
TAWGIH	Alberto, R., *et al.*, *Inorg Chem*, **1996**, 35, 3420	2.605
TAWGON	Alberto, R., *et al.*, *Inorg Chem*, **1996**, 35, 3420	2.590
TDECAG	Hittenhausen, H., *et al.*, *Cryst Struct Comm*, **1978**, 7, 385	2.572
VEBKOD	Seo, J., *et al.*, *Inorg Chem*, **2006**, 45, 952	2.602
VEBLEU	Seo, J., *et al.*, *Inorg Chem*, **2006**, 45, 952	2.679
VEDTUU	Awaleh, M.O., *et al.*, *Inorg Chem*, **2006**, 45, 1560	2.640
VOZNON	de Groot, B., *et al.*, *Inorg Chem*, **1992**, 31, 203	2.618
WAYLOX	Demirhan, F., *et al.*, *Dalton Trans*, **1993**, 2765	2.564
WEMMIM	Lee, E., *et al.*, *CrystEngComm*, **2013**, 15, 1814	2.583
XANNAB	Suenaga, Y., *et al.*, *Dalton Trans*, **2000**, 3620	2.591
XIXPUQ	Kim, H. J. *et al.*, *New J Chem*, **2008**, 32, 258	2.586
XOLNUH	Bu, X.-H., *et al.*, *Inorg Chem*, **2002**, 41, 3477	2.604
ZAQYUL	Neve, F., *et al.*, *Chem Mater*, **1995**, 7, 688	2.573

Table 11: Survey of AgS_2 THIOLATE structures in CSD version 5.40 (Nov 2018)

CSD Code	Reference	Av. Ag-S (Å)
ADIPAF	Yoshinari, N., *et al.*, *Acta Cryst E*, **2006**, 62, m1229	2.396
ARAYOJ	Lee, P.-S. *et al.*, *Chem Lett*, **2016**, 45, 740	2.421
ARAZAW	Lee, P.-S. *et al.*, *Chem Lett*, **2016**, 45, 740	2.436
BEPWEB	Yan, H., *et al.*, *Nature (London)*, **2018**, 554, 505	2.378
BEPWIF	Yan, H., *et al.*, *Nature (London)*, **2018**, 554, 505	2.382
BIVGIY	Najafabadi, B. K., *et al.*, *Dalton Trans*, **2014**, 43, 2104	2.370
BIVGOE	Najafabadi, B. K., *et al.*, *Dalton Trans*, **2014**, 43, 2104	2.363
BIVGUK	Najafabadi, B. K., *et al.*, *Dalton Trans*, **2014**, 43, 2104	2.371
BIVHAR	Najafabadi, B. K., *et al.*, *Dalton Trans*, **2014**, 43, 2104	2.401
CAYZOR	Dance, I., *et al.*, *Chem Comm*, **1984**, 17	2.372
CAYZOR10	Dance, I. G., *et al.*, *Inorg Chem*, **1989**, 28, 1853	2.372
CAYZUX	I.Dance, *et al.*, *Chem Comm*, **1984**, 17	2.372
CAYZUX10	I.G.Dance, *et al.*, *Inorg Chem*, **1989**, 28, 1853	2.374
CEPKIR	I.G.Dance, *et al.*, *Inorg Chem*, **1983**, 22, 3785	2.362
CUTYIA	S. Ahmar, *et al.*, *Angew Chem, Int Ed*, **2010**, 49, 4422	2.401
DAPTUJ	J. T. Sampanthar, *et al.*, *Dalton Trans*, **1999**, 3153	2.359
DAPVUL	J. T. Sampanthar, *et al.*, *Dalton Trans.*, **1999**, 3153	2.359
DENGOT	N. Yoshinari, *et al.*, *Bull. Chem. Soc. Jpn.*, **2006**, 79, 1066	2.386
DENGUZ	N. Yoshinari, *et al.*, *Bull. Chem. Soc. Jpn.*, **2006**, 79, 1066	2.437
ECOLIT	M. Tamura, *et al.*, *Inorg Chem*, **2009**, 48, 8998	2.387
ENCOAG	M. J. Heeg, *et al.*, *Inorg Chem*, **1980**, 19, 554	2.371
FATGAJ	Y.-D. Chen, *et al.*, *Inorg Chem,* **2004**, 43, 7493	2.425
FATGEN	Y.-D. Chen, *et al.*, *Inorg Chem*, **2004**, 43, 7493	2.390
FATNEW	X. Chu, *et al.*, *Inorg Chem Front*, **2017**, 4, 706	2.391
FEZGID	Dong, X.-Y., *et al.*, *Chem Mater*, **2018**, 30, 2160	2.389
FIMFIQ	Tang, K., *et al.*, *Inorg Chem*, **1987**, 26, 1488	2.459
FIMFOW	Tang, K., *et al.*, *Inorg Chem*, **1987**, 26, 1488	2.379
FIMFUC	Tang, K., *et al.*, *Inorg Chem*, **1987**, 26, 1488	2.396
FOGLOC	Gonzalez-Duarte, P., *et al.*, *Chem Comm*, **1987**, 1641	2.289
HAWZIP	Aridomi, T., *et al.*, *Chem Lett*, **2005**, 34, 770	2.456
HOBWIE	Fujisawa, K., *et al.*, *Chem Lett*, **1998**, 167	2.349
LAHDEE	Rao, P. V., *et al.*, *Inorg Chem*, **2004**, 43, 5833	2.385
LIQMUT	Habibi, D., *et al.*, *Polyhedron*, **1999**, 18, 2977	2.395
LOVJUB	Konno, T., *et al.*, *Angew Chem, Int Ed*, **2000**, 39, 4098	2.372
MARYUA	Chikamoto, Y., *et al.*, *Inorg Chem*, **2005**, 44, 1601	2.447
NIQWOB	Leung, B. O., *et al.*, *Inorg Chem*, **2013**, 52, 4593	2.395
OMIZEQ	Chen, P., *et al.*, *Euro. J Inorg Chem*, **2010**, 5239	2.384
OPAJIZ	Yuan, H. Q., *et al.*, *Chem Lett*, **2011**, 40, 285	2.417
PELRAC	Chen, Z.-Y., *et al.*, *Chem Asian J*, **2017**, 12, 2763	2.465

PIFGER	Tamura, M., *et al.*, *Acta Cryst. E*, **2007**, 63, m1641	2.394
RITJEJ	Konno, T., *et al.*, *Inorg Chem*, **1997**, 36, 1403	2.363
SPTSIN	Strickler, P., *Helvetica Chim Acta*, **1969**, 52, 270	2.400
TINDIE	Tamura, M., *et al.*, *Inorg Chem*, **2007**, 46, 6834	2.370
UCIJUM	Konno, T., *et al.*, *Chem Lett*, **2006**, 35, 316	2.408
UCIKAT	Konno, T., *et al.*, *Chem Lett*, **2006**, 35, 316	2.434
UFIJIC01	Konno, T., *et al.*, *Bull Chem Soc Jpn*, **2002**, 75, 2185	2.400
WURCER	Konno, T., *et al.*, *Angew Chemie, Int Ed*, **2002**, 41, 4711	2.476
WUYSIS	Hirotsu, M., *et al.*, *Mol Cryst Liquid Cryst*, **2002**, 379, 461	2.400
XAGRUU	Saito, K., *et al.*, *Euro J Inorg Chem,* **2010**, 3909	2.357
XAGSAB	Saito, K., *et al.*, *Euro J Inorg Chem,* **2010**, 3909	2.390
XANJAY	Li, J.-R., *et al.*, *Polyhedron*, **2005**, 24, 481	2.404
XINWIA	Heinl, U., *et al.*, *Z Anorg Allg Chem*, **2002**, 628, 770	2.388
XOZHUP	T. Konno, *et al.*, *Chem Lett*, **2002**, 304	2.386
YOMPIB	Yang, X., *et al.*, *Inorganica Chim Acta*, **2014**, 421, 233	2.371
YOMPOH	Yang, X., *et al.*, *Inorganica Chim Acta*, **2014**, 421, 233	2.363
YONCOV	Yang, X., *et al.*, *Inorganica Chim Acta*, **2014**, 421, 233	2.365
YONDAI	Yang, X., *et al.*, *Inorganica Chim Acta*, **2014**, 421, 233	2.372

Table 12: Survey of AgS_3 THIOLATE structures in CSD version 5.40 (Nov 2018)

CSD Code	Reference	Av. Ag-S (Å)
BALPEL	N.Yoshinari, *et al.*, *Dalton Trans*, **2011**, 40, 12191	2.494
BEPSIZ	P. C. Zachariadis, *et al.*, *Euro J Inorg Chem*, **2004**, 1420	2.574
BIVGOE	B. K. Najafabadi, *et al.*, *Dalton Trans*, **2014**, 43, 2104	2.485
BIVHAR	B. K. Najafabadi, *et al.*, *Dalton Trans*, **2014**, 43, 2104	2.553
CAYZUX	I.Dance, *et al.*, *Chem Comm*, **1984**, 17	2.563
CAYZUX10	I.G.Dance, *et al.*, *Inorg Chem*, **1989**, 28, 1853	2.565
CUTYIA	S.Ahmar, *et al.*, *Angew Chemie, Int Ed*, **2010**, 49, 4422	2.540
FIYMAC	M.L.Golden, *et al.*, *Inorg Chem*, **2005**, 44, 875	2.515
FOGLOC	P.Gonzalez-Duarte, *et al.*, *Chem Comm*, **1987**, 1641	2.508
IWIJUU	D.G.MacDonald, *et al.*, *Chem Euro J*, **2011**, 17, 5890	2.574
MEHYIJ	Ying Xiao, *et al.*, *Chem Euro J*, **2012**, 18, 11184	2.526
MEHYOP	Ying Xiao, *et al.*, *Chem Euro J*, **2012**, 18, 11184	2.530
RITJEJ	T.Konno, *et al.*, *Inorg Chem*, **1997**, 36, 1403	2.491
SOJFON	J.L.Hess, *et al.*, *J Mol Struct*, **2008**, 890, 70	2.464
WIDWOX	Zhong-Yi Li, *et al.*, *Cryst Growth Des*, **2013**, 13, 918	2.516
WURCER	T.Konno, *et al.*, *Angew Chemie, Int Ed*, **2002**, 41, 4711	2.514
XINWIA	U.Heinl, *et al.*, *Z Anorg Allg Chem*, **2002**, 628, 770	2.569
XOZJAX	T.Konno, *et al.*, *Chem Lett*, **2002**, 304	2.520
YOMPIB	Yang, X., *et al.*, *Inorganica Chim Acta*, **2014**, 421, 233	2.560
YOMPOH	Yang, X., *et al.*, *Inorganica Chim Acta*, **2014**, 421, 233	2.519
YONDAI	Yang, X., *et al.*, *Inorganica Chim Acta*, **2014**, 421, 233	2.516

Table 13: Survey of AgS_4 THIOLATE structure in CSD version 5.40 (Nov 2018)

CSD Code	Reference	Av. Ag-S (Å)
JOMBIW	Nadasdi, T.T., Stephan, D.W., *Organomet*, **1992**, 11, 116	2.600
KIXVAO	Stephan, D.W., *Organomet*, **1991**, 10, 2037	2.495
QUCGAW	McLauchlan, C.C., Ibers, J.A., *Inorg Chem*, **2001**, 40, 1809	2.563
RECNEV	Luo, G.-G., *et al.*, *Chem Euro J*, **2017**, 23, 14420	2.576
VIJHIF	Stephan, D.W., *Chem Comm*, **1991**, 129	2.626
VIJHIF10	Stephan, D.W., *Organomet*, **1991**, 10, 2037	2.626

Table 14: Survey of AgN_2 AMINE structures in CSD version 5.40 (Nov 2018)

CSD Code	Reference	Av. Ag-N (Å)
ACAFIV	Cheng, L., *et al.*, *CrystEngComm*, **2012**, 14, 7502	2.325
ACAFOB	Cheng, L., *et al.*, *CrystEngComm*, **2012**, 14, 7502	2.325

AGENPC11	Zhu, H.-L., *et al.*, *Z Krist New Cryst Struct*, **2003**, 218, 307	2.151
AKEDAX	Roy, S., *et al.*, *Cryst Growth Des*, **2016**, 16, 2814	2.185
AKIZEZ	Zhu, H.-L., *et al.*, *Z Krist New Cryst Struct*, **2003**, 218, 249	2.128
ANAYAQ	Garg, S., *et al.*, *J Am Chem Soc*, **2010**, 132, 8888	2.118
APIXED	Cai, Y. J., *et al.*, *Koord khim*, **2010**, 36, 501	2.147
AQAVAP	Wang, R., *et al.*, *Inorganica Chim Acta*, **2004**, 357, 103	2.237
AQAVUJ	Wang, R., *et al.*, *Inorganica Chim Acta*, **2004**, 357, 103	2.135
AROTUW	You, Z.-L., *et al.*, *Acta Cryst C,* **2004**, 60, m117	2.147
ASAVAS	Zerbe, E.-M., *et al.*, *Z Naturforsch B: J Chem Sci*, **2011**, 66, 449	2.171
ASAVUM	Zerbe, E.-M., *et al.*, *Z Naturforsch B: J Chem Sci*, **2011**, 66, 449	2.172
BAFFIZ	Kokunov, Y. V., *et al.*, *Z Neorg Khim*, **2011**, 56, 43	2.202
BAFTIO	Sun, C., *Guangpu Shiyanshi*, **2012**, 29, 1781	2.240
BAFTOU	Sun, C., *Guangpu Shiyanshi*, **2012**, 29, 1781	2.231
BIQVUU	Binnemans, K., *et al.*, *ChemPlusChem*, **2013**, 78, 578	2.141
BIQWAB	Binnemans, K., *et al.*, *ChemPlusChem*, **2013**, 78, 578	2.133
BIQWOP	Binnemans, K., *et al.*, *ChemPlusChem*, **2013**, 78, 578	2.144
BURQOV	Li, Y-G., *et al.*, *Z Anorg Allg Chem*, **2009**, 635, 2572	2.153
CAFHIC	Zhang, Q.-L., *Fenzi Kexue Xuebao*, **2011**, 27, 112	2.210
DAHFOJ	J. A. Flores, *et al.*, *Dalton Transactions*, **2011**, 40, 10351	2.140
DEWTOP	Laye, R. H., *Inorganica Chimica Acta*, **2007**, 360, 439	2.189
EQOJUP	Chen, S.-H., *et al.*, *Z Krist New Cryst Struct*, **2003**, 218, 301	2.130
EQOKEA	Zhu, H.-L., *et al., Z Krist New Cryst Struct*, **2003**, 218, 305	2.154
EVOHIG	You, Z.-L., *et al.*, *Acta Cryst C*, **2004**, 60, m231	2.144
FAXFOA	You, Z.-L., *et al.*, *Acta Cryst E*, **2005**, 61, m6	2.149
FIBPUE	Spinelli, F., *et al.*, *Dalton Trans*, **2018**, 47, 5725	2.165
FIBQAL	Spinelli, F., *et al.*, *Dalton Trans*, **2018**, 47, 5725	2.173
FUPGIG	Richmond, T. G., *et al.*, *Chem Comm*, **1988**, 96	2.148
GAXGIY	Noamane, M. H., *et al.*, *Euro J Org Chem*, **2017**, 3327	2.173
GAXJIB	Noamane, M. H., *et al.*, *Euro J Org Chem*, **2017**, 3327	2.163
GEKYOM	Lou, S.-F., *et al.*, *Z Strukturnoi Khimii*, **2011**, 52, 1129	2.148
GOBNAN	Tsai, H.-A., *et al.*, *Polyhedron*, **2008**, 27, 2035	2.203
GOBNER	Tsai, H.-A., *et al.*, *Polyhedron*, **2008**, 27, 2035	2.143
HAYXEM	Meyer, G., *et al.*, *Des Const Coord Poly*, **2009**	2.507
HAYXIQ	Meyer, G., *et al.*, *Des Const Coord Poly*, **2009**	2.513
HAZBER	Meyer, G., *et al.*, *Des Const Coord Poly*, **2009**	2.170
IHUPEG	Patra, G. K., Goldberg, I., *Cryst Growth Des*, **2003**, 3, 321	2.383
IKEWIE	Zhu, H.-L., *et al.*, *Z Anorg Allg Chem*, **2003**, 629, 1986	2.125
IMAWIC	Zhu, H.-L., *et al.*, *Z Anorg Allg Chem*, **2003**, 629, 1986	2.138
IMAWOI	Zhu, H.-L., *et al.*, *Z Anorg Allg Chem*, **2003**, 629, 1986	2.152
INATOG	Zhu, H.-L., *et al.*, *New Crystal Structures*, **2003**, 218, 309	2.151
IQEFAL	Ren, C.-X., *et al.*, *Inorganica Chim Acta*, **2004**, 357, 443	2.273
IQEFEP	Ren, C.-X., *et al.*, *Inorganica Chim Acta*, **2004**, 357, 443	2.219
JAFPEM	Erxleben, A., *Inorganica Chim Acta*, **2003**, 348, 107	2.208
KILQIF	Smith, G., *et al.*, *Aust J Chem*, **1999**	2.123
KIRWIS	Fielden, J., *et al.*, *Inorg Chem*, **2007**, 46, 9090	2.141
KIRWUE	Fielden, J., *et al.*, *Inorg Chem*, **2007**, 46, 9090	2.141
KIRXAL	Fielden, J., *et al.*, *Inorg Chem*, **2007**, 46, 9090	2.139
KIRXEP	Fielden, J., *et al.*, *Inorg Chem*, **2007**, 46, 9090	2.152
KONXOC	Arjmand, F., *CSD Comm*, **2014**	2.137
KUYNOI	Golder, R. K., *et al.*, *Acta Cryst E,* **2010**, 66, m1324	2.258
LEDWIB	Feazell, R. P., *et al.*, *Inorg Chem*, **2006**, 45, 2635	2.126
LEDXOI	Feazell, R. P., *et al.*, *Inorg Chem*, **2006**, 45, 2627	2.132
LEDYID	Feazell, R. P., *et al.*, *Inorg Chem*, **2006**, 45, 2627	2.145
LUFYIV	Duriska, M. B., *et al.*, *Chem Comm*, **2009**, 5579	2.308
MAGVOG	Sarkar, M., Biradha, K., *CrystEngComm*, **2004**, 6, 310	2.112
MAGVOG01	Dai, J.-X., *et al.*, *Z Naturforsch,B Chem Sci*, **2007**, 62, 1112	2.103
MAGVUM	Sarkar, M., Biradha, K., *CrystEngComm*, **2004**, 6, 310	2.117
MAGWAT	Sarkar, M., Biradha, K., *CrystEngComm*, **2004**, 6, 310	2.118
MINZUE	Crespo, O., *et al.*, *Dalton Trans*, **2002**, 1319	2.254
MOBJIW	Fenton, R. R., *et al.*, *Dalton Trans*, **2002**, 2185	2.189

NAYCEX	Cao, Y., *et al.*, *J Chem Cryst*, **2012**, 42, 401	2.152
NAYCEX01	Liu, J., *et al.*, *Acta Cryst B*, **2012**, 68, 401	2.152
NEPSEJ	Yousuf, I., *et al.*, *New J Chem*, **2018**, 42, 506	2.135
NUNRUL	Huang, J., *et al.*, *Dalton Trans*, **2015**, 44, 5837	2.363
NUNSAS	Huang, J., *et al.*, *Dalton Trans*, **2015**, 44, 5837	2.381
OBIHUD	Pickering, A. L., *et al.*, *Inorg Chem*, **2004**, 43, 4953	2.139
OBIJAL	Pickering, A. L., *et al.*, *Inorg Chem*, **2004**, 43, 4953	2.141
OBIJEP	Pickering, A. L., *et al.*, *Inorg Chem*, **2004**, 43, 4953	2.151
ODERAR	Song, Y.-F., *et al.*, *J Mater Chem*, **2007**, 17, 1903	2.178
OQIKOP	Wang, Y., U. Englert, *Inorganica Chim Acta*, **2010**, 363, 2539	2.180
OQILEG	Wang, Y., Englert, U., *Inorganica Chim Acta*, **2010**, 363, 2539	2.127
OQILOQ	Wang, Y., Englert, U., *Inorganica Chim Acta*, **2010**, 363, 2539	2.142
OQIMAD	Wang, Y., Englert, U., *Inorganica Chim Acta*, **2010**, 363, 2539	2.161
PAHVIE	You, Z.-L., Zhu, H.-L., *Acta Cryst C*, **2004**, 60, m515	2.143
QAQKID	Braga, D., *et al.*, *Chem Comm*, **2005**, 2915	2.168
QAYFUR	Fei, B.-L., *et al.*, *Inorganica Chim Acta*, **2000**, 306, 106	2.372
QEMJEY	Liu, J.-T., *et al.*, *Acta Cryst E*, **2006**, 62, m1992	2.165
RAHCAG	Kokunov, Y. V., *et al.*, *Koord khim*, **2011**, 37, 96	2.196
RAWTOZ	Bowmaker, G. A., *et al.*, *Inorganica Chim Acta*, **2005**, 358, 4327	2.232
RAYYIA	Bowmaker, G. A., *et al.*, *Inorganica Chim Acta*, **2005**, 358, 4342	2.157
RAYYOG	Bowmaker, G. A., *et al.*, *Inorganica Chim Acta*, **2005**, 358, 4342	2.167
RUMTID	Rios, D., *et al.*, *Inorg Chem*, **2009**, 48, 5279	2.138
RUMTOJ	Rios, D., *et al.*, *Inorg Chem*, **2009**, 48, 5279	2.174
RUSTOP	Sun, D., *et al.*, *Inorg Chem Comm*, **2010**, 13, 290	2.053
SUFTUK	Li, J., *et al.*, *J Inclu Phenom Macro Chem*, **2015**, 81, 485	2.150
SURVAS	Li, J., *et al.*, *J Inclu Phenom Macro Chem*, **2015**, 81, 485	2.161
SUTPED	Zhong, D.-C., *et al.*, *J Coord Chem*, **2010**, 63, 3146	2.193
TAFDIO	Zhu, H.-L., *et al.*, *Z Anorg Allg Chem*, **2003**, 629, 1059	2.162
TASHEC	Clauss, C., *et al.*, *Euro J Inorg Chem,* **2012**, 978	2.177
UGEKUM	Nomiya, K., *et al.*, *Dalton Trans*, **2002**, 2483	2.150
UMEWOY	Zhu, H.-L., *et al.*, *Acta Cryst E*, **2003**, 59, m906	2.158
UMEZIV	Zhu, H.-L., *et al.*, *Acta Cryst E* **2003**, 59, m942	2.123
UMOCOO	Zhu, H.-L., *et al.*, *Acta Cryst E*, **2003**, 59, m1048	2.136
UPUVEH	Liu, H.-Y., *et al.*, *Jiegou Huaxue*, **2011**, 30, 211	2.192
VARKIL	Xiao, Y.-H., *et al.*, *J Solid State Chem*, **2017**, 251, 255	2.251
VAYYOK	Brito, I., *et al.*, *Acta Cryst E*, **2005**, 61, m2626	2.176
VEJQIM	Zerbe, E.-M., *et al.*, *Z Naturforsch B Chem Sci*, **2012**, 67, 1263	2.164
VENCUP	Ren, M., *et al.*, *IUCrData*, **2018**, 3, x180101	2.417
VESWEW	Kalf, I., *et al.*, *CrystEngComm*, **2006**, 8, 916	2.144
VESWIA	Kalf, I., *et al.*, *CrystEngComm*, **2006**, 8, 916	2.165
VEXMOB	Kalf, I., *et al.*, *CrystEngComm*, **2006**, 8, 916	2.148
WEKLOQ	Gonzalez, J., *et al.*, *J Coord Chem*, **2015**, 68, 863	2.133
WIKGED	Dai, J.-X., *et al.*, *Z Naturforsch B Chem Sci*, **2007**, 62, 1112	2.139
WUXBIA	Usman, A., *et al.*, *Acta Cryst C*, **2003**, 59, m97	2.141
XAMDEU	Reiss, P., *et al.*, *Angew Chemie, Intl Ed*, **2000**, 39, 3925	2.149
XIFWAK	Kunze, A., *et al.*, *Dalton Trans*, **2002**, 1217	2.142
XUYSAL	Usman, A., *et al.*, *Acta Cryst E*, **2003**, 59, m131	2.167
YERWUQ	Li, S., *et al.*, *J Am Chem Soc,* **2018**, 140, 594	2.219

Table 15: Survey of AgN_3 AMINE structures in CSD version 5.40 (Nov 2018)

CSD Code	Reference	Av. Ag-N (Å)
ABIRAF	Pickering, A. L., *et al.*, *Polyhedron*, **2004**, 23, 2075	2.283
ABIRIN	Pickering, A. L., *et al.*, *Polyhedron*, **2004**, 23, 2075	2.227
CAPZUP	Zhang, G.-Q., *et al.*, *Euro J Inorg Chem*, **2005**, 1919	2.336
EZOZIE	Jones, P. G., *et al.*, *CSD Comm*, **2016**	2.277
GIXSAJ	Zhang, Q.-L., *et al.*, *J Solid State Chem*, **2014**, 210, 178	2.395
HAMSAJ	Liu, Z.-D., *et al.*, *Acta Cryst E,* **2004**, 60, m1883	2.266
HAZBIV	Meyer, G., *et al.*, *Des Const Coord Poly*, **2009**	2.315
IKOQOO	Arii, H., *et al.*, *Euro J Inorg Chem*, **2003**, 2917	2.292

ILAPES	Kovalev, V. V., *et al.*, *Koord khim*, **2015**, 41, 332	2.316
IQUZID	Pickering, A. L., *et al.*, *Chem Comm*, **2004**, 136	2.284
IQUZOJ	Pickering, A. L., *et al.*, *Chem Comm*, **2004**, 136	2.285
KILQEB	Smith, G., *et al.*, *Aust J Chem*, **1999**, 52, 317	2.289
LAJGEK	Wolper, C., *et al.*, *Z Naturforsch B Chem Sci*, **2010**, 65, 1249	2.321
NAYBOE	Plappert, E., *et al.*, *Dalton Trans*, **1997**, 2119	2.286
OBIJIT	Pickering, A. L., *et al.*, *Inorg Chem*, **2004**, 43, 4953	2.280
OBIJOZ	Pickering, A. L., *et al.*, *Inorg Chem*, **2004**, 43, 4953	2.309
OBIJUF	Pickering, A. L., *et al.*, *Inorg Chem*, **2004**, 43, 4953	2.290
QUDKIJ	Zhang, H., *et al.*, *Inorg Chem Comm*, **2001**, 4, 241	2.282
RAFROF	Carlucci, L., *et al.*, *Inorganic Chemistry*, **1997**, 36, 1736	2.346
RIFRIJ	Chen, C.-N., *et al.*, *J Mater Chem C*, **2013**, 1, 5161	2.297
TAWJOR	Brown, P. O., *et al.*, *Chem Comm*, **2005**, 4402	2.275
UJUXIG	Seeber, G., *et al.*, *Chem Comm*, **2003**, 2002	2.300
UJUXOM	Seeber, G., *et al.*, *Chem Comm*, **2003**, 2002	2.289
VAQFOL	Litecká, M., *et al.*, *J Coord Chem*, **2017**, 70, 1698	2.434
YOLKOA	Lee, J.-E., *et al.*, *Polyhedron*, **2008**, 27, 3004	2.300
YOLKUG	Lee, J.-E., *et al.*, *Polyhedron*, **2008**, 27, 3004	2.306
YOLLAN	Lee, J.-E., *et al.*, *Polyhedron*, **2008**, 27, 3004	2.299
YOLLER	Lee, J.-E., *et al.*, *Polyhedron*, **2008**, 27, 3004	2.319
ZEPWUO	Kokunov, Y. V., *et al.*, *Z Neorg Khim*, **2012**, 57, 1027	2.319

Table 16: Survey of AgN_4 AMINE structures in CSD version 5.40 (Nov 2018)

CSD Code	Reference	Av. Ag-N (Å)
AMEVUJ	Xie, Y., *et al.*, *Euro J Inorg Chem*, **2003**, 4010	2.366
ARABUR	Moon, J. R., *et al.*, *Inorganica Chim Acta*, **2010**, 363, 2682	2.145
ARUZAO	Ouyang, X.-M., *et al.*, *J Solid State Chem*, **2004**, 177, 350	2.352
BEGSAJ	Habata, Y., *et al.*, *Org Lett*, **2012**, 14, 4576	2.446
BEGSIR	Habata, Y., *et al.*, *Org Lett*, **2012**, 14, 4576	2.475
BEGSOX	Habata, Y., *et al.*, *Org Lett*, **2012**, 14, 4576	2.451
BEGTAK	Habata, Y., *et al.*, *Org Lett*, **2012**, 14, 4576	2.454
BEGTEO	Habata, Y., *et al.*, *Org Lett*, **2012**, 14, 4576	2.452
BEGTOY	Habata, Y., *et al.*, *Org Lett*, **2012**, 14, 4576	2.453
BERJUF	Habata, Y., *et al., Dalton Trans*, **2013**, 42, 8212	2.453
EYEXEM	Tao, X., *et al., Z Anorg Allg Chem*, **2011**, 637, 1394	2.379
FAXJEU	Liu, Z.-D., *et al.*, *Acta Cryst E*, **2005**, 61, m44	2.384
FINROK	Ma, Z., *et al.*, *J Mol Struct*, **2005**, 738, 137	2.402
GAFZIX	Habata, Y., *et al.*, *J Incl Phenom Macro Chem*, **2004**, 49, 17	2.418
GIMKIY	Chaloner, L., *et al.*, *Tetrahedron Lett*, **2013**, 54, 3363	2.417
HALCEC	Po, H. N., *et al., Acta Cryst C*, **1993**, 49, 1914	2.162
HAZBOB	Meyer, G., *et al.*, *Des Const Coord Poly*, **2009**	2.422
ICADIA	Iida, M., *et al.*, *Euro J Inorg Chem*, **2004**, 3920	2.375
IKOQII	Arii, H., *et al.*, *Euro J Inorg Chem*, **2004**, 2003, 2917	2.367
IXOFAC	Bharadwaj, P. K., *CSD Comm*, **2004**	2.484
JAGBEZ	Ouyang, X.-M., *et al.*, *Dalton Trans*, **2003**, 1836	2.384
JIFSIA	Charland, J.-P., *et al.*, *J Cryst Spectroscopic Res*, **1985**, 15, 581	2.388
JIFSIA02	Bowmaker, G. A., *et al., Inorganica Chim Acta*, **2005**, 358, 4327	2.402
KAPGEP	Zhang, Q.-L., *et al.*, *Gaodeng Xuexiao Huaxue Xuebao*, **2011**, 2187	2.392
KOFCAJ	Po, H. N., *et al.*, *Acta Cryst C*, **1991**, 47, 2310	2.195
LAJGIO	Wolper, C., *et al.*, *Z Naturforsch B Chem Sci,* **2010**, 65, 1249	2.356
LEBZID	Moon, J. R., *et al.*, *Bull Korean Chem Soc*, **2011**, 32, 325	2.161
MIGFUF	Habata, Y., *et al.*, *Inorg Chem*, **2013**, 52, 2542	2.477
MIGGAM	Habata, Y., *et al.*, *Inorg Chem*, **2013**, 52, 2542	2.478
NAYBUK	Plappert, E. C., *et al.*, *Dalton Trans*, **1997**, 2119	2.382
NIQYER	Darr, J. A., *et al., Dalton Trans*, **1997**, 2869	2.395
PEQMEG	Moon, D., *et al.*, *Acta Cryst E*, **2018**, 74, 461	2.180
QIBTOL	Choi, K. S., *et al.*, *Bull Korean Chem Soc*, **2006**, 27, 747	2.390
QIWPOB	Wang, Q.-M., *et al.*, *Chem Comm*, **2001**, 807	2.192
QOWNEX	Ikeda, M., *et al., Inorg Chem*, **2014**, 53, 10514	2.465

REPWUF	Brown, P. O., *et al.*, *Chem Asian J*, **2006**, 1, 529	2.403
TECCIO	Liu, X.-T., *et al.*, *Huaxue Yanjiu*, **2005**, 16, 1-4	2.372
TZTDAG01	Mertes, K. B., *Inorg Chem*, **1978**, 17, 49	2.161
UFAVEC	Yoon, I., *et al.*, *Acta Cryst C*, **2002**, 58, m165	2.393
VIBNEB	Habata, Y., *et al.*, *Org Biomolecular Chem*, **2013**, 11, 4265	2.452
XIZHOD	Wang, Q.-M., *et al.*, *New J Chem*, **2002**, 26, 513	2.186
YEMCUP	Ray, D., *et al.*, *Euro J Inorg Chem*, **2006**, 1771	2.466
YIJFAZ	Chun, I. S., *et al.*, *Bull Korean Chem Soc*, **2006**, 27, 1005	2.402
ZIDYOA	Carlucci, L., *et al.*, *Inorg Chem,* **1995**, 34, 5698	2.386

Table 17: Survey of AgO_2 CARBOXYLATE structures in CSD version 5.40 (Nov 2018)

CSD Code	Reference	Av. Ag-O (Å)
AFUJAN	Lin, H.-H., *et al.*, *J Chinese Chem Soc*, **2008**, 55, 45	2.420
AGTFAC01	Karpova, E. V., *et al.*, *Koord khim*, **1999**, 25, 70	2.241
ANATAM	Miao, S.-B., *et al.*, *CrystEngComm*, **2016**, 18, 4636	2.535
APIXED	Cai, Y. J., *et al.*, *Koord khim*, **2010**, 36, 501	2.165
AQUYUI	Song, Y., *et al.*, *CrystEngComm*, **2016**, 18, 6411	2.366
ATOJID	Gong, H.-Y., *et al., J Am Chem Soc*, **2011**, 133, 1526	2.177
AYAVIH	Thuéry, P., *et al.*, *Cryst Growth Des*, **2016**, 16, 7083	2.461
BAHPIL	Liu, C., *et al.*, *J Coord Chem*, **2012**, 65, 165	2.417
BEMRES	Wang, J.-J., *et al., Z Anorg Allg Chem*, **2012**, 638, 1531	2.218
BOKPOH	Zhao, L., *et al.*, *Chem Euro J*, **2008**, 14, 10437	2.417
BOMGER	Zorlu, Y., *et al.*, *J Mol Struct*, **2014**, 1076, 629	2.627
CAJKOQ	Kan, W.-Q., *et al.*, *Polyhedron*, **2015**, 85, 246	2.119
COHBEI	Wang, Z.-H., *et al., CrystEngComm*, **2014**, 16, 5028	2.495
DACJUO	Li, B., *et al.*, *Dalton Trans*, **2011**, 40, 10071	2.477
DACKAV	Li, B., *et al.*, *Dalton Trans*, **2011**, 40, 10071	2.144
DACKEZ	Li, B., *et al.*, *Dalton Trans*, **2011**, 40, 10071	2.133
DOQQUX	Mei, L., *et al.*, *Inorg Chem*, **2018**, 57, 4673	2.433
DUBXAA	Zhu, X.-F., *et al.*, *Acta Cryst E*, **2009**, 65, m994	2.659
EMOVEI	Sun, D., *et al.*, *CrystEngComm*, **2011**, 13, 1591	2.452
EQOJUP	Chen, S.-H., *et al., Z Krist New Cryst Struct*, **2003**, 218, 301	2.119
EQOKEA	Qiu, X.-Y., *et al.*, *Synth React Inorg Met-Org Nano-Met Chem*, **2005**	2.119
EWAFAJ	Suenaga, Y., *et al.*, *Inorganica Chim Acta*, **2003**, 351, 379	2.308
EWASOK	Dong, Y.-B., *et al.*, *Organometallics*, **2004**, 23, 1604	2.569
EXELID	Hao, H.-J., *et al.*, *Cryst Growth Des*, **2011**, 11, 3564	2.275
FAQPIY	Gondi, S. R., *et al.*, *J Sulfur Chem*, **2011**, 32, 17	2.404
FAXFOA	You, Z.-L., *et al.*, *Acta Cryst E*, **2005**, 61, m6	2.106
FAYMUO	Liu, S.-Q., *et al.*, *Acta Cryst E*, **2005**, 61, m251	2.157
FIJRAS	Liu, S.-Q., *et al.*, *Inorganica Chim Acta*, **2005**, 358, 919	2.267
GEVPIG	Mak, T. C. W., *et al.*, *Aust J Chem*, **1988**, 41, 683	2.217
GIHXIF	Abu-Youssef, M. A. M., *et al.*, *Inorg Chem*, **2007**, 46, 5893	2.215
GIMHOA	Wang, G.-L., *Acta Cryst C*, **2007**, 63, m479	2.445
GIMLAP	Mak, T. C. W., *et al.*, *Dalton Trans*, **1988**, 2353	2.187
GIWNOR	Xue, C.-M., *et al.*, *J Inorg Organomet P*, **2013**, 23, 1468	2.395
GUJCEU	Zhang, Y.-N., *et al.*, *Inorg Chem Comm*, **2009**, 12, 611	2.154
HAYWUB	Meyer, G., *et al.*, *Des Construct Coord P*, **2009**	2.276
HAYXAI	Meyer, G., *et al.*, *Des Construct Coord P*, **2009**	2.289
HUDQUU	Patterson, S., *et al.*, *CSD Comm*, **2015**	2.575
HUTQUJ	Zhao, X.-Q., *et al.*, *Inorg Chem*, **2009**, 48, 11048	2.498
HUTREU	Zhao, X.-Q., *et al.*, *Inorg Chem*, **2009**, 48, 11048	2.496
HUTRIY	Zhao, X.-Q., *et al.*, *Inorg Chem*, **2009**, 48, 11048	2.497
HUTROE	Zhao, X.-Q., *et al.*, *Inorg Chem*, **2009**, 48, 11048	2.745
IFOHIV	Zang, X.-Q., *et al.*, *Organomet*, **2008**, 27, 2396	2.381
IFUTUY	Wang, X.-J., *et al.*, *Z Anorg Allg Chem*, **2002**, 628, 1158	2.398
IJOMAW	Fischer, A., *Acta Cryst E*, **2011**, 67, m255	2.559
ILOXUE	Huang, H.-Q., *et al.*, *Inorg Chem Comm*, **2016**, 68, 21	2.370
ISABAH	Churakov, A. V., *et al.*, *Mendeleev Comm*, **2016**, 26, 295	2.596
ISARIE	Burrows, A. D., *et al.*, *Dalton Trans*, **2011**, 40, 5483	2.325

JEXLEG	Xia, C.-K., *et al., Cryst Growth Des*, **2018**, 18, 1978	2.554
KAMTOH04	Wolcyrz, M., *et al.*, *Z Krist Cryst Mater*, **2006**, 221, 270	2.188
KAMTOH05	Wolcyrz, M., *et al.*, *Z Krist Cryst Mater*, **2006**, 221, 270	2.224
KAMTOH07	Poyraz, M., *et al.*, *Inorganica Chim Acta*, **2011**, 375, 114	2.196
KAMTUN	Smith, G., *et al.*, *Z Krist Cryst Mater*, **1988**, 184, 275	2.221
KEGYEB	Wang, J., *et al., Euro J Inorg Chem*, **2006**, 2069	2.377
KOLWIS	Wang, Y.-L., *et al.*, *CrystEngComm*, **2008**, 10, 1667	2.412
LAFPUE	Ma, J.-L., *et al.*, *Z Krist - New Cryst Struct*, **2004**, 219, 159	2.126
LELPID	Sun, D., *et al.*, *CrystEngComm*, **2013**, 15, 1185	2.351
LERDUJ	Altaf, M., *et al.*, *Acta Cryst C,* **2013**, 69, 127	2.736
LIQGOI	Zhao, L., *et al.*, *Chem Asian J*, **2007**, 2, 1240	2.325
LIQHEZ	Zhao, L., *et al.*, *Chem Asian J*, **2007**, 2, 1240	2.517
LOSZAW	Lin, Y.-M., *et al.*, *Dalton Trans*, **2015**, 44, 2439	2.320
LUPJOW	Aprea, A., *et al.*, *Solid State Sci*, **2010**, 12, 795	2.255
MIDZUV	Li, X.-P., *et al.*, *Inorganica Chim Acta*, **2007**, 360, 2990	2.383
MOGYAI	Wang, Q.-M., *et al.*, *J Cluster Sci*, **2002**, 13, 63	2.307
MOXFUA	Brandys, M.-C., *et al.*, *J Am Chem Soc*, **2002**, 124, 3946	2.357
MOXFUA01	Marsh, R. E., *et al.*, *Inorganica Chim Acta*, **2007**, 360, 4017	2.352
MURPAR	Wang, L., *et al.*, *Wuji Huaxue Xuebao*, **2010**, 26, 725	2.368
NAMNUM	Park, K.-M., *et al.*, *Inorg Chem*, **2011**, 50, 12085	2.352
NUKRAO	Li, B., *et al.*, *J Organomet Chem*, **2011**, 696, 2820	2.441
NUKRES	Li, B., *et al.*, *J Organomet Chem*, **2011**, 696, 2820	2.397
OMAWOP	Wan, C.-Q., *et al.*, *New J Chem*, **2011**, 35, 319	2.487
OWACAR	Sun, D., *et al.*, *Cryst Growth Des*, **2011**, 11, 1427	2.368
PANXEE	Bruno, G., *et al.*, *Inorganica Chim Acta*, **1992**, 197, 9	2.218
PELQUV	Chen, Z.-Y., *et al.*, *Chem Asian J*, **2017**, 12, 2763	2.395
PIYGOV	Hau, S. C. K., *et al.*, *J Chinese Chem Soc*, **2013**, 60, 877	2.621
QATXUH	Shahangi, F., *et al.*, *Inorg Chem Comm*, **2017**, 82, 6	2.201
QUDLEH	Yin, P.-X., *et al.*, *Cryst Growth Des*, **2009**, 9, 4884	2.321
QUNWIG	Jin, J.-C., *et al.*, *Dalton Trans*, **2009**, 10181	2.143
RADYOM	Jin, J., *et al., New J Chem*, **2010**, 34, 1176	2.397
RADYUS	Jin, J., *et al., New J Chem*, **2010**, 34, 1176	2.414
RADZAZ	Jin, J., *et al., New J Chem*, **2010**, 34, 1176	2.397
RADZED	Jin, J., *et al., New J Chem*, **2010**, 34, 1176	2.415
RUDQAJ01	Zhang, T., *et al.*, *Dalton Trans*, **2009**, 7688	2.402
SASKUV	Zhang, J., *et al.*, *J Mol Struct*, **2017**, 1136, 196	2.378
TAYZAX	Yang, Y.-Y., *et al.*, *Polyhedron*, **2017**, 134, 345	2.390
TEQPOV	Frisch, M., *et al.*, *Dalton Trans*, **2006**, 4679	2.380
TIPZUP	Hu, M., *et al.*, *Euro J Inorg Chem*, **2013**, 5476	2.492
TIQCIH	Hu, T., *et al.*, *Euro J Inorg Chem*, **2013**, 5476	2.559
TIVGEK	Wu, D.-D., *et al.*, *Aust J Chem*, **1996**, 49, 689	2.126
UGEKUM	Nomiya, K., *et al.*, *Dalton Trans*, **2002**, 2483	2.125
UWIHUE	Ren, Y.-P., *et al.*, *Wuji Huaxue Xuebao*, **2011**, 27, 1015	2.205
VEDWAD	Awaleh, M. O., *et al.*, *Inorg Chem*, **2006**, 45, 1560	2.346
VEDWEH	Awaleh, M. O., *et al.*, *Inorg Chem*, **2006**, 45, 1560	2.269
VOYVEM	Huang, H.-Q., *et al.*, *J Mol Struct*, **2015**, 1086, 99	2.414
VUQQUV	Yang, Y.-D., *et al., J Am Chem Soc*, **2015**, 137, 12966	2.187
WAMWIS	Li, Y.-H., *et al.*, *Dalton Trans*, **2012**, 41, 2289	2.471
WUYFEB	Konaka, H., *et al.*, *Inorg Chem*, **2003**, 42, 1928	2.324
WUYFIF	Konaka, H., *et al.*, *Inorg Chem*, **2003**, 42, 1928	2.338
WUYFOL	Konaka, H., *et al.*, *Inorg Chem*, **2003**, 42, 1928	2.314
WUYMOS	Zhu, H.-L., *et al.*, *Supramol Chem*, **1999**, 11, 119	2.157
XOBDOI	Zheng, G.-L., *et al.CrystEngComm*, **2008**, 10, 658	2.356
XOCGOL	Karpova, E. V., *et al.*, *Koord khim*, **2001**, 27, 311	2.221
XORCOX	Liu, J.-Q., *et al.*, *Inorganica Chim Acta*, **2009**, 362, 1295	2.445
XORXUY	Sun, Y., *et al.*, *Canadian J Chem*, **2009**, 87, 188	2.180
XUXWOD	Wang, Y., *et al.*, *Struct Chem*, **2010**, 21, 203	2.136
YEGSIO	Wang, J.-J., *et al., J Coord Chem*, **2012**, 65, 3614	2.157
YOKPIY	Luo, G.-G., *et al.*, *Polyhedron*, **2008**, 27, 2791	2.580
ZIZXEN	Hau, S. C. K., *et al.*, *Acta Cryst B,* **2014**, 70, 37	2.468

ZUGJES	Hau, S. C. K., *et al.*, *J Organomet Chem*, **2015**, 792, 123	2.409

Table 18: Survey of AgO_3 CARBOXYLATE structure in CSD version 5.40 (Nov 2018)

CSD Code	Reference	Av. Ag-O (Å)
AQAZEX	Rombke, P., *et al.*, *Inorganica Chim Acta*, **2004**, 357, 235	2.285
AWORUA	Meng, Z.-H., *Acta Cryst E*, **2011**, 67, m1112	2.281
BADDUG	Neo, Y. C., *et al.*, *Dalton Trans*, **2002**, 337	2.272
BIDVAM	Xia, J., *et al.*, *Z Krist New Cryst Struct*, **2004**, 219, 163	2.303
CADXOU	Roesky, H. W., *et al.*, *Chem Comm*, **1983**, 981	2.458
CEVGUI	Altay, A., *et al.*, *Polyhedron*, **2018**, 151, 160	2.253
IFUTUY	Wang, X.-J., *et al.*, *Z Anorge Allg Chem*, **2002**, 628, 1158	2.289
JOFHIX	Wang, J.-J., *et al.*, *Jiegou Huaxue*, **2014**, 33, 729	2.286
KIMZUE	Zhu, Y., *et al.*, *Inorganica Chim Acta*, **2019**, 484, 42	2.269
KOLWIS	Wang, Y.-L., *et al.*, *CrystEngComm*, **2008**, 10, 1667	2.313
LELPID	Sun, D., *et al.*, *CrystEngComm*, **2013**, 15, 1185	2.315
MURPEV	Wang, L., *et al.*, *Wuji Huaxue Xuebao*, **2010**, 26, 725	2.322
NEYWAR	Hau, S. C. K., *et al.*, *Polyhedron*, **2013**, 52, 992	2.495
OCIVIF	Iyoda, M., *et al.*, *Tetrahedron Lett*, **2001**, 42, 6883	2.291
PANXEE	Bruno, G., *et al.*, *Inorganica Chim Acta*, **1992**, 197, 9	2.241
PELQUV	Chen, Z.-Y., *et al.*, *Chem Asian J*, **2017**, 12, 2763	2.578
QAFMEQ	Zhong, J. C., *et al.*, *Inorganica Chim Acta*, **2003**, 342, 202	2.312
QATRIO	Liu, F.-J., *et al.*, *Inorg Chem Comm*, **2012**, 15, 136	2.268
QIFTIK	Hu, T., *et al.*, *Organomet*, **2012**, 31, 7539	2.284
QIFTOQ	Hu, T., *et al.*, *Organomet*, **2012**, 31, 7539	2.295
QUBLUV	Hudson, Z. M., *et al.*, *Acta Cryst C,* **2009**, 65, m328	2.398
QUNWIG	Jin, J.-C., *et al.*, *Dalton Trans*, **2009**, 10181	2.325
ROJFUS	Akhbari, K., *et al.*, *J Mol Struct*, **2008**, 891, 132	2.313
UMIDIF	Han, J., *et al.*, *Z Anorg Allg Chem*, **2016**, 642, 584	2.267
VEDVEG	Awaleh, M. O., *et al.*, *Inorg Chem*, **2006**, 45, 1560	2.330
VEDVIK	Awaleh, M. O., *et al.*, *Inorg Chem*, **2006**, 45, 1560	2.334
VEDVOQ	Awaleh, M. O., *et al.*, *Inorg Chem*, **2006**, 45, 1560	2.333
VUJCOS	Kozitsyna, N. Y., *et al.*, *Mendeleev Comm*, **1992**, 100	2.350
WUYMOS	Zhu, H.-L., *et al.*, *Supramol Chem*, **1999**, 11, 119	2.293
XUXWUJ	Wang, Y., *et al.*, *Struct Chem*, **2010**, 21, 203	2.296

Table 19: Survey of AgO_4 CARBOXYLATE structures in CSD version 5.40 (Nov 2018)

CSD Code	Reference	Av. Ag-O (Å)
BESJUG	Artner, C., *et al.*, *Dalton Trans*, **2013**, 42, 6694	2.383
DOCNIT	Nockemann, P., *et al.*, *Cryst Growth Des*, **2008**, 8, 1353	2.403
DUCQEZ	Wright, J. S., *et al.*, *IUCrJ*, **2015**, 2, 188	2.327
EJUWOW	Yeung, A. D., *et al.*, *J Organomet Chem*, **2011**, 696, 112	2.345
LELLOF	Chen, S.-C., *et al.*, *Chem Comm*, **2013**, 49, 1270	2.365
ONEWEK	Kozitsyna, N. Y., *et al.*, *Inorganica Chim Acta*, **2011**, 370, 382	2.383
PABBOM	Han, J., *et al.*, *Inorganica Chim Acta*, **2016**, 442, 124	2.347
TIDSEE	Wang, Q.-M., *et al.*, *J Am Chem Soc*, **2001**, 123, 7594	2.343
XUYSER	Mei, H.-X., *et al.*, *J Mol Struct*, **2016**, 1108, 126	2.506
YAYKAK	Mak, T. C. W., *et al.*, *Inorganica Chim Acta*, **1993**, 203, 97	2.350

Appendix 3.9.3 Unfiltered blood EXAFS spectra

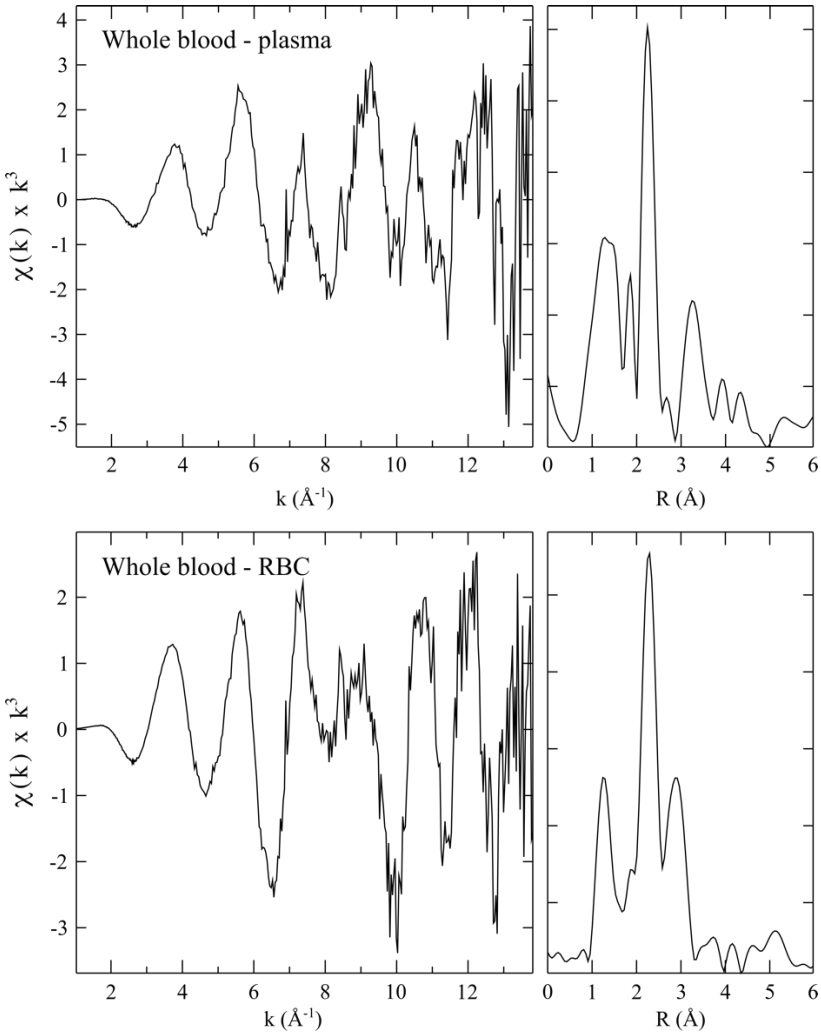

Figure 8: Unfiltered Ag K-edge EXAFS spectra (**left panel**) and corresponding Fourier Transform (**right panel**) of human whole blood plasma fraction (**top**), and RBC fraction (**bottom**).

Chapter Four: Development of silver-containing materials for use as antibacterial agents

4.1 Abbreviations

AS	Australian Synchrotron
ASBDC	2,5-bis(allylsulfanyl)benzene dicarboxylic acid
BDC	1,4-benzene dicarboxylic acid
EXAFS	extended X-ray absorption fine structure
HAI	health care-associated infection
LCF	linear combination fitting
MOF	metal-organic framework
NMR	nuclear magnetic resonance
NP	nanoparticles
PCL	polycaprolactone
PSBDC	2,5-bis(propylsulfanyl)benzene dicarboxylic acid
PXRD	powder X-ray diffraction
SBU	secondary building unit
SCXRD	single crystal X-ray diffraction
XANES	X-ray absorption near-edge structure
XAS	X-ray absorption spectroscopy
UiO-66	Universitet i Oslo-66

4.2 Introduction

Health care-associated infections (HAIs) are acquired while a patient is admitted to a health care facility. In developed countries HAIs have been reported to impact between 5 and 15% of hospitalised patients.[1] The US Center for Disease Control and Prevention estimates that 1.7 million patients are affected by HAIs and that ~100,000 die as a result of the infection.[2] In addition to the risk to human life these infections pose, the cost of combatting HAIs annually has been estimated to range from $28-45 billion (USD).[3] An increase in antibiotic resistant bacteria, and a lack of novel antibiotic discovery/development has further compounded the problem of health care associated infections.[4-5]

The discovery of penicillin in 1928 by Alexander Flemming, and the clinical testing/commercialisation of the drug by Howard Florey in the 1940s enabled highly effective treatment/prevention of bacterial infections.[6] However, while effective, molecular antibiotics often elicit their bactericidal activity through a singular mode of action, making it easier for resistances to form.[7] Coupled with misuse/over-prescription, and a lack of novel antibacterial drug discovery an antibiotic resistance crisis is a possibility.[4-5]

The antibacterial properties of silver have been known for centuries; Persian kings were thought to only drink from silver vessels as it was observed that drinks stored in them remained fresh for longer.[8] In modern day, silver is still used in the treatment of burns, ulcers and other wounds[9] in addition to being incorporated into a myriad of different medical and commercial items to imbue them with antibacterial properties.[10] Largely this is due to the high toxicity of the metal ions/nanoparticles against bacteria (μM $AgNO_3$) as well as the perceived lack of toxicity against mammals and humans. The *estimated* acute lethal dose of silver for humans ranges from 1.4 to 40 x 10^5 μg/kg,[11] and The World Health Organisation (WHO) has actively listed no health-based guideline for the amount of silver in drinking water.[12] The discrepancy in toxicity between bacteria and humans is possibly due to the high structural and functional redundancy of multicellular organisms vs. prokaryotes (like bacteria); an argument that implies inherent toxicity on a cellular level. Additionally, humans have detoxification mechanisms such as pacification by sedimentation or adsorption to biomolecules. Such a broad difference in toxic levels provides a broad 'therapeutic window' for the use of silver as an antibacterial agent.

Silver's efficacy as an antibacterial agent is thought to be, in part, due to a multifaceted attack on the organism. Four broad ways in which the metal can disrupt cellular processes have been identified and substantiated in literature: interaction with the

cell wall/membrane, DNA, inhibition of proteins/enzymes, generation of reactive oxygen species (ROS).[13] The benefit of a multimodal mechanism is that were the organism to develop resistance against one pathway, silver can still elicit its antibacterial properties in other ways.

According to Pearson, Ag(I) is classified as a 'soft' cation, similar to Cu(I), and has preference for polarizable 'soft' ligands such as those containing sulfur or nitrogen.[14] In addition to this, an affinity between silver ions and pi systems has also been observed. Indeed, the crystal structure of a major Cu^+ homeostatic protein (CusF) crystallised in the presence of silver ions reveals interaction between not only coordinating methionine and histidine residues but cation-pi interactions with a tryptophan residue.[15] Materials containing thioether units functionalised with pendant alkene groups have been shown to have increased selectivity for noble metals, like palladium.[16-17]

As the antibacterial properties of silver are well known, antibacterial assays of silver-containing materials/compounds are common. It has been identified that carboxylate-silver interactions in a structure are favourable and provide a stronger antibacterial response than either nitrogen or sulfur donors;[18] thought to be due to weak Ag-O interactions facilitating release of Ag^+.

Silver nanoparticles (AgNPs) also possess broad-spectrum antimicrobial properties against bacteria, fungi and viruses.[19] However, their mode(s) of action are still unclear; namely, whether the NPs act as a Trojan horse from which silver ions are released or whether the NPs themselves are the bactericidal agent (or both). In general a decrease in particle size has been observed to yield greater antibacterial activity due to increased surface area of the particle allowing more efficient oxidative dissolution of Ag^+.[20]

In medical instrumentation and implants, controlled release of bactericidal concentrations of silver are sought after.[21-23] The coating of metallic silver onto implants has been shown to have variable leaching of silver into the wound site, presumed to be due to a combination of the slow rate of oxidation of bulk silver, as well as sequestration of silver ions that are released by biomolecules or formation of insoluble salts. Attempts to combat both issues have seen silver ions and/or NPs incorporated into many devices, such as deposition onto surfaces as ions, NPs or composite materials; silver-doped phosphate glasses which release their cargo as they degrade; and adhesion of polymers or porous

materials onto the device.[11] Metal-organic frameworks are a class of porous materials of particular interest.

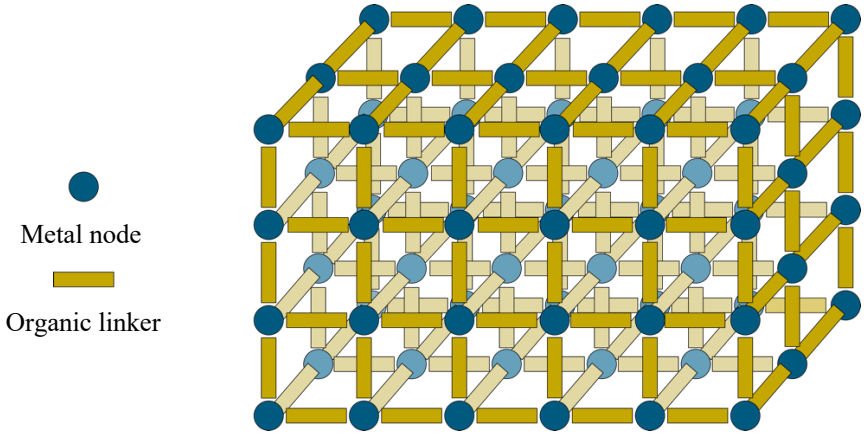

Figure 1: A schematic of MOF synthesis from a metal node and organic linker.

Metal-organic frameworks (MOFs) are crystalline, hybrid materials consisting of metal cluster nodes coordinated in a directional mode by organic linker molecules (**Figure 1**).[24] Metals such as zinc, copper, and zirconium are commonly used as 'metal nodes' while the organic linkers are often bi/trivalent carboxylic acids or nitrogen containing aromatic molecules.[25] In the last twenty years, the MOF field has expanded greatly and many possible applications have been reported, including: storage/separation of gas and hydrocarbons,[26-27] energy storage,[28] sensing,[29] catalysis,[30] and drug delivery.[31] Regarding medicinal drug delivery from MOFs, a wide range of applications have been investigated, including release/sensing of biologically-relevant gases (nitric oxide, carbon monoxide, hydrogen sulfide);[32-34] encapsulation of drugs like ibuprofen, doxorubicin, caffeine, vancomycin, and silver nanoparticles;[35-38] and incorporation of the bioactive component into the MOF structure such as the use of silver, copper or zinc in the metal cluster.[39-41]

A metal-organic framework of particular interest in this research is UiO-66 (*Universitet i Oslo*-66); comprised of zirconium-based $[Zr_6O_4(OH)_4]$ metal nodes, or secondary building unit (SBU), linked by twelve 1,4-benzene dicarboxylic acids (BDC) (**Figure 2**). The connectivity of the BDC linkers with the metal nodes results in two different pore environments, octahedral pores (~9 Å diameter) and tetrahedral pores (~7 Å diameter).[42] However, the synthesis of UiO-66 often requires inclusion of a modulator in the reaction mixture, often an organic, monotopic carboxylic acid or mineral acid (HCl). The role of the modulator is to impede crystal growth by competing with the BDC linker for coordination sites on the zirconium nodes.[43] While many of the modulator molecules are eventually replaced by BDC, some can be retained by the material, thereby introducing

defect sites which perturb the pore distribution of the MOF;[44] i.e. instead of twelve BDC linkers bound to the zirconium node, a mixture of BDC and modulator will be present and, given the modulator is a monotopic acid, provide less well-defined pore environments. Toxicity of zirconium against mammals is relatively low (LD_{50} ~4 g/kg) compared to other metals (LD_{50} Cu ~0.025 g/kg, and Zn ~0.35 g/kg)[45] suggesting that adverse health effects of the Zr-component of the MOF would be minimal.

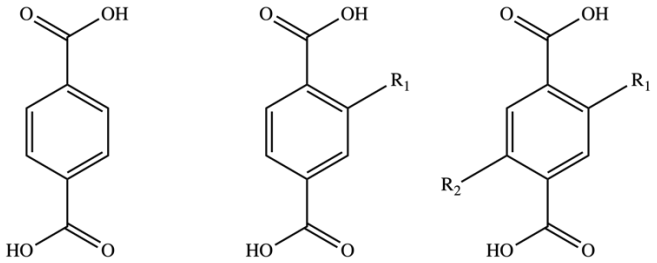

(a) **(b)** **(c)**

Figure 2: Structures of 1,4-benzene dicarboxylic acid (BDC) (**a**) and derivatives; 2- (**b**), and 2,5- (**c**) functionalised BDC. $R_1 = R_2$; R_1 = OH, NH_2, SH, etc.

A benefit that metal-organic frameworks provide over other porous materials, like zeolites, is their ability to be tailored for specific purpose. For example, while the UiO-66 morphology was initially discovered using the BDC linker, it has since been identified that structurally similar linkers, bearing different functional groups (**Figure 2**), can provide materials isostructural with UiO-66. Thus, it is possible to design a pore environment in the material that is favourable for a particular application (such as loading and releasing silver). Other modifications involve the elongation of the BDC linker by addition of a second phenyl core, resulting in the isoreticulated material, UiO-67, which has similar topology to UiO-66 but with larger pores.[46]

However, like most MOFs, UiO derivatives are prepared as crystalline powders, which, unlike composite materials, are not amenable to coating or incorporation onto medicinal surfaces, such as prosthetics or implants. Titanium is used for load-bearing implants due to its good biocompatibility, and strength, however, the metallic form of the transition metal has little, if any, antibacterial properties.[11] In order to imbue an implant with antibacterial properties it needs to be modified or coated with an antibacterial agent. From the synthesis of silver nanoparticles in titanium oxide nanoparticles[47] to hydrogels doped with silver ions or nanoparticles,[48] a multitude of different methods to incorporate silver into titanium structures have been investigated. Resins have been shown to be able to trap AgNPs within their matrices by immersion of the material in a solution containing

ionic silver followed by a reducing agent, which forms the NPs *in situ*.[49] Benefits observed by allowing the diffusion of the ionic silver species into the material include deeper impregnation into the resin or polymer which, in turn, leads to a slower release of the synthesised NPs.[11] Examples of polymers or materials previously explored for use in implant technology include lactose-substituted chitosan (Chitlac),[50] polyacrylamide,[51] polyethylene,[39] poly(L-lysine) (PLL),[52] and poly(L-lactic acid) (PLLA),[53] among others. It has been shown that the rate of release of ions or AgNPs from a polymer matrix is dependent on a number of factors such as the crystallinity of the matrix, concentration of silver, the morphology of the enveloped NPs, structural changes in the material caused by the inclusion of silver, as well as the strength of the interaction between silver and the material.[11] If the silver in the material is weakly bound it is shown that the release into media is faster relative to that of a more strongly bound silver species.[48]

A particular polymer of interest is polycaprolactone (PCL), which has been approved for use by the US Food and Drug Administration (FDA).[54] PCL was widely used in the biomaterials and drug delivery fields in the 70's and 80's but fell out of favour as other aliphatic polymers, such as polylactides and polyglycolides were developed.[55] However, with FDA approval, the reasonably inexpensive cost of production, and ease of use the polymer has come to the fore.[54] The solubility of the polymer in non-aqueous solvents means that it is easier to work with (compared to other polymers) and can be prepared by simple solvent casting techniques.[55]

4.2.1 Research aims

The aims of the work presented herein were to design and synthesise functionalised analogues of UiO-66 and, in doing so, determine whether uptake of silver (and controlled release) by the material can be manipulated to allow their use as antibacterial agents. Incorporation of chemical motifs known to have affinity for soft metals (like sulfur-containing functional groups and pi systems) were explored. Ionic and nanoparticulate silver were loaded into the structures to probe the effect of Ag oxidation state on release of silver. To extend the applications of silver-loaded UiO-66 derivatives, the materials were embedded into PCL matrices. The speciation of the loaded silver was investigated through use of X-ray absorption spectroscopy (XAS), to provide insight into the chemistry of the loaded cargo in a material unable to be characterised by single crystal X-ray crystallography. As controlled release of medicinally relevant species (like silver) is highly sought after, the release kinetics of silver from the PCL-embedded and non-embedded materials into aqueous media were characterised in both bacterial broth as well as ultra-

pure MilliQ water. Finally, the antibacterial efficacy of the materials was investigated against two clinically relevant strains of bacteria: *Escherichia coli* (*E. coli*), and *Staphylococcus aureus* (*S. aureus*).

4.3 Experimental and methods

Materials

All chemicals were purchased from Sigma Aldrich and used as received. Where necessary, additional preparation of reagents, including drying of solvents, is stated and were carried out by literature procedures.

Experimentals and methods

Instrumentation. NMR spectra were recorded on a Varian 500 MHz spectrometer at 23°C using a 5 mm probe. ^{1}H NMR spectra were referenced to either TMS (0 ppm) or DMSO-d^{6} (2.50 ppm). Infrared spectra were collected on a Perkin-Elmer Spectrum 11 using a UATR sampling accessory. Powder X-ray diffraction data was collected using a Cu Kα (1.542 Å) source on a Bruker D8 Advanced X-ray powder diffractometer (parallel X-ray, capillary loaded) or a Co Kα (1.789 Å) Bruker D4, Endeavour X-ray power diffractometer. Samples run on the Bruker D8 and D4 were mounted in 0.5 mm diameter glass capillaries or silicon low diffraction mirrors, respectively. Data was collected between 2θ of 2 to 52.94, phi rotation was 20 rotations per minute and 1 second exposure per step for 5001 steps. Raw data was converted to .xye format and WinPlotr 2006 software used for background subtraction. Simulated X-ray diffraction patterns were generated using Mercury from single crystal X-ray diffraction data.

X-ray absorption spectroscopy

Data collection. Silver K-edge X-ray absorption spectra were recorded on the X-ray absorption spectroscopy (XAS) beamline at the Australian Synchrotron (AS), Victoria, Australia. The energy of the electron beam was 3.0 GeV with a current of ~200 mA, and an X-ray beam was sourced from a wiggler monochromated by the Si(111) monochromator and harmonic rejection achieved using a rhodium-coated mirror. Samples were measured in transmission mode; the energy ranges used for EXAFS spectra collection were; pre-edge region 25.3140 – 25.4941 keV (0.003 eV steps); XANES region 25.4941 – 25.5641 keV (0.0003 eV steps); and EXAFS region 25.5641 – 25.700 keV. During data collection the samples were maintained at a temperature of ~ 10 K using a Cryo Industries (Manchester, NH, USA) cryostat. The spectrum of a silver foil, recorded in transmission downstream from the sample, was used as an internal standard to calibrate the energy scale for the first peak of the first derivative of the elemental silver edge (25.5156 keV); 1 to 4 scans per samples were collected for EXAFS spectra.

Data analysis. Calibration, averaging, background subtraction of all spectra and principle component, target, and multiple linear regression analyses of XANES spectra were performed using the EXAFSPAK software package (G. N. George, SSRL). Single-scattering fits of EXAFS data were carried out using EXAFSPAK and the FEFF8 code.[56] The model compounds for target analysis and XANES linear combination fitting were prepared, and spectra recorded at the AS, Victoria, Australia.

Single crystal X-ray diffraction

Single crystals of AgMOF-3 or 2D [$Zn(ox)_2BDC\text{-}(SO_3)_2$] material were mounted under paratone-N oil on a MiTeGen crystal mount, and X-ray diffraction data was collected at 100K on the MX2 beamline at the Australian Synchrotron using the Blue-ice software interface, λ=0.7108 or 0.7109 Å.[57] The data sets were corrected for absorption, the structures solved by direct methods using SHELXS or SHELXT and refined by full matrix least-squares on F^2 by SHELXL, interfaced through the programs X-Seed and/or Olex.[58-61] In general, all non-hydrogen atoms were refined anisotropically, and hydrogen atoms were included as invariants at geometrically estimated positions. Details of data collection and structure refinement are given in **Appendix 4.8.1**.

Synthesis of linkers

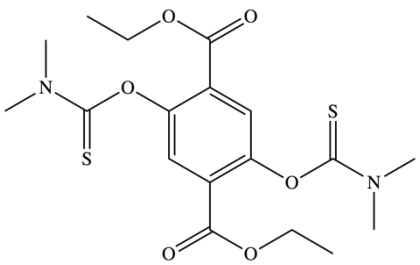

Diethyl 2,5-bis(dimethylthiocarbamoyloxy)benzene dicarboxylate.[62] To a solution of diethyl 2,5-dihydroxyl benzene dicarboxylate (2.04 g, 8.01 mmol) in DMF (100 mL) was added DABCO (3.71 g, 32.04 mmol) and the solution allowed to stir for several minutes. Dimethylthiocarbamoyl chloride (3.98 g, 32.04 mmol) was then added, the reaction mixture allowed to warm to room temperature and left to react for 6 h. The resultant suspension was poured over water (500 mL), filtered under reduced pressure and washed extensively with water to give diethyl 2,5-bis(dimethylthiocarbamoyloxy)benzene dicarboxylate as a fluffy white solid (3.41 g, 99%). ^{1}H NMR (500 MHz, $CDCl_3$): δ 7.73 (s, 2H), 4.30 (q, J = 7.1 Hz, 4H), 3.46 (s, 6H), 3.40 (s, 6H), 1.33 (t, J = 7.1 Hz, 6H); consistent with literature.

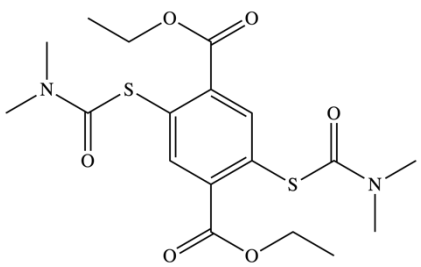

Diethyl 2,5-bis(dimethylthiocarbamoylsulfanyl) benzene dicarboxylate.[62] Diethyl 2,5-bis(dimethylthiocarbamoyloxy)benzene carboxylate (1.01 g, 2.40 mmol) was heated to 220ºC for 1 h under nitrogen protection. The crude product was cooled slowly to room temperature and recrystallised from ethanol to give diethyl 2,5-bis(dimethylthiocarbamoylsulfanyl) benzene carboxylate as pale brown plate-like crystals (0.93 g, 92%). ^{1}H NMR (500 MHz, $CDCl_3$): δ 8.11 (s, 2H), 4.34 (q, J = 7.1 Hz, 4H), 3.17 (s, 6H), 3.02 (s, 6H), 1.35 (t, 6H); consistent with literature.

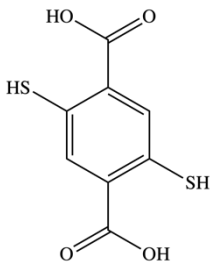

2,5-Dimercaptobenzene dicarboxylic acid (DMBDC).[62] Diethyl 2,5-bis(dimethylthiocarbamoylsulfanyl)benzene dicarboxylate (2.79 g, 6.51 mmol) was added to a degassed solution of potassium hydroxide (1.3 M) in 1:1 ethanol/water (150 mL). The mixture was degassed for a further 15 min and heated at reflux for 1 h under nitrogen protection. The solution was cooled to RT and acidified using hydrochloric acid (32%), the precipitate collected via vacuum filtration, washed extensively with degassed water and dried under nitrogen to give 2,5-dimercaptobenzene dicarboxylic acid as a bright yellow solid (1.46 g, 98%). ^{1}H NMR (500 MHz, DMSO-d^6): δ 8.03 (s, 2H); consistent with literature.

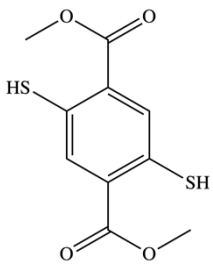

Dimethyl 2,5-dimercaptobenzene dicarboxylate.[17] A yellow suspension of 2,5-dimercaptobenzene dicarboxylic acid (1.00 g, 4.34 mmol) in methanol (30 mL) was degassed with nitrogen for 15 min. Sulfuric acid (98%, 1 mL) was added and the mixture heated at reflux for 4.5 h. The clear yellow solution was poured over a large amount of water, the product was collected by vacuum filtration and washed with water to give dimethyl 2,5-dimercaptobenzene dicarboxylic acid as a pale-yellow solid (1.10 g, 99%). ^{1}H NMR (500 MHz, $CDCl_3$): δ 7.96 (s, 2H), 4.68 (s, 2H), 3.94 (s, 6H); consistent with literature.

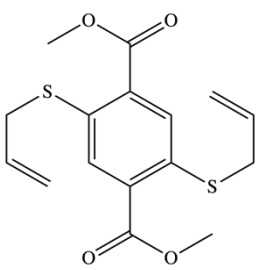

Dimethyl 2,5-bis(allylsulfanyl)benzene dicarboxylate.[17] To a suspension of dimethyl 2,5-dimercaptobenzene dicarboxylate (53 mg, 0.20 mmol) in acetone (10 mL) was added, under nitrogen protection, potassium carbonate (0.13 g) and potassium iodide (0.10 g, 0.61 mmol). A solution of allyl bromide (0.052 mL, 0.58 mmol) in acetone (5 mL) was added dropwise to the reaction vessel via a cannula. Upon complete addition of the allyl bromide, the reaction mixture was left to stir at room temperature for 3 h. The solvent was removed *in vacuo* and the crude product purified via a silica gel plug (1:2 hexane/dichloromethane) to give a dimethyl 2,5-bis(allylsulfanyl)benzene dicarboxylate as a bright yellow solid (64 mg, 92%). ^{1}H NMR (500 MHz, $CDCl_3$): δ 7.90 (s, 2H), 5.88 (ddt, J = 16.9, 10.1, 6.8 Hz, 2H), 5.32 (d, J = 17.0 Hz, 4H), 5.19 (d, J = 10.1 Hz, 4H), 3.94 (s, 6H), 3.62 (d, J = 6.8 Hz, 4H); consistent with literature.

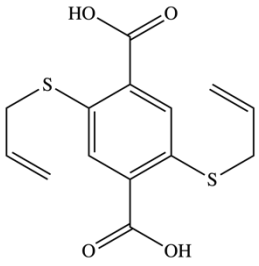

2,5-Bis(allylsulfanyl)benzene dicarboxylic acid (ASBDC).[17] Dimethyl 2,5-bis(allylsulfanyl)benzene dicarboxylate (0.36 g, 1.58 mmol) was added to a solution of potassium hydroxide in methanol (3 M, 90 mL) and the suspension was stirred overnight at room temperature. Water (20 mL) was added to the cloudy, white suspension, acidified with hydrochloric acid (32%) and the product isolated via vacuum filtration to give 2,5-bis(allylsulfanyl)benzenedicarboxylic acid as a bright yellow solid (0.28 g, 78%). ^{1}H NMR (500 MHz, DMSO-d^6): δ 13.43 (s, 2H), 7.80 (s, 2H), 5.84 (ddt, J = 16.6, 6.8 Hz, 2H), 5.29 (d, J = 17.0 Hz, 4H), 5.15 (d, J = 10.0 Hz, 4H), 3.65 (d, J = 6.2 Hz, 4H); consistent with literature.

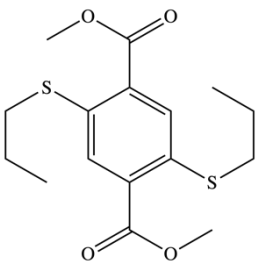

Dimethyl 2,5-bis(propylsulfanyl)benzene dicarboxylate. A suspension of dimethyl 2,5-dimercaptobenzene dicarboxylate (0.52 g, 2.01 mmol) in acetone (40 mL) was degassed for ~15 min. Potassium carbonate (1.14 g, 8.04 mmol) and sodium iodide (1.22 g, 8.04 mmol) were then added to the suspension under nitrogen protection and allowed to stir for 30 min. A mixture of 1-bromopropane (0.75 mL, 8.04 mmol) and acetone (5 mL) was injected via a cannula under N_2, the resultant mixture was left to stir at room temperature for 3 hours and monitored via TLC (2:1 CH_2Cl_2/Pet. Spirit). The mixture was gravity filtered, the solvent removed *in vacuo*, and the yellow oil purified via silica plug (silica gel, 2:1 CH_2Cl_2/Pet. Spirit) to give dimethyl 2,5-

bis(propylsulfanyl)benzene dicarboxylate as a bright yellow solid (0.50 g, 72%). ^{1}H NMR (500 MHz, $CDCl_3$): δ 7.84 (s, 2H), 3.95 (s, 6H), 2.92 (t, *J* = 7.3 Hz, 4H), 1.75 (sx, *J* = 7.3, 7.3 Hz, 4H), 1.09 (t, *J* = 7.3 Hz, 6H).

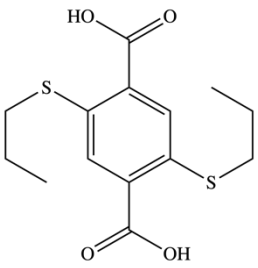

2,5-Bis(propylsulfanyl)benzene dicarboxylic acid (PSBDC). Dimethyl 2,5-bis(propylsulfanyl)benzene dicarboxylate (100 mg, 0.32 mmol) was added to a solution of potassium hydroxide in methanol (3 M, 5 mL) and the suspension was stirred overnight at room temperature. Water (20 mL) was added to the cloudy, white suspension, the mixture acidified with hydrochloric acid (32%) and the product isolated via vacuum filtration to give 2,5-bis(propylsulfanyl)benzene dicarboxylate acid as a bright yellow solid (65 mg, 70%). ^{1}H NMR (500 MHz, DMSO-d^6): δ 7.75 (s, 1H), 2.90 (t, *J* = 7.2 Hz, 2H), 2.55 – 2.45 (m, 1H), 1.69 – 1.52 (sx, 4H), 1.00 (t, *J* = 7.3 Hz, 6H).

Synthesis of materials

UiO-66. Procedure followed as reported by Katz *et al*.[43] $ZrCl_4$ (125.8 mg, 0.54 mmol) was dissolved in DMF (7.5 mL), benzene-1,4-dicarboxylic acid (BDC) (124.6 mg, 0.75 mmol) was dissolved in DMF (7.5 mL) and both solutions sonicated for 10 min. Upon dissolution, the two solutions were combined and concentrated hydrochloric acid (1 mL) was added and the resultant mixture sonicated for a further 10 min. The solution was heated at 85°C overnight, cooled to room temperature, the solid isolated by centrifugation (10,000 rpm, RT, 5 min), washed with DMF (2 x 5 mL), and CH_2Cl_2 (2 x 5 mL), and dried under vacuum overnight. This yielded UiO-66 as a white microcrystalline powder.

ASUiO-66. $ZrCl_4$ (100.1 mg, 0.43 mmol) was dissolved in DMF (10 mL), ASBDC (200 mg, 0.64 mmol) was dissolved in DMF (10 mL) and both solutions sonicated for 10 min. Upon dissolution, the two solutions were combined and formic acid (661 μL) was added and the resultant mixture sonicated for a further 10 min. The solution was heated at 120°C overnight, cooled to room temperature, the solid isolated by centrifugation (10,000 rpm, RT, 5 min), washed with DMF (2 x 5 mL), and CH_2Cl_2 (2 x 5 mL), and dried under vacuum overnight. This yielded ASUiO-66 as a yellow microcrystalline powder.

PSUiO-66. $ZrCl_4$ (98.8 mg, 0.42 mmol) was dissolved in DMF (10 mL), ASBDC (200 mg, 0.64 mmol) was dissolved in DMF (10 mL) and both solutions sonicated for 10 min. Upon dissolution, the two solutions were combined and formic acid (653 μL) was

added and the resultant mixture sonicated for a further 10 min. The solution was heated at 85°C overnight, cooled to room temperature, the solid isolated by centrifugation (10,000 rpm, RT, 5 min), washed with DMF (2 x 5 mL), and CH_2Cl_2 (2 x 5 mL), and dried under vacuum overnight. This yielded PSUiO-66 as a yellow microcrystalline powder.

AgMOF-3 (single crystal). ASBDC (42.6 mg, 0.14 mmol) and silver trifluoroacetate (8.52 mg, 0.036 mmol) were separately dissolved in DMSO (2 x 2 mL). The two solutions were combined, and ethyl acetate diffused into the mixture over ~2 weeks to produce colourless needle-like crystals.

AgMOF-3 (microcrystalline powder). ASBDC (42 mg, 0.14 mmol) and silver trifluoroacetate (8.49 mg, 0.035 mmol) were separately dissolved in DMF (2 x 2 mL). The solution of ligand was added, dropwise, to that of the stirred solution of the silver salt and the mixture allowed to stir for a further 15 min after addition. The resultant beige suspension was isolated by centrifugation (10,000 rpm, 5 min), washed with DMF (3 x 1 mL), and acetone (3 x 1 mL) and dried under vacuum at 50°C.

2D [$Zn(ox)_2BDC$-$(SO_3)_2$] material. DMBDC (12.5 mg, 0.040 mmol) and $Zn(NO_3)_2.6H_2O$ (36.2 mg, 0.122 mmol) were dissolved in DEF (2 mL). To the solution was added HNO_3 (70%, 1-2 drops). The solution was split between multiple vials which were flame sealed. The solution was heated at 120°C for 3 days followed by a cooling rate of 6°C/h to room temperature to yield clear, colourless plate crystals.

Impregnating materials with silver

Ionic silver: Ag(I)-MOF. Dried MOF was soaked in a solution of silver nitrate in acetonitrile (100 mM) at a ratio of 0.25 mL/mg MOF overnight in the dark. The solid was isolated by centrifugation (10,000 rpm, RT, 10 min) washed briefly with acetonitrile (5 mL), centrifuged immediately - as above - and dried under vacuum overnight.

Mixed oxidation state silver: Ag(I/0)-MOF. Procedure adapted from Plesser, *et al.*[63] Dried MOF was soaked in a solution of silver nitrate in water/ethanol (100 mM, 1:5 v/v) at a ratio of 0.25 mL/mg MOF under a nitrogen atmosphere, overnight in the dark. The solid was isolated by centrifugation (10,000 rpm, RT, 10 min) washed briefly with 1:5 v/v water/ethanol (5 mL), centrifuged immediately - as previous – washed with CH_2Cl_2 (2 x 5 mL) and dried under vacuum, in the dark, overnight.

Nanoparticulate silver loading: Ag(0)-MOF. The material was prepared as above, however, the solid was isolated by centrifugation (10,000 rpm, RT, 10 min) and washed thoroughly over 1 h with water/ethanol (6 x 5 mL, 1:5 v/v). After which time no - or minimal - silver chloride precipitate was observed when the supernatant of the wash was treated with a saturated sodium chloride solution. The material was then washed with CH_2Cl_2 (2 x 5 mL) and dried under vacuum, in the dark, overnight.

Embedding materials in a polycaprolactone (PCL) matrix

Dried silver-loaded MOF (20 mg) was suspended in CH_2Cl_2 (2 mL) with sonication and, separately, PCL (60 mg) was dissolved in CH_2Cl_2 (2 mL). Upon dissolution of the polymer, the two components were combined and sonicated for a further 10 min. The suspended mixture was transferred to a glass petri dish (6 cm) and the solvent allowed to evaporate in the dark overnight.

Silver leaching studies

To ultrapure water or Luria-Bertani (LB) broth (10 mL) was added shredded MOF-PCL composite material (80 mg). The mixture was stirred for 24 h and aliquots (0.5 mL) were removed at 1, 2, 4, 8, and 24 h intervals. The aliquots were analysed by AAS by comparison of absorbance relative to known silver standards. At least three technical replicates of the leaching profile of each material were recorded and averaged.

Microbiological studies

The antibacterial properties of the silver-loaded materials were tested against *Escherichia coli* (*E. coli*) MG1655 and *Staphylococcus aureus* (*S. aureus*) Newman strains. All assays were performed in technical and biological triplicate and averaged. Positive and negative controls were performed by using $AgNO_3$ embedded PCL, and PCL, respectively. Antibacterial tests was carried out as per the procedure outlined by Young *et al*.[64] LB broth (20 mL) was inoculated with *S. aureus* or *E. coli* to an OD_{600} of 0.05 and incubated at 37°C with shaking (200 rpm) for 6 h. The cultures were then diluted to an OD_{600} of 0.8 in LB broth and 100 μL spread onto LB + 1.5% (w/v) agar plates. The embedded disks were placed on the plates and inhibition zone measured after incubation overnight at 37°C by visual inspection.

X-ray absorption spectroscopy

Powders. Materials were mixed with polyethylene (3:1 w/w) and compressed into disks with a hand press. The disks were then sandwiched between Kapton tape in an XAS sample holder and presented to the beamline.

MOF-PCL composite materials. PCL/MOF thin films were folded upon themselves until a sufficient size to be loaded inside a Lucite sample holder and held in place with Kapton tape.

Defect analysis

As-synthesised UiO-66 was soaked in a solution of benzoic acid in DMF (8%) overnight at 85°C. Each material (1-2 mg) was digested in DMSO-d^6 (700 μL), and D_2SO_4 (5 drops) at 80°C for 2 h to give a clear solution. The integration of the ^1H NMR peaks corresponding to the formic or benzoic acid modulator (A) were compared to that of the MOF linker (L). The number of defects per metal node (X) was found by using the following equation:

$$X = \frac{6(A:L)}{(1+0.5)A:L}$$

See **Appendix 4.8.2** for details.

4.4 Results and Discussion

4.4.1 Synthesis of organic linkers

According to a literature procedure, 2,5-dimercaptobenzene dicarboxylic acid (DMBDC) (**Figure 3**) was successfully synthesised from diethyl 2,5-dihydroxybenzene dicarboxylate and dimethyl thiocarbamoyl chloride *via* a Newman Kwart rearrangement.[62] Thioetherification of DMBDC with allyl or propyl bromide produced 2,5-bis(allylsulfanyl)benzene dicarboxylic acid (ASBDC) or 2,5-bis(propylsulfanyl)benzene dicarboxylic acid (PSBDC), respectively; ASBDC has previously been reported[16] while PSBDC has not been examined as a linker.

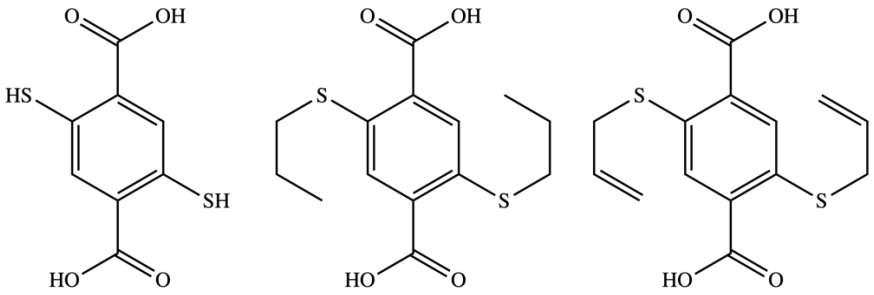

Figure 3: Structures of the organic linkers synthesised in this project: (**a**) 2,5-dimercaptobenzene dicarboxylic acid (DMBDC); (**b**) 2,5-bis(propylsulfanyl)benzene dicarboxylic acid (PSBDC); (**c**) 2,5-bis(allylsulfanyl)benzene dicarboxylic acid (ASBDC).

4.4.2 Synthesis of metal-organic frameworks (MOFs)

Synthesis of an ASBDC analogue of UiO-66 (ASUiO-66) has previously been reported.[17] The procedure included 30 equivalents of acetic acid (relative to $ZrCl_4$) as a modulator and heating at 120°C for 24 hours; however, when repeated in this work it was found that only amorphous yellow solid was formed under these conditions (or with any ratio of acetic acid to metal salt). However, substitution of acetic acid with formic acid yielded ASUiO-66 as a yellow, microcrystalline powder. Any ratio of formic acid to zirconium chloride used – except zero – produced ASUiO-66, and for all subsequent studies 40 equivalents were used as this was the lowest ratio that produced highly crystalline material (data not shown). The same conditions used to synthesise ASUiO-66 were successfully applied to the synthesis of the PSBDC analogue of UiO-66 (PSUiO-66).The solvothermal synthesis of unfunctionalized UiO-66 was adapted from work by Katz, *et al*.[43]

In addition to the three materials mentioned above, a dimercapto analogue of UiO-66 (DMUiO-66) was synthesised using DMBDC, as per literature conditions.[65] When

treated with aqueous hydrogen peroxide, the thiolates of DMUiO-66 could be post-synthetically oxidised to produce a disulfonate-functionalised UiO-66 analogue (DSUiO-66)[66] further extending the library of isoreticular materials (**Figure 4**). DM- and DSUiO-66 were included as materials to investigate the effect of soft, and hard, negatively charged pore environments on the uptake/release of ionic silver, respectively.

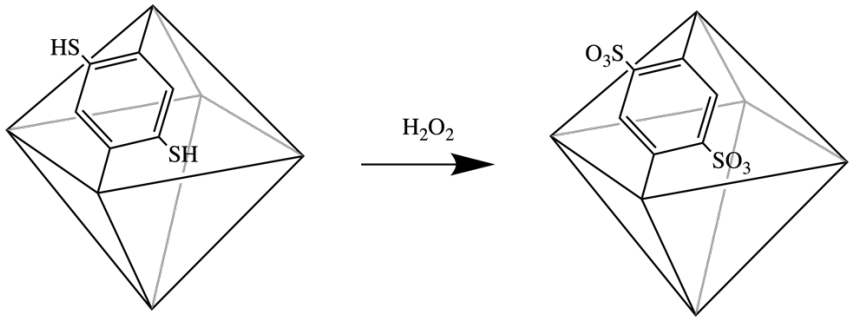

Figure 4: Schematic of the post synthetic modification of dimercapto UiO-66 (DMUiO-66) to disulfonate UiO-66 (DSUiO-66) using hydrogen peroxide. Only the octahedral UiO-66 pores are shown for clarity.

Powder X-ray diffraction (PXRD) patterns of all as-synthesised functionalised and unfunctionalized UiO-66 materials (**Figures 5b, 6b, 7b, 8b, 9b**) matched the powder pattern of UiO-66 simulated from single crystal data.[67] The PXRD data indicated that the materials were isostructural to that of the unfunctionalized material, with $Zr_6O_4(OH)_4$ secondary building units (SBUs) connected by twelve 1,4-benzenedicarboxylic acid (BDC) linkers in the absence of defects. As noted, this connectivity has been shown to produce two types of pore environments; an octahedral cage, and a tetrahedral cage with diameters of ~9 and ~7 Å, respectively.[68]

4.4.3 Synthesis and characterisation of silver-loaded MOFs

Silver nitrate was loaded into the dried materials by soaking them in an acetonitrile solution of the metal salt in the dark for ~16 h. The solids were isolated, washed briefly with fresh acetonitrile (to remove surface-bound silver) and dried under vacuum. Any materials treated in such a way were assigned the prefix of 'Ag(I)-' e.g. Ag(I)ASUiO-66.

Upon addition of silver nitrate solution (clear) to UiO-66 (white), the material immediately turned brown; an indication that the Ag(I) may have been reduced to Ag(0). AS/PS/DSUiO-66 did not undergo any colour change upon treatment of silver ions; however, despite already being bright yellow in colour, DMUiO-66 appeared to become an even more intense shade of yellow upon exposure to $AgNO_3$.

To further expand the library of silver-containing materials investigated, the *in-situ* reduction of silver ions to nanoparticles was carried out. Ethanol has previously been used as a mild reductant which allows silver ions to diffuse into the material and, over time, be reduced to nanoparticles.[69] AS-, PS-, and unfunctionalized UiO-66 were soaked in aqueous ethanol solutions of silver nitrate in the dark, under nitrogen protection for ~16 h; DMUiO-66 and DSUiO-66 were not included in these treatments. The batches of materials were then split in half and either washed extensively with fresh ethanol/water to remove unreacted Ag(I) (monitored visually by precipitation of AgCl when wash supernatant liquid was added to a saturated solution of NaCl in EtOH/H_2O) or washed briefly to removed surface-bound silver. Materials that were washed thoroughly to remove ionic silver were given the prefix 'Ag(0)-' denoting that only reduced silver was proposed to remain in the material. Materials that were briefly washed were given the prefix 'Ag(I/0)-' to show that a mixture of silver oxidation states were likely present in the structure. PXRDs were recorded for all silver-loaded materials showing that crystallinity was retained during the loading process (**Figure 5** to **9**). No PXRD patterns recorded for the silver-treated materials differed significantly from the as-synthesised patterns suggesting that loading silver into the materials did not change the structure of the material and were still isostructural with UiO-66.

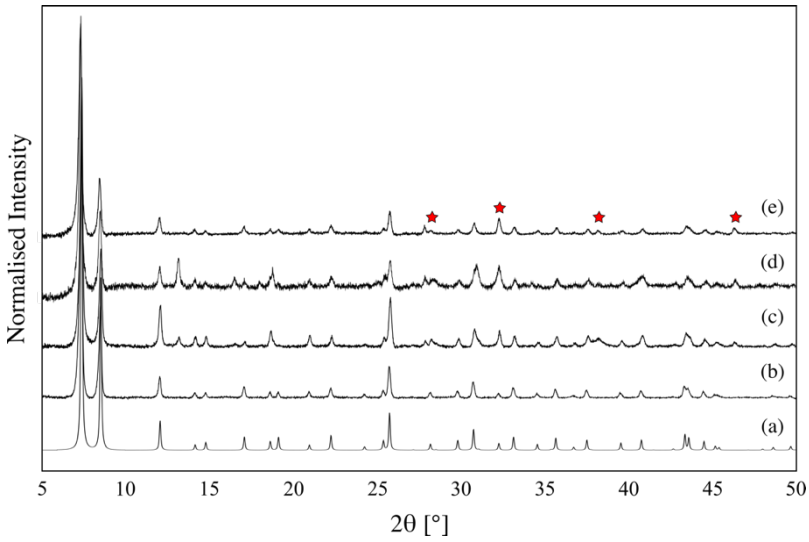

Figure 5: Powder X-ray diffraction patterns (Cu Kα, λ = 1.5418Å) of UiO-66: (**a**) simulated pattern from single crystal structure of UiO-66; (**b**) as-synthesised; (**c**) treated with 100 mM solution of $AgNO_3$ in acetonitrile; (**d**) treated with 100 mM solution of $AgNO_3$ in 5:1 ethanol/water; (**e**) treated as per sample (d) but extensively washed with 5:1 ethanol/water to remove traces of ionic silver. Red stars highlight peaks inconsistent with the 'as-synthesised' material.

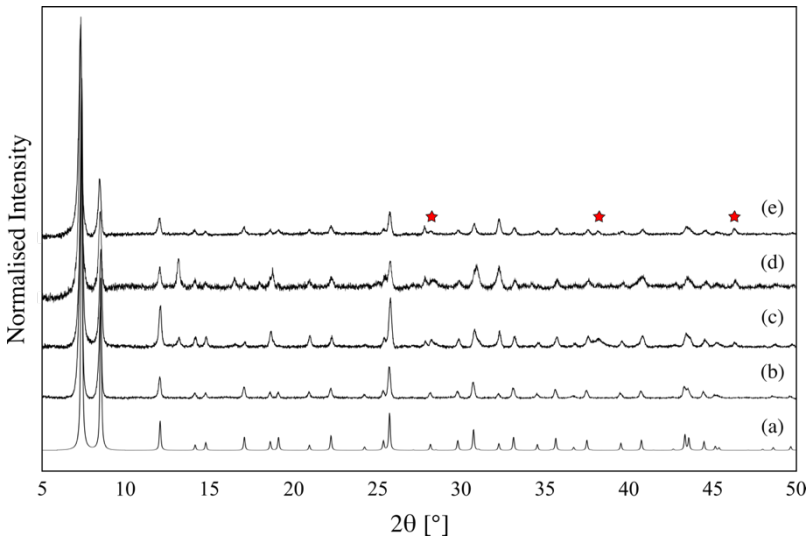

Figure 6: Powder X-ray diffraction patterns (Cu Kα, λ = 1.5418Å) of PSUiO-66: (**a**) calculated pattern from single crystal structure of UiO-66; (**b**) as-synthesised; (**c**) treated with 100 mM solution of $AgNO_3$ in acetonitrile; (**d**) treated with 100 mM solution of $AgNO_3$ in 5:1 ethanol/water; (**e**) treated as per sample (d) but extensively washed with 5:1 ethanol/water to remove traces of ionic silver. Red stars highlight peaks inconsistent with the 'as-synthesised' material pattern.

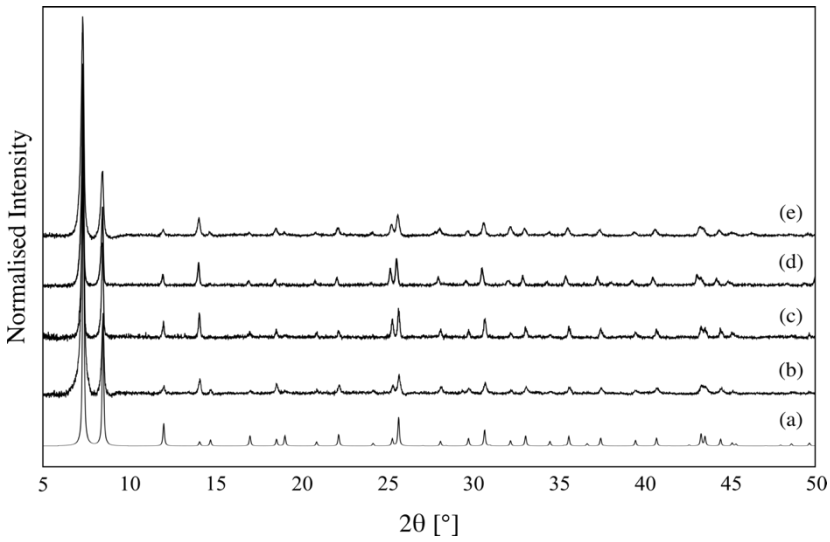

Figure 7: Powder X-ray diffraction patterns (Cu Kα, λ = 1.5418Å) of ASUiO-66: (**a**) calculated pattern from single crystal structure of UiO-66; (**b**) as-synthesised; (**c**) treated with 100 mM solution of $AgNO_3$ in acetonitrile; (**d**) treated with 100 mM solution of $AgNO_3$ in 5:1 ethanol/water; (**e**) treated as per sample (d) but extensively washed with 5:1 ethanol/water to remove traces of ionic silver.

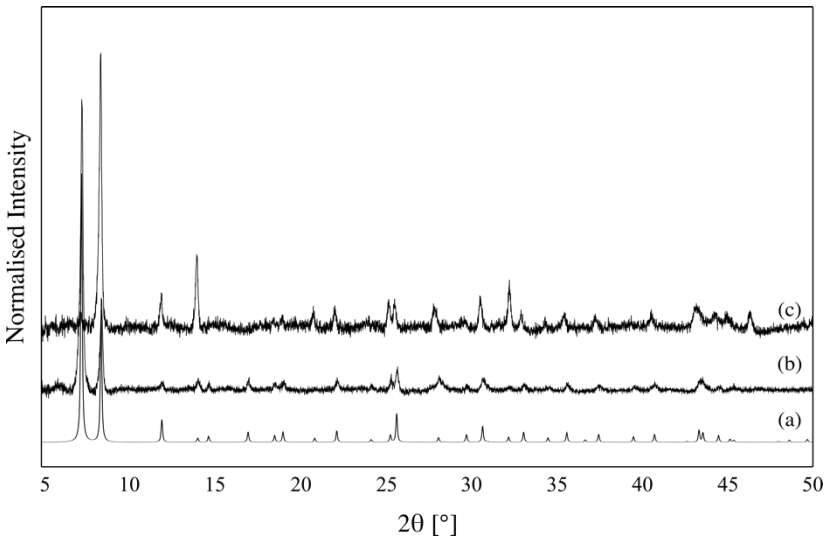

Figure 8: Powder X-ray diffraction patterns (Cu Kα, λ = 1.5418Å) of DMUiO-66: (**a**) calculated pattern from single crystal structure of UiO-66; (**b**) as-synthesised; (**c**) treated with 100 mM solution of $AgNO_3$ in acetonitrile.

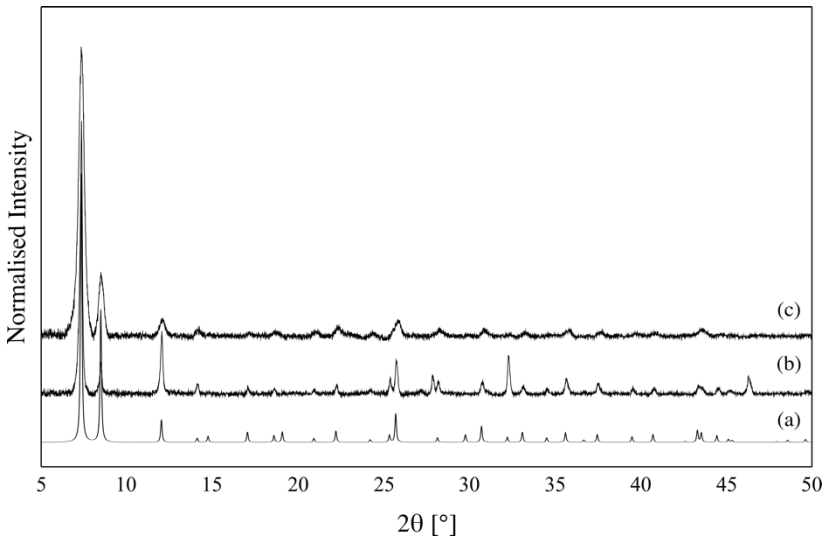

Figure 9: Powder X-ray diffraction patterns (Cu Kα, λ = 1.5418Å) of DSUiO-66: (**a**) calculated pattern from single crystal structure of UiO-66; (**b**) as-synthesised; (**c**) treated with 100 mM solution of $AgNO_3$ in acetonitrile.

Crystalline silver nanoparticles have been shown to diffract X-rays at large 2θ values, however, the absence of such peaks do not preclude the presence of nanoparticles as they can be amorphous or two small to diffract. Peaks inconsistent with those of the 'as-synthesised' MOF materials were observed at 27.8°, 37.4°, and 46.3° in the PXRD patterns of UiO-66 and PSUiO-66 treated with silver (**Figure 5** and **6**, annotated with stars). These peaks may have been the result of diffraction by crystalline silver/silver oxide nanoparticles as the [110] plane of Ag_2O NPs have been shown to diffract at 27.84°.[70] Similarly, the [111] and [211] planes of *fcc* Ag NPs have been shown to diffract at 38.3°,

and 46.34, respectively;[71] the presence of diffraction from the AgNP [111] plane is often attributed to aggregation of NPs with diameters >10 nm. In phase-pure UiO-66, with no defects, any pore-contained nanoparticles would be restricted to diameters <9 Å due to the materials pore size distribution. Thus, the presence of these reflections would indicate that not all silver was confined to the pores of PSUiO-66 and UiO-66 and could have been located in the interstitial spaces between crystallites, or in larger pore regions associated with defect sites in the MOF. To determine whether the latter scenario might have been the case, defect analysis was carried out to determine the number of defects in the MOF samples.

4.4.4 Defect analysis

Defect analysis of dried as-synthesised, Ag(I)-, Ag(I/0)-, and Ag(0)-treated PS- and ASUiO-66 materials was carried out. After heating samples at 85°C in DMSO-d_6 and D_2SO_4, clear, yellow solutions were obtained and ^{1}H NMR spectra recorded (**Appendix 4.8.2**). The thioether-functionalised materials were all synthesised in the presence of formic acid modulator, which introduces defect sites into the structure, replacing, or binding in preference to the organic linker to the zirconium-oxo SBU. Integration and comparison of the formic acid ^{1}H NMR peak relative to the aryl MOF linker signal enabled calculation of the number of defects per node in the material. **Figure 10** summarises the results of the defect analysis of AS and PSUiO-66 materials.

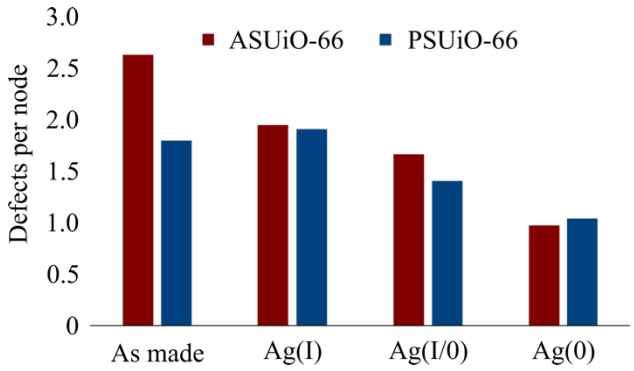

Figure 10: Number of defects of formic acid modulated PS- and ASUiO-66 materials. See **Appendix 4.8.2** for calculations.

The number of defects per node for 'as-synthesised' PS- and ASUiO-66 were ~1.75 and 2.6, respectively. Relative to 'as-synthesised' ASUiO-66, all silver treatments resulted in a decrease in the number of defects per metal node, with the largest decrease being for the Ag(0)ASUiO-66 materials (~1.0 defects per node). However, for the PSUiO-66

materials, the number of defects only decreased in the Ag(I/0)- and Ag(0)-treatments. Decreases in the defects indicated that the ratio of formic acid to organic linker decreased during the silver treatments or washing procedures. Given the way in which the Ag(0) materials were prepared, i.e. extensive washing to remove silver ions, the hydrolysis of defect acid site was not surprising; this does not mean that defects were removed or healed but that the measure of defects in the MOF (i.e. formic acid) was removed. If equal amounts of formic acid modulator and organic linker were leached from the materials, the number of defects per node would appear to remain constant, however, this would not preclude the assumption that the material was degraded by extensive washing, it merely suggested that unequal amounts of formic acid and organic linker were leached.

Defect analysis was not conducted for UiO-66 as hydrochloric acid was used as the modulator as per literature procedure.[43]

Determination of silver-loading

Samples of all dried UiO-66 analogues soaked in 100 mM $AgNO_3$ in acetonitrile were acid digested and the ratio of zirconium to silver quantified by ICP-MS. As the number of zirconium atoms per unit cell of UiO-66 is known, and the functionalised materials were known to be isostructural with UiO-66, the amount of silver per unit cell could be calculated. **Table 1** summarises the mole percent of silver in the unit cell of the material as loaded in by each silver treatment.

Table 1: Mole percent of silver per unit cell of UiO-66 and derivatives thereof soaked in solutions of $AgNO_3$ in acetonitrile, as determined by ICP-MS.

Ag(I) loaded material	mol % Ag in MOF sample
UiO-66	9.07
PSUiO-66	13.2
ASUiO-66	18.4
DMUiO-66	37.7
DSUiO-66	17.7

Of the five materials investigated, unfunctionalised UiO-66 had the lowest uptake of silver ions from a solution of $AgNO_3$, while DMUiO-66 had the highest (**Table 1**). A high uptake of silver by DMUiO-66 was likely due to the strong affinity soft thiolate donors have for silver, as well as electrostatic attraction between the negative sulfur and positive silver ions. Conversely, DSUiO-66 had a moderate uptake of silver, likely due to the electrostatic attraction between the silver cations and the negative sulfonates. However, sulfonates are not known to have strong affinity for Ag(I) like thiolates. Of the two

thioether-containing materials, ASUiO-66 had a greater uptake of Ag(I) than did PSUiO-66, possibly due to the inclusion of the allyl functionality in the structure of the former, which has been reported to have an affinity for noble metals.[16]

The leaching profiles of DM- and DSUiO-66 (**Figure 11**, page 173) revealed that a strong affinity for the metal ions, as well as electrostatic forces, significantly limited the release of silver from the materials. Thus, only UiO-66, PS- and ASUiO-66 were used in subsequent studies where *in-situ* reduction of silver ions by ethanol was investigated. Similar to the Ag(I) treated materials, the silver loading of Ag(I/0) and Ag(0) treated materials was determined by acid digestion and analysis of Zr/Ag ratios by ICP-MS (**Table 2**).

Of the three silver treatments the mixed oxidation state Ag(I/0) treatment resulted in the highest uptake of silver of each of the three materials. The increase in silver loading may be attributed to the close packing of reduced silver in the materials relative to Ag(I), allowing a greater uptake of the metal. The uptake of silver in the Ag(I/0)UiO-66 only increased by ~1% which was likely due to the fact that, when exposed to Ag(I) in the absence of a reducing agent, the material already appeared to reduce the ions (observable as a colour change from white to brown).

Table 2: Mole percent of silver calculated for UiO-66, PSUiO-66, and ASUiO-66 for three silver treatments, as determined by ICP-MS.

	mol % Ag		
Material	Ag(I)	Ag(I/0)	Ag(0)
UiO-66	9.1(1)	10.9	6.0
PSUiO-66	13.2(1)	17.1	16.5
ASUiO-66	18.4(8)	23.4	15.6

Values in brackets represent the standard error. Ag(I/0) and Ag(0) values

The Ag(0) treated materials were washed thoroughly with ethanolic water to remove residual silver ions (ideally leaving only silver in the zero oxidation state). Thus it was unsurprising that the percentage of silver in all three Ag(0) materials was lower relative to Ag(I/0). Six washes per material were carried out over the course of 1 hr with the MOF suspended in EtOH/H_2O in the dark for 10 min between centrifugation and replacement of the supernatant liquid. Six washes were deemed sufficient since addition of the supernatant liquid from the sixth wash to a saturated solution of sodium chloride did not result in precipitation of AgCl. The fresh ethanolic water used to wash the materials

was deaerated by sonication prior to use, however, all washings were carried out under atmospheric conditions and may have contributed to the formation of Ag_2O NPs, the diffraction from which was possibly observed in the PXRD patterns for UiO-66 and PSUiO-66 (**Figures 5** and **6**). The speed of washing meant that oxidative dissolution of the silver nanoparticles in the materials was likely to be minimal.

During washing, the supernatant liquid of ASUiO-66 became faintly yellow in colour. Suspensions of silver nanoparticles have been reported to have colours ranging from yellow to brown due to surface plasmon resonance of the NPs.[72] To investigate the source of the colour of the supernatant liquid, a UV-Vis spectrum was recorded for the supernatant liquid as well as a solution of ASBDC (in the same solvent system – 5:1 EtOH/H_2O). A λ_{max} of 385 nm was recorded for the supernatant liquid, as well as the solution of ASBDC, thus the colour was attributed to degradation of ASUiO-66 and liberation of the organic linker into solution (rather than leaching of silver nanoparticles) – data not shown.

4.4.5 Leaching profiles of silver-loaded metal-organic frameworks

The silver leaching profiles of the five Ag(I)-loaded, powdered materials into ultra-pure water were measured by stirring suspensions of the dried material in water (in the dark) for 24 hours. At each time point all supernatant liquid was removed and replaced (**Figure 11**). For all frameworks the greatest percentage of silver was released within the first hour of the study. Despite a higher loading of silver ions into the allylsulfanyl (ASUiO-66) material relative to the propylsulfanyl (PSUiO-66) derivative, PSUiO-66 released a larger percentage of total loaded silver within the first hour than did ASUiO-66 (~55% vs. ~40%, respectively, **Table 3**); over 24 hours ASUiO-66 released 56% of total silver compared to 77% for PSUiO-66. This observation added weight to the hypothesis that addition of an alkene group in the thioether unit of the organic linker (the major difference between AS and PSUiO-66) could influence the uptake, and retention, of silver ions. Control over the uptake and release of biologically relevant molecules (like silver) by tailoring the MOF pore environment is a favourable property in materials to be used in clinical settings to prevent bacterial infections.

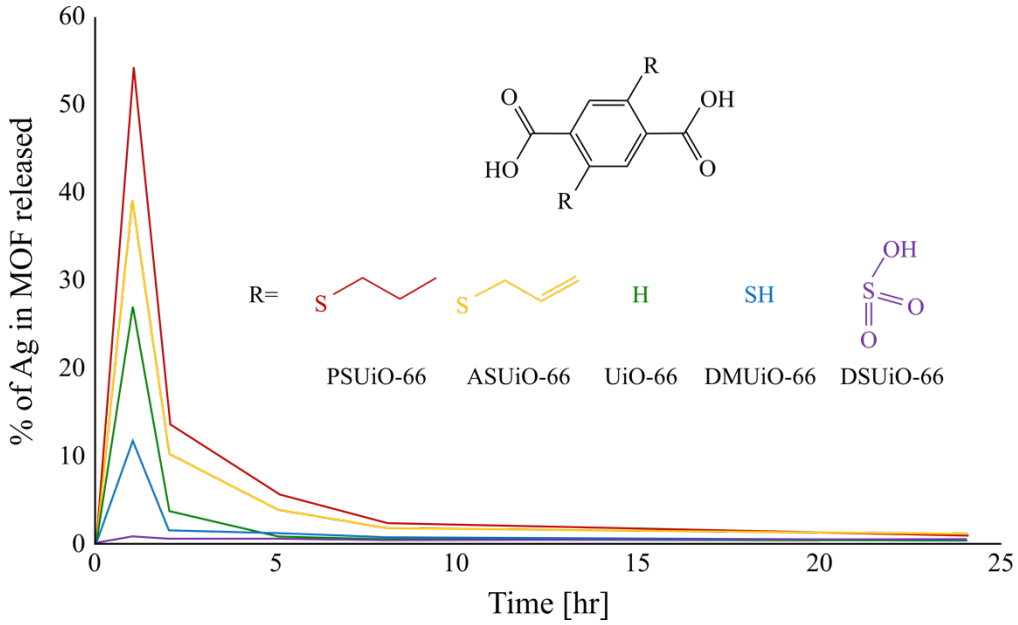

Figure 11: Silver leaching profiles of powdered: Ag(I)PSUiO-66 (red); Ag(I)ASUiO-66 (yellow); Ag(I)UiO-66 (green); Ag(I)DMUiO-66 (blue); and Ag(I)DSUiO-66 (purple) stirred in MilliQ water in the dark for 24 h. Supernatant liquid was removed and replaced with fresh water at 1, 2, 5, 8, and 24 h and analysed by ICP-MS. Lines are direct connection between adjacent measured points. Point markers were not included due to the closeness of measurement at larger time.

The two materials with negatively charged linkers (DM and DSUiO-66) released the lowest percentage of total loaded silver over 24 hours; 15%, and 2%, respectively. Sulfonic acids are highly acidic (pKa ~ -7),[73] thus, at the pH of ultra-pure water (pH 6 to 7), all of the sulfonic acid groups in the material would be expected to be deprotonated. Electrostatic forces between the silver cations and the anionic sulfonate functional groups would be expected to be the dominant interaction as oxygen is considered a 'hard' Lewis base with low affinity for soft metals like silver.[74] Conversely, the pKa of thiophenol,[75] which is analogous to the mercapto linker in DMUiO-66, is only 6.6 in water. Thus, at pH 6-7, only ~50% of the thiol groups in the material may be deprotonated.

Table 3: Percentage of silver released from UiO-66 and derivatives thereof after 1 hour of stirring in MilliQ water and the total percentage released over the duration of the experiment (24 h).

Silver loaded material	Silver released at T = 1 hr (%)	Total silver released (%)	Total loading (mol%)
UiO-66	26.9	32.2	9.07
PSUiO-66	54.3	76.9	13.2
ASUiO-66	39.1	56.2	18.4
DMUiO-66	11.6	15.1	37.7
DSUiO-66	0.73	2.4	17.7

4.4.6 Embedding silver-loaded metal-organic frameworks into polymer matrices

Powdered, crystalline solids serve little use in medical settings; thus, to extend the application of these materials they were embedded into polycaprolactone (PCL) polymer matrices. PCL is a polymer approved for use by the United States Food and Drug Administration (FDA) and offers ease of processing as the polymer can be solution cast from volatile solvents.[76] A maximum loading of 25% w/w MOF in PCL was achievable before the structural integrity of the polymer was visually compromised (data not shown). All materials were embedded into the polymer at 25 wt% and retained their crystallinity (**Appendix 4.8.3**). All MOF-derived peaks in the PXRD were significantly reduced in intensity and broadened as a result of the reduced amount of crystalline material presented to the X-ray beam. All peaks not associated with the PCL matrix were in good agreement with the UiO-66 materials, suggesting no significant change in the morphology of the microcrystalline powders occurred during solvent casting of the films.

4.4.7 X-ray absorption spectroscopy

Single crystal X-ray diffraction (SCXRD) is a powerful technique to study crystalline materials but is limited by the ability to grow suitable crystals and the necessity of a well-ordered structure to provide useful information. The UiO-66 family of materials often form as microcrystalline powder, the crystals of which are too small for synchrotron or home-lab SCXRD experiments. Single crystal structures of UiO-66 have been reported in literature,[67] however, the conditions for growth are not universally applicable between analogous materials. Additionally, the presence of poorly ordered thioether units in the materials, as well as variability in the orientation of a 2,5-substituted BDC linker, results in a high degree of disorder in the materials, frustrating data collection and analysis. Finally, a lack of well-defined binding sites for silver cations in the pores of the (un)functionalised UiO-66 derivatives provided yet another layer of difficulty in determining the structure of the silver-impregnated materials. X-ray absorption spectroscopy (XAS) is an element specific technique that has previously been used to study speciation of heavy elements loaded into crystalline materials.[77] Both X-ray absorption near edge structure (XANES) and extended X-ray absorption fine structure (EXAFS) were recorded for all microcrystalline powders as well as select PCL-MOF films.

XANES of silver-loaded metal-organic frameworks

Silver K-edge XANES spectra of silver-loaded UiO-66, PSUiO-66, and ASUiO-66 are presented in **Figures 12** and **14**, respectively. Principal component analysis (PCA) of

the MOF XANES dataset indicated that three spectral components were required to describe these data (not shown). Target transformation against a library of Ag K-edge XANES model spectra allowed visual identification of similarities between the experimental, and model spectra. Bulk silver metal, aqueous silver nitrate, and a buffered solution of the thioether-containing amino acid methionine with silver were identified as possible spectral components of the experimental spectra. The relative proportions of each model spectrum required to describe the experimental data were calculated by linear combination fitting (LCF) (**Figures 13**/**15**, and **Table 4**).

Figure 12 shows the XANES spectra for the three silver treatments of UiO-66 (**a** to **c**), PCL embedded Ag(0)UiO-66 (**d**), and bulk elemental silver (**e**). The three peaks of the elemental silver spectrum annotated with red stars were prominent features of each of the four UiO-66 spectra; only the relative intensities of these peaks changed between samples. A point of differentiation in the experimental spectra was between the Ag(I/0) and Ag(0) materials (**b** and **c**, respectively). The post-edge oscillations of samples (**a**) and (**b**) (Ag(I)-, and Ag(I/0)UiO-66), while bearing similarities to the spectrum of bulk silver, were reduced in intensity relative to the Ag(0)-containing samples, which may have been due to the inclusion of Ag^{+} in the structure. The spectrum of bulk silver metal was not a perfect model for the speciation of silver in the Ag(0)UiO-66 samples (**c** and **d**) as the post-edge oscillations were more intense for the bulk metal than for the materials. Additionally, the edge position of the silver metal was higher in energy than all of the experimental spectra.

The LCF results of the UiO-66 XANES spectra are shown in **Figure 13** and **Table 4**. The silver methionine model spectrum was included for the UiO-66 dataset despite the absence of thioether units in the unfunctionalized material, as, when the data were fit, the features of the methionine spectrum were so obscured that the contribution from the methionine spectrum appeared to be to 'bulk up' the other spectral components (particularly silver metal). I.e. the bulk silver model spectrum was fit at a ratio where the intensity of the oscillations of the model matched the intensity of the oscillations of the experimental spectra (**Figure 13A**, **C** and **D**). It has been observed that the XANES spectra of nanoparticles share similar but dampened post-edge features with that of the bulk element.[78-79] The reason for this is unclear, but may be due to the reduction in long-range order when transitioning from a bulk material to nanoparticles. Hence, the resemblance of the Ag(0) treated materials to that of bulk silver does not preclude the presence of silver nanoparticles in the material. While an imperfect model, the spectrum of bulk silver

provided a better fit to the experimental data than did PVP-capped silver nanoparticles. Better quality XANES data of a suspension of small-diameter (<10 nm), unfunctionalized silver nanoparticles could act as a better model but is not available in the current Ag K-edge XANES model library.

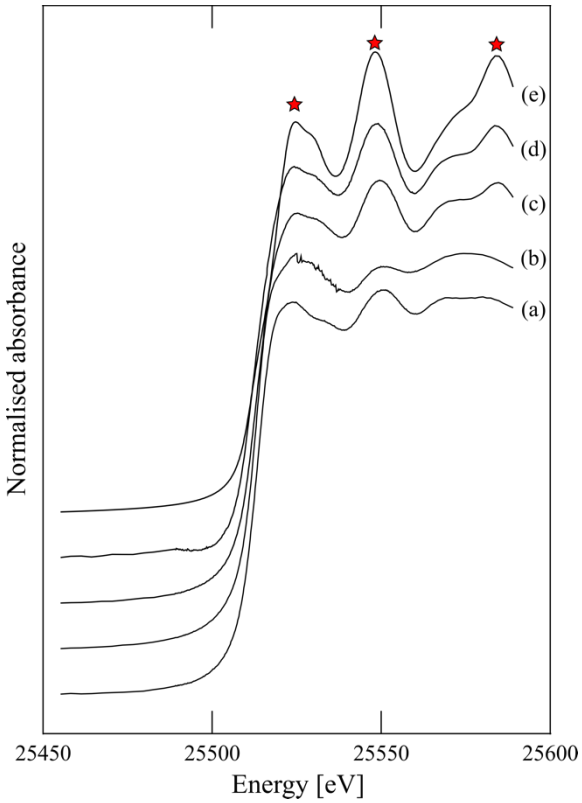

Figure 12: Ag K-edge X-ray absorption near-edge spectra of UiO-66 treated with: (**a**) 100 mM solution of $AgNO_3$ in acetonitrile; (**b**) 100 mM solution of $AgNO_3$ in 5:1 ethanol/water; (**c**) as per (b), but extensively washed with 5:1 ethanol/water to remove ionic Ag; (**d**) as per (c) but embedded in a polycaprolactone matrix; (**e**) bulk silver metal. Some of the loose, powdered MOF was combined with granulated polyethylene (~3:1 w/w) and compressed into a pellet prior to presentation to the beamline; the MOF/polymer composite (d) was secured in a Lucite holder by Kapton tape. All spectra were measured in transmission. PXRD patterns of the samples were recorded pre and post XAS analysis (**Appendix 4.9.4**).

The Ag K-edge XANES of Ag(0)UiO-66 (**Figure 13C**) and Ag(0)UiO-66 in polycaprolactone (**D**) revealed that no significant change in the speciation of silver occurred when the MOF was embedded in the polymer matrix. The polymers were cast by suspending the silver-loaded framework in a solution of polymer followed by evaporation of solvent overnight (in the dark). A visible difference between the two spectra was the diminution of the intensities of the post-edge peaks in the polymer-embedded sample, which may have resulted in the difference in the ratio of model components fit by LCF. The reduction in intensity was most likely due to the amount of sample presented to the beamline. The films were <100 μm thick and simply folded on themselves until an

appropriate size to fit into the sample holder used. At 25% w/w loading, a significantly lower amount of silver-loaded MOF was present than for the loose, powdered material (**Figure 13C**) which was compressed into a pellet of ~0.5 cm thickness.

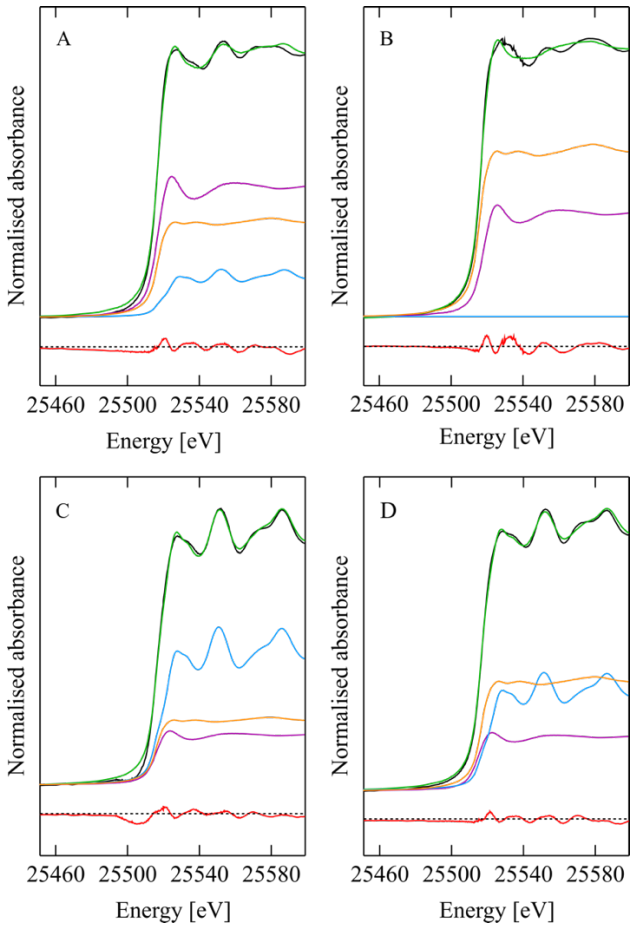

Figure 13: Linear combination fits of Ag K-edge XANES of UiO-66 treated with: (**A**) 100 mM solution of $AgNO_3$ in acetonitrile; (**B**) 100 mM solution of $AgNO_3$ in 5:1 ethanol/water; (**C**) as per (B), but extensively washed with 5:1 ethanol/water to remove ionic Ag; (**D**) as per (C) but embedded in a polycaprolactone matrix. The experimental spectra (black) were fit with a linear combination fit (green) comprised of model XANES spectra of solid bulk silver metal (light blue); aqueous silver nitrate (purple); a buffered solution of the thioether-containing amino acid methionine with silver (orange) with the residual (red) shown offset. Results of linear combination analysis are shown in **Table 4**.

The post edge XANES oscillations of the thioether-containing materials (**Figure 14**) were significantly different from those of the unfunctionalized MOF with the most intense peak atop the rising edge and lower intensity oscillations occurring at higher energy. For both PS- and ASUiO-66 treated with Ag(I) (**Figure 14a**) the post-edge features were almost identical, which suggested that the speciation of silver in both materials was similar. This similarity was reflected in the LCF results shown in **Figure 15** and **Table 4**.

In contrast to the UiO-66 LCF data (**Figure 13**), similarities between the silver-methionine model spectrum and the experimental PS/ASUiO-66 spectra were visually present (**Figure 15**, **orange**), e.g. the broad peaks at ~25,540 eV and ~25,575 eV. Similarly, features of the aqueous silver nitrate XANES spectrum (**Figure 15**, **purple**) could be identified in the experimental data such as the peak atop the rising edge and the broad peak at ~25,545 eV.

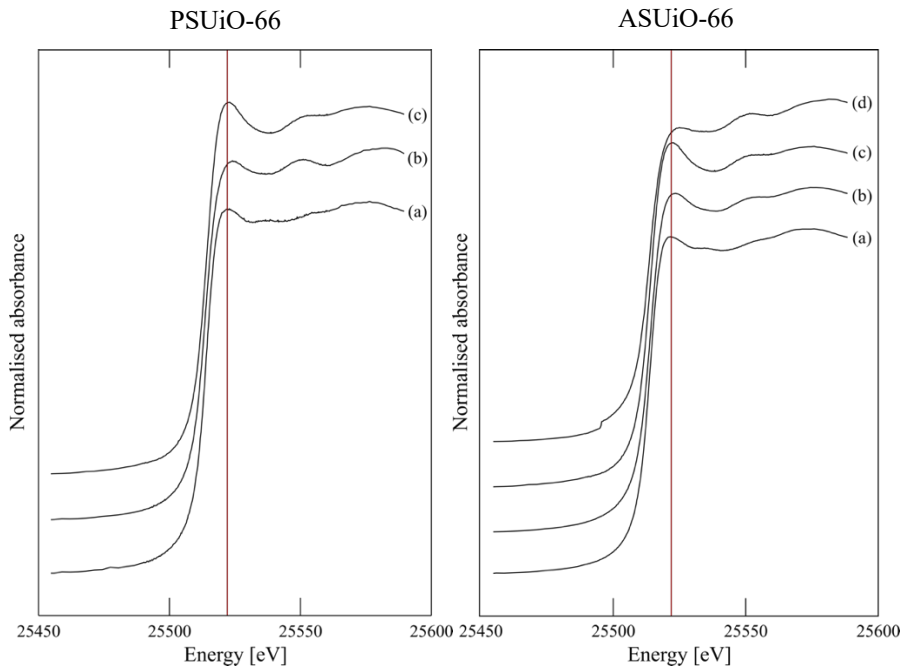

Figure 14: Ag K-edge X-ray absorption spectra of PSUiO-66 (**left**), and ASUiO-66 (**right**) treated with: (**a**) 100 mM solution of $AgNO_3$ in acetonitrile; (**b**) 100 mM solution of $AgNO_3$ in 5:1 ethanol/water; (**c**) as per (b), but extensively washed with 5:1 ethanol/water to remove ionic Ag; (**d**) as per (c) but embedded in a polycaprolactone matrix. Some of the loose, powdered MOF was combined with granulated polyethylene (~3:1 w/w) and compressed into a pellet prior to presentation to the beamline; the MOF/polymer composite (d) was secured in a Lucite holder by Kapton tape. All spectra were measured in transmission. PXRD patterns of the samples were recorded pre and post XAS analysis (**Appendix 4.9.4**).

The XANES spectra of Ag(0)ASUiO-66 and the PCL-embedded equivalent (**Figure 14c** and **d**) displayed different post-edge features which suggested that the speciation of silver in the material may have been perturbed by the evaporation of solvent when casting the Ag(0)ASUiO-66/PCL composite material. The LCF results showed an increase in the bulk silver metal contribution (2.5% to 39%) and a reduction in the methionine component (61% to 39%) which could indicate aggregation of nanoparticulate silver during the polymer casting.

When ethanol was included as a reductant, a colour change from yellow to brown was observed for both PS- and ASUiO-66 after soaking for ~16 h. Despite this observation silver-methionine was the dominant component fit to almost all thioether-containing materials. The absence of metallic or nanoparticulate character in the XANES spectra of Ag(I/0) and Ag(0) treated PS/ASUiO-66 could indicate that the silver was largely located within the pores of the materials and interacted strongly with the pendant thioether units. Any silver located outside of the pores would likely have been reduced to metallic silver in the presence of the ethanol.

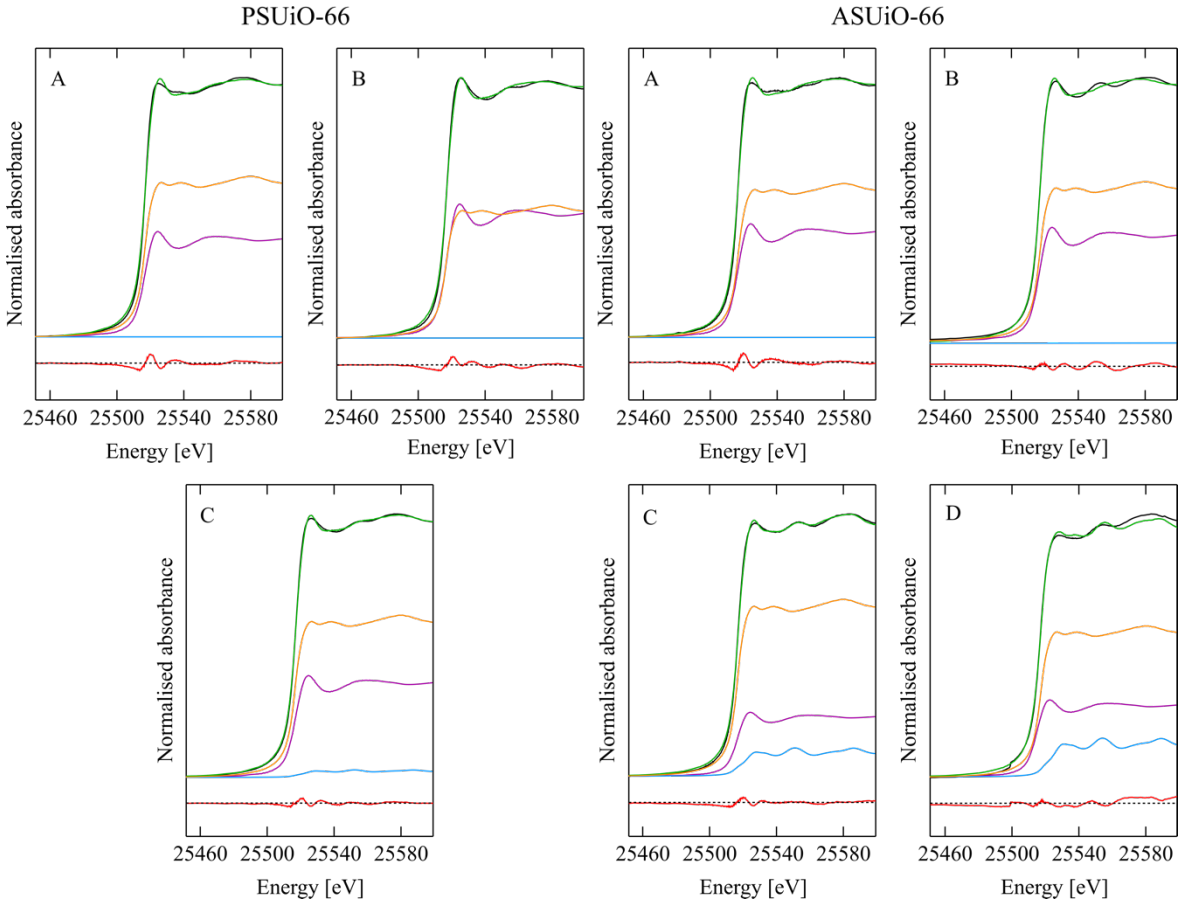

Figure 15: Linear combination fits of Ag K-edge XANES of PSUiO-66 treated with: (**A**) 100 mM solution of $AgNO_3$ in acetonitrile; (**B**) 100 mM solution of $AgNO_3$ in 5:1 ethanol/water; (**C**) as per (B), but extensively washed with 5:1 ethanol/water to remove ionic Ag; (**D**) as per (C) but embedded in a polycaprolactone matrix. The experimental spectra (black) were fit with a linear combination fit (green) comprised of model XANES spectra of solid bulk silver metal (light blue); aqueous silver nitrate (purple); a buffered solution of the thioether-containing amino acid methionine with silver (orange) with the residual (red) shown offset. Results of linear combination analysis are shown in **Table 4**.

Table 4: Calculated ratios of Ag species in UiO-66, PSUiO-66, and ASUiO-66 treated with silver, as estimated by linear combination of model XANES spectra.

Sample	Ratio of component fitted[a]			N_{tot}[b]	Residual
	Silver nitrate	Bulk silver	Methionine		
Ag(I)UiO-66	0.50(2)	0.168(9)	0.36(2)	1.02	0.41
Ag(I/0)UiO-66	0.34(2)	-	0.67(1)	1.00	0.54
Ag(0)UiO-66	-	0.52(1)	0.49(1)	1.01	0.75
Ag(0)UiO-66/PCL	0.23(2)	0.391(7)	0.39(2)	1.01	0.19
Ag(I)PSUiO-66	0.41(2)	-	0.59(2)	1.00	0.30
Ag(I/0)PSUiO-66	0.39(1)	0.077(5)	0.53(1)	1.00	0.11
Ag(0)PSUiO-66	0.24(1)	0.095(6)	0.67(1)	1.00	0.14
Ag(I)ASUiO-66	0.38(2)	-	0.61(2)	1.00	0.30
Ag(I/0)ASUiO-66	0.53(2)	-	0.47(2)	1.00	0.26
Ag(0)ASUiO-66	0.365(9)	0.025(4)	0.61(1)	1.00	0.08
Ag(0)ASUiO-66/PCL	0.23(2)	0.391(7)	0.39(2)	1.01	0.19

[a]Values in parentheses are the estimated standard deviation derived from the diagonal elements of the covariance matrix and are a measure of precision. [b]N_{tot} is the sum of the fractions

EXAFS of silver-loaded metal-organic frameworks

Figures 16 and **17** show the EXAFS oscillations (left panel) and phase-corrected Fourier Transforms (FTs) (right panel) of all powdered materials. The oscillations of the UiO-66 materials (all treatments) were dampened until ~4 $Å^{-1}$ at which point the amplitude of the oscillations increased and continued until the cessation of data collection at 14 $Å^{-1}$, suggesting a high degree of interaction between the absorbing Ag atoms and other heavy elements. The maximum amplitudes of the oscillations shifted to larger *k* from Ag(I) ~8.5 $Å^{-1}$ to Ag(0) >14 $Å^{-1}$ which indicated an increase in heavy element interactions in the absorbing Ag coordination sphere, consistent with the premise of AgNP formation and removal of Ag^{+} *via* thorough washing. The FTs of the EXAFS oscillations for all UiO-66 materials displayed an intense peak at ~2.8 Å which, for the Ag(I) and Ag(I/0) materials was adequately described by single scattering silver and oxygen backscattering interactions. However, the EXAFS of Ag(0)UiO-66 and the PCL-embedded equivalent were successfully fitted with multiple scattering models calculated from a crystal structure of *fcc* silver metal[80] (**Table 5**). When applied to the EXAFS recorded from Ag(0)UiO-66, the generated MS model required minimal relaxation as the model and the experimental spectrum were almost superimposable, suggesting coordination of silver in the material similar to that in the bulk metal. Such an observation brought into question the location of the silver in unfunctionalised UiO-66. In the absence of defects, the pores of UiO-66 are 7 and 9 Å in diameter which could accommodate – assuming close-packed *fcc* geometry and a silver Van de Waals radius of 1.72 Å[81] – between 7 and 14 atoms of silver; so few atoms are unlikely to result in the intense oscillations and similarities to the bulk metal. The similarity of the experimental spectrum with elemental silver may suggest that, for UiO-66, the washing steps caused aggregation of silver.

Despite the absence of a reducing agent when a solution of silver nitrate in acetonitrile was diffused into UiO-66, the intensity of the EXAFS of Ag(I)UiO-66 suggested that some of the silver was in the Ag(0) oxidation state, possibly reduced by the material itself; corroborated by the LCF analysis. This rendered the putative prefix of 'Ag(I)-' not entirely correct for the unfunctionalised material, however, it was employed to describe the conditions to which the material was exposed to silver (i.e. no reducing agent).

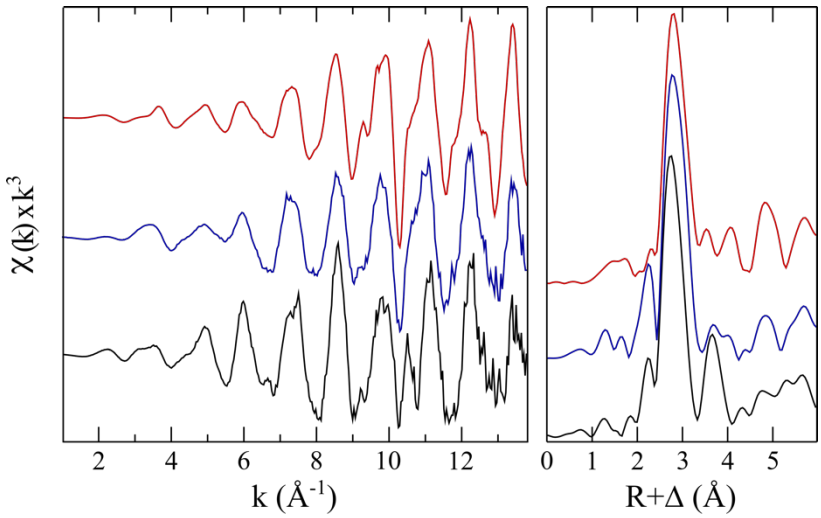

Figure 16: Ag K-edge EXAFS spectra (left panel) and corresponding Fourier Transform (right panel) of UiO-66 treated with: 100 mM solution of $AgNO_3$ in acetonitrile (**black**); 100 mM solution of $AgNO_3$ in 5:1 ethanol/water (blue); as per previous, but extensively washed with 5:1 ethanol/water to remove ionic Ag (red). EXAFS fits shown in **Appendix 4.9.5**.

Table 5: Parameters fit to EXAFS spectra of Ag(I), Ag(I/0), Ag(0)UiO-66, and Ag(0)UiO-66/PCL, shown in **Figure 16**. See **Appendix 4.8.5** for calculated fits.[a]

Sample	Scatterer	CN	Distance (Å)	DWF (Å^2)	-E_0	Fit error
Ag(I)UiO-66	O	2	2.536(8)	0.0030(7)	19	0.42
	Ag	5	2.840(3)	0.0068(1)		
	Ag	2	3.913(5)	0.0046(3)		
Ag(I/0)UiO-66	O	2	2.219(5)	0.0032(5)	14	0.39
	Ag	3	2.881(2)	0.0041(1)		
Ag(0)UiO-66	010	12	2.896(2)	0.0036(1)	11	0.34
	010	5	4.096	0.0051		
	010	24	5.017	0.0062		
	0110	96	5.405	0.0067		
	010	12	5.793	0.0072		
	0110	24	5.793	0.0072		
	01010	12	5.793	0.0072		
	01110	12	5.793	0.0072		
Ag(0)UiO-66/PCL	010	12	2.885(2)	0.0045(1)	13	0.35
	010	5	4.080	0.0064		
	010	24	4.996	0.0078		
	0110	96	5.382	0.0084		
	010	12	5.769	0.0090		
	0110	24	5.769	0.0090		
	01010	12	5.769	0.0090		
	01110	12	5.769	0.0090		

[a] k-ranges used for fitting each spectrum were 1-14 Å with a scale factor (S_0^2) of 0.9. $\Delta E_0 = E_0 - 25515$ eV where E_0 is the threshold energy. Values in parentheses are the estimated standard deviation derived from the diagonal elements of the covariance matric and are a measure of precision. The fit error is defined as $[\Sigma k^6(\chi_{exp}-\chi_{calc})^2/\Sigma k^6\chi_{exp}^2]^{½}$.

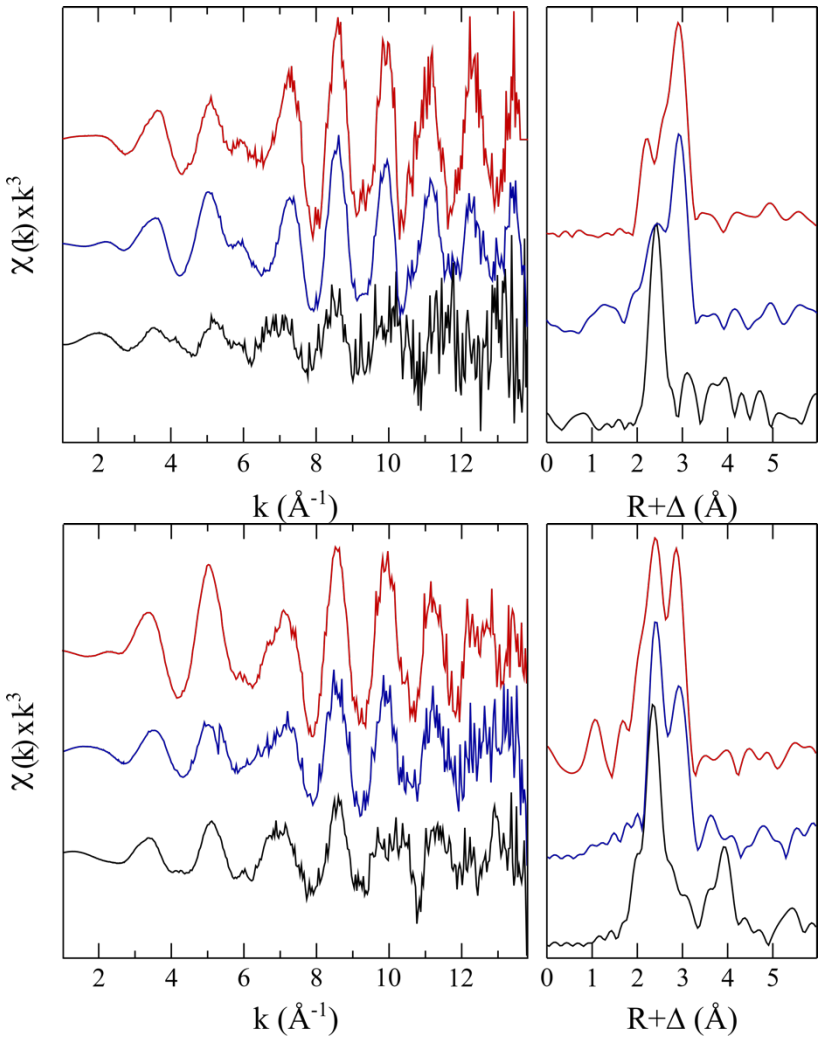

Figure 17: Ag K-edge EXAFS spectra (left panel) and corresponding Fourier Transform (right panel) of PSUiO-66 (**top**) and ASUiO-66 (**bottom**) treated with: 100 mM solution of $AgNO_3$ in acetonitrile (**black**); 100 mM solution of $AgNO_3$ in 5:1 ethanol/water (blue); as per previous sample, but extensively washed with 5:1 ethanol/water to remove ionic Ag (red). EXAFS fits are shown in **Appendix 4.8.5**.

Table 6: Parameters fit to EXAFS spectra of Ag(I), Ag(I/0), Ag(0)PS and ASUiO-66, and Ag(0)ASUiO-66/PCL, shown in **Figure 17**. See **Appendix 4.8.5** for calculated fits.[a]

Sample	Scatterer	CN	Distance	DWF	$-E_0$	Fit error
Ag(I)PSUiO-66	S	1	2.506(8)	0.0025(4)	15(2)	0.84
Ag(I/0)PSUiO-66	S	2	2.479(5)	0.0028(3)	18(1)	0.43
	Ag	6	2.854(3)	0.0071(3)		
Ag(0)PSUiO-66	O	1	2.30(1)	0.004(1)	16(1)	0.42
	S	1	2.48(2)	0.009(1)		
	Ag	2	2.863(3)	0.0052(1)		
Ag(I)ASUiO-66	C/O	2	2.40(1)	0.014(3)	13(1)	0.55
	S	1	2.502(4)	0.0038(3)		
	C/O	1	3.02(1)	0.0044(3)		
	Ag	1	3.939(8)	0.0066(4)		
Ag(I/0)ASUiO-66	S	1	2.496(4)	0.0024(3)	18(1)	0.51
	S	1	2.67(1)	0.007(1)		
	Ag	1	2.852(5)	0.0062(3)		
Ag(0)ASUiO-66	C/O	2	2.30(1)	0.017(2)	19(1)	0.36
	S	1	2.494(5)	0.0066(4)		
	Ag	1	2.824(3)	0.0070(1)		

[a]k-ranges used for fitting each spectrum were 1-14 Å with a scale factor (S_0^2) of 0.9. $\Delta E_0 = E_0 - 25515$ eV where E_0 is the threshold energy. Values in parentheses are the estimated standard deviation derived from the diagonal elements of the covariance matric and are a measure of precision. The fit error is defined as $[\Sigma k^6(\chi_{exp}-\chi_{calc})^2/\Sigma k^6\chi_{exp}^2]^{½}$.

The phase-correct Fourier Transforms of the Ag(I)PS and ASUiO-66 (**Figures 17**, **black**) both displayed intense peaks at ~2.5 Å which were fit by sulfur backscattering interactions at distances of 2.5 Å, and 2.7 Å. A survey of the CSD indicated that bond lengths of ~2.5 Å are consistent with silver-thioether interactions, while the longer distances were likely due to bridging of the thioether units between multiple silver atoms. Carbon/nitrogen/oxygen backscattering interactions were fit to the low R peak in the FTs of Ag(I)PS and ASUiO-66 but resulted in physically unrealistic fit parameters. Silver-silver interactions were successfully fit to both spectra but yielded very different distances. The allyl sulfanyl material was fit with an Ag-Ag distance of 3.9 Å while the same component fit to the propyl sulfanyl material resulted in a distance of 2.9 Å. The difference in distances could possibly be due to multiple scattering (e.g. Ag-S-Ag pathways). The orientations of the pi system in the pendant allyl sulfanyl groups in UiO-66 are not known, however, if they were to form pi-pi interactions with adjacent allyl groups or the benzene core of the ligand (see novel materials section) then the additional rigidity provided by this interaction may have facilitated multiple scattering. In contrast to the EXAFS oscillations

of Ag(I)UiO-66 the oscillations of the Ag(I)PS and ASUiO-66 materials (**Figure 17**, **black**) were reduced in intensity up to the end of data collection (14 $Å^{-1}$), confirming the absence of elemental silver.

The Ag(I/0) and Ag(0) treatments of both PS- and ASUiO-66 displayed strong contributions from silver-silver backscattering interactions, evident from the emergence of a prominent peak at ~2.9 Å in the EXAFS FTs of the corresponding materials. While the Ag-Ag interaction became the dominant feature of the PSUiO-66 FTs, it did not for the ASUiO-66 with the peak at ~2.5 Å remaining the most intense feature.

Both Ag(0)PSUiO-66 and Ag(0)ASUiO-66 were fit with Ag-O interactions at 2.30 Å. The emergence of PXRD peaks corresponding to the formation of Ag_2O nanoparticles in the Ag(0)PSUiO-66 materials supported this fitting, however, it was unclear why the interaction was only seen in the Ag(0) material EXAFS. It was possible that the Ag(I/0), overall, contained less significant contribution of Ag-O interactions than did the Ag(0) materials, which had been washed extensively with water/ethanol in air.

4.4.8 Silver leaching from MOF/polymer composite materials

Solid-state materials are unlikely to find application as consumable medicines to fight established bacterial infections, however, the premise of coating surfaces to prevent infection in clinical settings provides a wealth of opportunity. For example, coating prostheses, instruments, and components with antibacterial materials. Unlike some natural bactericidal materials[82] metal-organic frameworks have not been shown to elicit an antibacterial response through the topology/morphology of the material and their brittle, powdered nature precludes them from such applications. Instead the medicinally relevant attribute of the materials is usually the release of a payload, degradation of the material itself to release molecular entities or generation by external stimuli.[31, 83] If preventative action is required (i.e. preventing biofilms from forming at wound or implant) sites then a prolonged release of, in this case, silver would be desirable. Thus, an understanding of the kinetics of release of silver from the MOF/polymer composite materials is crucial.

To investigate the silver leaching profiles of all PCL-embedded materials they were stirred in water or Luria Bertani bacterial broth for 24 hours. Aliquots were removed at 1, 2, 4, 8, and 24 hour and analysed by atomic absorption spectroscopy (AAS) by comparison to a silver calibration curve. The release of silver from the MOF/PCL films was

significantly reduced relative to release from the loose, powdered MOFs (**Figure 11**) due to the silver having to diffuse through the polymer matrix in addition to out of the material itself.

The leaching profile of the PSUiO-66 materials (**Figure 18**) did not follow the trend observed for the loading of silver into the material (**Table 1**, above). Ag(I)PSUiO-66 had the lowest loading of silver (~13 mol%), but the greatest release of silver after 24 hours (15.4% of total loaded silver), followed by Ag(I/0) and Ag(0). The lower release of silver from the materials in which reduced silver was present was possibly due to the mode of release from the materials. From the leaching profile it was clear that the silver nanoparticles (and elemental silver) in the materials were prevented from diffusing, out of the materials into the aqueous medium, likely limited by oxidative dissolution, an additional process on top of diffusion of Ag^{+} out of the MOF/polymer composite. Logarithmic release was observed for all PSUiO-66 materials with a plateau beginning to appear after 8 h that would likely have been reached if the studies were conducted for a longer period of time. The error bars displayed for all silver leaching profiles were representative of both technical and material batch replicates which suggested that the loading of silver into the PSUiO-66 materials was consistent for the Ag(I) and Ag(0) treatments, however, a higher level of variation was observed for release from the Ag(I/0) material.

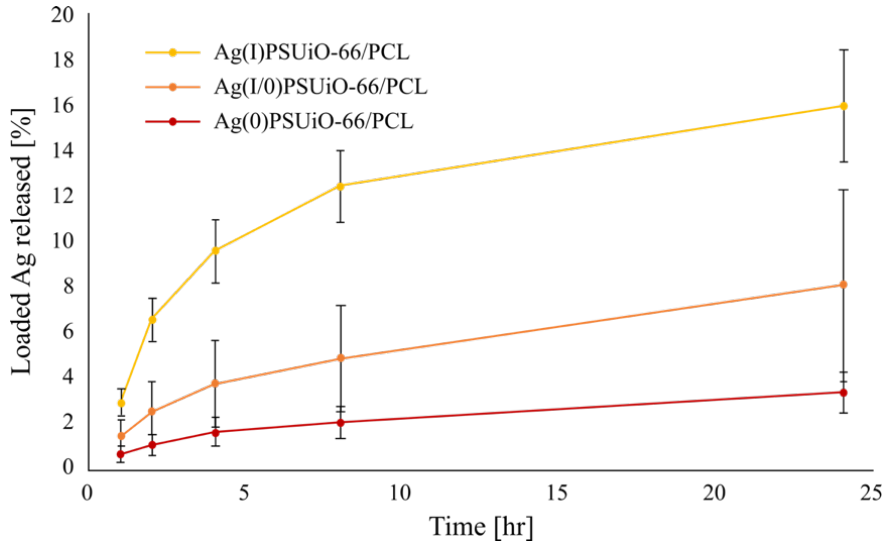

Figure 18: Percentage of total loaded silver in PSUiO-66/PCL composites released into MilliQ water over 24 hours. Error bars are representative of the standard error calculated from multiple replicates.

Similar to PSUiO-66 composite materials, the leaching profile of the ASUiO-66/PCL materials into water did not adhere to the trend of loading reported in **Table 1**. Both the Ag(I) and Ag(I/0) materials released similar percentages of total loaded silver over 24 hours despite the latter having the highest loading of all ASUiO-66 materials (~23 mol%). The standard error of the measurements of silver released from Ag(I/0)ASUiO-66 was greater than that of Ag(I)ASUiO-66 which, again, suggested variable results when loading silver into the material in this way. Both the Ag(I) treated PS and ASUiO-66 materials released similar percentages of total loaded silver into water after 24 hours (15.9 vs. 14.3%, respectively). However, both the Ag(I/0) and Ag(0) treatments of ASUiO-66 released approximately twice as much Ag than did the equivalent PSUiO-66 materials.

Silver-silver interactions were the dominant features of the Ag(I/0) and Ag(0)PSUiO-66 EXAFS FTs (**Figure 17**). Conversely, the EXAFS of the ASUiO-66 materials maintained a strong contribution from the thioether sulfur in the coordination sphere of silver for both the Ag(I/0) and Ag(0) samples. An increased contribution could indicate a strong interaction between the pendant allyl thioether and the loaded silver. If this interaction increased the rate of oxidative dissolution of the reduced silver, it could help explain the increased release of Ag^{+} from ASUiO-66, relative to PSUiO-66. Alternatively, the silver ions may have been stabilised and prevented from being reduced to Ag(0) in the presence of ethanol.

The leaching profiles discussed thus far were carried out in ultra-pure MilliQ water, a poor comparison for a wound site. To better understand the kinetics of release into biological systems, leaching studies were carried out in Luria Bertani (LB) broth. LB broth is an ‘undefined’ media commonly used in microbiology to culture bacteria. It is considered undefined as it is composed of reconstituted water-soluble yeast extract (5 g/L), digested casein (tryptone) (10 g/L), and sodium chloride (5 g/L). The results of silver leaching from the ASUiO-66 family of materials into LB broth are displayed in **Figure 19**, **bottom** and key points summarised in **Table 7**. Overall the release of silver from all Ag-treatments of ASUiO-66 were reduced, relative to release into water. For all time points, the Ag(I/0)ASUiO-66 material released the greatest percentage of total loaded silver which was consistent with the mol% loading of silver discussed above. It was unclear why the trend of silver release changed between water and broth; however, it may have been that some of the solute dissolved in the broth (short chain peptides, amino acids, minerals, etc.) aided in the oxidative dissolution of the nanoparticles (or elemental silver)

in Ag(I/0)ASUiO-66. Similarly, the Ag(0)ASUiO-66 material (despite having the lowest loading of the three silver treatments – 15.6 mol%) released the second highest percentage of silver after 24 hours. Ag(I)ASUiO-66 released the lowest percentage of silver into broth of the three materials, which was possibly a result of impeded diffusion out of the MOF/PCL composite due the high ionic strength of the broth reducing the concentration and diffusion gradient from material to medium. Given the significantly reduced release of silver from the ASUiO-66 materials into broth (**Figure 19**, **bottom**), the same experiments were not carried out for the PS analogues.

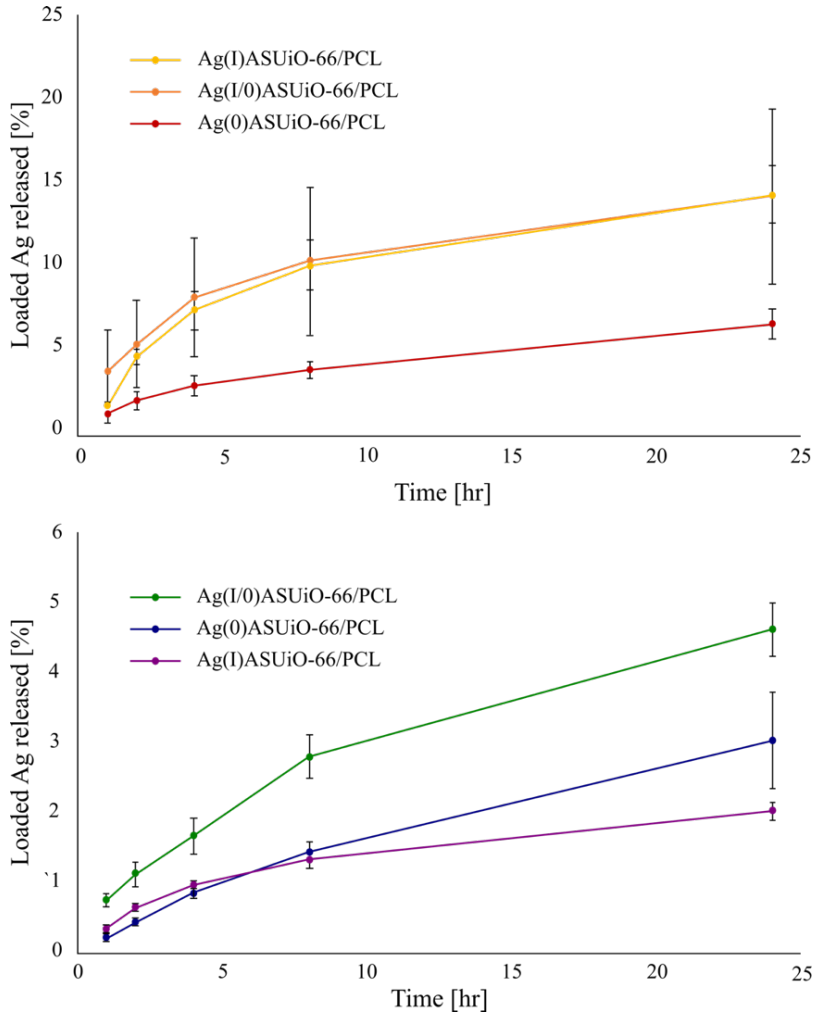

Figure 16: Percentage of total loaded silver in ASUiO-66/PCL composites released into MilliQ water (**top**) and Luria Bertani broth (**bottom**) over 24 hours. Error bars are representative of the standard error calculated from multiple replicates.

For almost all silver treatments, measuring the leaching of silver from the unfunctionalised UiO-66 materials gave inconsistent results. A high degree of variability in the release of silver from the Ag(I/0) and Ag(0) materials was observed even within the

same batch of processed material; tables of UiO-66 leaching data are shown in **Appendix 4.8.6**. The variability was likely a result of non-specific interactions between the silver and the material resulting in inhomogeneous distribution within the sample. Leaching from Ag(I)UiO-66, however, was consistent and the silver release profile into water and broth is shown in **Figure 20**. Similar to the ASUiO-66 materials, the overall release of silver into broth was reduced compared to release into water. After 24 hours, 15.4% of total loaded silver was released into water, while only 0.7% was released into broth over the same period.

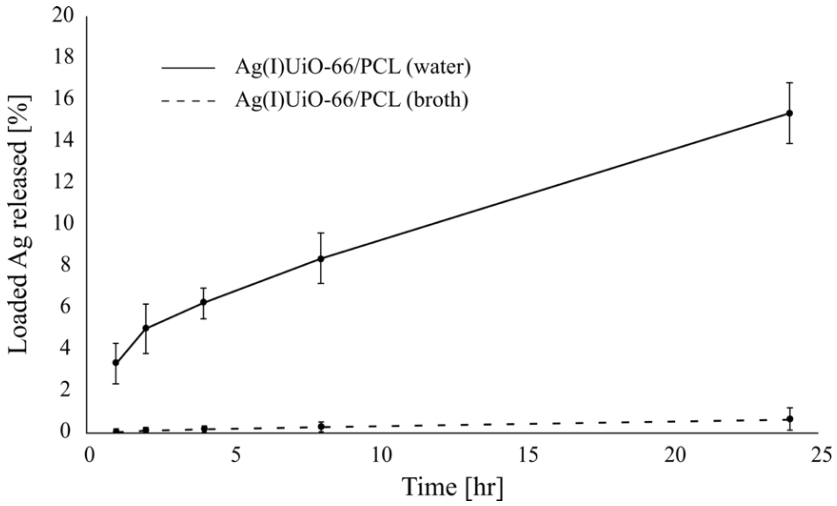

Figure 20: Percentage of total loaded silver in Ag(I)UiO-66/PCL composites released into MilliQ water (solid) and LB broth (dashed) over 24 hours. Error bars are representative of the standard error calculated from multiple replicates.

Table 7: Concentrations and percentage of silver released into water or broth by MOF/PCL composite materials after 24 hours.[a]

Material	Medium	[Ag] after 24 h [ppm]	Released Ag after 24 h [%]
Ag(I)UiO-66	Water	30.7 (2.5)	15.4 (1.5)
Ag(I)UiO-66	Broth	3.0 (0.6)	0.7 (0.5)
Ag(I)PSUiO-66	Water	44.1 (7.0)	15.9 (2.5)
Ag(I/0)PSUiO-66	Water	32.7 (20.3)	8.1 (4.2)
Ag(0)PSUiO-66	Water	13.0 (3.4)	3.4 (0.9)
Ag(I)ASUiO-66	Water	42.2 (5.0)	14.3 (1.7)
Ag(I/0)ASUiO-66	Water	72.3 (25.9)	14.2 (5.2)
Ag(0)ASUiO-66	Water	27.9 (5.9)	6.7 (0.9)
Ag(I)ASUiO-66	Broth	6.6 (1.1)	2.0 (0.4)
Ag(I/0)ASUiO-66	Broth	24.9 (0.8)	3.0 (0.7)
Ag(0)ASUiO-66	Broth	10.1 (1.7)	4.6 (0.1)

[a]Values in parentheses are calculated standard errors of replicates

4.4.9 Antibacterial disk diffusion assays of silver-loaded MOF/PCL composites

The antibacterial activity of all materials was tested by disk diffusion assays on 1.5% LB broth agar plates inoculated with cultures of Gram-negative (*E. coli*) and Gram-positive (*S. aureus*) bacteria. Disks of polymer-embedded silver-loaded MOF (5 mm diameter) were cut from the bulk cast films and placed on the surface of the inoculated plates along with disks of PCL alone, and 25% w/w $AgNO_3$ in PCL as negative and positive controls, respectively (**Figure 21**). For all silver-loaded MOF/PCL materials the antibacterial response was greater against the Gram-positive *S. aureus* compared to the Gram-negative *E. coli*, shown by larger zones of inhibited growth around the MOF-polymer disks. It has been reported in literature that Gram-negative bacteria can be more tolerant of higher metal concentrations.[84] The higher resistance of the *E. coli* to the leached silver could be due to a wealth of copper efflux genes in the bacterial strain used herein (MG1655). Due to similarities in chemistry, removal of Ag(I) from bacterial cells is often associated with Cu(I) transport and regulation.[85] The proteome of the Newman strain of *S. aureus* only contains one known copper-efflux protein, while that of the strain of *E. coli* used (MG1655) contains up to 10 copper-efflux proteins. The ability for *E. coli* to efflux endogenous silver could have resulted in the overall reduced zones of inhibition (ZOIs) and antibacterial response in the disk diffusion assays.

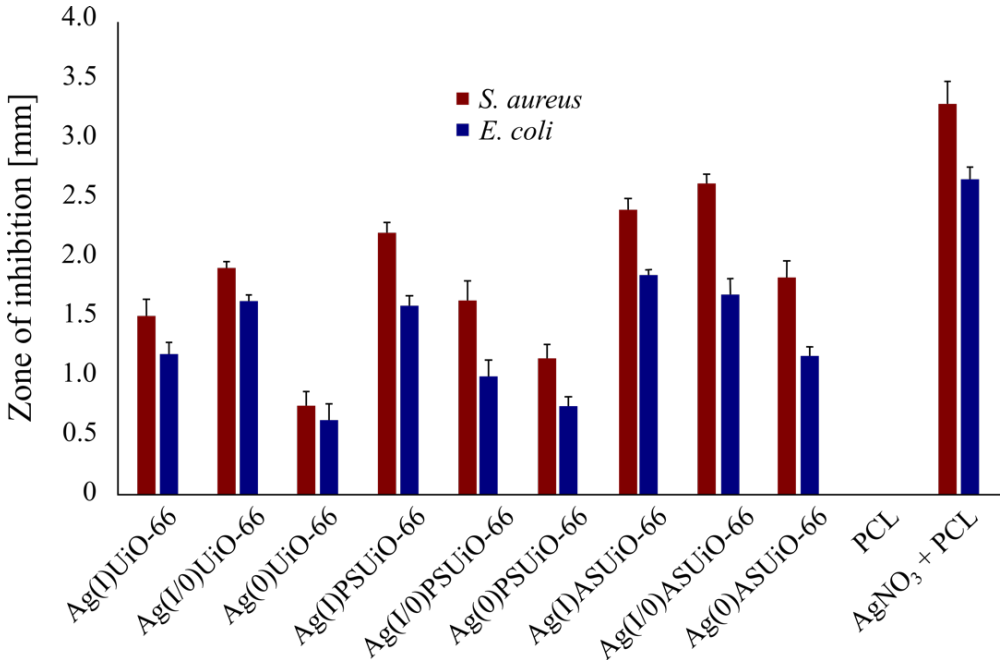

Figure 21: Measured zones of inhibited growth of S. aureus (red) and E. coli (blue) around 5 mm disks of PCL-embedded, silver-loaded UiO-66 materials (25 wt%). Disks of untreated PCL, and silver nitrate embedded in PCL (25 wt%) were used as negative and positive controls, respectively. Error bars are representative of biological and technical replicates.

The ZOI for all silver treatments of unfunctionalised UiO-66, and ASUiO-66 reflected the relative amounts of silver loaded into each material (**Table 2**). For example, the mixed oxidation state material (Ag(I/0)) had the highest loading of silver and the highest ZOI, followed by ionic silver (Ag(I)), and nanoparticulate silver (Ag(0)). However, the difference between the ZOIs of the Ag(I) and Ag(I/0)ASUiO-66 samples were within the margin of error for the measurements. The trend observed for the PSUiO-66 materials did not match the relative loadings of silver into each material, instead the ionic silver treated material had the greatest antibacterial response with the ZOI decreased for Ag(I/0), and Ag(0), respectively.

No materials had a greater antibacterial response than the positive control of silver nitrate in PCL, however, upon analysis of the relative amount of silver in each sample, the results of the disk diffusion assays changed significantly. The 5 mm disks punched from the bulk cast films for the disk diffusion assays had an average mass of 2.2 ± 0.3 mg. Knowing the mass of the disks used, weight loading of solid into the PCL, and percentage of silver per unit cell of MOF enabled the mass of silver in each disk to be calculated. Thus, the zone of inhibition data in **Figure 21** could be weighted relative to the mass of silver in the disks tested (**Figure 22**).

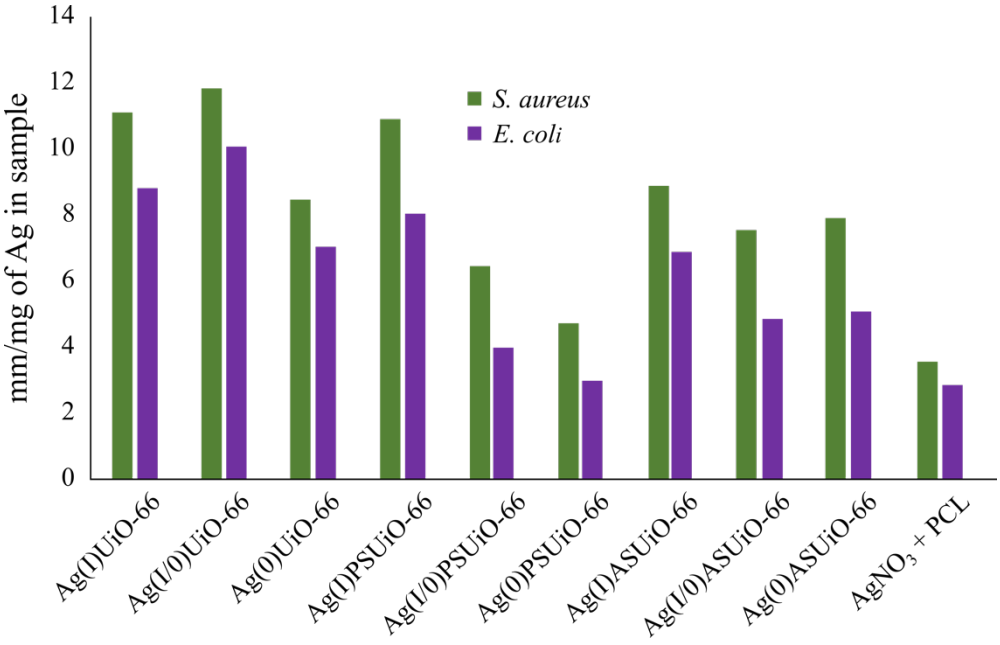

Figure 22: Zone of inhibition distances – from **Figure 21** – against *S. aureus* (green) and *E. coli* (purple) weighted by the mass of silver in each 5 mm disk of MOF/PCL composite. Error bars omitted for clarity; same as Figure 21.

The weighted zone of inhibition data revealed that the positive control of 25% w/w $AgNO_3$ in polycaprolactone had the lowest clearance zone per mg of silver against both *S. aureus* and *E. coli*. Additionally, it was found that for the PS- and ASUiO-66 materials the Ag(I) treatments had the highest ZOI per mg Ag and were the best performing materials of the same MOF type. By viewing the data in this way, it also highlighted that the amount of silver loaded into each framework was not the governing factor in the antibacterial properties of the composite materials. If this was the case, the Ag(I/0) material of each analogue would have had the greatest zone of clearance per mg of silver according to the silver-loading results in **Table 2**. Once weighted, unfunctionalised UiO-66/PCL samples were found to have the greatest antibacterial efficacy for each silver treatment. However, while the unfunctionalised materials may have been the best performing in the short term, the disk diffusion assays were only conducted over ~16 h and did not take into consideration the longevity of silver release from the materials. Conducting longer duration disk diffusion assays would likely have resulted in erroneous results due to the natural death of the microorganisms.

4.4.10 Novel materials

AgMOF-3

As has been detailed elsewhere, having a material loaded with an antibacterial agent and made from an antibacterial metal node (silver) could increase bactericidal efficacy (**4.7 Future directions**); either additive or synergistic. It was found that reaction of the ASBDC linker with silver trifluoroacetate, in a DMSO/ethyl acetate solvent mixture provided single crystals suitable for single crystal X-ray crystallography (parameters shown in **Appendix 4.8.1**). The structure of the material, $[Ag_2(ASBDC)]$, is a three-dimensional framework comprised of silver ions and the ASBDC linker and reveals a rather unusual coordination environment for Ag ions comprising carboxylate and thioether donors. The asymmetric unit of AgMOF-3 comprises two silver ions chelated by sulfur and oxygen atoms from half an ASBDC linker ($Ag_2C_7O_2S_1$) (**Figure 23**). Pillars of silver atoms coordinated by both carboxylate oxygen and sulfur atoms from the ASBDC linkers project along the *c* axis (**Figure 24**). Two silver S_2O_4 coordination spheres are formed in the material, both with distorted octahedral geometry, with one located in the interior of the pillar and the second on the periphery. One distinction between the two silver coordination spheres is that in one the two sulfur donors coordinate in a linear fashion (S-Ag-S angle: 169.4°) while the other has them arranged at right angles (S-Ag-S angle:

88.8°). The pillars are coordinated to three carboxylate linkers at each repeat giving rise to hexagonal pores with apertures ~7 Å in diameter (**Figure 25**).

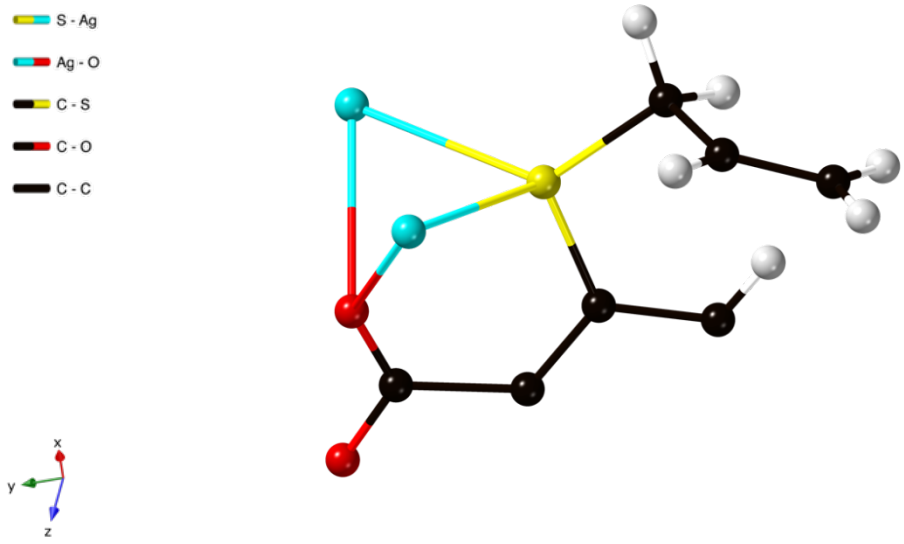

Figure 23: Asymmetric unit of the single crystal structure of AgMOF-3.

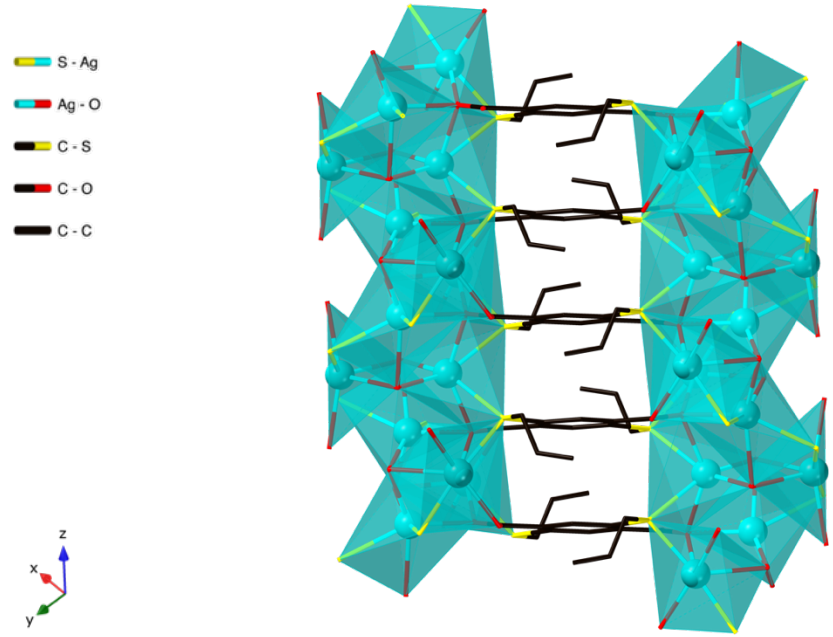

Figure 24: AgMOF-3 has pillars of silver ions running along the c-axis of the structure. Two S_2O_4 coordination spheres of the silver ions are formed, both with distorted octahedral geometries; one coordination sphere has the thioether sulfurs coordinating the Ag ion linearly (S-Ag-S angle: 169.4°) while the other forms right angle geometry (S-Ag-S angle: 88.8°).

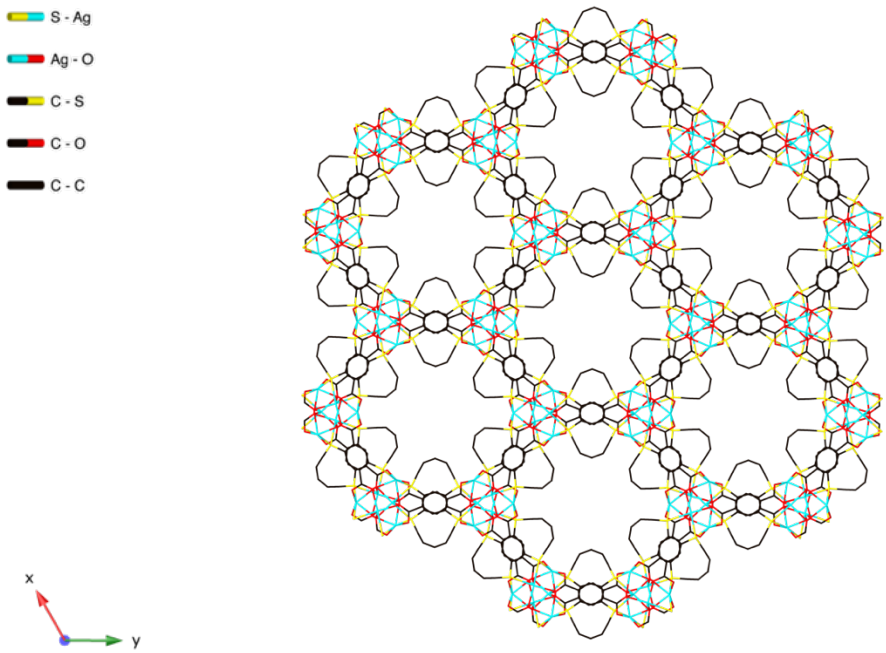

Figure 25: Hexagonal pores that run along the c-axis of the framework with ~9 Å apertures. The allyl pi systems are projected into the pore space of the material.

The structure of [Ag_2(ASBDC)] is further stabilised by pi stacking interactions. The benzene rings of the ASBDC linkers are separated by 4.054 Å, which is within the distance range normally ascribed to pi stacking interactions.[86] When viewed down the *c*-axis the hexagonal pores are lined by interdigitated allyl groups from the ASBDC linkers. The pendant allylsulfanyl ether units also appear to form intermolecular pi-pi contacts with nearby ASBDC thioether groups with a C-C distance of 4.054 Å (**Figure 26**, **right**). Furthermore, close contacts between the pendant allyl group and the linker benzene core are also formed with distances of 3.426 and 3.501 Å (**Figure 26**, **left**).

A simulated powder X-ray diffraction pattern was generated from the single crystal data presented here of AgMOF-3 and is shown in **Figure 27a**. Once grown by vapour diffusion, the single crystals of AgMOF-3 were crushed under solvent and wet-loaded into a capillary to obtain a powder diffraction pattern of the bulk material (**Figure 27b**). Additionally, room temperature conditions to synthesise the material were also identified (**Figure 27c**). As the simulated powder pattern accounts for all major peaks, and their relative intensities, it can be said that the single crystal structure presented here is representative of the bulk material generated from this experiment. No further

characterisation of this material was undertaken, but future work has been detailed elsewhere (see **4.7 Future directions**).

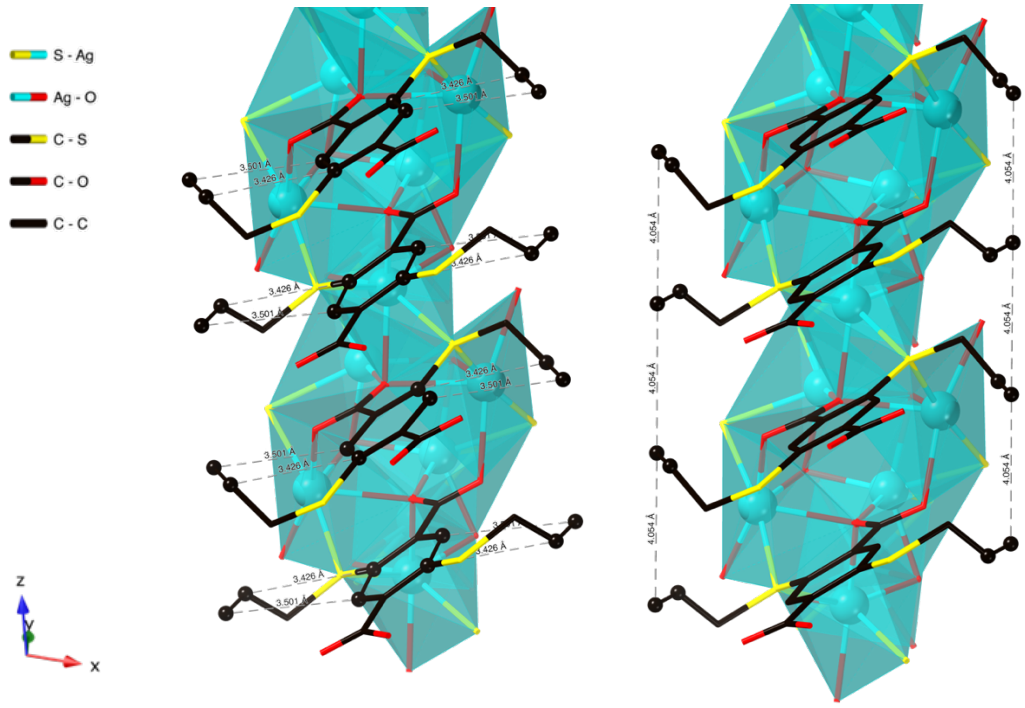

Figure 26: Intramolecular (left) and intermolecular (right) pi-pi bonds formed in and between ASBDC linkers.

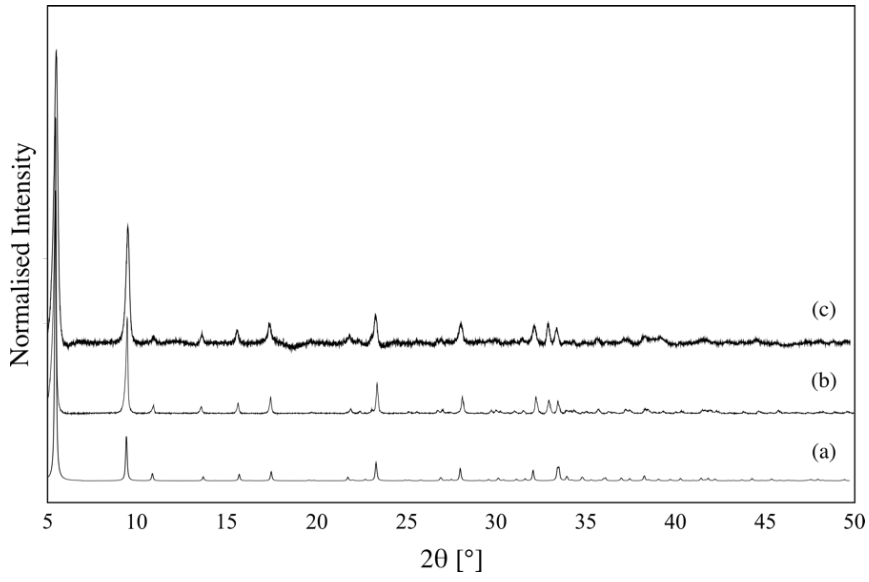

Figure 27: Powder X-ray diffraction patterns (Cu Kα, λ = 1.5418Å) of AgMOF-3: **(a)** simulated pattern from single crystal structure; **(b)** bulk material (vapour diffusion); **(c)** bulk material (room temperature).

The hexagonal channels running through the structure of AgMOF-3 are similar to (albeit more hydrophobic than) those of M-MOF-74 (M = Zn, Ni, Co, Mg), a family of stable materials in which the organic linker is 2,5-dihydroxy BDC.[87-88] Investigated uses of

MOF-74 include gas separation, proton mobility, sensing, catalysis, and drug delivery, although in the present case the permanent porosity of AgMOF-3 has not been established. The large channels running throughout the material could potentially facilitate flow-through chemistry and reactions. Were the stability and porosity of AgMOF-3 to approach that of MOF-74, then it could present some interesting opportunities. Silver and the noble metals have been shown to have affinity for pi-systems and be potentially useful in alkene/alkane separation.[26] The decoration of the hexagonal channels with the alkene of the allylthioether also presents opportunities for tailoring of the pore by Diels Alder chemistry, and substitution of different functional groups onto the alkene.[89] MOF-74 derivatives have also been prepared with longer linkers which suggests the intriguing possibility that AgMOF-3 may also be able to be prepared with an even larger pore aperture.[90]

2D [Zn(ox)$_2$BDC-(SO$_3$)$_2$] material

While no data is included in this thesis, an early stage focus of this project involved the synthesis of the archetypal MOF-5 materials, which were comprised of ZnO_4 clusters and BDC linkers, the latter decorated with a range of sulfur-containing functional groups. This aspect of the project was eventually discarded due to the poor aqueous stability of the MOF-5 analogues which arises from easily hydrolysed Zn-O bonds.[91] However, while still in consideration, a thiol-functionalised MOF-5 analogue was pursued. One attempt to form this material, involving reaction of zinc nitrate hexahydrate and 2,5-dimercapto benzene dicarboxylic acid in *N,N*-diethyl formamide and nitric acid, yielded clear colourless crystals suitable for analysis by SCXRD (parameters in **Appendix 4.8.1**). The structure of the resulting material turned out to be a 2D layered structure $(H_2NEt_2)_2[Zn(ox)_2BDC\text{-}(SO_3)_2]$ comprising five-coordinate zinc cations with distorted square pyramidal geometry coordinated by oxalate (ox) ligands and the oxidised ligand, disulfonate BDC (BDC-$(SO_3)_2$). These zinc centres form a strand down the *b* axis with oxalate ligands chelating the metal in the four basal positions; the direction of the apices of these polyhedra alternate at each zinc centre (ca. 5.33 Å) which causes the strand to zig-zag (**Figure 28**). The apices of the polyhedra were occupied by one of the oxygen atoms from the carboxylic acid group of the disulfonate BDC (DSBDC) linker which bridged between the zinc-oxalate strands and forms anionic sheets which propagate in the *bc* plane. The crystal packing was completed by well-ordered molecules of protonated diethylamine (DEA) which lie between the zinc-oxalate-DSBDC sheets and are associated with the sheets through hydrogen bonding interactions. Both the oxalate and the diethylamine were likely

degradation products of the *N*,*N*-diethylformamide; upon heating, DEF/DMF are well known to degrade to di(m)ethylamine and formic acid, however, the formation of oxalate from the formic acid was less clear. It is possible that the highly acidic reaction medium and high heat (100°C) enabled conversion of formic acid to oxalic acid which can usually only be achieved at ~400°C or with a catalyst.[92] The flame-sealed glass vials in which the crystals were grown popped and bubbled when broken open, an indication that a gas had formed during the synthesis (possibly H_2). The ordering of the DEA molecules between the layers was due to hydrogen bonding between a sulfonate oxygen on the organic linker and the secondary amine as well as an oxygen from an oxalate linker secondary amine (**Figure 29**, **left** & **Table 8**). The diethylamine counterions within the cavities of the anionic 2D sheets of the material have their orientation fixed by hydrogen bonding interactions from the sulfonate oxygens of two adjacent DSBDC linkers as well as one of the non-coordinated oxygens in the carboxylic acid group of the linker (**Figure 29**, **right** & **Table 8**).

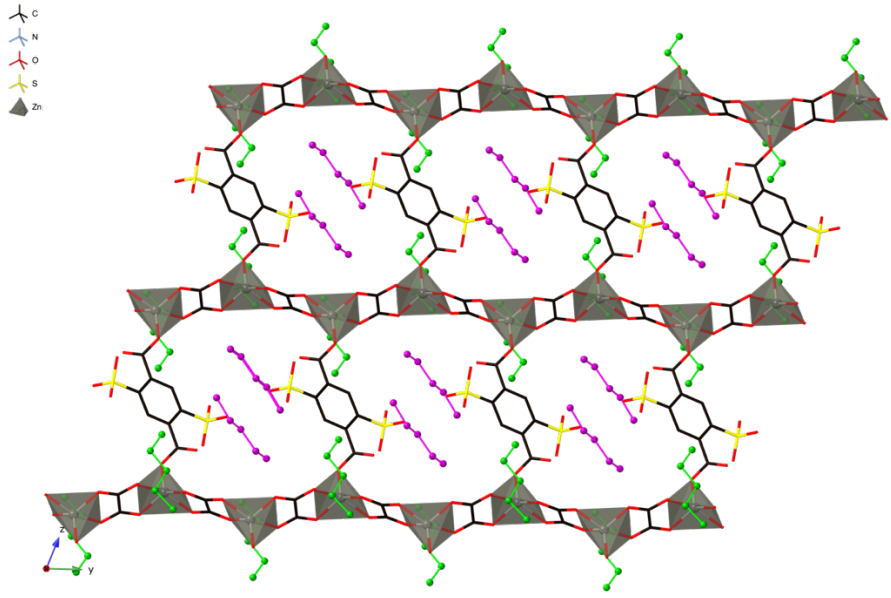

Figure 28: A view of the 2D layered structure of $(H_2NEt_2)_2[Zn(ox)_2BDC\text{-}(SO_3)_2]$ showing the 1D Zn-oxalate chains which are bridged to form the 2D structure. Localisation of diethyl ammonium cations is highlighted in purple and green (within and between the layers, respectively).

Table 8: Summary of hydrogen bonding interactions in 2D layered $(H_2NEt_2)_2[Zn(ox)_2BDC\text{-}(SO_3)_2]$ in **Figure 29**.

DEA[a]	Interaction	D···A (Å)	DH···A (Å)	DH···A angle (°)
Purple	$O_{SO3}\cdots N_{DEA}$	2.826	1.900	173.02
	$O_{ox}\cdots N_{DEA}$	2.864	1.942	169.74
Green	$O_{COOH}\cdots N_{DEA}$	2.842	2.079	138.31
	$O_{SO3}\cdots N_{DEA}$	2.844	2.229	122.88
	$O_{SO3}\cdots N_{DEA}$	2.874	1.963	168.71

[a]Diethyl amine

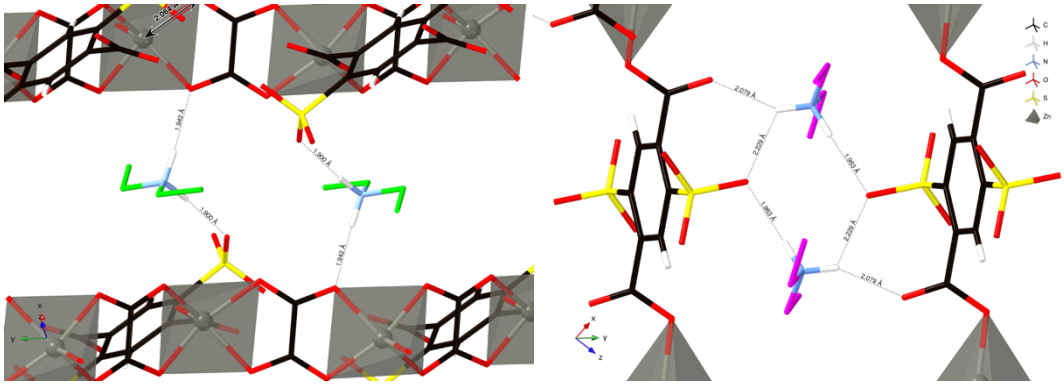

Figure 29: Hydrogen bonding interactions between diethyl ammonium molecules and sulfonates/oxalates (left), and diethyl ammonium molecules and DSBDC linkers (right). Hydrogen bonding distances shown in **Table 8**.

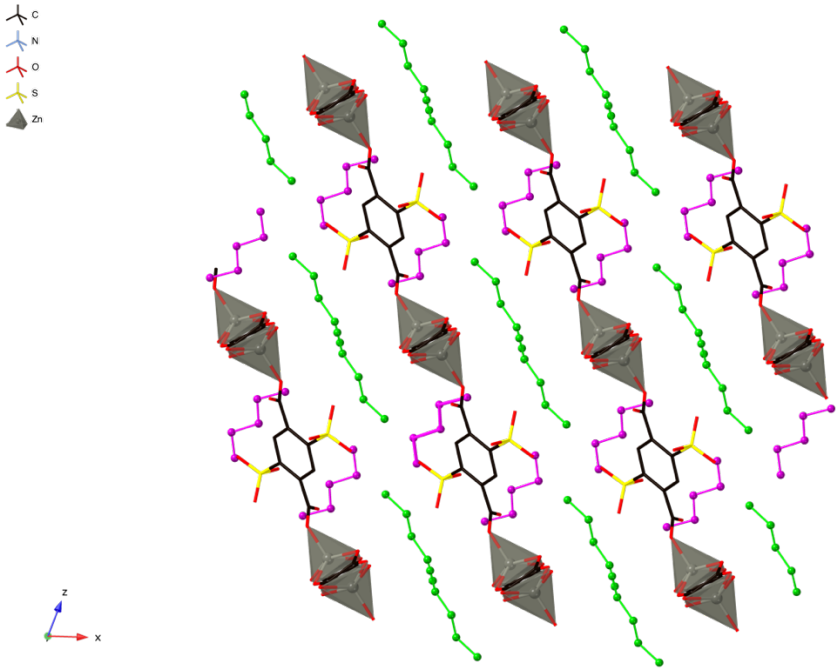

Figure 30: Diethyl ammonium solvent molecules held in place between layered sheets of material (green) due to hydrogen bonding (**Table 8**).

4.5 Conclusions

This chapter described the effect of the inclusion of a range of sulfur-containing organic linkers on the uptake and release kinetics of silver in UiO-66 and its analogues. It was found that, overall, incorporation of sulfur-containing functionality in the material resulted in a higher uptake of silver ions relative to unmodified UiO-66. A thiolate-containing MOF (DMUiO-66) had the highest uptake of silver ions from solution, however, the material had poor release properties. Inclusion of thioether units greatly decreased the uptake of silver relative to DMUiO-66, but the release of silver from these materials were greatly improved, likely due to the absence of electrostatic forces. The allyl thioether-containing material (ASUiO-66) had a higher uptake of silver relative to the alkyl thioether derivative (PSUiO-66), possibly highlighting an affinity between the pi-system and the silver ions. When silver ions were diffused into each material and reduced *in situ* to give nanoparticle or mixed oxidation state materials the relative trend in uptake of silver between the materials remained unchanged.

Ag XAS revealed that silver ions loaded into unfunctionalised UiO-66 were partially reduced to Ag(0), possibly by the framework itself. The interactions of the added metal in UiO-66 were almost exclusively with other silver atoms (resembling the spectrum of metallic silver), with some small contribution from oxygen. Conversely, XAS of the thioether-containing materials showed strong interaction between the silver ions and the thioether sulfur. Interestingly, the ASUiO-66 material appeared to stabilise the silver ions in the presence of a reductant, as silver-sulfur interactions were the dominant interaction observed in the EXAFS FT for all silver treatments of ASUiO-66; a feature not observed for the propyl thioether derivative.

Composites of all silver-loaded materials were successfully prepared by embedding them into a polycaprolactone matrix. Incorporation into the polymer further slowed silver release from the materials and release kinetics were determined for all composites. Ag(I)AS/PS/UiO-66-PCL composites all released ~15% of total loaded silver into ultra-pure water after 24 hours. Release of silver into a more biologically relevant medium, such as bacterial broth, resulted in a 5 to 10-fold decrease in the amount of total bound silver released from the materials tested suggesting that ionic strength of the solution could play a role in material release kinetics.

All silver-loaded UiO-66 derivatives embedded in a PCL matrix were shown to have antibacterial activity against both *S. aureus* and *E. coli*. Overall, the materials were more effective against the Gram-positive *S. aureus* with Ag(I/0)ASUiO-66 having the greatest antibacterial effect, based on disk diffusion assays. The positive control of silver

nitrate embedded in PCL (25 wt. %) had greater antibacterial efficacy than all tested materials, however, weighting the results of the disk diffusion assay based on the mass of silver in each sample revealed that with less silver content, the MOF-containing species (i.e. not the positive control) produced a greater antibacterial response. Whether the increased response was due to the controlled release of the silver from the materials or possibly leaching of other material components having an additive effect is unclear but could be clarified by testing the antibacterial activity of all components of the material individually.

4.6 Future directions

Loading a bioactive payload into a framework is only one way of delivering medicinally relevant species to a wound site. Copper and zinc have been shown to have antibacterial properties and are also common metal nodes in MOF chemistry.[93] Examples of such frameworks are MOF-5, composed of Zn_4O clusters joined by BDC linkers or the copper-based HKUST-1 which used benzene tricarboxylic acid.[40, 94] Both materials are known to degrade in aqueous media through hydrolysis of the Zn/Cu-$O_{carboxylate}$ bonds, liberating zinc and copper ions.[91, 95] Were such a framework loaded with silver to be released by material degradation then two bioactive metals would be released into solution possibly having an additive or synergistic effect. Design of an antibacterial linker could provide a third prong of attack in the degradation of the material; sulfonamides, camphor, and beta lactams are all known to be potent antibacterial functional groups.[96-97] Finally, embedding of a material comprising an antibacterial metal, linker, and payload into an antibacterial polymer, such as chitosan,[98] could provide yet another layer of efficacy as well as extending the applicability of the material for medical use. Such experiments were attempted here with MOF-5 and the thioether-containing linkers, however, the degradation of the material complicated characterisation, handling, and processing.

Permanently porous silver-based MOFs or coordination polymers are a class of materials for which there are only limited reports.[99] As such, the discovery of AgMOF-3 which has large, hexagonal channels running throughout it could provide an interesting material to further investigate, especially as both single crystal and room temperature syntheses have been identified. To test the stability and porosity of the new framework thermogravimetric analysis, and gas adsorption isotherms would need to be carried out.

The channels decorated with well-ordered allyl thioether units provides an opportunity for saturation of the double bond with other functionality, and Diels Alder

chemistry. Additionally, rearrangement reactions of allyl ethers have been reported previously which could liberate the thiolate functionality as well as retain the pi-system.[100]

4.7 References

1. Haque, M.; Sartelli, M.; McKimm, J.; Abu Bakar, M, Health care-associated infections - an overview. *Infect Drug Resist* **2018,** *11*, 2321-2333.
2. Reed, D.; Kemmerly, S. A., Infection control and presentation: A review of hospital-acquired infections and the economic implications. *Ochsner J* **2009,** *9* (1), 27-31.
3. Revelas, A., Healthcare-associated infections: A public health problem *Nigeria Med J* **2012,** *53* (2), 59-64.
4. Ventola, C. L., The antibiotic resistance crisis. *P&T* **2015,** *40* (4), 277-283.
5. Alanis, A. J., Resistance to antibiotics: are we in the post-antibiotic era? *Arch Med Res* **2005,** *36* (6), 697-705.
6. Aminov, R. I., A brief history of the antibiotic era: lessons learned and challenges for the future. *Front Microbiol* **2010,** *1* (134), 1-7.
7. Munita, J. M.; Arias, C. A., Mechanisms of antibiotic resistance. *Microbiol Spectr* **2016,** *4* (2), 1-37.
8. Alexander, J. W., History of the medical use of silver. *Surg Infect (Larchmt)* **2009,** *10* (3), 289-292.
9. Medici, S.; Peana, M.; Crisponi, G.; Nurchi, V. M.; Lachowicz, J. I.; Remelli, M.; Zoroddu, M. A., Silver coordination compounds: A new horizon in medicine. *Coordination Chemistry Reviews* **2016,** *327-328*, 349-359.
10. Sim, W.; Barnard, R. T.; Blaskovich, M. A. T.; Ziora, Z. M., Antimicrobial silver in medicinal and consumer applications: A patent review of the past decade (2007-2017). *Antibiotics (Basel)* **2018,** *7* (93), 1-15.
11. Eckhardt, S.; Brunetto, P. S.; Gagnon, J.; Priebe, M.; Giese, B.; Fromm, K. M., Nanobio silver: its interactions with peptides and bacteria, and its uses in medicine. *Chem Rev* **2013,** *113* (7), 4708-4754.
12. Silver in drinking water. In *Guidelines for drinking-water quality*, 2 ed.; World Health Organisation: Geneva, 1996; Vol. 2.
13. Choi, O.; Deng, K. K.; Kim, N. J.; Ross, L., Jr.; Surampalli, R. Y.; Hu, Z., The inhibitory effects of silver nanoparticles, silver ions, and silver chloride colloids on microbial growth. *Water Res* **2008,** *42* (12), 3066-3074.
14. Chernousova, S.; Epple, M., Silver as antibacterial agent: ion, nanoparticle, and metal. *Angew Chem* **2013,** *52* (6), 1636-1653.
15. Xue, Y.; Davis, A. V.; Balakrishnan, G.; Stasser, J. P.; Staehlin, B. M.; Focia, P.; Spiro, T. G.; Penner-Hahn, J. E.; O'Halloran, T. V., Cu(I) recognition *via* cation-pi and methionine interactions in CusF. *Nat Chem Biol* **2008,** *4* (2), 107-109.
16. He, J.; Zha, M.; Cui, J.; Zeller, M.; Hunter, A. D.; Yiu, S. M.; Lee, S. T.; Xu, Z., Convenient detection of Pd(II) by a metal-organic framework with sulfur and olefin functions. *J Am Chem Soc* **2013,** *135* (21), 7807-7810.
17. Zha, M.; Liu, J.; Wong, Y. L.; Xu, Z., Extraction of palladium from nuclear waste-like acidic solutions by a metal–organic framework with sulfur and alkene functions. *J Mater Chem A* **2015,** *3* (7), 3928-3934.
18. Nomiya, K.; Azaumaya, I.; Kasuga, N. C.; Kato, T., Molecular design and synthesis of water-soluble silver(I) complexes exhibiting a wide spectrum of effective antimicrobial activities. *Curr Top Biochem Res* **2008,** *10* (1), 1-10.
19. Chen, X.; Schluesener, H. J., Nanosilver: a nanoproduct in medical application. *Toxicol Lett* **2008,** *176* (1), 1-12.
20. Panacek, C.; Kvitek, L.; Prucek, R.; Kolar, M.; Vecerova, R.; Pizurova, N.; Sharma, V. K.; Nevecna, T.; Zboril, R., Silver colloid nanoparticles: Synthesis, characterization and their antibacterial activity. *J. Phys. Chem.* **2006,** *110*, 16248-16253.

21. Getzlaf, M. A.; Lewallen, E. A.; Kremers, H. M.; Jones, D. L.; Bonin, C. A.; Dudakovic, A.; Thaler, R.; Cohen, R. C.; Lewallen, D. G.; van Wijnen, A. J., Multi-disciplinary antimicrobial strategies for improving orthopaedic implants to prevent prosthetic joint infections in hip and knee. *J Orthop Res* **2016,** *34* (2), 177-186.
22. Schmidt-Braekling, T.; Streitbuerger, A.; Gosheger, G.; Boettner, F.; Nottrott, M.; Ahrens, H.; Dieckmann, R.; Guder, W.; Andreou, D.; Hauschild, G.; Moellenbeck, B.; Waldstein, W.; Hardes, J., Silver-coated megaprostheses: review of the literature. *Eur J Orthop Surg Traumatol* **2017,** *27* (4), 483-489.
23. Wyszogrodzka, G.; Marszalek, B.; Gil, B.; Dorozynski, P., Metal-organic frameworks: mechanisms of antibacterial action and potential applications. *Drug Discov Today* **2016,** *21* (6), 1009-1018.
24. Stock, N.; Biswas, S., Synthesis of metal-organic frameworks (MOFs): routes to various MOF topologies, morphologies, and composites. *Chem Rev* **2012,** *112* (2), 933-969.
25. Lee, Y.-R.; Kim, J.; Ahn, W. S., Synthesis of metal-organic frameworks: A mini review. *Korean Journal of Chemical Engineering* **2013,** *30* (9), 1667-1680.
26. Wang, Y.; Hu, Z.; Cheng, Y.; Zhao, D., Silver-decorated hafnium metal–organic framework for ethylene/ethane separation. *Ind Eng Chem Res* **2017,** *56* (15), 4508-4516.
27. Li, H.; Wang, K.; Sun, Y.; Lollar, C. T.; Li, J.; Zhou, H.-C., Recent advances in gas storage and separation using metal–organic frameworks. *Mater Today* **2018,** *21* (2), 108-121.
28. Baumann, A. E.; Burns, D. A.; Liu, B.; Thoi, V. S., Metal-organic framework functionalization and design strategies for advanced electrochemical energy storage devices. *Comm Chem* **2019,** *2* (1), 1-14.
29. Kumar, P.; Deep, A.; Kim, K.-H., Metal organic frameworks for sensing applications. *Trend Anal Chem* **2015,** *73*, 39-53.
30. Dhakshinamoorthy, A.; Li, Z.; Garcia, H., Catalysis and photocatalysis by metal organic frameworks. *Chem Soc Rev* **2018,** *47* (22), 8134-8172.
31. Cao, J.; Li, X.; Tian, H., Metal-organic framework (MOF)-based drug delivery. *Curr Med Chem* **2019**.
32. Taylor-Edinbyrd, K.; Li, T.; Kumar, R., Effect of chemical structure of S-nitrosothiols on nitric oxide release mediated by the copper sites of a metal organic framework based environment. *Phys Chem Chem Phys* **2017,** *19* (19), 11947-11959.
33. Li, H.; Hill, M. R., Low-energy CO2 release from metal-organic frameworks triggered by external stimuli. *Acc Chem Res* **2017,** *50* (4), 778-786.
34. Ma, Y.; Li, X.; Li, A.; Yang, P.; Zhang, C.; Tang, B., H_2S-activable MOF nanoparticle photosensitizer for effective photodynamic therapy against cancer with controllable singlet-oxygen release. *Angew Chem* **2017,** *56* (44), 13752-13756.
35. Dong, Z.; Sun, Y.; Chu, J.; Zhang, X.; Deng, H., Multivariate metal-organic frameworks for dialing-in the binding and programming the release of drug molecules. *J Am Chem Soc* **2017,** *139* (40), 14209-14216.
36. Sarker, M.; Jhung, S. H., Zr-MOF with free carboxylic acid for storage and controlled release of caffeine. *J Mol Liquids* **2019,** *296*, 1-6.
37. Lin, S.; Liu, X.; Tan, L.; Cui, Z.; Yang, X.; Yeung, K. W. K.; Pan, H.; Wu, S., Porous iron-carboxylate metal-organic framework: A novel bioplatform with sustained antibacterial efficacy and nontoxicity. *ACS Appl Mater Interfaces* **2017,** *9* (22), 19248-19257.
38. Han, C.; Yang, J.; Gu, J., Immobilization of silver nanoparticles in Zr-based MOFs: induction of apoptosis in cancer cells. *J Nano Res* **2018,** *20* (3), 1-11.

39. Young, R. J.; Begg, S. L.; Coghlan, C. J.; McDevitt, C. A.; Sumby, C. J., Exploring the use of structure and polymer incorporation to tune silver ion release and antibacterial activity of silver coordination polymers. *Eur J Inorg Chem* **2018,** *2018* (30), 3439-3518.
40. Lis, M. J.; Caruzi, B. B.; Gil, G. A.; Samulewski, R. B.; Bail, A.; Scacchetti, F. A. P.; Moises, M. P.; Maesta Bezerra, F., *In-situ* direct synthesis of HKUST-1 in wool fabric for the improvement of antibacterial properties. *Polymers (Basel)* **2019,** *11* (4), 1-11.
41. Tamames-Tabar, C.; Imbuluzqueta, E.; Guillou, N.; Serre, C.; Miller, S. R.; Elkaïm, E.; Horcajada, P.; Blanco-Prieto, M. J., A Zn azelate MOF: Combining antibacterial effect. *CrystEngComm* **2015,** *17* (2), 456-462.
42. Wang, H.; Wang, Q.; Teat, S. J.; Olson, D. H.; Li, J., Synthesis, structure, and selective gas adsorption of a single-crystalline zirconium based microporous metal–organic framework. *Cryst Growth Des* **2017,** *17* (4), 2034-2040.
43. Katz, M. J.; Brown, Z. J.; Colon, Y. J.; Siu, P. W.; Scheidt, K. A.; Snurr, R. Q.; Hupp, J. T.; Farha, O. K., A facile synthesis of UiO-66, UiO-67 and their derivatives. *Chem Comm* **2013,** *49* (82), 9449-9451.
44. Bueken, B.; Van Velthoven, N.; Krajnc, A.; Smolders, S.; Taulelle, F.; Mellot-Draznieks, C.; Mali, G.; Bennett, T. D.; De Vos, D., Tackling the defect conundrum in UiO-66: A mixed-linker approach to engineering missing linker defects. *Chem Mater* **2017,** *29* (24), 10478-10486.
45. Horcajada, P.; Gref, R.; Baati, T.; Allan, P. K.; Maurin, G.; Couvreur, P.; Ferey, G.; Morris, R. E.; Serre, C., Metal-organic frameworks in biomedicine. *Chem Rev* **2012,** *112* (2), 1232-1268.
46. Ali-Moussa, H.; Navarro Amador, R.; Martinez, J.; Lamaty, F.; Carboni, M.; Bantreil, X., Synthesis and post-synthetic modification of UiO-67 type metal-organic frameworks by mechanochemistry. *Mater Lett* **2017,** *197*, 171-174.
47. Santillán, M. J.; Quaranta, N. E.; Boccaccini, A. R., Titania and titania–silver nanocomposite coatings grown by electrophoretic deposition from aqueous suspensions. *Surface and Coatings Technology* **2010,** *205* (7), 2562-2571.
48. Kumar, R.; Munstedt, H., Silver ion release from antimicrobial polyamide/silver composites. *Biomaterials* **2005,** *26* (14), 2081-8.
49. de Santa Maria, L. C.; Souza, J. D. C.; Agular, M. R. M. P.; Wang, S. H.; Mazzei, J. L.; Felzenszwalb, I.; Amico, S. C., Synthesis, characterization, and bactericidal properties of composites based on crosslinked resins containing silver. *Journal of Applied Polymer Science* 2008, *107* (3), 1879-1886.
50. Travan, A.; Pelillo, C.; Donati, I.; Marsich, E.; Benincasa, M.; Scarpa, T.; Semeraro, I.; Turco, G.; Gennaro, R.; Paoletti, S., Non-cytotoxic silver nanoparticle-polysaccharide nanocomposites with antimicrobial activity. *Biomacromolecules* **2009,** *10*, 1429-1435.
51. Song, J.; Kang, H.; Lee, C.; Hwang, S. H.; Jang, J., Aqueous synthesis of silver nanoparticle embedded cationic polymer nanofibers and their antibacterial activity. *ACS Appl Mater Interfaces* **2012,** *4* (1), 460-465.
52. Hyldgaard, M.; Mygind, T.; Vad, B. S.; Stenvang, M.; Otzen, D. E.; Meyer, R. L., The antimicrobial mechanism of action of epsilon-poly-l-lysine. *Appl Environ Microbiol* **2014,** *80* (24), 7758-7770.
53. Masters, J. R., HeLa cells 50 years on: the good, the bad and the ugly. *Nat Rev Cancer* **2002,** *2* (4), 315-319.
54. Woodruff, M. A.; Hutmacher, D. W., The return of a forgotten polymer - Polycaprolactone in the 21st century. *Prog Polym Sci* **2010,** *35* (10), 1217-1256.

55. Woodruff, M. A.; Hutmacher, D. W., The return of a forgotten polymer—Polycaprolactone in the 21st century. *Progress in Polymer Science* 2010, *35* (10), 1217-1256.
56. Ankudinov, A. L.; Ravel, B.; Rehr, J. J.; Conradson, S. D., Real-space multiple-scattering calculation and interpretation of X-ray absorption near-edge structure. *Phys Rev B* **1998,** *58* (12), 7565-7576.
57. McPhillips, T. M.; McPhillips, S. E.; Chiu, H.-J.; Cohen, A. E.; Deacon, A. M.; Ellis, P. J.; Garman, E.; Gonzalez, A.; Sauter, N. K.; Phizackerly, R. P.; Soltis, S. M.; Kuhn, P., Blu-Ice the distributed control system: Software for data acquisition and instrument control at macromolecular crystallography beamlines. *J Synchrotron Rad* **2002,** *9*, 401-406.
58. Sheldrick, G. M., Phase annealing in SHELX-90: Direct methods for larger structures. *Acta Cryst* **1990,** *A46*, 467-473.
59. Sheldrick, G. M., SHELXL-2014. University of Göttingen: Göttingen, Germany, 2014.
60. Barbour, L. J., X-Seed - A software for supramolecular crystallography. *J Supramol Chem* **2003,** *1* (4-6), 189-191.
61. Dolomanov, O. V.; Bourhis, L. J.; Gildea, R. J.; Howard, J. A. K.; Puschmann, H., OLEX2: a complete structure solution, refinement and analysis program. *J Appl Cryst* **2009,** *42* (2), 339-341.
62. Skowron, P. T.; Dumartin, M.; Jeamet, E.; Perret, F.; Gourlaouen, C.; Baudouin, A.; Fenet, B.; Naubron, J. V.; Fotiadu, F.; Vial, L.; Leclaire, J., On-demand cyclophanes: substituent-directed self-assembling, folding, and binding. *J Org Chem* **2016,** *81* (2), 654-661.
63. Plessers, E.; De Vos, D. E.; Roeffaers, M. B. J., Chemoselective reduction of α,β-unsaturated carbonyl compounds with UiO-66 materials. *J Catal* **2016,** *340*, 136-143.
64. Young, R. J.; Begg, S. L.; Coghlan, C. J.; McDevitt, C. A.; Sumby, C. J., Exploring the use of structure and polumer incorporation to tune silver ion release and antibacterial activity of silver coordination polymers. *Eur J Inorg Chem* **2018,** (30).
65. Yee, K. K.; Reimer, N.; Liu, J.; Cheng, S.Y.; Yiu, S. M.; Weber, J.; Stock, N.; Xu, Z., Effective mercury sorption by thiol-laced metal–organic frameworks: in strong acid and the vapor phase. *J Am Chem Soc* **2013,** *135* (21), 7795-7798.
66. Phang, W. J.; Jo, H.; Lee, W. R.; Song, J. H.; Yoo, K.; Kim, B.; Hong, C. S., Superprotonic conductivity of a UiO-66 framework functionalized with sulfonic acid groups by facile postsynthetic oxidation. *Angew Chem* **2015,** *54* (17), 5142-5146.
67. Trickett, C. A.; Gagnon, K. J.; Lee, S.; Gandara, F.; Burgi, H. B.; Yaghi, O. M., Definitive molecular level characterization of defects in UiO-66 crystals. *Angew Chem* **2015,** *54* (38), 11162-11167.
68. Han, Y.; Liu, M.; Li, K.; Zuo, Y.; Wei, Y.; Xu, S.; Zhang, G.; Song, C.; Zhang, Z.; Guo, X., Facile synthesis of morphology and size-controlled zirconium metal–organic framework UiO-66: the role of hydrofluoric acid in crystallization. *CrystEngComm* **2015,** *17* (33), 6434-6440.
69. Plessers, E.; De Vos, D. E.; Roeffaers, M. B. J., Chemoselective reduction of α,β-unsaturated carbonyl compounds with UiO-66 materials. *J Cat* **2016,** *340*, 136-143.
70. Dhoondia, Z. H.; Charkraborty, H., *Lactobacillus* mediated synthesis of silver oxide nanoparticles. *Nanomater nanotechnol* **2012,** *2*, 1-7.
71. Hsueh, Y. H.; Lin, K. S.; Ke, W. J.; Hsieh, C. T.; Chiang, C. L.; Tzou, D. Y.; Liu, S. T., The antimicrobial properties of silver nanoparticles in *Bacillus subtilis* are mediated by released Ag+ ions. *PLoS One* **2015,** *10* (12), 1-17.

72. Endo, T.; Shibata, A.; Yanagida, Y.; Higo, Y.; Hatsuzawa, T., Localized surface plasmon resonance optical characteristics for hydrogen peroxide using polyvinylpyrrolidone coated silver nanoparticles. *Mater Lett* **2010,** *64* (19), 2105-2108.
73. Kozlov, V., Solubility and dissociation of sulfonic acids in water-acid systems. *Z Fizich Khim* **1983,** *57* (6), 1404-1408.
74. Pearson, R. G., Hard and soft acids and bases. *J Am Chem Soc* **1963,** *85* (22), 3533-3539.
75. Reimers, J. R.; Ford, M. J.; Halder, A.; Ulstrup, J.; Hush, N. S., Gold surfaces and nanoparticles are protected by Au(0)-thiyl species and are destroyed when Au(I)-thiolates form. *PNAS* **2016,** *113* (11), E1424-E1433.
76. Tang, Z. G.; Black, R. A.; Curran, J. M.; Hunt, J. A.; Rhodes, N. P.; Williams, D. F., Surface properties and biocompatibility of solvent-cast poly[epsilon-caprolactone] films. *Biomaterials* **2004,** *25* (19), 4741-4748.
77. Chen, S.; Lucier, B. E. G.; Luo, W.; Xie, X.; Feng, K.; Chan, H.; Terskikh, V. V.; Sun, X.; Sham, T.-K.; Workentin, M. S.; Huang, Y., Loading across the Periodic Table: Introducing 14 different metal ions to enhance Metal–Organic Framework performance. *ACS Appl Mater Interfaces* **2018,** *10* (36), 30296-30305.
78. Doolette, C. L.; McLaughlin, M. J.; Kirby, J. K.; Batstone, D. J.; Harris, H. H.; Ge, H.; Cornelis, G., Transformation of PVP coated silver nanoparticles in a simulated wastewater treatment process and the effect on microbial communities. *Chem Cent J* **2013,** *7* (46), 1-18.
79. Anderson, D. P.; Adnan, R. H.; Alvino, J. F.; Shipper, O.; Donoeva, B.; Ruzicka, J.-Y.; Qahtani, H. A.; Harris, H. H.; Cowie, B.; Aitken, J. B.; Golovko, V. B.; Metha, G. F.; Andersson, G. G., Chemically synthesised atomically precise gold cluster deposited and activated on titania. Part II. *Phys Chem Chem Phys* **2013,** *15*, 14806-14813.
80. Anubhav, J.; Ong, S. P.; Hautier, G.; Chen, W.; Richards, W. D.; Dacek, S.; Cholia, S.; Gunter, D.; Skinner, D.; Ceder, G.; Persson, K. A., The Materials Project: A materials genome approach to accelerating materials innovation. *J Chem Phys* **2018,** *148* (24), 1-11.
81. Aylward, G.; Findlay, T., *SI Chemical Data*. 6 ed.; Wiley: 2008.
82. Ivanova, E. P.; Hasan, J.; Webb, H. K.; Truong, V. K.; Watson, G. S.; Watson, J. A.; Baulin, V. A.; Pogodin, S.; Wang, J. Y.; Tobin, M. J.; Löbbe, C.; Crawford, R. J., Natural bactericidal surfaces: Mechanical reupture of *Pseudomonas aeruginosa* cell by Cicada wings. *Small* **2012,** *8* (16), 2489-2494.
83. Cai, W.; Wang, J.; Chu, C.; Chen, W.; Wu, C.; Liu, G., Metal-Organic Framework-based stimuli-responsive systems for drug delivery. *Adv Sci (Weinh)* **2019,** *6* (1), 1-20.
84. Randall, C. P.; Gupta, A.; Jackson, N.; Busse, D.; O'Neill, A. J., Silver resistance in Gram-negative bacteria: A dissection of endogenous and exogenous mechanisms. *J Antimicrob Chemother* **2015,** *70* (4), 1037-1046.
85. Gudipaty, S. A.; Larsen, A. S.; Rensing, C.; McEvoy, M. M., Regulation of Cu(I)/Ag(I) efflux genes in *Escherichia coli* by the sensor kinase CusS. *FEMS Microbiol Lett* **2012,** *330* (1), 30-37.
86. Gung, B. W.; Emenike, B. U.; Alverez, C. N.; Rakovan, J.; Kirschbaum, K.; Jain, N., Relative substituent position on the strength of pi-pi stacking interactions. *Tetrahedron Lett* **2010,** *51* (13), 1648-1650.
87. Xiao, T.; Liu, D., The most advanced synthesis and a wide range of applications of MOF-74 and its derivatives. *Micro Meso Mater* **2019,** *283*, 88-103.

88. Hwang, S.; Lee, E. J.; Song, D.; Jeong, N. C., High proton mobility with high directionality in isolated channels of MOF-74. *ACS ApplMater Inter* **2018,** *10* (41), 35354-35360.
89. Tanaka, K.; Nagase, S.; Anami, T.; Wierzbicki, M.; Urbanczyk-Lipkowska, Z., Enantioselective Diels–Alder reaction in the confined space of homochiral metal–organic frameworks. *RSC Adv* **2016,** *6* (112), 111436-111439.
90. Jawahery, S.; Simon, C. M.; Braun, E.; Witman, M.; Tiana, D.; Vlaisavljevich, B.; Smit, B., Adsorbate-induced lattice deformation in IRMOF-74 series. *Nat Commun* **2017,** *8*, 1-9.
91. Ming, Y.; Kumar, N.; Siegel, D. J., Water adsorption and insertion in MOF-5. *ACS Omega* **2017,** *2* (8), 4921-4928.
92. Yepez, A.; Hidalgo, J. M.; Pineda, A.; Černý, R.; Jíša, P.; Garcia, A.; Romero, A. A.; Luque, R., Mechanistic insights into the hydroconversion of cinnamaldehyde using mechanochemically-synthesized Pd/Al-SBA-15 catalysts. *Green Chem* **2015,** *17* (1), 565-572.
93. Chandrangsu, P.; Rensing, C.; Helmann, J. D., Metal homeostasis and resistance in bacteria. *Nat Rev Microbiol* **2017,** *15* (6), 338-350.
94. Bhardwaj, N.; Pandey, S. K.; Mehta, J.; Bhardwaj, S. K.; Kim, K. H.; Deep, A., Bioactive nano-metal-organic frameworks as antimicrobials against Gram-positive and Gram-negative bacteria. *Toxicol Res (Camb)* **2018,** *7* (5), 931-941.
95. Todaro, M.; Buscarino, G.; Sciortino, L.; Alessi, A.; Messina, F.; Taddei, M.; Ranocchiari, M.; Cannas, M.; Gelardi, F. M., Decomposition process of carboxylate MOF HKUST-1 unveiled at the atomic scale level. *J Phys Chem C* **2016,** *120* (23), 12879-12889.
96. Tang, S. S.; Apisarnthanarak, A.; Hsu, L. Y., Mechanisms of beta-lactam antimicrobial resistance and epidemiology of major community- and healthcare-associated multidrug-resistant bacteria. *Adv Drug Deliv Rev* **2014,** *78*, 3-13.
97. Patel, N. B.; Patel, J. N.; Lilakar, J. D., Sulfonamides of 2-[(2,6-dichlorophenyl)amino]phenyl acetoxyacetic acid and their antibacterial studies. *Polish Pharma Soc* **2010,** *67* (4), 351-359.
98. Rinaudo, M., Chitin and chitosan: Properties and applications. *Progress in Polymer Science* **2006,** *31* (7), 603-632.
99. Zhang, J.-P.; Kitagawa, S., Supramolecular isomerism, framework flexibility, unsaturated metal center, and porous property of Ag(I)/Cu(I) 3,3',5,5'-tetramethyl-4,4'-bipyrazolate. *J Am Chem Soc* **2008,** *130*, 907-917.
100. Burrows, A. D.; Hunter, S. O.; Mahon, M. F.; Richardson, C., A reagentless thermal post-synthetic rearrangement of an allyloxy-tagged metal-organic framework. *Chem Commun (Camb)* **2013,** *49* (10), 990-992.

4.8 Appendices

Appendix 4.8.1 Single crystal X-ray experimental data

Table 9: X-ray experimental data for Ag_2ASBDC

Compound	AgMOF-3
Identification code	AgMOF-3
Empirical formula	$C_7H_6AgO_2S$
Formula weight	309.31
Crystal system	*trigonal*
Space group	R-3c
a/Å	32.531(10)
b/Å	32.531(10)
c/Å	8.1040(16)
α/°	90
β/°	90
γ/°	120
Volume/$Å^3$	7427(5)
Z	36
$\rho_{calc}g/cm^3$	2.424
μ/mm^{-1}	3.146
F(000)	5256.0
Radiation	Synchrotron (λ = 0.71073)
2Θ range for data collection/°	5.008 to 64.636
Reflections collected	42024
Independent reflections	2712 [R_{int} = 0.7445, R_{sigma} = 0.5168]
Data/restraints/parameters	2712/0/101
Goodness-of-fit on F^2	0.945
Final R indexes [I>=2σ (I)]	R_1 = 0.1466, wR_2 = 0.3264
Final R indexes [all data]	R_1 = 0.2821, wR_2 = 0.4180
Largest diff. peak/hole / e $Å^{-3}$	2.20/-10.08

Table 10: X-ray experimental data for [Zn(ox)$_2$BDC-(SO$_3$)$_2$]

Compound	2D [Zn(ox)2BDC-(SO3)2] material
Identificantion code	[Zn(ox)2BDC-(SO3)2]
Empirical formula	$C_{14}H_{25}N_2O_9SZn$
Formula weight	462.79
Temperature/K	100.15
Crystal system	*triclinic*
Space group	P-1
a/Å	9.0420(18)
b/Å	10.017(2)
c/Å	13.172(3)
α/°	69.38(3)
β/°	70.39(3)
γ/°	85.36(3)
Volume/Å^3	1050.9(5)
Z	2
ρ_{calc}g/cm^3	1.463
μ/mm^{-1}	1.313
F(000)	482.0
Crystal size/mm^3	0.2 × 0.2 × 0.2
Radiation	Synchrotron (λ = 0.71073)
2Θ range for data collection/°	4.348 to 66.188
Index ranges	-13 ≤ h ≤ 13, -12 ≤ k ≤ 14, -19 ≤ l ≤ 19
Reflections collected	17721
Independent reflections	5871 [R_{int} = 0.1106, R_{sigma} = 0.1178]
Data/restraints/parameters	5871/4/248
Goodness-of-fit on F^2	1.176
Final R indexes [I>=2σ (I)]	R_1 = 0.0783, wR_2 = 0.2304
Final R indexes [all data]	R_1 = 0.0888, wR_2 = 0.2479
Largest diff. peak/hole / e Å^{-3}	1.26/-1.54

Appendix 4.8.2 Defect calculations of PS- and ASUiO-66 materials

MOF formulas $Zr_6O_4(OH)_4L_{(6-0.5X)}A_X$, where L is the linker, and A the acid modulator, were obtained from ^{1}H NMR spectra using the following equation:

$$X = 6R/(1+0.5R)$$

where R is the ratio of A to L determined from the integration of the formic acid and aromatic linker signals in the ^{1}H NMR spectrum of digested MOF (obtained from the figures below).

Table 11: Calculated number of defects per node of PS and ASUiO-66 derivatives for all silver treatments

Material	Formic acid integration [A]	Aromatic linker integration [L]	Ratio [A/L]	6-0.5X	X
PSUiO-66	0.31	2	0.24	5.37	1.27
Ag(I)PSUiO-66	0.34	2	0.25	5.32	1.35
Ag(I/0)PSUiO-66	0.22	2	0.18	5.50	0.99
Ag(0)PSUiO-66	0.15	2	0.13	5.63	0.73
ASUiO-66	0.58	2	0.37	5.07	1.86
Ag(I)ASUiO-66	0.35	2	0.26	5.31	1.38
Ag(I/0)ASUiO-66	0.28	2	0.22	5.41	1.18
Ag(0)ASUiO-66	0.14	2	0.12	5.65	0.69

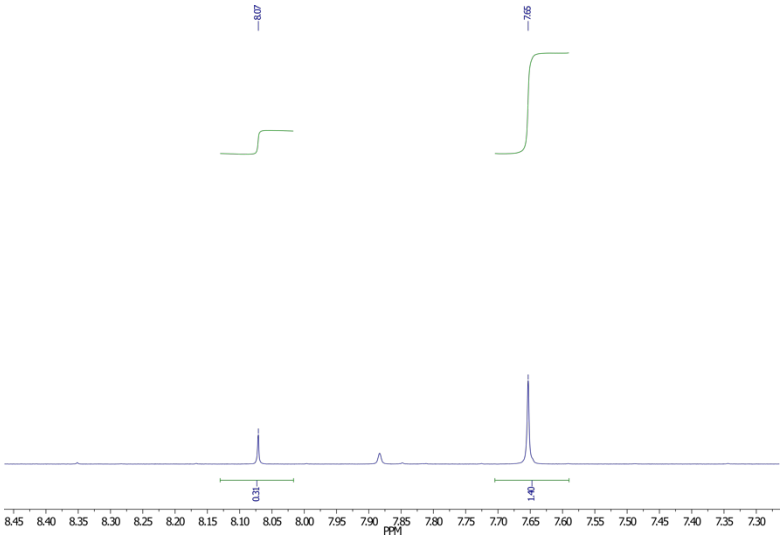

Figure 7: ^{1}H NMR spectrum of digested untreated PSUiO-66 synthesised using 30 equivalents of formic acid. Integration of PSBDC linker aromatic signal (7.65 ppm, 1.40 integration) and acid modulator (8.07 ppm, 0.31 integration) shown.

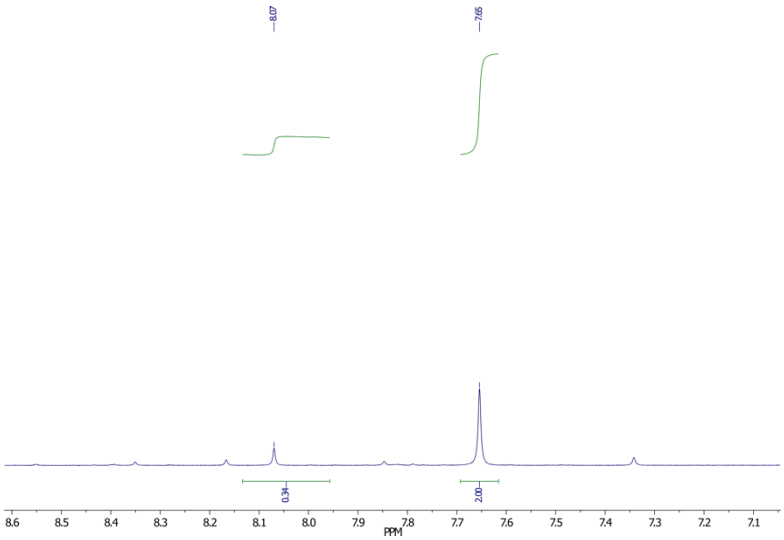

Figure 32: [1]H NMR spectrum of digested Ag(I)PSUiO-66 synthesised using 30 equivalents of formic acid. Integration of PSBDC linker aromatic signal (7.65 ppm, 2.00 integration) and acid modulator (8.07 ppm, 0.34 integration) shown.

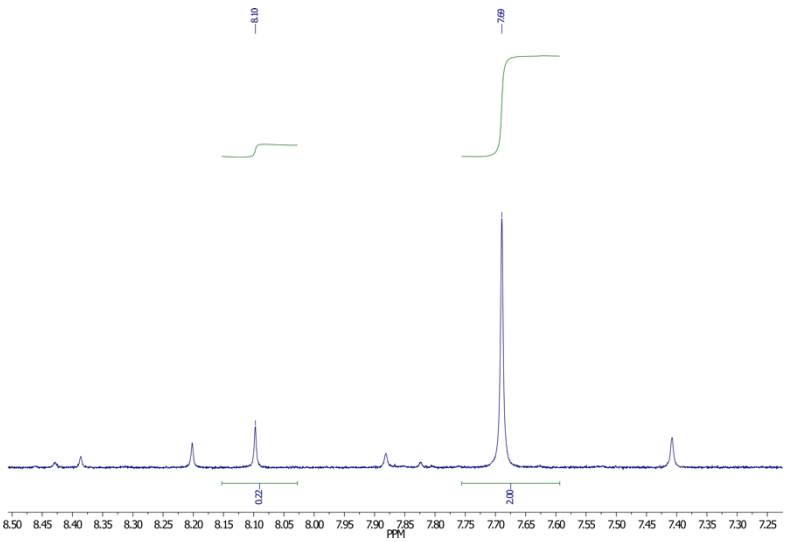

Figure 33: [1]H NMR spectrum of digested Ag(I/0)PSUiO-66 synthesised using 30 equivalents of formic acid. Integration of PSBDC linker aromatic signal (7.69 ppm, 2.00 integration) and acid modulator (8.10 ppm, 0.22 integration) shown.

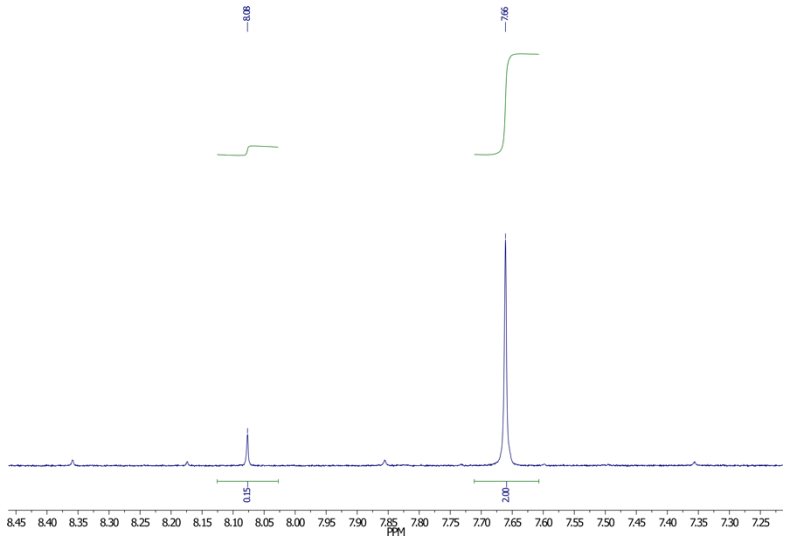

Figure 34: [1]H NMR spectrum of digested Ag(0)PSUiO-66 synthesised using 30 equivalents of formic acid. Integration of PSBDC linker aromatic signal (7.66 ppm, 2.00 integration) and acid modulator (8.08 ppm, 0.15 integration) shown.

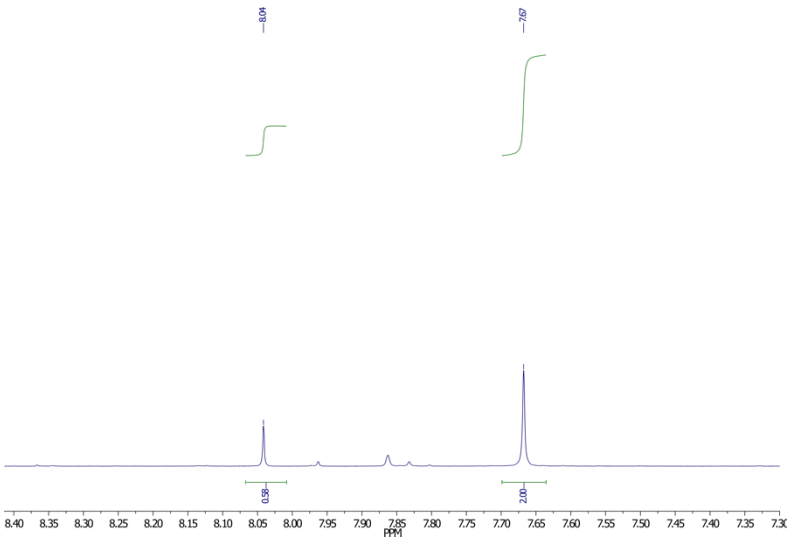

Figure 35: [1]H NMR spectrum of digested untreated ASUiO-66 synthesised using 30 equivalents of formic acid. Integration of ASBDC linker aromatic signal (7.75 ppm, 2.00 integration) and acid modulator (8.04 ppm, 0.58 integration) shown.

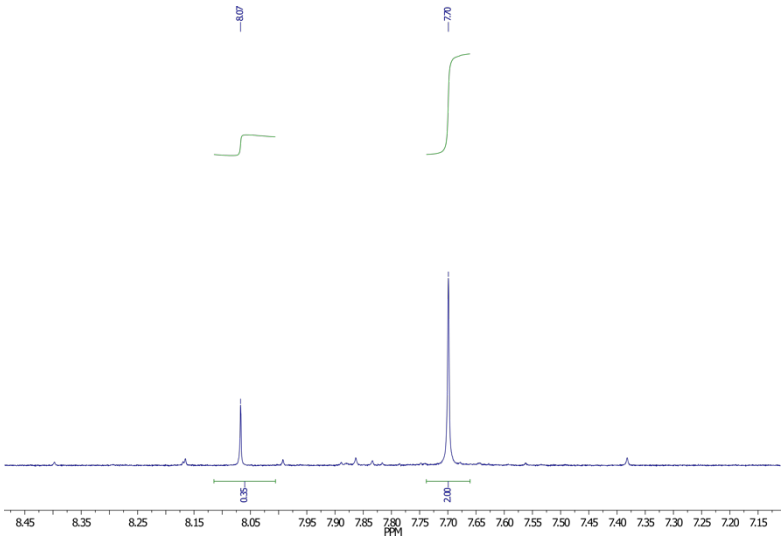

Figure 36: [1]H NMR spectrum of digested Ag(I)PSUiO-66 synthesised using 30 equivalents of formic acid. Integration of ASBDC linker aromatic signal (7.70 ppm, 2.00 integration) and acid modulator (8.07 ppm, 0.35 integration) shown.

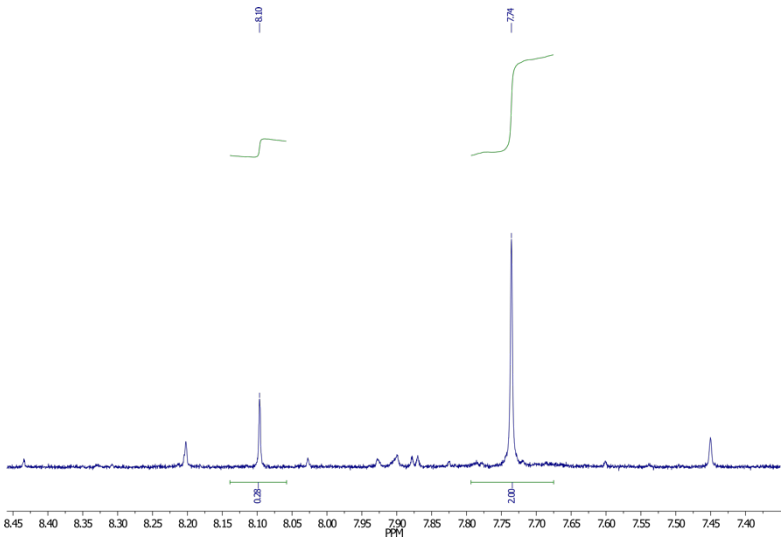

Figure 37: [1]H NMR spectrum of digested Ag(I/0)ASUiO-66 synthesised using 30 equivalents of formic acid. Integration of ASBDC linker aromatic signal (7.74 ppm, 2.00 integration) and acid modulator (8.10 ppm 0.28 integration) shown.

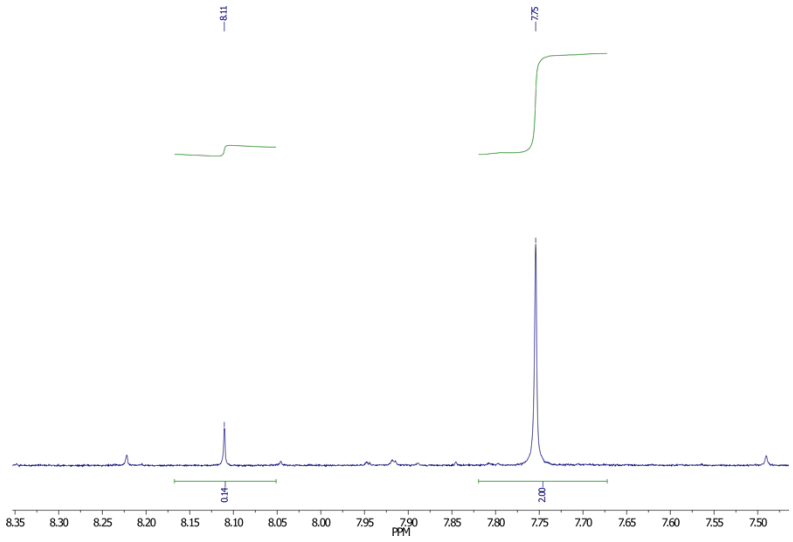

Figure 38: ^{1}H NMR spectrum of digested Ag(0)ASUiO-66 synthesised using 30 equivalents of formic acid. Integration of ASBDC linker aromatic signal (7.65 ppm, 2.00 integration) and acid modulator (8.07 ppm, 0.14 integration) shown.

Appendix 4.8.3 Powder X-ray diffraction data for polymer-embedded UiO-66 derivatives

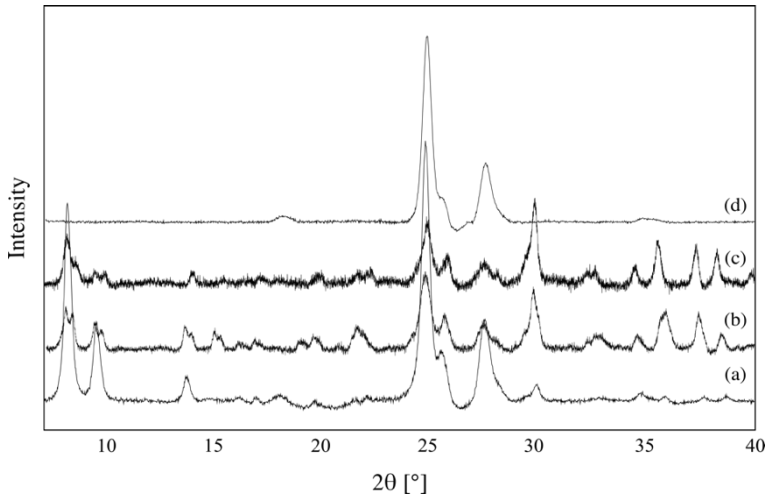

Figure 39: Baseline-corrected powder X-ray diffraction patterns (Co Kα, λ = 1.789 Å) of UiO-66 embedded in a polycaprolactone matrix: **(a)** treated with 100 mM solution of $AgNO_3$ in acetonitrile; **(b)** treated with 100 mM solution of $AgNO_3$ in 5:1 ethanol/water; **(c)** treated as per sample (b) but extensively washed with 5:1 ethanol/water to remove traces of ionic silver, and **(d)** polycaprolactone alone.

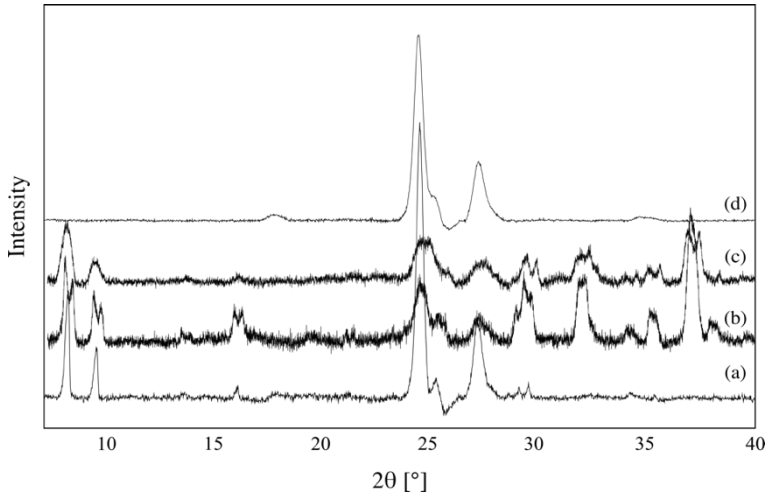

Figure 40: Baseline-corrected powder X-ray diffraction patterns (Co Kα, λ = 1.789 Å) of PSUiO-66 embedded in a polycaprolactone matrix: **(a)** treated with 100 mM solution of $AgNO_3$ in acetonitrile; **(b)** treated with 100 mM solution of $AgNO_3$ in 5:1 ethanol/water; **(c)** treated as per sample (b) but extensively washed with 5:1 ethanol/water to remove traces of ionic silver, and **(d)** polycaprolactone alone.

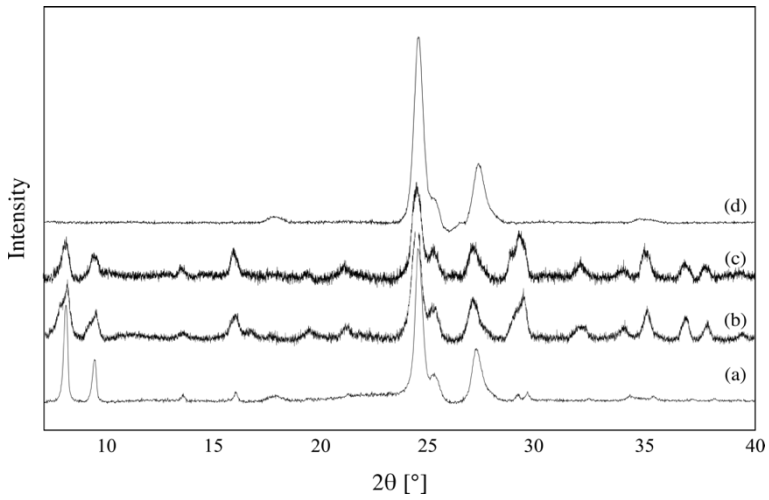

Figure 41: Baseline-corrected powder X-ray diffraction patterns (Co Kα, λ = 1.789 Å) of ASUiO-66 embedded in a polycaprolactone matrix: **(a)** treated with 100 mM solution of $AgNO_3$ in acetonitrile; **(b)** treated with 100 mM solution of $AgNO_3$ in 5:1 ethanol/water; **(c)** treated as per sample (b) but extensively washed with 5:1 ethanol/water to remove traces of ionic silver, and **(d)** polycaprolactone alone.

Appendix 4.8.4 Powder X-ray diffraction data pre and post XAS experiments

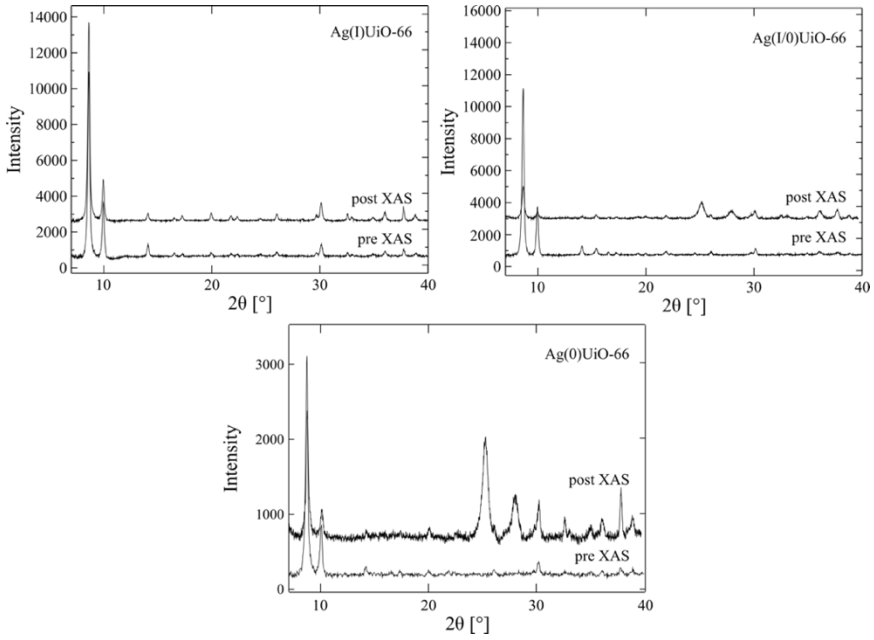

Figure 42: Powder X-ray diffraction patterns (Cu Kα, λ = 1.5418 Å) of silver-treated UiO-66 pre and post XAS experiments. Some of the powdered materials were compressed into a pellet with granulate polyethylene before being presented to the beam which led to the appearance of the broad peaks starting at ~25°. The peaks were cross referenced with an XRD of PE alone (not shown).

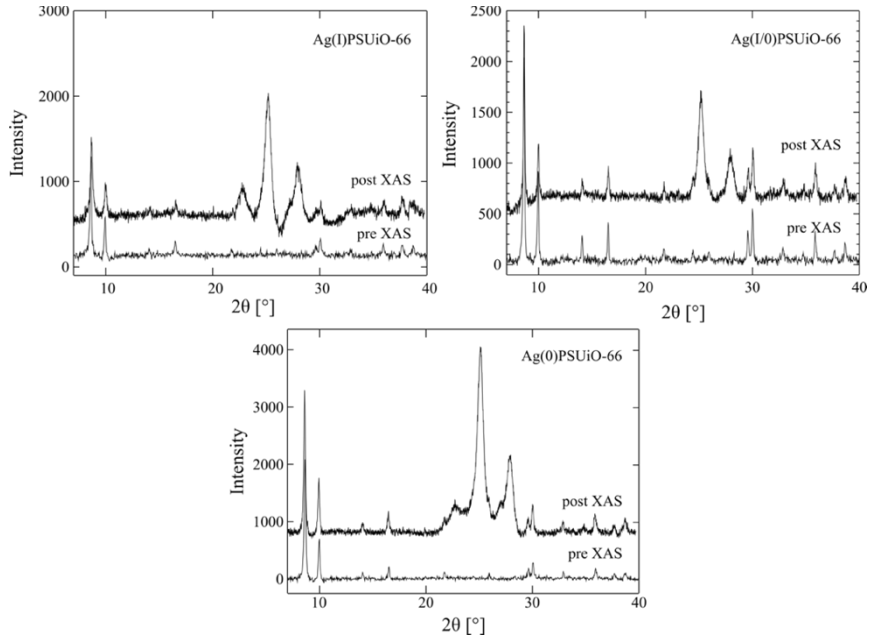

Figure 43: Powder X-ray diffraction patterns (Cu Kα, λ = 1.5418 Å) of silver-treated PSUiO-66 pre and post XAS experiments. Some of the powdered materials were compressed into a pellet with granulate polyethylene before being presented to the beam which led to the appearance of the broad peaks starting at ~25°. The peaks were cross referenced with an XRD of PE alone (not shown).

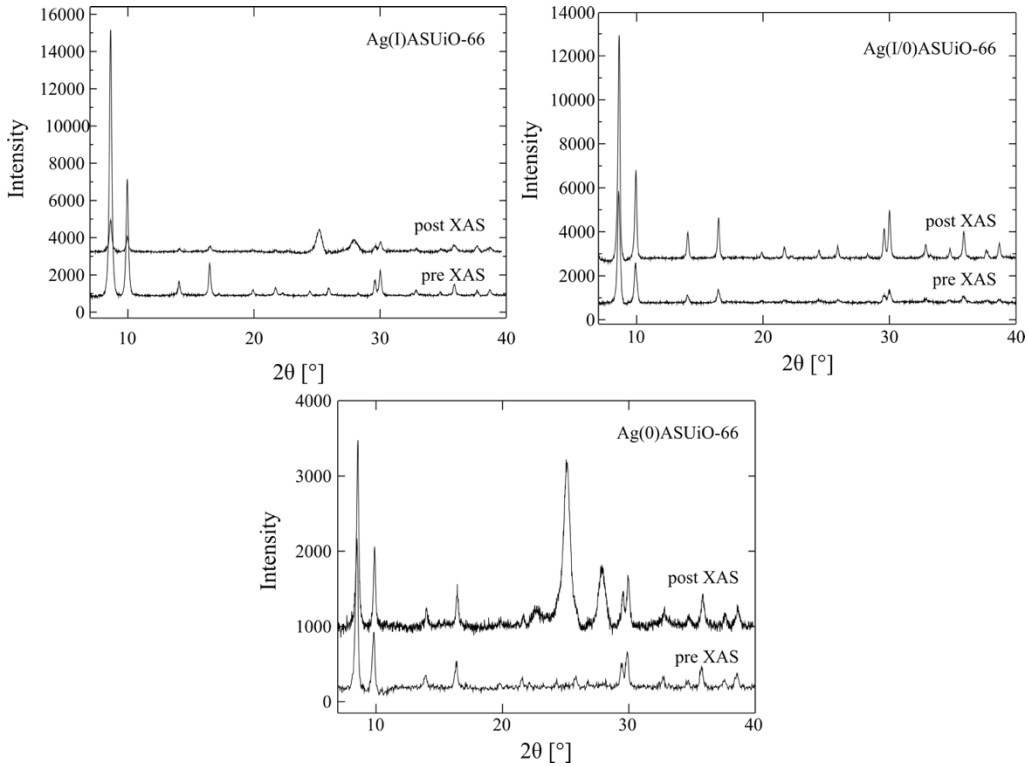

Figure 44: Powder X-ray diffraction patterns (Cu Kα, λ = 1.5418 Å) of silver-treated ASUiO-66 pre and post XAS experiments. Some of the powdered materials were compressed into a pellet with granulate polyethylene (PE) before being presented to the beam which led to the appearance of the broad peaks starting at ~25°. The peaks were cross referenced with an XRD of PE alone (not shown).

Appendix 4.8.5 MOF EXAFS fits

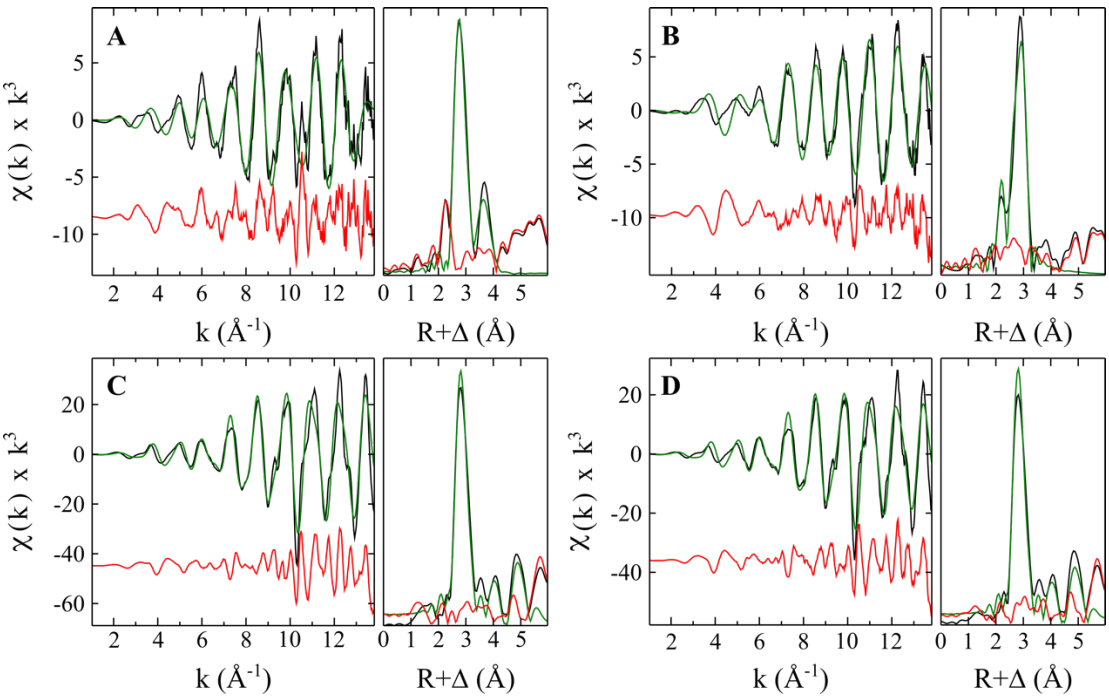

Figure 45: Ag K-edge EXAFS spectra (left panel) and corresponding Fourier Transform (right panel) of UiO-66: (**A**) treated with 100 mM solution of $AgNO_3$ in acetonitrile; (**B**) treated with 100 mM solution of $AgNO_3$ in 5:1 ethanol/water; (**C**) treated as per sample (B) but extensively washed with 5:1 ethanol/water to remove traces of ionic silver, and (**D**) sample (C) embedded in a polycaprolactone matrix. Experimental (black) and calculated (green) data with the residual (red) shown offset. Fit parameters are shown in **Table 5**.

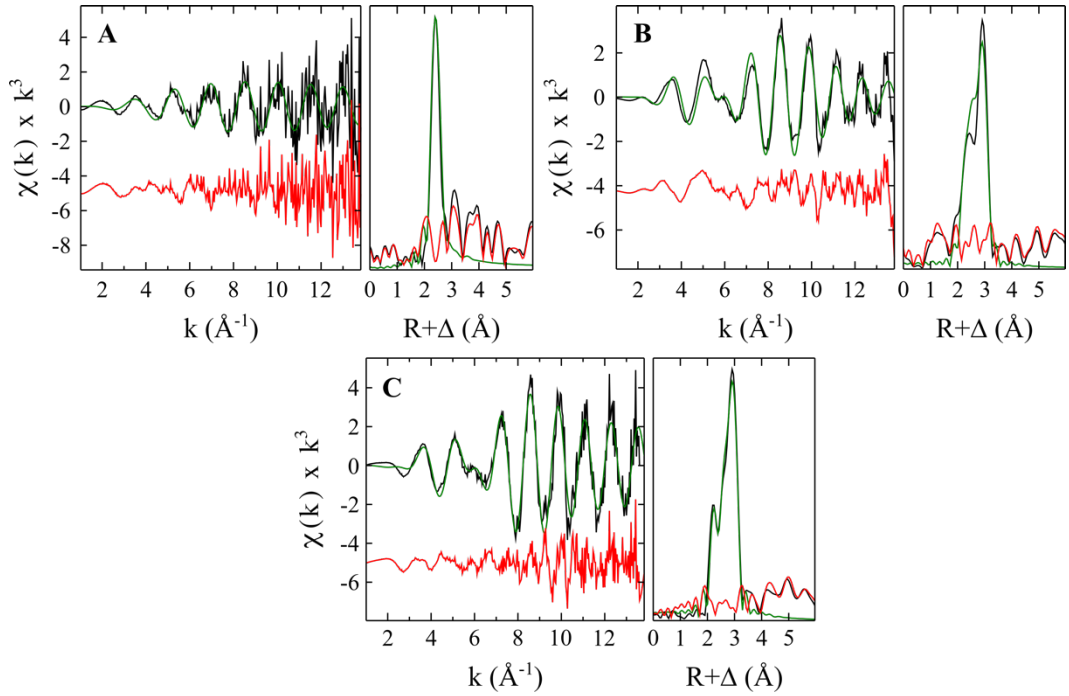

Figure 46: Ag K-edge EXAFS spectra (left panel) and corresponding Fourier Transform (right panel) of PSUiO-66: (**A**) treated with 100 mM solution of $AgNO_3$ in acetonitrile; (**B**) treated with 100 mM solution of $AgNO_3$ in 5:1 ethanol/water; (**C**) treated as per sample (B) but extensively washed with 5:1 ethanol/water to remove traces of ionic silver. Experimental (black) and calculated (green) data with the residual (red) shown offset. Fit parameters are shown in **Table 6**.

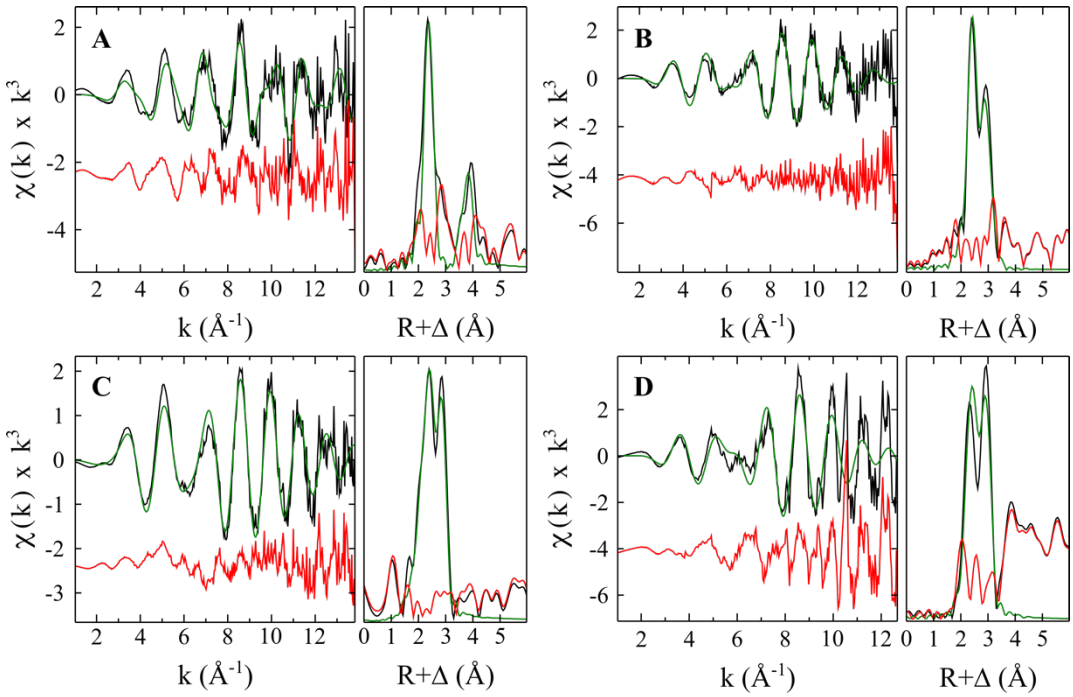

Figure 47: Ag K-edge EXAFS spectra (left panel) and corresponding Fourier Transform (right panel) of ASUiO-66: (**A**) treated with 100 mM solution of $AgNO_3$ in acetonitrile; (**B**) treated with 100 mM solution of $AgNO_3$ in 5:1 ethanol/water; (**C**) treated as per sample (B) but extensively washed with 5:1 ethanol/water to remove traces of ionic silver, and (**D**) sample (C) embedded in a polycaprolactone matrix. Experimental (black) and calculated (green) data with the residual (red) shown offset. Fit parameters are shown in **Table 6**.

Appendix 4.8.6 Silver leaching results for UiO-66 treated with Ag(I/0) and Ag(0)

Table 12: Ag(I/0)UiO-66/PCL in water

Time	Conc. of Ag [ppm] & replicate			
	1	2	3	4
1	45.9	1.7	115.1	14.6
2	64.7	4.2	126.1	26.8
4	84.0	7.2	134.0	81.7
8	98.7	9.6	138.1	54.8
24	115.0	15.6	149.3	84.4

Table 13: Ag(0)UiO-66/PCL in water

Time	Conc. of Ag [ppm] & replicate			
	1	2	3	4
1	1.04	0.60	0.26	1.50
2	1.44	0.93	0.66	2.01
4	1.26	1.43	1.10	2.36
8	4.19	1.46	1.68	2.37
24	7.49	2.65	2.54	2.53

Chapter Five: Conclusions and future work

5.1 Conclusions and future work

Presented herein was an in-depth analysis of the biochemical fate of silver ions in bacterial and mammalian systems by metallomics techniques: X-ray absorption spectroscopy, and size exclusion chromatography hyphenated with inductively coupled plasma mass spectrometry. In addition, silver-loaded metal-organic frameworks with chemically-programmed pore enviornments were synthesised, characterised and tested for antibacterial efficacy.

At sublethal concentrations, silver ions in Luria Bertani broth were determined to be predominantly bound by cysteine, or thiolate-containing low to medium molecular weight species, likely partially degraded protein species or agglomerations of short-chain peptides. Interestingly, no silver chloride was identified in the XAS data of silver in broth, despite the medium containing ~5 g/L NaCl. This would suggest that the silver species in solution is highly stable against precipitation as AgCl but was still bioavailable to the bacteria grown in the broth. Such a silver-species could potentially be an antibiotic drug candidate if successfully isolated and characterised further. The speciation of the silver ions was found to be concentration dependent, with a twenty-fold increase in [$AgNO_3$] resulting in formation of distinct, new complexes, possibly due to aggregation of smaller molecular weight species peptides. At such a concentration, $AgNO_3$ would be well above the MIC of both strains of bacteria used.

Analysis of post bacterial growth silver-treated broth found that no detectable silver remained in the *S. aureus* depleted broth, and a significantly reduced silver signal was detected from the *E. coli* depleted broth. Interestingly, the post growth broth SEC traces did not differ significantly from that of the pre growth broth. From this it could be concluded that the silver concentration was indeed ‘sublethal’ as, if cell death had occurred due to the presence of silver ion, the post growth chromatogram would be expected to be significantly altered as a result of cell lysis. Additionally, the complete uptake of silver ions by *S. aureus* from the broth indicated that efflux from the organism was not occurring. Taking these observations into consideration it could be concluded that the bacteria were taking up the silver containing molecules and not identifying them as a toxicant to be effluxed from the cell.

Intracellular silver was also found to be coordinated by sulfurous donors like cysteine. However, SEC-ICP-MS of the bacterial lysates indicated that intracellular silver ions were associated with high molecular weight species. Comparison of the *S. aureus* and

E. coli ^{107}Ag and ^{65}Cu traces revealed the silver ions were nonuniformly colocalised with copper ions. Such confluence of the two elements could suggest that the cells were processing the endogenous Ag^+ ions as if they were nutrient copper ions. For this to have occurred, the short-chain peptide-bound silver ions would have to have been stripped of their exogenous ligands (e.g. peptide or partially digested protein), transported by a chaperone through the cell to metallate a cuproenzyme or homeostatic copper protein. Extension of the Irving-Williams series would suggest that the silver ions would form more stable complexes with cuproenzymes than their native copper cofactors. Silver's lack of accessible oxidation states would likely result in inhibition of redox-active species. Thus, it is possible that in the initial stages of bacterial cell death, silver is incorporated into copper metabolic pathways which would be overwhelmed as the concentration rose.

While ~20 copper-binding proteins have been identified in the proteome of *E. coli* MG1655, only two have been identified in the proteome of *S. aureus* Newman. However, the ^{65}Cu trace of *S. aureus* lysate revealed many more than two copper-binding proteins. Isolation, purification and characterisation of these species by techniques like anion exchange chromatography and mass spectrometry could provide great insight into the copper homeostatic pathways of bacteria. Following the fate of silver through these additional proteomics techniques would also yield more information about the molecular mechanisms through which silver ions elicit their antibacterial response.

Given the close association between silver and copper reported here, it would be informative to carry out transcriptomics analysis of the organisms at concentrations of $AgNO_3$ approaching the MIC with particular attention paid to the scores associated with copper-binding protein expression. However, for this to be useful, greater knowledge about the copper-binding proteins in the organisms would be required.

In human whole blood, silver nitrate was found to rapidly associate with the red blood cell fraction where ~90% of Ag^+ was localised, 5 minutes post exposure. Significant lysis of the RBCs was also observed to occur in the presence of 2 mM $AgNO_3$, which was consistent with previously reported observations. Within the red blood cells, silver was predominantly associated with haemoglobin and bound by cysteine residues present in the protein, a small portion of the silver was also found to be associated with carbonic anhydrase.

Due to haemolysis, the plasma fraction of whole blood treated with 2 mM silver nitrate was contaminated with RBC cellular contents. SEC-ICP-MS of the plasma fraction revealed that the greatest proportion of Ag^+ was associated with contaminant haemoglobin.

After Hb, human serum albumin was found to be the dominant silver-binding species, as well as a range of higher molecular weight protein species. Interestingly, in isolated plasma the speciation of silver nitrate was found to be predominantly silver chloride, which was suspected to be present as a colloidal suspension. Conversely, in a sample of plasma fractionated from whole blood treated with silver nitrate, no silver chloride was determined to be present. This would suggest that studies carried out elsewhere in isolated plasma or serum are correct in conclusion that the antibacterial properties of silver are reduced in such systems due to sequestration as silver chloride, however, that appears to not be representative of 'true' or 'complete' biological fluids as reported here. At a lower concentration of silver nitrate (0.1 mM) lysis of RBCs did not visibly occur, as validated by the absence of a haemoglobin peak in the SEC-ICP-MS plasma chromatogram. However, this could merely indicate that the degree of lysis that did occur was successfully managed by the haemoglobin scavenging protein, haptoglobin.

A second dimension of separation and purification of the size exclusion chromatograms by anion exchange chromatography would possibly allow more precise identification of silver-binding protein species in plasma and red blood cells. To do this, the buffer system would need to be changed to one that is not anionic at physiological pH, like Tris or bis-Tris. Isolation of protein samples could enable testing for enzymatic activity for validation of plasma proteins that may bind silver.

Finally, the pore environment of UiO-66 was successfully modified and tailored for increased uptake and prolonged release of silver ions. This was acheived through synthesis of alkyl thioether- and allyl thioether-functionalised analogues of the parent material. Soaking of the materials in solutions of silver nitrate enabled loading of the materials with silver ions and, depending on the solvent system used, silver could be loaded in as Ag^{+}, Ag(I)/Ag(0) or Ag(0) with slow *in situ* reduction. Embedding the silver loaded MOFs into a polymer matrix slowed the release of silver from all MOF/polymer composites relative to the free MOF as well as extending the applicability of the material for use in clinical settings as an antibacterial coating. Comparison of the leaching of silver from the polymer-embedded materials into water and into bacterial broth revealed that release into broth was significantly suppressed. Reduced release of silver was likely due to the high ionic strength of the medium which provides useful information regarding the behaviour of the materials in biological settings. Additionally, it was found that release of silver from the unfunctionalised UiO-66 was highly variable for all silver treatments which could have been due to heterogenous distribution of the silver in the framework given that this

variability was even observed within a single batch of the material. Antibacterial testing of the silver-loaded, polymer-embedded materials revealed that all silver-containing material had antibacterial properties against Gram-positive and Gram-negative bacteria. Comparing raw bacterial growth inhibition zones between the silver-loaded materials and silver nitrate in the polymer at an equivalent weight loading, none of the materials performed better than the $AgNO_3$/PCL sample. However, weighting the inhibition zones by the mass of silver in each sample, it was revealed that almost all materials outperformed the positive control (based on mm of inhibited growth per mg of silver). The material with the greatest zone of inhibition per mg of silver was the unfunctionalised UiO-66; however, the disk diffusion assays did not take into account the longevity of the materials.

The only known antibacterial component of the UiO-66 analogues presented herein was the loaded silver. The antibacterial properties of the materials could be further optimised by using of a framework which comprises another antibacterial metal (like Cu or Zn) and/or inclusion of a linker with antibacterial properties, possibly a sulfonamide derivative. Coupled with embedding into an antibacterial polymer matrix like chitosan and loaded with silver ions or another antibiotic, a material entirely comprised of antibacterial components could be produced.